

**Modelling and Practical Set-up to Investigate the
Performance of Permanent Magnet Synchronous
Motor through Rotor Position Estimation at
Zero and Low Speeds**

Mazen Makki Ali Al Ibraheemi

**A thesis submitted to the Cardiff University in Candidature for the degree of
Doctor of Philosophy**

Wolfson Centre for Magnetics Technology

Cardiff School of Engineering

Cardiff University

Wales, United Kingdom

September, 2018



DECLARATION

This work has not been submitted in substance for any other degree or award at this or any other university or place of learning, nor is being submitted concurrently in candidature for any degree or other award.

Signed (candidate) **Date**.....

STATEMENT 1

This thesis is being submitted in partial fulfilment of the requirements for the degree of PhD

Signed (candidate) **Date**.....

STATEMENT 2

This thesis is the result of my own independent work/investigation, except where otherwise stated, and the thesis has not been edited by a third party beyond what is permitted by Cardiff University's Policy on the Use of Third Party Editors by Research Degree Students. Other sources are acknowledged by explicit references. The views expressed are my own.

Signed (candidate) **Date**.....

STATEMENT 3

I hereby give consent for my thesis, if accepted, to be available for photocopying and for interlibrary load, and for the title and summary to be made available to outside organisations.

Signed (candidate) **Date**.....

STATEMENT 4: PREVIOUSLY APPROVED BAR ON ACCESS

I hereby give consent for my thesis, if accepted, to be available online in the University's Open Access repository and for inter-library loans **after expiry of a bar on access previously approved by the Academic Standards & Quality Committee.**

Signed (candidate) **Date**.....

ABSTRACT

This thesis provides a study for the rotor position estimation in SM-PMSMs, particularly at zero and low speeds. The method for zero rotor speed is based on injection of three high frequency voltage pulses in the motor stator windings. Then, the voltage responses at the motor terminals are exploited to extract the rotor position. Two approaches, modelling and practical implementations, are presented. The obtained results have showed a verification of a high-resolution position estimation (a position estimation of 1 degree angle), a simplicity and cost effective implementation and a no need for current sensors is required to achieve the estimation process. It should be noticed that the implementation of rotor position estimation at zero speed is only attended when the rotor is at standstill or very low speed. Therefore, the motor driver is not expected to be active at this condition. Thereby, the zero speed estimation does not provide a robust torque control. In future, this should be taking into consideration to overcome this drawback and to make the estimator more reliable.

At low speed running, the primary goal is to start spinning the under test motors, and then the rotor position estimation is achieved. The motor spinning is based on adopting a virtual injected signal to generate the voltage components, V_α and V_β , of the space vector pulse width modulation technique. Then, generating the eight space vectors is conducted through storing the standard patterns of the six space vector sectors in a memory structure together with the timing sequences of each sector. The presented strategy of motor running includes a proposed motor speed control scheme, which is based on controlling the frequency of the power signal, at the inverter output, through controlling the timing period of execution the power delivery program. The thesis presents a proposed method to achieve the estimation goal depends on tracking the magnetic saliency on one motor line voltage. Thereby, the rotor position estimation

The introduced proposed method, for rotor position estimation at zero speed, verifies the following contributions:

- Presents a simple and cost effective zero speed rotor position estimator for the motor under test.
- The aimed resolution in this thesis is an angle 1 degree.

- Adopting solely the measuring of motor terminal voltages.
- Eliminating the detection of the rotor magnet polarity as a necessary technique for completing the position estimation.

At low speed running, the following contributions are verified:

- Rather than a real frequency signal, a virtual injected signal is adopted to generate the voltage components, V_α and V_β of the space vector pulse width modulation technique.
- The proposed method for generating the eight space vectors is based on storing the standard patterns of the six sectors in a memory structure together with the timing sequence.
- The strategy of motor speed control is based on controlling the period of execution the power delivery program.
- The strategy of low speed rotor position employs one motor line voltage from which the low speed estimation is achieved.

ACKNOWLEDGEMENTS

I would like to thank the Wolfson Centre for Magnetics Technology for their support, especially my supervisor **Dr Fatih J. Anayi** for his patience and valuable guidance.

In addition, I would like to give a special thank you to my wife *Zainb Al Kafagy* for her patience and cooperation, and to my family members *Haider, Aulla, Tabarek and Yaqeen* who have supported me throughout.

This work was made possible through; the moral support by the Establishment of Martyrs/Iraq and the gratefully received financial support of my sponsor, the Ministry of Higher Education/Iraqi government, via its representative, the Iraqi Cultural Attache, London ... Many Thanks.

List of symbols and abbreviations

A, B

ac	alternating current
A/D	Analogue to Digital converter
ACM	Alternating Current Machine
ACIM	Alternating Current Induction Machine
B	Magnetic field density [Wb/m^2]
BaFe	Barium Ferrite
BDCM	Brushless direct current motor
BPF	Band pass filter

C, D

CCI	Current Control Inverter
CPM	Claw Permanent Magnet
cwSM-PMSM	Concentrated windings surface mounted permanent magnet machine
d	Direct direction in rotary reference frame
DAC	Digital to Analogue Converter
dc	direct current

DFIG Double Fed Induction Generator

DOL Direct On Line

DTC Direct Torque Control

E, F

EEPROM Electrical Erasable Read-Only Memory

EMF Electro-Motive Force [V]

ESM Electrical-energized Synchronous Motor

EV Electric Vehicle

f Electric frequency (Hz)

FI-PMSM Flux Intensified Permanent Magnet Synchronous Motor

FOC Field Oriented Control

f_s Sampling frequency [Hz]

H, I

H Magnetic field intensity [A/m]

HEV Hybrid Electric Vehicle

HFSI	High Frequency Signal Injection
HPF	High Pass Filter
I, i	Electric current [A]
IGBT	Isolated Gate Bipolar Transistor
IP	Ingress Protection
I_p	Peak current [A]
IPMSM	Interior Permanent Magnet Synchronous Motor
I_s	Stator rating current [A]
I_{ph}, i_{ph}	Phase current [A]
IM	Induction Motor
<u>L, J</u>	
J	Motor moment of inertia [kg.m^2]
L	Inductance [H]
L_d	d-axis synchronous inductance [H]
LPF	Low Pass Filter
L_q	q-axis synchronous inductance [H]
LSRPE	Low Speed Rotor Position Estimation

M, N

MMF	Magneto Motive Force [AT]
MEC	Magnetic Equivalent Circuit
MOSFET	Metal-Oxide Semiconductor Field-Effect Transistor
MTPA	Maximum Torque Per Amber [N.m/A]
NdFeB	Neodymium Iron Boron

O, P

p	Number of pole-pair
P	Electric power [W]
PC	Personal computer
PM	Permanent Magnet
PMSM	Permanent Magnet Synchronous Motor
PWM	Pulse Width Modulation

Q, R

q	Quadrature direction in rotary reference frame
R_{ph}	Phase resistance [Ω]
r_{ph}	Direct current phase resistance [Ω]

REM	Rare Earth Magnets
RMS	Root Mean Square
RP	Rotor Position
RPE	Rotor Position Estimation
<u>S, T</u>	
SG	Synchronous Generator
SmCo	Samarium Cobalt
SM-PMSM	Surface Mounted Permanent Magnet Synchronous Motor
SPWM	Sine Pulse Width Modulation
SRAM	Static Random Access Memory
SrFe	Strontium Ferrites
SRM	Switched Reluctance Motor
SVPWM	Space Vector Pulse Width Modulation
T_e	Electromagnetic Torque [Nm]
T_L	External applied torque [Nm]
T_m	Mechanical Torque [Nm]
T_s	Full period of sampling frequency [sec]

U, V

V_a , V_b , and V_c	Motor terminal voltages [V]
VCI	Voltage Control Inverter
V_d	direct voltage in rotary reference frame [V]
V_{dc}	DC Supply Voltage [V]
VIPM	V-shape Interior Permanent Magnet
V_q	quadrature voltage in rotary reference frame [V]
VLSI	Very Large Scale Integrated
V_α	horizontal voltage in stationary reference frame [V]
V_β	vertical voltage in stationary reference frame [V]

W, Y, Z

ZSRPE	Zero Speed Rotor Position Estimation
-------	--------------------------------------

Greek

α	Horizontal direction in stationary reference frame
β	Vertical direction in stationary reference frame
θ	Rotor position angle [degree]
θ_e	Estimated rotor position angle [degree]

θ_E	actual Electrical rotor position angle [degree]
θ_r	Mechanical rotor position angle [degree]
μC	Microcontroller
λ_d	direct permanent magnetic flux [Wb]
λ_m	Permanent magnetic flux [Wb]
λ_q	quadrature permanent magnetic flux [Wb]
ω	Angular electric frequency [rad/sec]
ω_c	Carrier angular frequency [rad/sec]
ω_e	Electrical rotor speed [rpm]
ω_m	Mechanical rotor speed [rpm]

Table of contents

Summary	III
Acknowledge	V
List of symbols and abbreviations	VI
Table of contents	XIII
List of tables	XXIII
List of figures	XXIV
CHAPTER ONE	1
INTRODUCTION.....	1
1.1 Importance of permanent magnet motors.....	1
1.2 Thesis objectives.....	1
1.2.1 Zero-speed rotor position estimation	2
1.2.2 Low-speed machine driving and rotor position estimation.....	3
1.3 Thesis organization.....	4
CHAPTER TWO	6
THEORY OF PERMANENT MAGNET SYNCHRONOUS MOTORS	6
2.1 Introduction	6
2.2 Features of permanent magnet motors.....	8
2.3 Comparing PMSM and BDCM	10

2.4	Applications of permanent magnet synchronous motor	11
2.5	Magnetic materials	16
2.6	Types of the permanent magnet motors (PMMs).....	18
2.6.1	Interior permanent magnet synchronous motor (Salient-Pole)	19
2.6.2	SM-PMSM (Non-salient pole).....	19
2.6.3	CPM	20
2.6.4	Spoke FMM	21
2.6.5	VIPM.....	22
2.7	Electrical machine frame transformations	22
2.8	Operation of PMSM and importance of rotor position.....	25
2.8.1	Field Oriented Control (FOC).....	26
2.8.2	Direct Torque Control (DTC)	28
2.8.3	Speed Control.....	28
2.8.4	Non-linear Control	29
2.8.5	Sensorless Control.....	30
2.9	Methods of detecting the rotor position angle	30
2.9.1	Direct position-detection	30
2.9.2	Indirect position-detection	31
2.10	PMSM equations	32
2.11	Sensorless techniques and power electronic development.....	35
2.11.1	Concept of HF injection and machine core saturation	36

2.12	The inverters and PWM.....	36
2.13	Summary.....	37
CHAPTER THREE.....		39
LITERATURE REVIEW		39
3.1	Introduction	39
3.2	Structure modification	42
3.3	Improving the performance of PMSM drive	45
3.4	HFSI in the hybrid operation of PMSM.....	47
3.5	The noise in HFSI.....	48
3.6	Eliminating the filtering process.....	49
3.7	HFSI in the frame axes and saliency effect	51
3.8	Addressing the drawbacks in HFSI	53
3.9	HFSI in non-PMSM.....	56
3.10	Mathematical models for HFSI	57
3.11	Square wave injection.....	62
3.12	Improve the HFSI performance	65
3.13	The HFSI in different applications	67
3.14	Evaluation of HFSI estimation	68
3.15	State-Of-Art.....	69
3.16	Summary.....	73
CHAPTER FOUR.....		75

INVESTIGATION OF ZERO-SPEED ROTOR POSITION THROUGH MODELLING SYSTEM.....75

- 4.1 Introduction 75
- 4.2 The problem of rotor position estimation at zero-speed..... 76
- 4.3 Mathematical model of PMSM 77
 - 4.3.1 Transformation of stator variables to stationary reference frame 78
 - 4.3.2 Transformation between stationary and rotary reference frames..... 78
 - 4.3.2.1 Stationary to rotary reference frame..... 78
 - 4.3.2.2 Rotary to stationary reference frames..... 79
 - 4.3.3 Modelling the motor fields λ_d and λ_q 79
 - 4.3.4 Modelling the stator currents in the rotor reference frame 79
 - 4.3.5 Modelling the motor outputs 80
- 4.4 The proposed method for modelling the ZSRPE..... 81
 - 4.4.1 Basic concept 81
 - 4.4.2 Formatting the x-address from the voltage measurements 83
 - 4.4.2.1 Voltage waveform formations..... 83
 - 4.4.2.2 Defining a specific value for each waveform..... 85
 - 4.4.2.3 Rotor space sectors and x-address creation 86
 - 4.4.3 Formatting the y-address 88
 - 4.4.3.1 Formatting the y-address through current responses..... 88
 - 4.4.3.2 Formatting the y-address from a voltage measurement 91

4.4.4	Modelling blocks for deviation algorithm.....	92
4.5	Implementation of the proposed method for modelling the ZSRPE	93
4.5.1	ZSRPE for IPMSM	93
4.5.2	ZSRPE for SM-PMSM	94
4.6	Modelling the effect of saliency weakness on RPE	97
4.7	Mathematical modelling view	98
4.8	Simulation results	100
4.9	Summary.....	102
CHAPTER FIVE.....		104
PRACTICAL SET-UP AND VERIFICATION FOR ZERO-SPEED ROTOR POSITION ESTIMATION.....		104
5.1	Introduction	104
5.2	Construction of the practical platform for ZSRPE.....	105
5.2.1	The microcontroller.....	106
5.2.1.1	The microcontroller hardware and software integration	107
5.2.2	Inverter	108
5.2.3	The PMSMs under test.....	108
5.3	Describing the practical model	110
5.3.1	Generating of the triggering signals by software implementation	111
5.3.2	Triggering the inverter elements	112
5.3.3	Voltage offsets	113

5.3.4	Analogue to digital conversion	113
5.4	Sequence of triggering the inverter switching elements.....	114
5.5	Exciting the stator windings	115
5.6	Results	117
5.6.1	Results of the proposed practical platform.....	117
5.6.2	Processing the motor terminal voltages	117
5.6.3	Comparison between the “MATLAB” and practical model results.....	120
5.6.4	Comparing the proposed estimator with other relevant works	121
5.7	Summary.....	122
CHAPTER 6	124
SIMULATION ANALYSIS FOR ROTOR POSITION ESTIMATION OF SM-PMSM AT LOW SPEED	124
6.1	Introduction	124
6.2	General scheme for modelling the LSRPE.....	125
6.2.1	Modelling the forward path.....	126
6.2.1.1	Forward path with PWM via voltage comparison.....	126
6.2.1.1.1	Modelling procedure for generating the voltage V_β	127
6.2.1.1.2	Modelling procedure for generating the voltage V_α	127
6.2.1.2	Forward path with PWM via current comparisons	128
6.2.2	Modelling the feedback path.....	128
6.2.2.1	Modelling detection and estimation of motor currents	128

6.2.2.2	Modelling the estimation of rotor position and angular speed.....	129
6.3	Proposed modelling scheme for LSRPE	130
6.3.1	Blocks of forward path.....	131
6.3.1.1	Setting speed Block	131
6.3.1.2	Block of reference torque quadrature current.....	132
6.3.1.3	Reference current Block.....	133
6.3.1.4	Power management Block.....	133
6.3.1.5	PM motor model.....	134
6.3.1.6	Applied torque Block	134
6.3.2	Blocks of feedback path	135
6.3.2.1	Block of magnetic saliency detection.....	136
6.3.2.2	Unity peak normalization Block.....	136
6.3.2.3	Position estimation Block, θ_e	138
6.3.2.4	Block of speed estimation, ω_e	138
6.3.2.5	Position recovery Block	139
6.3.2.6	Block of Combining the initial and low speed positions.....	139
6.4	Modelling results of the LSRPE.....	140
6.5	Summary.....	146
CHAPTER SEVEN.....		148
REAL-TIME EXPERIMENTAL SET-UP TO PREDICTE ROTOR POSITION OF SM-PMSM AT LOW SPEED		148

7.1	Introduction	148
7.2	Development in real-time implementation	148
7.3	Description of the low-speed test bed.....	149
7.3.1	Forward path operations.....	150
7.3.1.1	Master microcontroller	150
7.3.1.1.1	Generating virtual injected voltages	153
7.3.1.1.2	Sector determination.....	153
7.3.1.1.3	Timing of motor excitation.....	154
7.3.1.1.4	Address counter	156
7.3.1.1.5	SVPWM and Memory	157
7.3.1.1.6	Speed control	163
7.3.1.2	Optocoupler	164
7.3.1.3	Bootstrap gate drive.....	165
7.3.1.4	Inverter	167
7.3.2	The feedback path operations.....	168
7.3.2.1	Amplifiers.....	168
7.3.2.2	Slave microcontroller	169
7.4	PMSMs under test	170
7.5	Encoders	170
7.6	Binary converter and DAC	171
7.7	Magnetic brake load	172

7.8	Startup strategy	173
7.9	Harmonic calculations	174
7.10	Avoiding microcontroller limitations	174
7.11	Practical Results	175
7.11.1	Results of rotor position estimation at low speed	177
7.11.2	Results of startup strategy and harmonic analysis	180
7.11.3	Results related to motors power delivering	183
7.12	Summary	190
CHAPTER EIGHT		192
8.1	Main conclusion points	192
8.2	Main contributions	197
8.3	Novelty	198
8.4	Suggestions for future works	200
References		202
Appendices		228
Appendix A, C-language codes for μ Cs programming		228
A.1	Codes of zero speed position estimation	228
A.2	Codes for low speed running and RPE	245
Appendix B, References for the main peripherals		270
B.1	Encoder inside the motor M0200	270
B.2	Incremental encoder 755HS	270

B.3 Binary converter	273
B.4 Pins out description for the μ C ATAmega328	274
B.5 Pins out description for the μ C ATAmega2560	275
B.6 Transducer Display Interface [E301/2]	279
Appendix C, Miscellaneous.....	281
C.1 Datasheets for electronic components	281
C.1.1 Brief datasheet for IGBT FGH40N60SFD	281
C.1.2 Brief datasheet for IGBT FGH40T100SMD	282
C.1.3 Brief datasheet for digit to analogue converter AD767.....	283
C.2 Snaps for load test results	284
C.3 Motor M0200 datasheet.....	285
C.4 Motor AC M2n0320 datasheet	286
C.5 Virtual voltages and sectors of the proposed SV sequence	287
C.6 The inverter printed circuit board, PCB	288
C.7 Standard patterns of space vector technique	291
C.8 Details of the block IGBT switching in figure 4.21	294

List of tables

Table 2. 1, Advantages of PM motor over the induction and brush machines	8
Table 2. 2, Various types of magnetic materials and their properties.....	18
Table 3. 1: Comparisons results given by reference [124].....	70
Table 4. 1: Division of the rotor spatial space into sectors and x-address creation	87
Table 4. 2: Parameters of the modelled IPMSM.....	94
Table 4. 3: Distribution of rotor position angles on main sectors and subsectors	95
Table 4. 4: The modelled SM-PMSM parameters	96
Table 5. 1, Specification parameters of the PMSMs in the ZSRPE practical platform	109
Table 5. 2, Comparison statements in calculating the x-address	118
Table 5. 3, Summary of errors in ZSRPE for the practical platform	120
Table 5. 4, Comparing `performance of the propose estimator with other works	122
Table 6. 1: Index for blocks numbering in figure 6.2	131
Table 7. 1: Summary of SVPWM voltages and currents analysis	159
Table 7. 2: Load test for both powered motors	190

Table of figures

Fig. 2. 1, Basic structure of (a) PM motor (b) Induction motor	6
Fig. 2. 2, Cross-section for (a) PMSM (b) induction motor.....	9
Fig. 2. 3, Schematic view for the construction of PM motor	9
Fig. 2. 4, PMSM in washing machine (a) the application (b) a closer look.....	11
Fig. 2. 5, PMSM in integrated mobile application	12
Fig. 2. 6, Classification of the electric vehicle drives	12
Fig. 2. 7, PM auxiliary generator in EV (a) Stator (b) Rotor (c) Flux distribution.....	13
Fig. 2. 8, Application of PM motor as a ship propulsion	13
Fig. 2. 9, Sketch for the application of PMSM as a boat propulsion	14
Fig. 2. 10, (a) PMSM topology centrifugal pumps (b) micro drill system	14
Fig. 2. 11, Application of PMSM on syringe pump (a) a cross-section view (b) the syringe description	15
Fig. 2. 12, Application of PMSM on paraglider	15
Fig. 2. 13, Comparison the magnetic strength of three different magnetic materials ...	16
Fig. 2. 14, Developing steps of magnetic materials	16
Fig. 2. 15, Interior configurations of PM (a) interior- circumferential (b) interior- radial	19
Fig. 2. 16, Surface configurations of PM (a) surface-mounted (b) surface-inserted	20
Fig. 2. 17, Claw pole PMSM (a) schematic of one disc (b) positioning the claw pole (c) real claw rotor	21

Fig. 2. 18, Basic structure of spoke FMM.....	21
Fig. 2. 19, V-shape rotor in an 18/16 PMSM.....	22
Fig. 2. 20, Clarke's transformations of stator voltages (V_a , V_b and V_c) to the stationary reference frame (V_α and V_β).....	23
Fig. 2. 21, Park's transformations of stator voltages (V_a , V_b and V_c) to the rotary reference frame (V_d and V_q).....	24
Fig. 2. 22, Park's transformations through Clarke's transformations	25
Fig. 2. 23, Speed control scheme with FOC	28
Fig. 2. 24, Scheme for nonlinear IPMSM control.....	29
Fig. 2. 25, The rotor position sensors (a) electromagnetic (b) photoelectric (c) magnetic (d) electrical	31
Fig. 2. 26, Methods of sensorless rotor position estimation.....	31
Fig. 2. 27, Basic structure for PMSM servo system.....	32
Fig. 2. 28, Vector representation for PMSM in rotor reference frame.....	33
Fig. 2. 29, Stator core saturation effect due to exciting current	36
Fig. 3. 1, Method of sensorless position estimation.....	40
Fig. 3. 2(a) schematic for the motor structure with nonmagnetic materials (b) effect of nonmagnetic material on magnetization characteristics	42
Fig. 3. 3, Effect of the treatment of zero current clamping on the accuracy of rotor position estimation (a) before (b) after.....	46
Fig. 3. 4, Basic idea of the injection axis-switch, IAS	46
Fig. 3. 5, Schematic for estimation procedure by the weighted coefficients algorithm	48

Fig. 3. 6, Method of substituting filters by transfer functions.....	50
Fig. 3. 7, RP detection from envelops of the stator current HF components	52
Fig. 3. 8, Schematic diagram for the electrically energized motor	57
Fig. 3. 9, Method of three levels converter normalized voltages	59
Fig. 3. 10, Estimation results given by reference [152]	72
Fig. 3. 11, Estimation results given by reference [153]	72
Fig. 3. 12, Estimation results given by reference [154]	73
Fig. 4. 1, Concept of magnetic polarity and its saturation effect	77
Fig. 4. 2, The complete modelling system for PMSM	81
Fig. 4. 3, Sketch of the injected pulses.....	82
Fig. 4. 4, The proposed memory structure for picking up the rotor position	82
Fig. 4. 5, Pulse injection in the zero speed “MATLAB” model	83
Fig. 4. 6, Excitation of coils A and B by the first pulse and the freewheeling reaction	84
Fig. 4. 7, Excitation of coils A and C by the second pulse and the freewheeling reaction	85
Fig. 4. 8, The zero-speed voltage measurements of PMSM at rotor positions 45°	86
Fig. 4. 9, Block diagram for voltage comparisons and x-address creation	87
Fig. 4. 10, The stator voltage waveforms and division of rotor space into sectors.....	88
Fig. 4. 11, Two injected pulses and the corresponding current responses	90
Fig. 4. 12, Block diagram for the circuitry of y-address extraction	90
Fig. 4. 13, Block diagram for y-address implementation through voltage response	92

Fig. 4. 14, The readings of current peaks in ZSRPE modelling.....	92
Fig. 4. 15, Modelling the ZSRPE by employing the motor output voltages and current	94
Fig. 4. 16, Modelling the ZSRPE by exploiting only the motor terminal voltages	96
Fig. 4. 17, Saliency effect on voltage oscillation in (a) IPM and SPM (b) SPM	97
Fig. 4. 18, Statistic analysis for the voltage at the terminals of (a) IPMSM (b) SMPMSM	98
Fig. 4. 19, Mathematical “Simulink” model view for rotor position estimation	100
Fig. 4. 20, The injected pulses and the corresponding voltage responses in the modelling system.....	100
Fig. 4. 21, Results of modelling the ZSRPE for (a) IPMSM (b) SM_PMSM	101
Fig. 4. 22, Outputs of the Mathematical model when estimating the rotor position 25°	102
Fig. 5. 1, Block diagram for practical platform of ZSRPE	105
Fig. 5. 2, Pin configurations for the microcontroller “ATmega328”	107
Fig. 5. 3, Basic structure of the 3-ph bridge inverter	108
Fig. 5. 4, PM motor “Ac M2n0320-4/2-3” and its abbreviation code	109
Fig. 5. 5, PM motor “M0200-104-4-000” and its abbreviation code.....	110
Fig. 5. 6, Memory address formatting in ZSRPE practical platform	110
Fig. 5. 7, The practical model injected pulses.....	112
Fig. 5. 8, Implementation of switching elements	113
Fig. 5. 9, Details of the practical platform	114

Fig. 5. 10, Flowchart for the procedure of ZSRPE by the practical platform.....	116
Fig. 5. 11, Injected pulses and waveform responses in ZSRPE practical platform	117
Fig. 5. 12, Graphical representation for obtained ZSRPEs from the practical platform	119
Fig. 5. 13, Estimation errors as difference between the estimated and actual positions	120
Fig. 5. 14, Comparing the estimation results (a) modelling (b) experimental	122
Fig. 6. 1, Overall scheme for modelling the LSRPE with voltage PWM	129
Fig. 6. 2, Modelling scheme for low speed position estimation	130
Fig. 6. 3, Forward path main blocks for LSRPE modelling scheme.....	134
Fig. 6. 4, Variation of the applied torque load in the LSRPE modelling system.....	135
Fig. 6. 5, Feedback path main blocks for LSRPE modelling scheme.....	135
Fig. 6. 6, Structure of the unity peak normalization block.....	137
Fig. 6. 7, Block diagram for speed estimation	139
Fig. 6. 8, Block of combining the zero and low speeds rotor positions	140
Fig. 6. 9, Motor currents, reference currents, and PWM	141
Fig. 6. 10, Waveforms at three output points in the saliency detection block	142
Fig. 6. 11, Input and output of unity peak normalisation block	143
Fig. 6. 12, Outputs of blocks unity peak normalization and position estimation.....	144
Fig. 6. 13, Speed and position estimation curves by LSRPE modelling.....	144
Fig. 6. 14, PMSM output curves by modelling system (at no-load)	145

Fig. 6. 15, PMSM output curves by modelling system (under load test).....	146
Fig. 7. 1, Block diagram for the practical test bed	150
Fig. 7. 2, Functional block diagram for the master controller tasks in practical LSRPE	151
Fig. 7. 3, Micro-computer 2560 (a) chip (b) development board	152
Fig. 7. 4, Sector divisions of the space vector.....	154
Fig. 7. 5, Space vectors representation in complex plane	159
Fig. 7. 6, Sequence of motor winding connections in sector 6	160
Fig. 7. 7, Prohibited regions in SV technique	162
Fig. 7. 8, Standard space vector firing sequence.....	162
Fig. 7. 9, Optocoupler HCPL2531	165
Fig. 7. 10, Principle of bootstrap operation.....	166
Fig. 7. 11, Bootstrap driver type L6338E.....	166
Fig. 7. 12, Schematic for the used in the practical test bed.....	167
Fig. 7. 13, Converting V_a and V_b into V_{ab}	168
Fig. 7. 14, Functional block diagram for the slave micro-controller in LSRPE	169
Fig. 7. 15, Encoder connection in the motor M0200-104-000.....	170
Fig. 7. 16, Encoder rotor position estimation.....	171
Fig. 7. 17, Details of the magnetic brake	172
Fig. 7. 18, Startup strategy	173
Fig. 7. 19, A snap for the practical test bed.....	176

Fig. 7. 20, Real view for master and slave microcontrollers and their peripherals.....	176
Fig. 7. 21, LSRPE for the motor M2n0320 (a) encoder and sensorless (b) saliency track	178
Fig. 7. 22, LSRPE for the motor M2n0320 encoder and sensorless	179
Fig. 7. 23, Error between sensorless and encoder RP estimations for M2n0320.....	179
Fig. 7. 24, LSRPE for motor M0200 encoder and sensorless	180
Fig. 7. 25, Error between sensorless and encoder RP estimations for M0200.....	180
Fig. 7. 26, Start-up currents for the motor M0200	181
Fig. 7. 27, No load currents of the motor M0200	181
Fig. 7. 28, Start-up time for the motors M0200 and M2n0320.....	182
Fig. 7. 29, Harmonics analysis for the practical inverter output by a MATLAB view	183
Fig. 7. 30, Line voltage V_{ab} and PWM switching signals S_A , S_B , and S_C	184
Fig. 7. 31, Variation of the output phase voltage V_{an}	185
Fig. 7. 32, Variation of the output line voltage V_{ab}	185
Fig. 7. 33, Instantaneous torque produced by the motor “M2n0320”	186
Fig. 7. 34, Speed growth of the motor M2n0320 for different modulation index	186
Fig. 7. 35, Speed growth of the motor M0200 for different modulation index	187
Fig. 7. 36, Actual and smoothed speed curves for the motor M2n0320	187
Fig. 7. 37, Speed growth of the motor M0200 for different levels of applied torque. .	188
Fig. 7. 38, Speed growth of the motor M2n0320 for different levels of applied torque	188

Fig. 7. 39, Speed growth of the motor M200 by the microcontroller plotter 189

CHAPTER ONE

INTRODUCTION

1.1 Importance of permanent magnet motors

The application for permanent magnet motors is mainly in field of variable speed ac servo or brushless dc systems. Although the conventional and well-known induction machines are able to achieve this task, the trend is always changes toward the PM motors when a high performance system is demanded, in spite of being these motors of high cost technology. A dedicated digital signal processor (DSP) techniques are required to support the operation of permanent magnet (PM) motors. From this point of view, the PM motors have recently been found in many fields of sensitive industrial applications, such as mechatronics applications, modern transverse vehicles, energy storage drives, compressors of centrifugal principle, ... etc.

1.2 Thesis objectives

As any other rotating motor, the function of permanent magnet motors is to convert the supplied electrical power into revolving mechanical torque. A permanent magnet (PM) is provided to the rotor to replace the rotor windings in producing an effectively strong magnetic field in the motor airgap sufficient to start the rotor spinning action. Accordingly, when this motor is running, a rotating magnetic field emerges in a synchronous speed to that of the field generated by the stator windings. So they have their name as permanent magnetic synchronous motors (PMSMs). They have started as competitive motors in industrial process since the 70s of the last century under the influence of cheap production of magnetic materials and the development in power electronic theories and applications.

Detection of the actual rotor position, with respect to stator windings, has a significant effect on the motor soft running; high performance speed control and torque ripple reduction. The literature review has showed that while the rotor position estimation is well solved at medium and high speeds, the topic is still need more improvements at zero and low speed.

As given in table 5.4, the zero-speed position estimation has verified an angle resolution of 22.5° , according to the impulse response method, while the low speed position estimation has predicted the position with high resolution but it still suffering from the problems of signals filtering and the acoustic noise. Therefore, this thesis aims to raise the resolution of the rotor position estimation of PMSM at zero speed and to verify a new strategy for rotor position estimation at low speed.

To achieve these goals, the thesis works focused on constructing a closed-loop microcontroller based system to achieve the estimation process and to control the operation of permanent magnet machine. The system involves a PC monitoring for the design performance. The thesis goals were primarily satisfied by simulated models based on “MATLAB/Simulink” environment models. Accordingly, real-time controllers were built to achieve an advance estimation for rotor position and, correspondingly, advance control on machine running. The works are designed to be fully sensorless through adopting only the voltage measurements as base to detect the rotor position. Finally, the performance of the proposed and verified controllers were tested practically and modified repeatedly to reach the optimum condition.

The thesis is introduced with two sections, zero-speed and low-speed rotor position estimations. In both sections, the inherent machine magnetic saliency feature was adopted as a base in detection the rotor position. Moreover, the thesis also considers addressing some problems related to operation of PMSM such as filter process and noise.

1.2.1 Zero-speed rotor position estimation

This thesis section aims to implement a high-resolution estimation system to estimate the rotor position of permanent magnet synchronous motors PMSMs at zero-speed condition. To achieve this goal, a system is built based on exploiting the impulse

responses to an injection of high frequency pulses, 3 kHz, into the motor stator windings. The responses are sensorlessly measured at the motor terminals. This section is primarily implemented through simulated models for surface mounted and salient pole permanent magnet motors. Then a practical system is setup depending on a microcontroller, type “ATMega328”. Its duty is limited into achieving three tasks, generating the high frequency pulses, measuring, manipulating and analysing the motor responses and finally displaying and monitoring the estimation progress. Three key points were taken into consideration in implementing the zero-speed rotor position estimations:

- ✓ To reduce the sector gap in rotor position estimation. This means not to determine the rotor location between points x and y where the gap between these two points is wide enough.
- ✓ To adopt only the motor terminal voltage variations, no current measurements contribution. This allows making the proposed approach fully sensorless.
- ✓ To be as cost effective as possible.

1.2.2 Low-speed machine driving and rotor position estimation

In this section, a variable speed drive servo system is built to run two types of surface mounted permanent magnet motors with high performance specifications. The system forward path drives the motors through a sensorless space vector control strategy. The system forward path drives the motors through a proposed method to modulate the space vector. It bases on inserting a virtual voltage, which causes in generating the optimum patterns in the space vector analysis. Whereas, the feedback path includes a sensorless rotor position estimator, which exploits the sinusoidal variations at the motor terminal voltages to calculate the rotor position angle. This system is firstly designated by the aid of mathematical modelling and then simulated by the “MATLAB/Simulink” environment. Accordingly, a practical representation is verified to obtain a real time low-speed implementation.

Advanced control algorithms were employed to meet the high implementation requirements of such systems. Therefore, two high specifications microcontrollers are exploited to effectively manage the controlling process and to achieve data analysis and manipulation. One of the microcontrollers, type “ATMega2560”, controlled the forward

path operations, whereas the other, type “ATmega328”, was employed to manage the feedback path operations. Software programming of the microcontrollers is achieved through the C-language codes. These microcontrollers are effectively exploited to generate the required frequencies and to display and monitor the system performance and rotor position estimation progress in conjunction with a host personal computer.

1.3 Thesis organization

This thesis is organized into eight chapters, in addition to appendices. The organization is explored as follow:

- **Chapter one** introduces an overall introduction for the thesis trends.
- **Chapter two** highlights the types and properties of magnetic materials and how they have been exploited in constructing permanent magnet rotors. Then, a demonstration is presented to the types of PM motors, comparison of the PMSM with other types of motors, PMSM operation methods, effect of rotor position detection on PM motor running, and the power electronic structures, which support the operation of PM motors.
- **Chapter three** gives a detail chronological literature review for the various methods of rotor position estimation. These methods were classified into nine categories and discussed accordingly. In addition, an assessment for the strengths and weaknesses in methods of rotor position estimations is also presented.
- **Chapter four** presents a modelling for the zero-speed rotor position estimation of permanent magnet motors type surface mounted and interior permanent magnet synchronous motors.
- **Chapter five** introduces a practical implementation for the proposed methods which aims to estimate the zero speed estimation for rotor position of permanent magnet motors. The obtained responses and results were compared with the corresponding results of the modelling approaches given in chapter four.
- **Chapter six** presents a modelling for the proposed view of rotor position estimation when the motor is running at low speed. The following points were addressed:
 - The speed stability comparing to the setting speed is investigated.

- The dynamic response, of the under test estimator, in case of sudden change in the input torque is examined.
 - The effect of PID controller parameters on the speed stability, system response and the accuracy of rotor position estimation is investigated.
- **Chapter seven:** A practical experimental bed test is introduced to run the PMSM at low-speed and to estimate its rotor position. This real time work includes a design, based on space vector, and implementing of open loop driving of PMSM as well as to closed loop operation. Both control schemes were controlled through employing of microcontrollers.
- **Chapter eight:** This chapter includes three points, they are:
- Conclusions according to the obtained modelling and practical results.
 - Mention of the verified novelties through this thesis.
 - Suggestions and future works for the expected works, which may represent continuing and improving trends for this thesis works.
- **Appendices:** It includes all the software algorithms to run the microcontrollers, in addition to the necessary data sheets. Pictures for some practical events, which thought to be included, are attached too.

CHAPTER TWO

THEORY OF PERMANENT MAGNET SYNCHRONOUS MOTORS

2.1 Introduction

The rotating Permanent Magnet Synchronous Motors, PMSMs, consist of a stationary part and rotary part, stator and rotor respectively. The stator is exactly similar to that of the induction motor. It includes three set of windings, which are excited by a three-phase ac power supply, through some form of power inverter, to produce a revolving magnetic field. Whereas the rotated part, rotor, composes from a set of permanent magnets rather than bar windings, as it is the case in the induction motors. Mainly, the rotor magnets are either embedded in the rotor structure to create a directive magnetic field, or mounted on the surface of the rotor structure to create a uniformly distributed magnetic field. Figure 2.1 illustrates the comparative basic structures of the PM and the induction motors as given by [1] . Meanwhile, the PMSM is called a synchronous motor because the rotor magnetic poles track the revolving stator magnetic field in a synchronous speed.

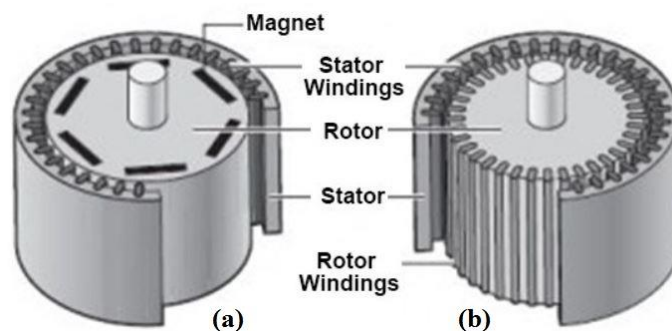


Fig. 2. 1, Basic structure of (a) PM motor (b) Induction motor

To run the PMSMs, its stator windings should be excited by a some form of an inverter, which is always controlled through an electronic system to be fired in a certain

sequence consistent to the instantaneous rotor position [2]. Therefore, the information about rotor position is an essential factor to ensure safe and soft running for these motors. Since the first use of PMSM, the sensor technique has been adopted to determine the rotor position. However, over the past three decades, there has been an increasing attention on sensorless techniques of rotor position estimation due to the noticeable drawbacks of sensor approaches. This has supported the importance of PMSMs. So, significant efforts, in field of machine controlling developments, have been directed toward these motors. Thereby, they become in a competitive situation to induction machines in many field of applications [3].

The reason behind this attention is the distinctive characteristics for PMSMs over the other types of motors, such as compact size, lower power consumption, higher ratio of torque to inertia, and faster performance [4]–[7]. Not only that, but also a significant progress in the reliability of these motors has been achieved through exclusion the sensors and the accessories, which support its operation [8]. Although there are a certain amount of magnetic losses in PM rotor due to the space harmonics, there is a little heat rising up from the rotor as a result of no exciting rotor current is required. Therefore, the motor temperature rising, which almost comes from the stator windings, is readily drawn off through the motor surface without needing to some form of cooling structure, as it is the case in induction motors. The promising result for this cooling ability is the manufacturing of the PMSM with a high ingress protection, IP factor [9].

This chapter is going to be organized into thirteen sections. After the introduction (2.1), the second section (2.2) discusses the PM motor features. Section three (2.3) gives a comparison for PMSM with Brushless Direct Current Motor, BDCM. The main applications of PM machines are explored in section four (2.4), while a historical review for magnetic materials is highlighted in section five (2.5). Sections six (2.6) and seven (2.7) illustrate the types of PM motors, classified according to geometric shape of the rotor, and the machine frame transformations respectively. The various methods of running the PM motors and the impact of rotor position are discussed in section eight (2.8). Section nine (2.9) introduces the various approaches for the rotor position detection. Section ten (2.10) gives a mathematical review for the PM motor equation. Then, the relation between sensorless technique and power electronic developments are

discussed in section eleven (2.11). While section twelve (2.12) gives a short review for the inverter and pulse width modulation.

2.2 Features of permanent magnet motors

The features of PM motors are briefly illustrated through comparing the performance of these motors with the performance of other types. Table 2.1 summarises the features of PM motors through showing the advantages of sensorless PM motors over the other competing types of motors [3][6][10]–[12].

Table 2. 1, Advantages of PM motor over the induction and brush machines

	Advantage	Reason
1	Higher power efficiency	(a) No power loss in rotor. (b) At any moment, only two stator windings may be excited.
2	Smaller size	(a) No sensor and cooling structures are required. (b) No commutator structure is needed.
3	Lower temperature	(a) Due to point 1 (b) Higher heat conductivity by radiating the stator heat through motor outer surface.
4	Higher ingress protection	Due to point 3.
5	Higher speed	(a) No mechanical speed limitations due to the absence of brushes or encoders. (b) The magnet retention at high speeds has been solved.
6	Higher reliability and lower RFI ¹	Less maintenance is required due to the absence of commutator and brushes, which regards the main source of the RFI.
7	Faster response	Due to the lower rotor inertia.
8	Linear speed-torque relation	Due to the closed loop operation of PM motors, which is regulated through a continuous monitoring for the rotor position.
9	Cheaper speed adjust	Due to the presence of electronic controller, which facilitates this issue.
10	Smaller rated power drivers	The lack of magnetizing current in PM motors and their higher efficiency comparing to IM reduce the required drive power.
11	Stator-rotor airgap is not critical factor	In contrast the case in IM, the PM generates a flux which is strong enough to softly avoid the airgap reluctance.
12	Higher Torque/inertia ratio	Due to the very low rotor inertia of PMSM.
13	Less sensitive to airgap width	Due to the influence of the strong magnetic field produced by the permanent magnets.

Whereas, figure 2.2 shows cross-sections to a permanent magnet motor and an induction motor to illustrate the structural differences [1].

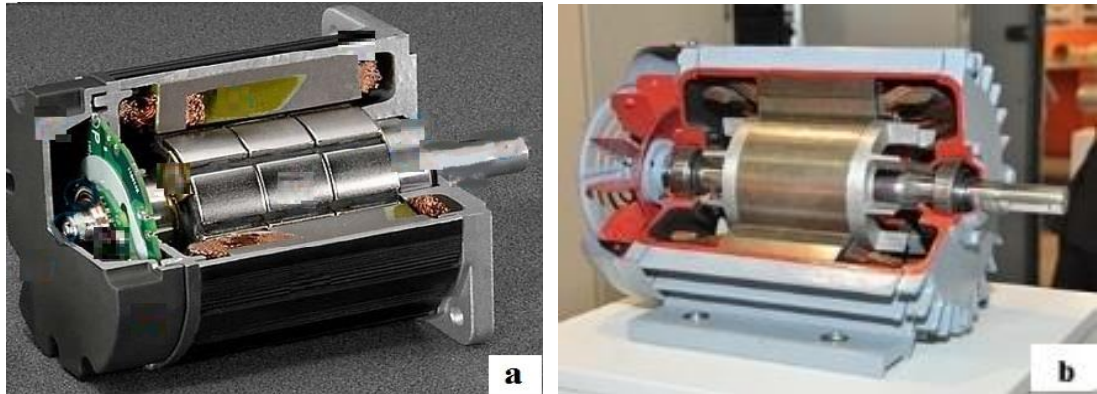


Fig. 2. 2, Cross-section for (a) PMSM (b) induction motor

In addition, figure 2.3 gives a detailed schematic view for the construction of PM motor [9].

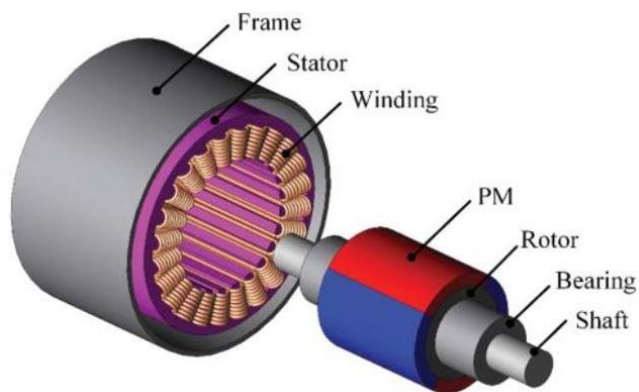


Fig. 2. 3, Schematic view for the construction of PM motor

From other side of view, the induction motor has a lower production cost, lower cogging torque¹, lower encoder cost which is incremental rather than absolute, suitable for higher temperature environment and easier in appliances application, DOL operation [12].

¹ Cogging torque appears due to the interaction between the fields of permanent magnet and stator teeth.

2.3 Comparing PMSM and BDCM

The precision of speed control and the dynamic response are the two criteria which determine the type of PM motors, PMSM or BDCM, to be used for a certain application [12]. The permanent magnet synchronous motors PMSMs and the brushless dc motors BDCMs have the same construction, a stator of three set of windings and a rotor of permanent magnets. In spite of this similarity, they are different by the next fundamental points: [10][12][13]

- The PMSM is more adequate than BDCM in certain application, and vice versa. It relies on the speed control precision and the dynamic requirements for that application.
- The windings of the PMSM stator are sinusoidally distributed while those of the BDCM are of a trapezoidal distribution.
- Accordingly, a sinusoidal source is required to supply the PMSM stator windings, whereas a BDCM is fed from a voltage source of a square waveform.
- Consequently, the induced back EMFs in the PMSM and BDCM are of sinusoidal and trapezoidal forms respectively. This leads to an important consequence which represented by being the PMSM runs softly with a less torque ripple comparing with the BDCM.
- For this reason, the PMSMs have found a wider range of industrial applications.
- The rotor of BDCM is mostly has higher amount of magnet than that of the PMSM.
- If I_{P-PMSM} represents the peak of the sinusoidal current of PMSM, and I_{P-BDCM} represents the corresponding peak of the trapezoidal current of BDCM, then $(I_{P-PMSM}/\sqrt{2})$ and $(\sqrt{2} I_{P-BDCM}/\sqrt{3})$ are the effective currents of both motors PMSM and BDCM respectively.
- If the two machines have equal parameters and core losses, then:

$$(I_{P-PMSM}/\sqrt{2})^2 * R_{ph} = (\sqrt{2} I_{P-BDCM}/\sqrt{3})^2 * R_{ph} \quad \dots (2.1)$$

From which yields:

$$I_{P-BDCM} = 1.15 * I_{P-PMSM} \quad \dots (2.2)$$

- Thereby, the BDCM has approximately 15% output power higher than that of the PMSM under the assumption that they have equal core losses.
- Accordingly, the BDCM possesses 15% torque rate higher than that of the PMSM under the same rated speeds.
- The BDCM drive system is noisier and has lower high-speed efficiency than the PMSM. However, the PMSM inverter electronic circuitry is more complicated than that of the BDCM [14].

2.4 Applications of permanent magnet synchronous motor

For the aforementioned features of the PMSMs, these motors have found many applications in the various branches of modern life. It is possible to summarise these applications as follow:

- In field of domestic appliances, the PMSMs are widely used in washing machines, air-conditioning and refrigerating as ac compressors. Figure 2.4 illustrates an example for the permanent magnet motor PMM in washing machine as given by[15].

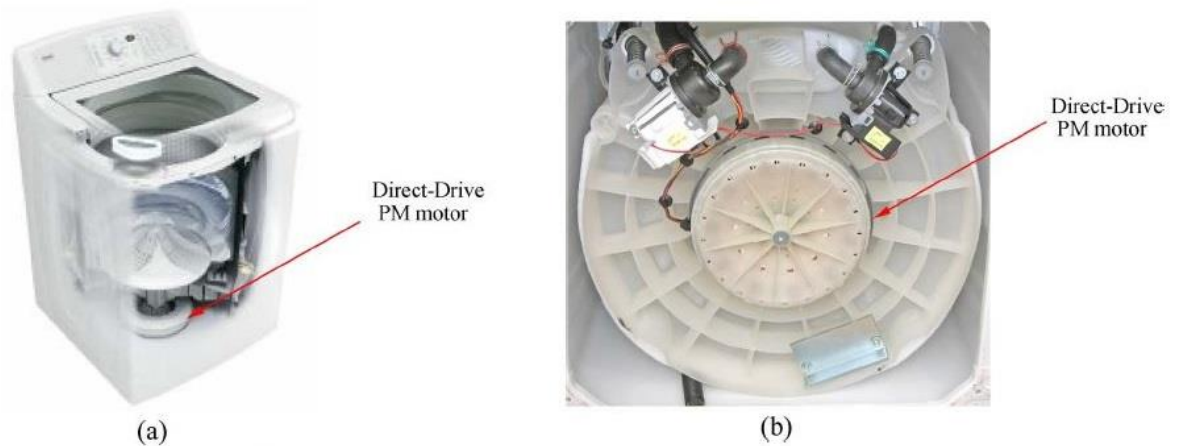


Fig. 2. 4, PMSM in washing machine (a) the application (b) a closer look

- Reference [3] highlighted that, in the manufacturing industry and automated assembly, the PM electric tools have used as alternatives to some hand-held pneumatic products. The main requirement should be available in these PM tools

are the high speed and torque as well as a small diameter. For instant, reference [14] presented such applications, which is shown in figure 2.5. The main considerations in such application are the; lower power consumption, light weight, quite operation and small size. To satisfy these conditions, an integrated motor system was designed. It based on a PMSM with a technology, of effective material density, to combine the machine and the inverter drive [14]. In a relevant application, reference [16] referred to the usage of the PMSMs as hard disc spindles in computer industries.



Fig. 2. 5, PMSM in integrated mobile application

- The automotive and railway manufacturing companies rely on the permanent magnet motors as a prime drive or power steering drive [17] [18] [19]. Figure 2.6 shows a classification for the electric vehicle, EV, drives as given by [20]. This figure highlights the leading position occupied by the permanent magnet drives in this field of application.

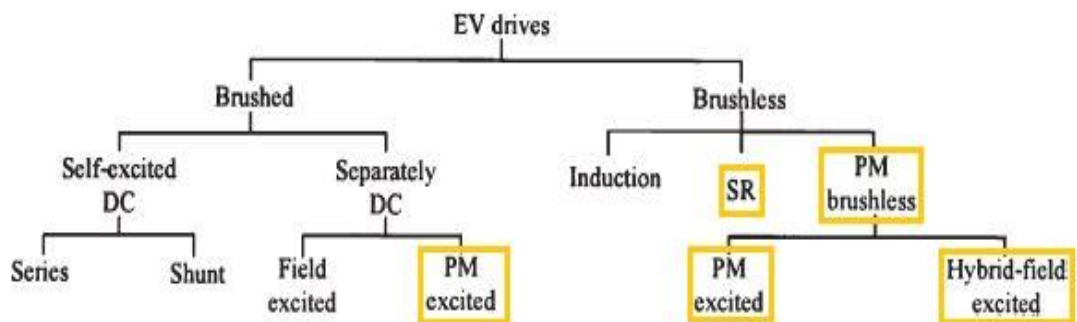


Fig. 2. 6, Classification of the electric vehicle drives

- In field of friendly environment applications, the conventional wind energy generators are classified into; the double fed induction generator DFIG, the induction generator IG and the synchronous generator SG. In the multi-MW wind generation, the synchronous generator is mostly employed to achieve this task. Commonly, the rotor type of this generator, SG, is permanent magnet or rotor windings, depending on the technical and cost considerations [21].
- As an auxiliary power unit in the electric vehicles. Figure 2.7 shows the structure of 9kW, 4200-rpm ferrite magnetic generator for EV application as given by [22].

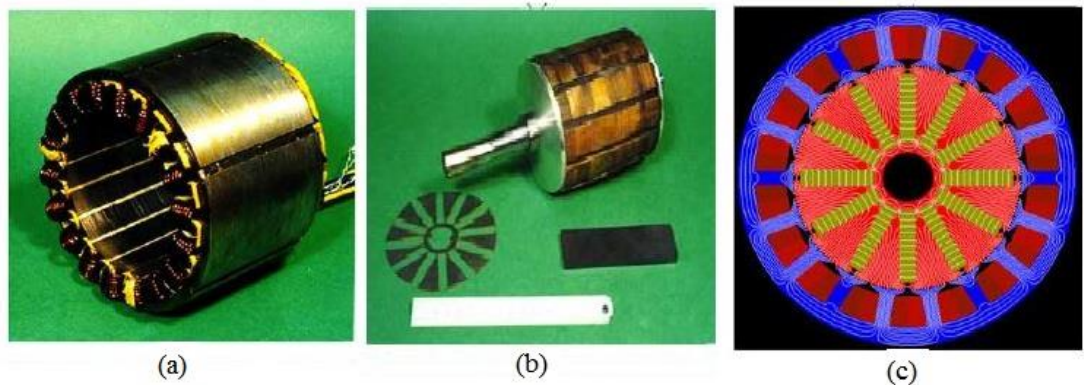


Fig. 2. 7, PM auxiliary generator in EV (a) Stator (b) Rotor (c) Flux distribution

- **Transport applications:** References [23] and [24] presented a practical application for the PM motors in field of boat propulsions, figures 2.8 and 2.9 respectively. This application, whose power range is between 50 and 250 kW, more or less according to passengers' capacity, is especially applied as a propulsion in the river transport for passengers.

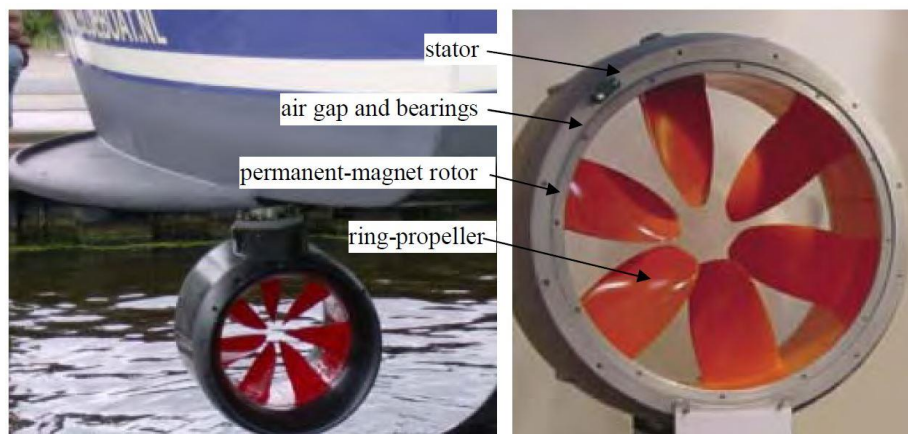


Fig. 2. 8, Application of PM motor as a ship propulsion

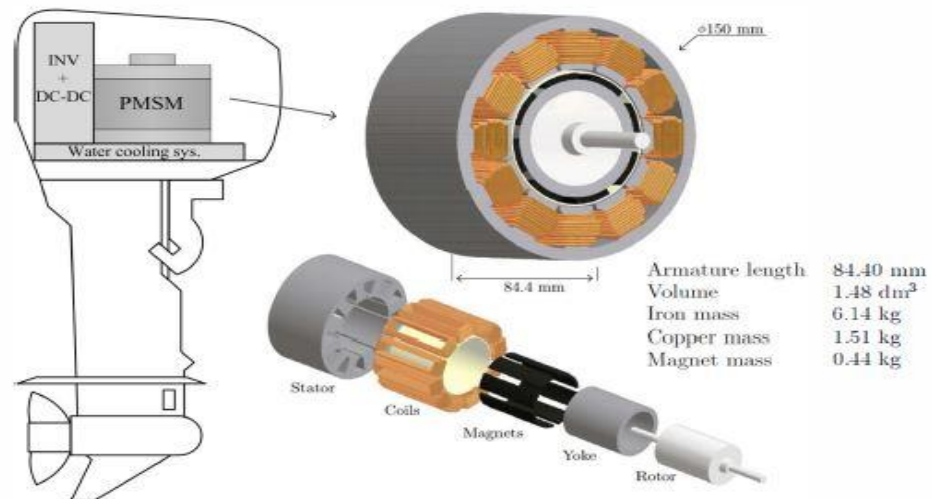


Fig. 2. 9, Sketch for the application of PMSM as a boat propulsion

- Sensitive and accurate applications:** Reference [25] introduced an application for an outer-rotor PMSM whose PM segments are mounted on the rotor surface. This application was developed to be applicable for small size, compact and direct driven centrifugal pumps. This is a sensitive application in field of vehicles fluids pumping systems such as fuel, lubrication, breaking and steering systems. Such application is further applied in aerospace industries and medical device industries. Figure 2.10 (a) presents a schematic for the PMSM in such application as it was given by [25]. Reference [26] presented a micro drill application for PMSM. A micro pipette holder forms the shaft of the drill. Thereby, it houses the injection pipettes for the piercing. Figure 2.10 (b) shows a block diagram for this application as introduced by [26].

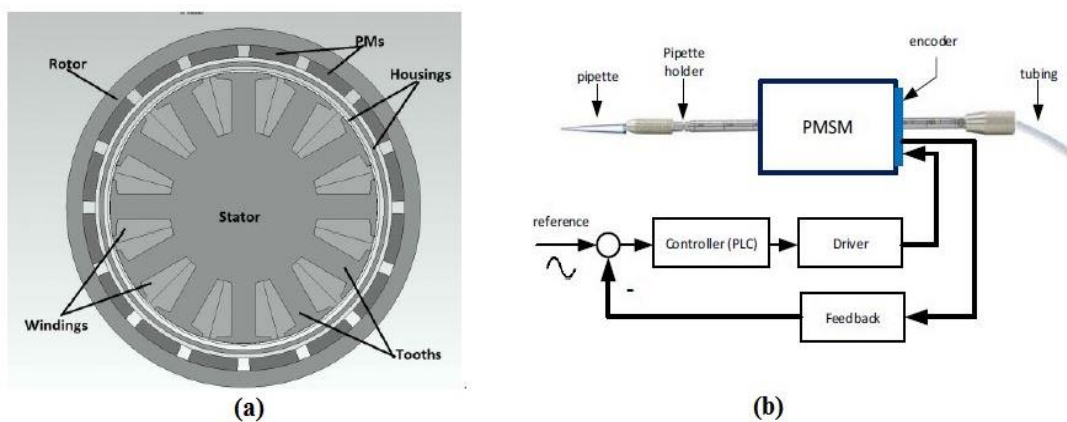


Fig. 2. 10, (a) PMSM topology centrifugal pumps (b) micro drill system

- References [27] presents an application for PMSM as a syringe pump. This pump has found different applications in the medical, gas, oil, and pharmaceutical industries and. Figure 2.11 illustrate the basic concept of the proposed application.

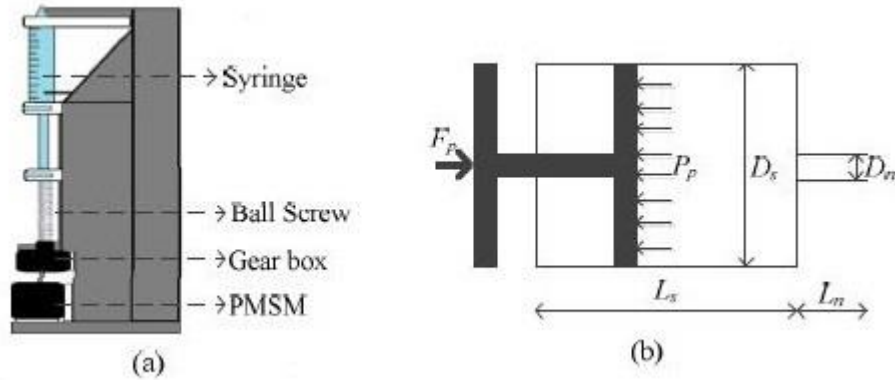


Fig. 2. 11, Application of PMSM on syringe pump (a) a cross-section view (b) the syringe description

Reference [28] discussed the application of PMSM as a propulsion unit in a single pilot paraglider. Figure 2.12 illustrate this application.

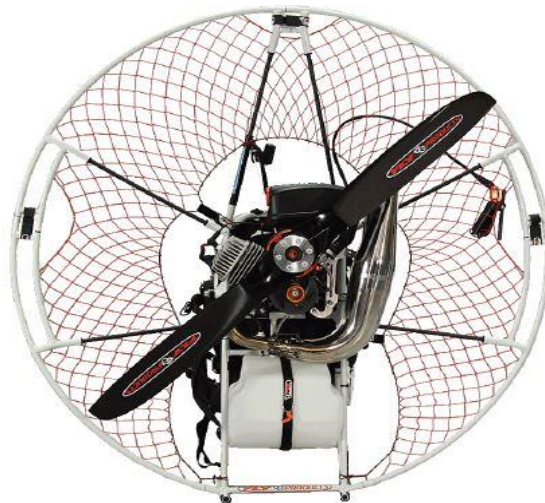


Fig. 2. 12, Application of PMSM on paraglider

2.5 Magnetic materials

The advancement in magnetic material has gradually step up through the years. Each step led to a born of a new magnetic material of new or improved characteristics. The main criterion in determining the improvement is the product of maximum energy product per mass, or volume, unit. Figure 2.13 shows the improvement in the strength of magnetic materials per mass unit. Three different magnetic materials are viewed in this figure, lodestone, ferrite and neodymium iron boron. Each of them carry the same magnetic energy, nearly 0.4J and iron of 70% per mass unit [29].

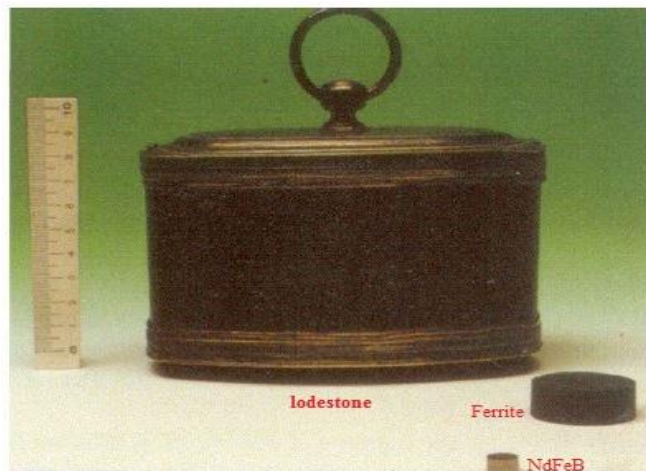


Fig. 2. 13, Comparison the magnetic strength of three different magnetic materials

Whereas Figure 2.14 highlights the developing steps of the magnetic material strengths within the period from 1920 to 2010 as given by [10].

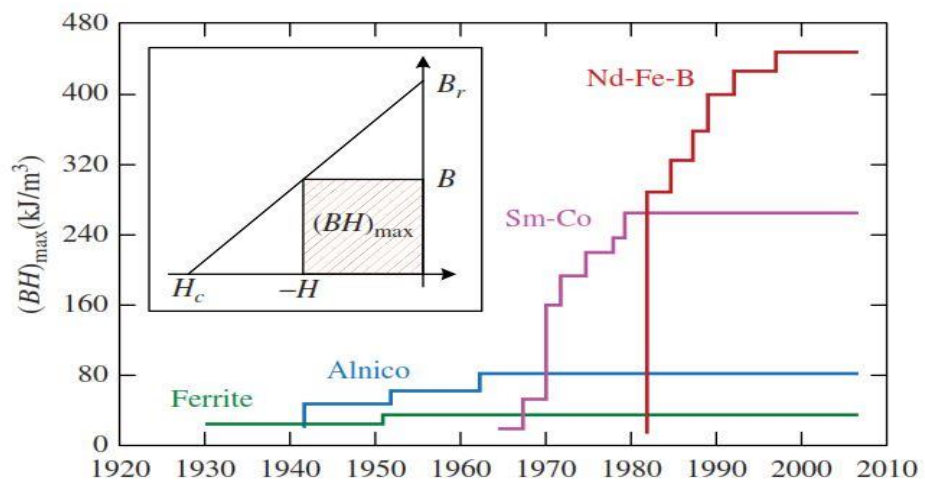


Fig. 2. 14, Developing steps of magnetic materials

The next is a brief historical review for most popular magnetic material and magnetic alloys:

- i. Lodestone: this is a permanent magnet of a weak magnetic field and high resistance to magnetization. It is thought to be the oldest discovered permanent magnets [29].
- ii. Magnetic Carbon Steel: this has a higher level of magnetic properties than the lodestone. It was firstly developed in the eighteenth century. It is always alloyed with other materials to be used in construction purposes [29].
- iii. Alnico Magnet: It is a permanent magnet, which was developed in the twenties of last century to produce a magnetic alloy harder than the magnetic steel [29]. Currently, they still have some applications due to their high Curie temperature², T_C , (more than 800° C).
- iv. Cobalt Platinum Magnet: this was developed in 50s of the last century for a certain mechanical property, high corrosion resistance. Therefore, it is still in use, but in a narrow band of applications, biomedical, because of its high cost of production[29].
- v. Hard Ferrite Magnets: although they have a weak energy, they still have a wide range of practical applications. This is because of the low cost production of these magnets, $BaFe_{12}O_{19}$ or $SrFe_{12}O_{19}$, and their mechanical properties, which permits to use them in forming of complicated shapes.
- vi. SmCo: the SmCo, Samarium Cobalt, is a magnetic alloy, which is formed from cobalt, iron, and rare earth. Since it was first alloyed, together with Alnico during 1960s, they regarded as the highest strength of permanent magnet field. However, the highly relative cost has limited their use [30], [31].
- vii. Neodymium: the first development of this material was in 1982. It came as an economic solution to reduce the high ratio problem of (cost/magnetic strength) which emerged with discovering the samarium magnet. Then, the well-known alloy Neodymium Iron Boron, NdFeB, has been formulated. The high magnetic characteristics of strong magnetic field and demagnetization resistance permitted to exploit this material over a wide range of applications, from the industry field to the mini home domestic appliances [32]. The main drawback for this alloy is the low

² Curie temperature is the environment temperature at which a certain material completely loses its magnetic properties.

Curie temperature, nearly 300° C, which prevents it to be used at high temperature applications [29].

Table 2.2 illustrates the most popular magnetic alloys with a brief idea about their more important magnetic characteristics [33]–[36].

Table 2. 2, Various types of magnetic materials and their properties.

	Energy	Demagnetization	Mech. Strength	Corrosion Res.	Curie Temp.
NdFeB	High	Difficult	Brittle	Low	Low
SmCo	High	Difficult	Low	High	V. Good
Alnico	Different	Easy	Medium	High	Good
Ferrite	High	Difficult	Brittle	High	Good

2.6 Types of the permanent magnet motors (PMMs)

At the end of 1980s, the mass product of new discovered magnetic materials, such as samarium-cobalt magnets and neodymium-iron-boron magnet, have made the manufacturing of permanent magnet rotors cheaper and more reliable [9], [10]. This has enhanced the opportunities of PMSMs to be hard competitive in many appliances [11]. Moreover, the sharp decrease in the cost of magnet materials during the past three decades beside the lower cost of sensorless techniques comparing to sensors types, have increased the demand on the PM machines [12].

In structure of permanent magnet brushless machines, the PM materials represent the essential part because they provide these machines by a continuous magnetic field. There are different magnetic materials in nature and different industrial magnetic alloys, which are manufactured to enhance the mechanical properties of pure magnetic materials. Those alloys are used to product the magnetic rotors of PMSMs in various shapes. Accordingly, the PMSMs can be categorised according to the used alloy and the rotor geometric shape. However, the more commonly used geometric shapes of permanent magnet rotors are classified as given below:

2.6.1 Interior permanent magnet synchronous motor (Salient-Pole)

It stands for Interior, buried or embedded, Permanent Magnet Synchronous Motor. Figure 2.15 shows a schematic view for the main two configurations of inserting permanent magnets into the rotor structure. Considering the fact that the permeability of permanent magnet can be omitted comparing to that of the stator iron, and according to the field distribution in this type of motors, it can be deduced that the IPM has the capability of high torque production. This is because the q-axis inductance, L_q , becomes much higher than the d-axis inductance, L_d , in the rotor reference frame. Consequently, the magnetic path inductance, d-axis, through the permanent magnet will be very small, the inductance ratio L_q/L_d will be very high, and the spatial saliency will be very high too. Accordingly, there will be a growing torque called the saliency torque, which act as reinforcing torque to the flux torque. Mathematically, this can be expressed by the following equation [37]–[39].

$$T = \frac{3}{2}p \{ (L_q - L_d)I_q I_d + \lambda_m I_q \} \quad (2.3)$$

where the first term in the sum between the brackets, represents the saliency torque and the second term is the flux term. As it is clear, the saliency torque is proportional to the difference between L_q and L_d .

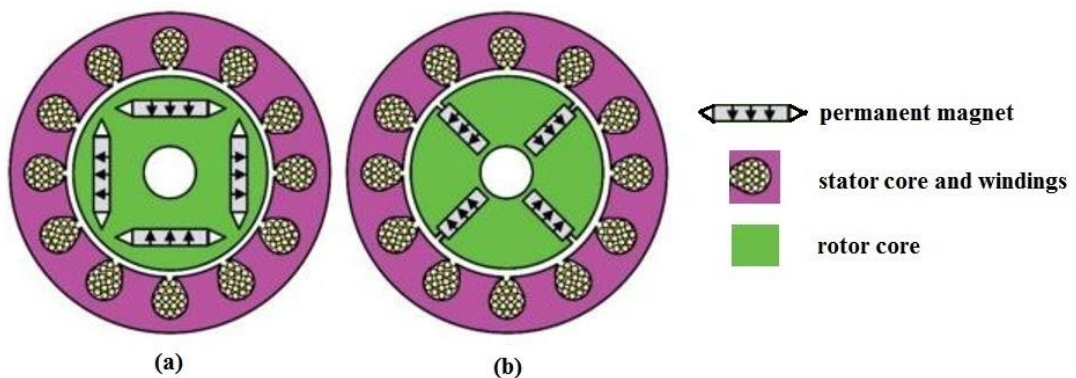


Fig. 2. 15, Interior configurations of PM (a) interior- circumferential (b) interior- radial

2.6.2 SM-PMSM (Non-salient pole)

It stands for a Surface Mounted Permanent Magnet Synchronous Motor. Figure 2.16 shows a schematic view for the main two configurations to mount the permanent

magnets on the rotor body. These configurations yield a uniform circular rotor construction, which make its reluctance equal in all directions. Thereby, in contrast the IPMSM, the surface mounted magnetics motor has a uniform magnetic field distribution. Accordingly, the inductances L_q and L_d are approximately equal. This leads to a low spatial saliency and a very close to unity inductance ratio. Consequently, the estimation of rotor position at low and zero speed becomes more difficult in SM-PMSMs [40].

Moreover, the SM-PMSM has a lower torque and speed performances than the IPMSM. The SM-PMSM resultant torque is lower than that of IPMSM due to the absence of the saliency torque term from the torque equation given in (2.3). This means that the electromagnetic torque is only the effective torque in this type of motors. Meanwhile, the SM-PMSM has a lower speed range, comparing with the IPM. Firstly, the buried magnets inside the IPM rotor steel structure comparing with the fixed magnets on the SM-PMSM rotor surface, by means of epoxy glue, make the former more reliable at high-speed applications than the latter. However, manufacturing of buried permanent magnets rotor is more complicated than that of surface mounted which reflects on the production cost to tend to benefit of the latter [10], [12].

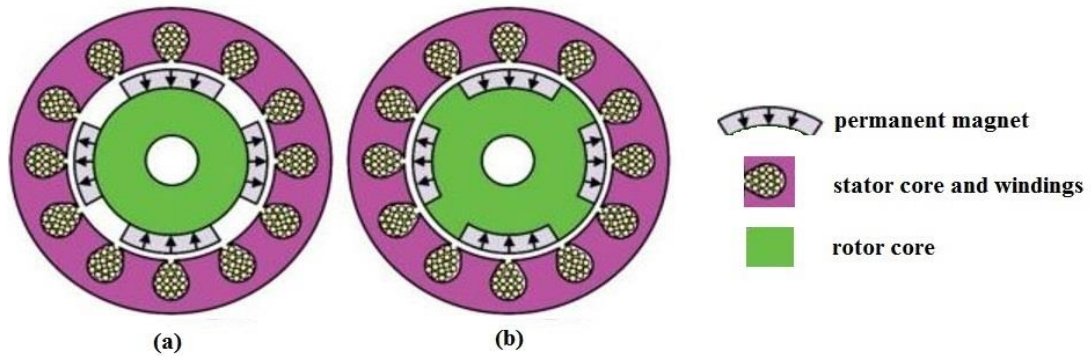


Fig. 2. 16, Surface configurations of PM (a) surface-mounted (b) surface-inserted

2.6.3 CPM

It stands for Claw Permanent Magnet. This type of rotors is usually constructed in form of three disks, which are fixed with 120° space angle between each other. The CPM is similar to SMPM by having a low inductance ratio. It is mainly useful when a production of a cheap motor by using ferrite magnet is required. In this case a rotor flux concentration has to be used, and the CPM is one of the solutions [41]. Figure 2.17 (a)

shows a schematic for one disc of the rotor discs as given by [41], whereas figures 2.17 (b) and (c) are schematic to illustrate fixing of the claw pole and a picture for a real claw pole rotor, respectively, as given by [42].

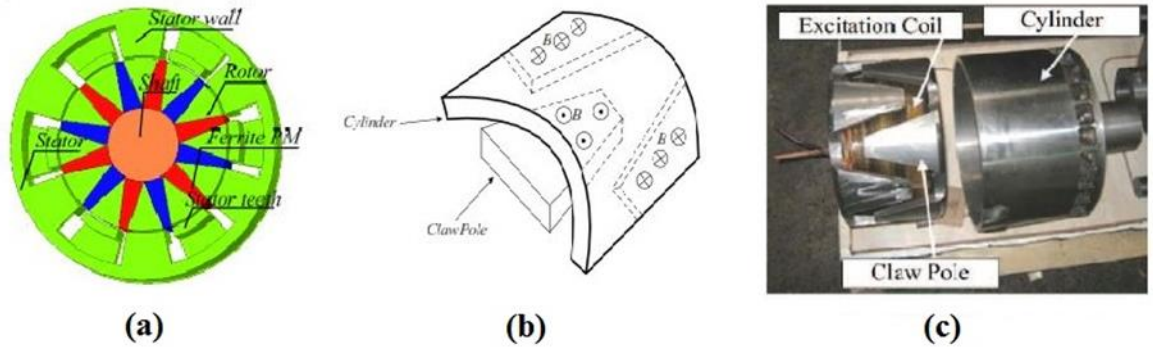


Fig. 2.17, Claw pole PMSM (a) schematic of one disc (b) positioning the claw pole (c) real claw rotor

2.6.4 Spoke FMM

It stands for Spoke Ferrite Magnet Motor. The rotor consists of ferrite magnets in trapezoidal forms. Thereby, a flux linkage is suppressed in the rotor spatial space to produce a strong magnetic field. The employment of ferrite has come to overcome the cost of rare-earth magnet in manufacturing the electric vehicle drives [43],[44]. Figure 2.18 shows the basic structure of the spoke FMM as given by [44].

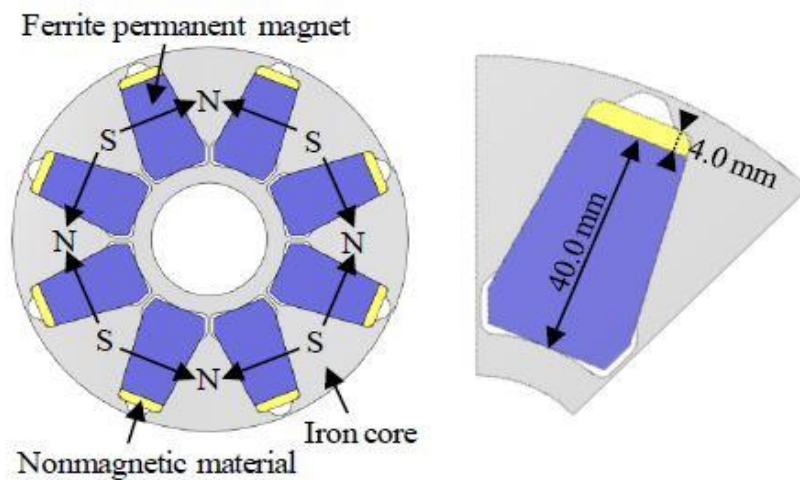


Fig. 2.18, Basic structure of spoke FMM

2.6.5 VIPM

It stands for V-shape Interior Permanent Magnet. It is similar to IPMSM but the magnet inside the rotor core is formed in V letter shape so as to maximise the rotor ferrite magnetic flux [45] [46]. Figure 2.19 illustrates a schematic drawing for a 3-phase (A, B, C) IPMSM whose stator has 18 slots and rotor has 16 V-shape magnetic segments as given by reference [46].

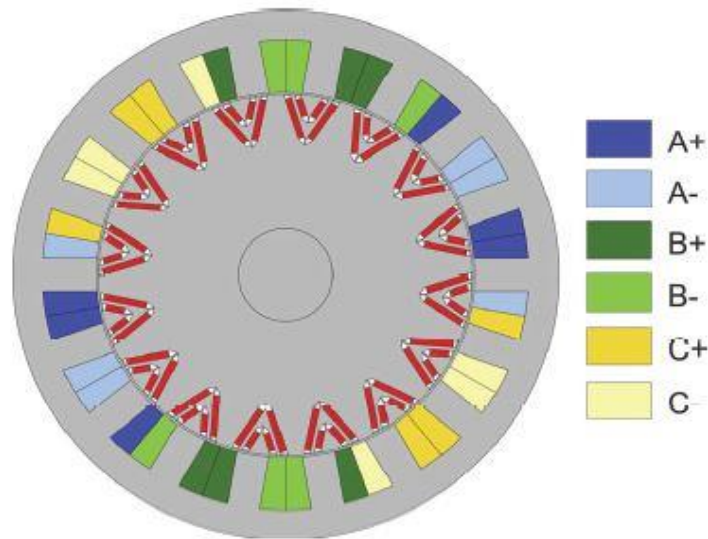


Fig. 2. 19, V-shape rotor in an 18/16 PMSM

2.7 Electrical machine frame transformations

In electrical machine theory, the properties of a 3-phase machine are always described by the stator voltage and current differential equations. The self and mutual inductances of the stator windings are significant terms in those equations. In PMSMs, the inductances are variant with rotor position, this makes the coefficients of machine equation dependent variables. Therefore, the coefficients become difficult to be directly used in machine analysis. To overcome this obstacle, the stator and rotor variables are transformed from one reference frame to another, stationary and rotary reference frames.

Clarke and Park transformations are employed to perform these transformations. Thereby, when the machine equations are transformed from the stator , stationary reference frame, to the rotor, rotary reference frame, the coefficients will be regarded as

constants with respect to rotor position. Moreover, these stationary and rotary frames have only two variables. Therefore, they will facilitate the machine analysis, where they permit to analysis the machine as two variables problem instead of three variables [10].

Figure 2.20 shows the transformation of the stator vectors into the stationary reference frame. Clarke introduced this transformation concept by which the three variables in the 3-phase stator frame are transformed into a stationary reference frame, which consists of two orthogonal vectors α , and β [10] [47]. The α -axis should in same direction with (a) winding current, I_a .

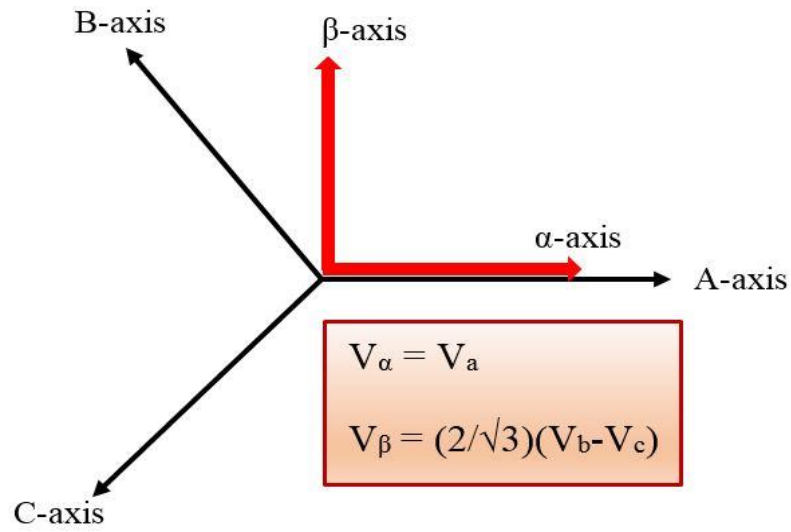


Fig. 2. 20, Clarke's transformations of stator voltages (V_a, V_b and V_c) to the stationary reference frame (V_{α} and V_{β})

By adding a third null vector to the formula of Clarke transformation, it becomes a reversible transformation formula to transform any quantity of three dimensions (f_{abc}) into two dimensions ($f_{\alpha\beta 0}$) through a conversion matrix (T_{Clarke}), as follow:

$$f_{\alpha\beta 0} = T_{Clarke} X f_{abc} \quad (2. 4)$$

$$T_{Clarke} = \begin{bmatrix} 1 & -0.5 & -0.5 \\ 0 & 0.866 & -0.866 \\ 0.5 & 0.5 & 0.5 \end{bmatrix} \quad (2. 5)$$

Inversely, it is possible to transform from two dimensions to three dimensions quantities through the inverse Clarke matrix (T_{Clarke}^{-1}), as follow:

$$f_{abc} = (T_{Clarke})^{-1} X f_{\alpha\beta 0} \quad (2.6)$$

$$(T_{Clarke})^{-1} = \begin{bmatrix} 1 & 0 & 1 \\ -0.5 & 0.866 & 1 \\ -0.5 & -0.866 & 1 \end{bmatrix} \quad (2.7)$$

Whereas, Park proposed to exploit Clarke stationary reference frame to transform the stator variables to the rotor, rotor reference frame. So, they are formulated by two orthogonal vectors, the direct d-axis and the quadrature q-axis. Thereby, Park transformations are used to control the relation between the stator winding current vectors and the rotor flux vector without the effect of rotor position on the winding inductances. This is because all the variables, with respect to rotor, will be observed as constants. Figure 2.21 illustrates the three stator voltages are represented in a space vector by two revolving quadrature vectors d and q [10] [47]. The d-axis vector should be in direction with the rotor field vector.

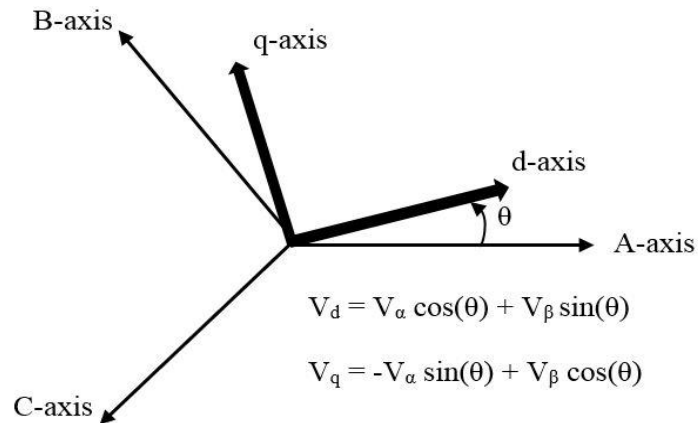


Fig. 2. 21, Park's transformations of stator voltages (V_a , V_b and V_c) to the rotary reference frame (V_d and V_q)

So, Park's transformation from the stator frame to the rotor reference frame, through Clarke transformations, is illustrated as following:

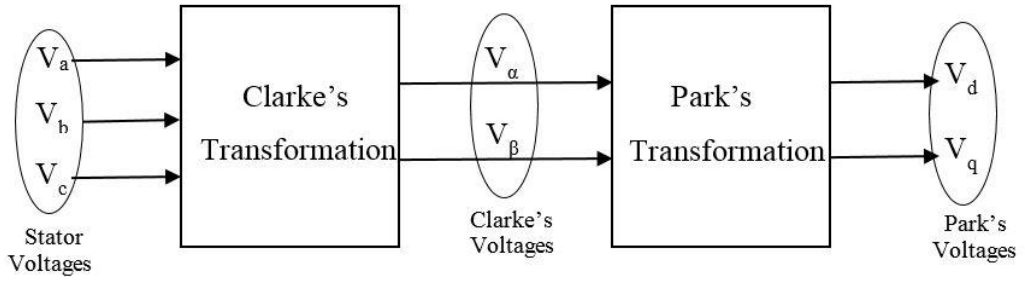


Fig. 2. 22, Park's transformations through Clarke's transformations

In figure 2.22, a formula is derived to express directly the stator variables into the rotary reference frame. This formula is given by:

$$\begin{bmatrix} V_d \\ V_q \end{bmatrix} = \frac{2}{3} \begin{bmatrix} \cos(\theta) & \cos(\theta - 120) & \cos(\theta + 120) \\ \sin(\theta) & \sin(\theta - 120) & \sin(\theta + 120) \end{bmatrix} \begin{bmatrix} V_a \\ V_b \\ V_c \end{bmatrix} \quad (2. 8)$$

In addition, to return back to the stator variables, the inverse Park's transformation is given by:

$$\begin{bmatrix} V_a \\ V_b \\ V_c \end{bmatrix} = \begin{bmatrix} \cos(\theta) & \sin(\theta) \\ \cos(\theta - 120) & \sin(\theta - 120) \\ \cos(\theta + 120) & \sin(\theta + 120) \end{bmatrix} \begin{bmatrix} V_d \\ V_q \end{bmatrix} \quad (2. 9)$$

Thereby, the machine parameters, flux, currents and voltages, are expressed either on the stator side or on the rotor side depending upon the machine analysis requirements.

2.8 Operation of PMSM and importance of rotor position

The stator windings of PMSMs are distributed in a certain manner, which is suitable to produce a sinusoidal flux shape within the motor air gap and correspondingly a sinusoidal back EMF [12]. This makes it having a higher response to sinusoidal supply voltages and more close to the stator structure of the alternating current induction machines ACIMs. From another side of view, the rotor of PMSM is self-magnetic field production due to the presence of the permanent magnet materials, which enable the motor to dispense the rotor induced current in producing the rotor magnetic field. Thereby, the PMSM is similar to the rotor structure of the brushless direct current motors BLDCMs. Accordingly, it may be possible to mention that the PMSM is sharing both ACIM and BLDCM their properties [33].

Principle of operation of PMSMs bases on generating a stator revolving magnetic field which should be synchronous with the direction of the rotor field. To achieve this topic, the stator windings should be energized by a proper sequence related to the rotor angle. So, the prior prediction of the PMSM rotor position plays a crucial role to ensure optimal soft running, torque maximizing, torque ripple minimizing and preventing the reverse start up. Moreover, the knowledge of rotor information enhances the opportunity of a perfect and dynamic torque control of permanent magnet synchronous machine PMSM. The instantaneous value of the rotor angle is either obtained by the mathematical integration of the rotor angular speed, or by a some form of sensor technique [47]. The currently adopted methods in rotor position detection will be discussed in detail through the next paragraphs.

In contrast to some of induction motor applications, fixed speed, the PMSM is not directly supplied from an ac source, but is supplied through a DC to AC inverter. This is to be able to run the machine within servo system. Two main strategies are used in controlling the inverter power flow; the voltage control strategy, VCI, and the current control strategy, CCI. Choosing one of these strategies to drive a certain PMSM is depending on the required performance of that PMSM or its application [47] [48]. The inverter elements are driven by pulse width modulated signals, PWM. Three main techniques are currently in use to perform the PWM; the sine wave PWM, SPWM, the third harmonic PWM, TRIPWM and the space vector PWM, SVPWM.

Currently, several methods are mainly used to control the running of PMSMs through controlling the stator field production. The most popular methods, according to their wide application, are the: field oriented control, FOC; speed control; direct torque control; nonlinear control; sensorless control [10]. These methods are briefly reviewed below.

2.8.1 Field Oriented Control (FOC)

The FOC [49], [50], which is also called vector control, has led to increase the ac machines torque response. It was firstly proposed in the 60s decade of last century as a method to drive the ac machines. The concept of FOC bases on controlling the rotary reference frame currents I_d and I_q to achieve maximum torque by minimum current, i.e.,

minimum torque to current ration, Maximum Torque Per Ampere MTPA. To clarify the concept, FOC, let us consider a 3-ph PMSM rotates at electrical speed ω_r when it is supplied with a stator vector current I_s . The stator vector current has an angle θ with the rotor permanent field direction. Then the motor three phase currents can be written as:

$$\begin{aligned} i_a &= I_s \sin(\omega_r t + \theta) \\ i_b &= I_s \sin\left(\omega_r t + \theta - \frac{2\pi}{3}\right) \\ i_c &= I_s \sin\left(\omega_r t + \theta + \frac{2\pi}{3}\right) \end{aligned} \quad (2. 10)$$

Transferring the stator currents to the rotor reference frame, Park transformations, produces the rotor currents i_d and i_q which are expressed by:

$$\begin{bmatrix} I_d \\ I_q \end{bmatrix} = I_s \begin{bmatrix} \cos(\theta) \\ \sin(\theta) \end{bmatrix} \quad (2. 11)$$

In this equation, as the stator vector current has a constant value and a constant angle with the rotor field, so I_d and I_q are correspondingly constants. This inherent feature of PMSM makes it operates in a manner similar to that of dc motor. The i_d current is equivalent to the dc motor field current whereas i_q is equivalent to the armature current. From this side of view, it is said that the PMSM possesses faster torque response as that of the dc motor. So, the PMSM electromagnetic torque is given by:

$$T_e = \frac{3}{2}p \left\{ \frac{1}{2}(L_q - L_d)I_s^2 \sin(2\theta) + \lambda_m i_q \right\} \quad (2. 12)$$

A constant torque control strategy is derived from the field oriented control, where the maximum possible torque is desired at all times like the case in the dc motor. As the magnetic field is permanently produced by the permanent magnet, consequently the field current i_d is no longer required. This permits to produce a torque current i_q equal to the supply current I_s while i_d is zero. To achieve this topic, the FOC system should work under the θ angle equals to 90° . By making the i_d current equal to zero, the term of saliency difference ($L_d - L_q$) in the electromagnetic torque equation (2.12) is eliminated and the equation is reduced to:

$$(T_e)_{FOC} = \frac{3}{2}p \lambda_m i_q \quad (2. 13)$$

From this equation, it can be concluded that the torque produced by the FOC is quite similar to that of a SM-PMSM. So the FOC is simply implemented in this motor by setting the direct current I_d to zero.

2.8.2 Direct Torque Control (DTC)

This method is based on the direct selection of a stator voltage vector depending on the comparison between actual and reference values for the stator flux linkage and electromagnetic torque. The comparison results are used to access a lookup table which is established to organize the firing voltage vectors of the inverter [10], [51]. So, the inverter switches are directly turned ON or OFF according to the calculated values of stator flux and torque. Reference [51] mentioned that DTC method is preferred in many applications being robust toward parameters changes and has a fast torque response.

2.8.3 Speed Control

This method is verified through employing a speed error signal to maintain the motor speed at a pre-set value, reference speed. Therefore, the reference speed, in the forward path, is compared with the actual motor speed, which should be measured through the feedback path, to obtain an error speed signal. The error signal is manipulated by proportional-integrator, PI, to produce quadrature reference current, I_{q-ref} . This current is either directly used to control the motor output speed or matched with a torque control scheme to control both outputs speed and torque [10]. Figure 2.23 shows an outline for the basic verification of speed control.

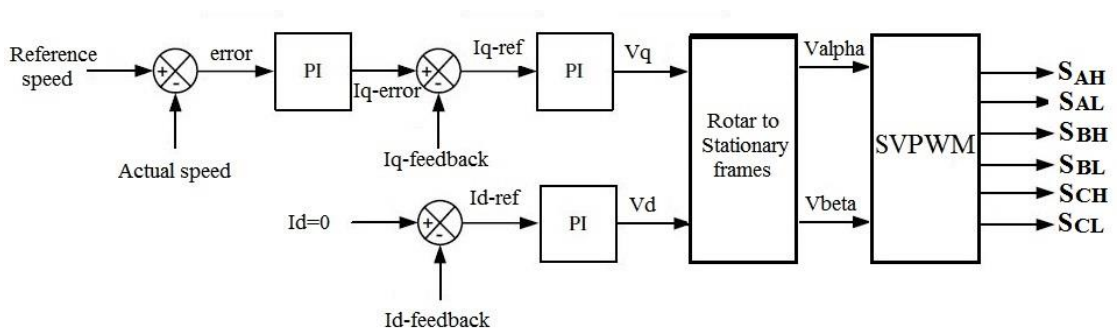


Fig. 2. 23, Speed control scheme with FOC

2.8.4 Non-linear Control

In running the PMSM, the linear strategies have found to be inefficient for the cases of accurate controlling of speed and high performance torque strategy. Reference [52] mentioned that the control engineers, who are interesting in non-linear control, have determined some points of weakness in linear control approaches. First, is the nonlinearity in relation between rotor speed information and the stator winding currents. Next, is the nonlinearity in the torque equation terms. Finally, the aforementioned factors have negative effect on the driving system linearity and it becomes harder when the rotor magnets are at position of field-weakening which leads to make I_d negative value. Consequently, this situation has a high drawback on the main torque assumption based on $I_d=0$.

In contrast, the nonlinear technique has shown more reliability in addressing the nonlinearity of the PM motors [52]. It was confirmed that the PMSM nonlinearity occurs because the motor stator currents has nonlinear relation with the rotor speed [53]. The theory of nonlinear method is based on controlling the motor operation through creating a feedback loop to vary the quadratic component, i_q , of the SM-PMSM stator currents, or both direct and quadratic currents, i_d and i_q respectively, in case of IPMSM [54]. Figure 2. 24 demonstrates a block diagram for a proposed IPMSM nonlinear operation control as given by reference [55].

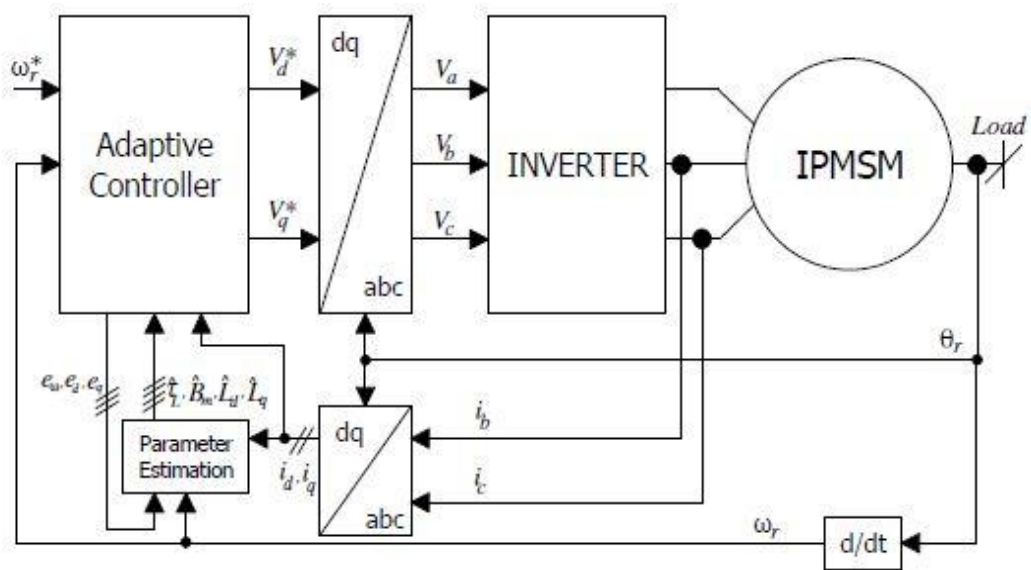


Fig. 2. 24, Scheme for nonlinear IPMSM control

2.8.5 Sensorless Control

To implement this controlling approach, the stationary reference frame voltages vectors, V_α and V_β , should be provided through a sensorless technique. Then, the estimation of rotor position angle, θ , is achieved by employing the orthogonal relation between V_α and V_β vectors of the voltage stationary reference frame [10]:

$$\theta = \arctan\left(\frac{V_\beta}{V_\alpha}\right) \quad (2.14)$$

Whereas the produced torque is calculated from the relation:

$$T_e = \frac{i_\alpha V_\alpha + i_\beta V_\beta}{\omega_r} \quad (2.15)$$

2.9 Methods of detecting the rotor position angle

Two main methods are adopted in detection of the rotor position of PMSM. They are the direct position-detection method, which is based on a position sensor, and the indirect position-detection method, which is based on a sensorless approach.

2.9.1 Direct position-detection

This method bases on using some form of a physical sensor to sense the rotor position. Basically and according to the principle of operation, there are four types of these sensors; the electromagnetic, the photoelectric, the magnetic sensors and the electrical (resolver). Figure 2.25 shows images for these types. Although this method has a higher accuracy in detection the rotor position, it includes few drawbacks, which make it not preferable in many applications. These drawbacks are summarized by; it has more system size, more wiring extensions, lower reliability under some environmental conditions, noisy operation and higher production cost [56].

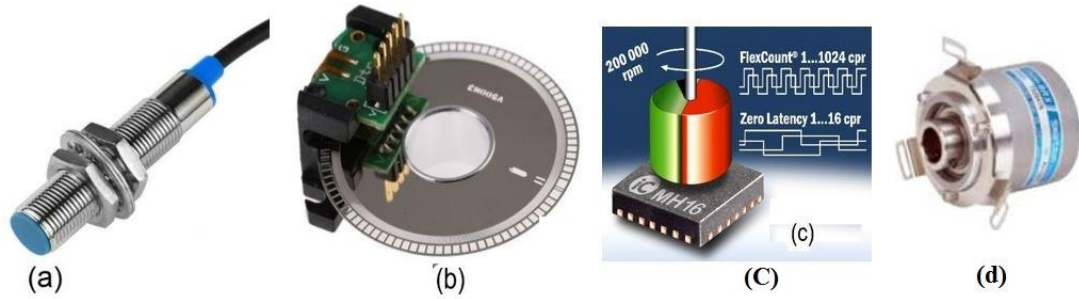


Fig. 2. 25, The rotor position sensors (a) electromagnetic (b) photoelectric (c) magnetic (d) electrical

2.9.2 Indirect position-detection

By this method, the motor terminal voltages and currents are sensed and an algorithm is used to extract the embedded data from which the rotor position can be estimated. So, this method is always called the sensorless technique in rotor position estimation. The estimation concept differs depending on the speed of rotor. Figure 2.26 shows a chart to illustrate a classification to the various types of sensorless estimation [57].

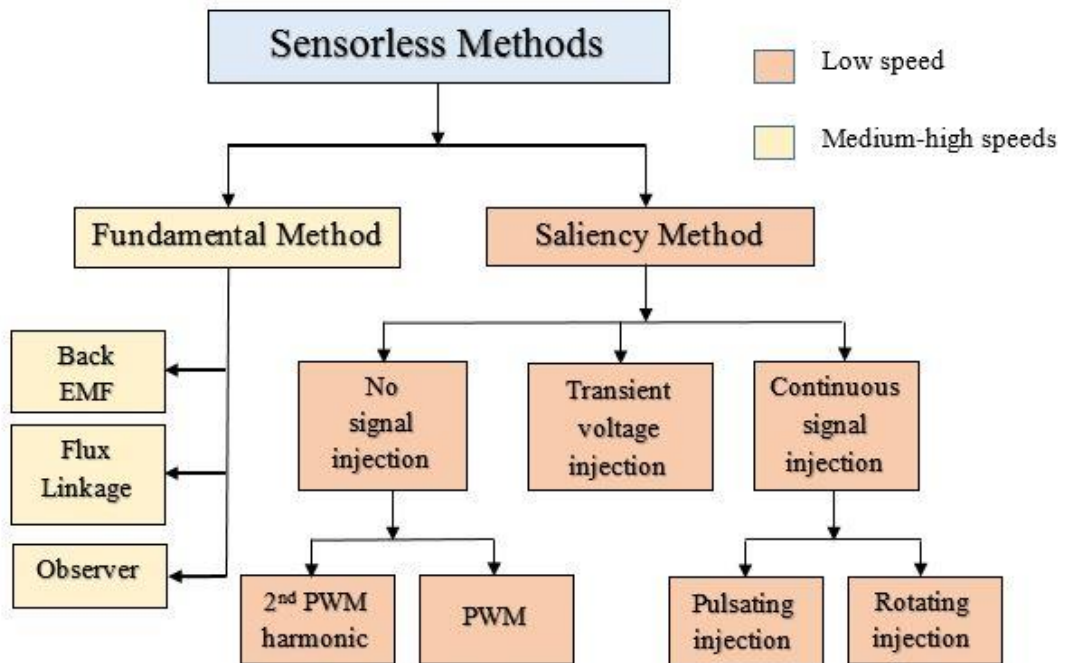


Fig. 2. 26, Methods of sensorless rotor position estimation

2.10 PMSM equations

Figure 2.27 shows the equivalent structure of a PMSM which is driven via a PWM excited inverter in a servo system. In addition to PM rotor, the construction of PMSM includes three stator windings, denoted A, B and C, connected in a star connection. Each winding is made of a number of copper turns (N_s). The internal resistances of the copper windings are shown in the figure as r_A , r_B and r_C , whereas L_A , L_B and L_C refer to the corresponding coil self-inductances. The stator windings are located at 120° from each other and they are assumed to be sinusoidally distributed in the stator slots.

The stator windings are electrically excited by the currents i_A , i_B and i_C which are fed by the inverter outputs. Meanwhile, the windings are magnetically excited by the magnetic flux of the rotor permanent magnet (λ_m). In this configuration, a mutual inductance between each winding-pair emerges added in series with the self-inductance of the corresponding winding. For instance, L_{mB} refers to the mutual inductance, which is added to phase B winding, under the influence of the other two phases A and C. When the motor is spinning, the induced back electromagnetic forces, EMF, in each phase are denoted e_A , e_B and e_C .

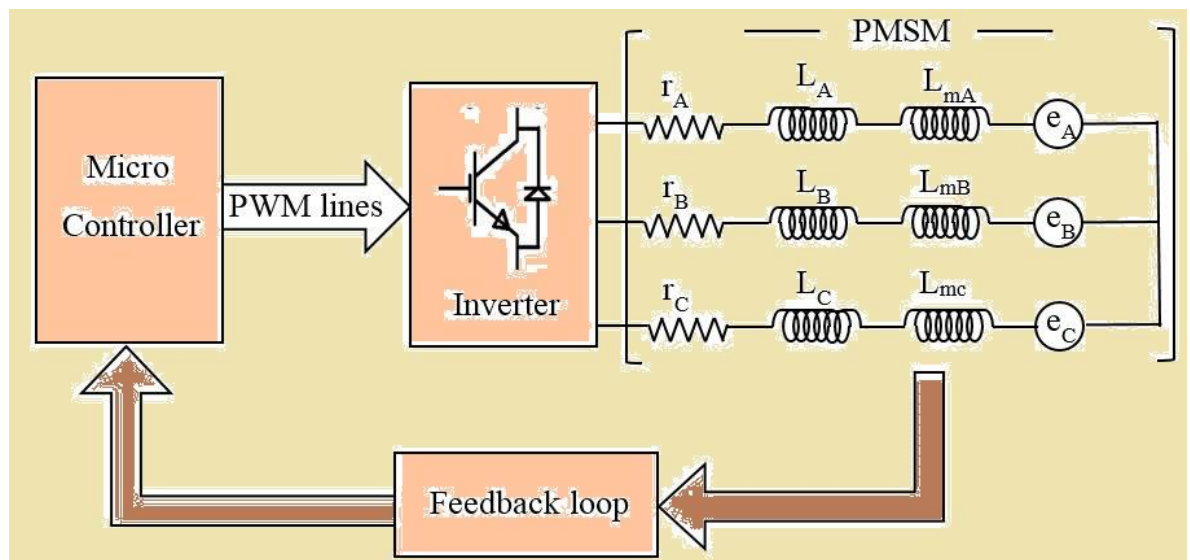


Fig. 2. 27, Basic structure for PMSM servo system

To simplify the analysis of ac machines, the Clarke-Park transformations are employed. Figure 2.28 shows the vector representation of a 3-phase PMSM in the rotor reference frame by means of Park transformations.

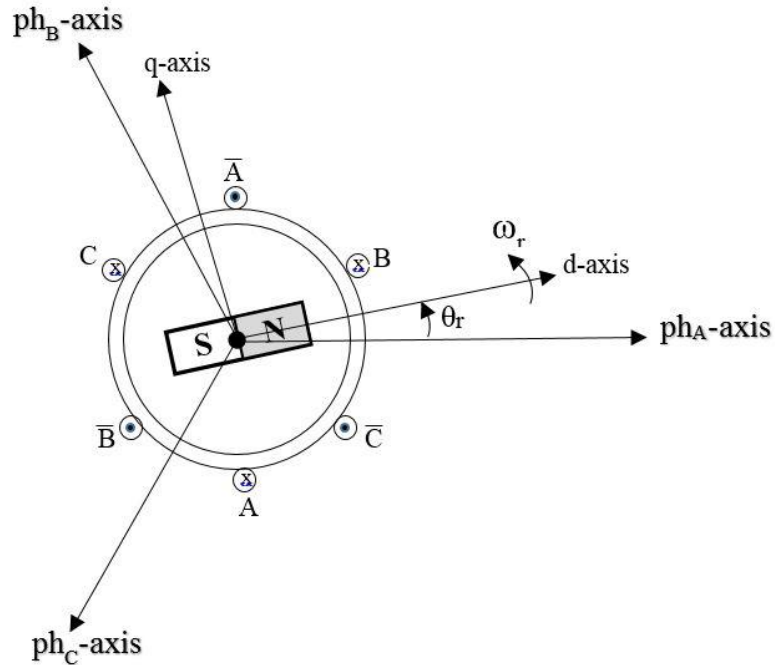


Fig. 2. 28, Vector representation for PMSM in rotor reference frame

According to these transformations, the three stator voltages, or currents, are represented in figure 2.28 by two vectors, d and q axes, which are to be exploited by the digital controller as a base to modulate the PWM signals. Moreover, they have an important contribution in deriving the basic equations of the PMSMs. The d-axis is always aligned with the rotor magnetic axis, whereas the q-axis is 90° ahead in the direction of rotation, which is assumed to be counter-clockwise. Both axes rotate at an angular speed ω_r with respect to the stator stationary reference frame.

Refer to figure 2.27, the voltage equation for each stator phase is rewritten as:

$$v_{sa} = i_a r_A + (L_A + L_{mA}) \frac{di_{sa}}{dt} + \omega_e \lambda_m \cos(\theta_e) \quad (2. 16)$$

$$v_{sb} = i_b r_B + (L_B + L_{mB}) \frac{di_{sb}}{dt} + \omega_e \lambda_m \cos(\theta_e - 2\pi/3) \quad (2. 17)$$

$$v_{sc} = i_c r_C + (L_C + L_{mC}) \frac{di_{sc}}{dt} + \omega_e \lambda_m \cos(\theta_e + 2\pi/3) \quad (2. 18)$$

These equations are formatted in matrix form as following:

$$[V_s]^T = [R_s]^T [I_s]^T + [L]^T \frac{d}{dt} [I_s]^T + \omega_e \lambda_m K(\theta_e) \quad (2.19)$$

where:

$$[V_s] = \begin{bmatrix} v_{sa} \\ v_{sb} \\ v_{sc} \end{bmatrix}, \quad [R_s] = \begin{bmatrix} r_A & 0 & 0 \\ 0 & r_B & 0 \\ 0 & 0 & r_C \end{bmatrix}, \quad K(\theta_e) = \begin{bmatrix} \cos(\theta_e) \\ \cos(\theta_e - 2\pi/3) \\ \cos(\theta_e + 2\pi/3) \end{bmatrix}$$

$$[I_s] = \begin{bmatrix} i_{sa} \\ i_{sb} \\ i_{sc} \end{bmatrix}, \quad [L] = \begin{bmatrix} (L_A + L_{mA}) & 0 & 0 \\ 0 & (L_B + L_{mB}) & 0 \\ 0 & 0 & (L_C + L_{mC}) \end{bmatrix}$$

Then, to consider the generated torque, it is important to point out that there are two sources for torque generation by the PMSMs. First, the torque that generates as a result of the intersection between rotor and stator magnetic fields. Second, the torque that appear from the machine magnetic saliency, and it is directly proportional to the difference between L_d and L_q [58]. So the PMSM develops an electromagnetic torque which is expressed by the following relation:

$$T_e = \frac{3}{2} p ((L_d - L_q) I_d I_q + \lambda_m I_q) \quad (2.20)$$

where L_d and L_q , p denote the inductances in d and q directions of rotor reference frame and the number of pole-pairs respectively. Whereas, I_d , I_q are the conversion of the three stator currents into the rotor reference frame according to the Park's transformations, as follow:

$$\begin{bmatrix} I_d \\ I_q \end{bmatrix} = \frac{2}{3} \begin{bmatrix} \cos(\theta) & \cos(\theta - 120) & \cos(\theta + 120) \\ \sin(\theta) & \sin(\theta - 120) & \sin(\theta + 120) \end{bmatrix} \begin{bmatrix} i_{sa} \\ i_{sb} \\ i_{sc} \end{bmatrix} \quad (2.21)$$

The electromagnetic torque has another relation that considers the motor parameters and the applied external torque. This relation is given by [59] :

$$T_e = T_L + B\omega_m + J \frac{d\omega_m}{dt} \quad (2.22)$$

where T_L , B and J refer to the external applied torque, the rotor viscous damping factor and the rotor inertia respectively. Whereas, ω_m denotes the rotor mechanical angular speed that relates with the electrical speed by:

$$\omega_e = p\omega_m \quad (2.23)$$

Then, combining the equations (2.22) and (2.23) gives a formula for determining the rotor electrical angular speed:

$$\omega_e = p \int \left(\frac{T_e - T_L - B\omega_m}{J} \right) dt \quad (2.24)$$

2.11 Sensorless techniques and power electronic development

In 1969, the world witnessed the first attempt to sensorless detection when Mieslinger presented a view for position estimation by a method called capacitor shifting [60]. However, it is concluded that there was not enough attention toward the sensorless subject at that time. This is because the next research in this field did not appear until 1983 when Davoine, Perret and Le-Huy presented their view in sensorless controlling of synchronous motor [61], and in 1985 when Iizuka et al proposed a senseless microprocessor based system to estimate the rotor position [62].

This long period is interpreted by the thought that the developed PMSM needs to be supported by a high level electronic applications to perform the sensorless position estimation. These required electronic techniques began to emerge during that period, 1970s to early of 1985s, where the microprocessor and microelectronics techniques started to be adopted with the development in VLSI technology in 1970s [63]. Moreover, reference [56] has pointed out two factors which contributed strongly in the wide spreading of BLDC motors and PMSMs starting from 1970s. They were the considerable development in field of power semiconductors and the discovering of the high quality magnetic materials. So the developed PMSM could not exploit those electronic applications until the middle of 1980s. As a result, it may be allowed to argue that the growing of sensorless techniques of rotor position estimation and the jumping to a higher level in this field of applications were based on the development in microelectronics techniques.

2.11.1 Concept of HF injection and machine core saturation

The topology of injection a sequence of high frequency pulsating voltages is employed to predict the rotor position at standstill. This topology is based on the concept of the PMSM stator core saturation and the machine saliency [64]. Figure 2.29 is a schematic curve to illustrate the relation between the stator exciting current and the flux that linkages the stator core.

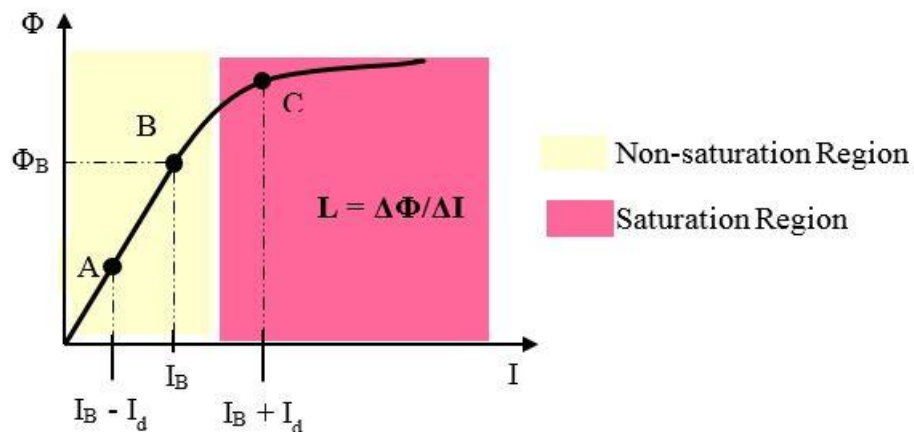


Fig. 2. 29, Stator core saturation effect due to exciting current

In this figure, point B is the supposed motor operating point of motor. Then, if a pulsating voltage is injected into the stator windings, a corresponding change in stator current (I_d) will take place. If I_d was negative, then it will shift point B, the operating point, toward point A, i.e., within the non-saturation region, and there will be a noticeable change in the inductance value. In contrast, if I_d was positive, then the operating point will move toward point C and it may enter the saturation region where the corresponding inductance change will be less sensible.

2.12 The inverters and PWM

The inverter is an electronic circuitry which inverts the dc input into an ac output. Basically, the inverters are classified into three types: the Pulse Width Modulation, PWM inverters, the Voltage Source Inverters, VSI, and the Current Source Inverters, CSI. These three inverter types perform the task of controlling motor speed and power

through controlling the motor supplied voltage and frequency. The choice of one of them for a certain application depends upon the nature of that application [65].

Currently, the PWM inverter has many advantages (such as its higher reliability, less harmonic effect on power supply and more compatible with digital systems) which make it preferable in most motor control applications. By this technique, the ac power is modulated on a set of pulses to modify the pulse width according to the voltage level of the ac power. This modulated pulses fire the gates of switching devices, which form the structure of the inverter. The switching devices are commonly high speed and high power MOSFETs or IGBTs respectively [65].

The switching frequency of the inverter plays an important role in maintaining pure sinusoidal output current, which supplies the PMSM. Choosing the value of switching frequency is a trade-off between the consequences of higher and lower values. The higher values of switching frequency causes in improving the sinusoidal shape of the output current through minimising the involved harmonics. This improvement comes accompanied with negative effect of raising the losses in the inverter switching elements. This will lead to reduce the output power and cause warming up the switching elements. In contrast, choosing a lower switching frequency will lead to reduce the power losses, but increases the output harmonics. Reference [10] mentioned that the range of switching frequency is between 3 and 10 kHz. However, the current applications for PM drives have witnessed wider range for switching frequency, up to 40 kHz. Typically, the frequency range between 6 and 20 kHz is avoidable being cause an audible noise.

2.13 Summary

This chapter presents a brief review for the theory of permanent magnet motor. This presentation is achieved through a discussion for the basic equations which govern the running process of these motors. The considerations of torque and speed generations and the crucial role for accurate rotor position estimation are highly investigated. Moreover, a review for history and types of permanent magnet materials, being the distinguished materials in construction of these motors, are explored. The basic power electronic requirements to establish the control boards of permanent motor running are shortly

discussed. The adopted strategies in controlling the operation of the permanent motors are explained.

In addition, this chapter sections provide a comparison between the permanent motors and the other types of rotating machines. The promised features of the permanent motors are highlighted through this comparison. Not only the positive view for permanent magnet motors is introduced, but a spot of light is also projected on the negative side of view for these motors. Being the permanent magnet motors of sinusoidal and trapezoidal back electro-motive force have many common features, a sufficient space of arguments is also provided in this chapter for the comparison between these two motor types. This comparison is to show the qualitative attributes which make one of these two motor types preferred in a certain application more than the other.

Different thoughts related to permanent magnet motors are also explored, such as:

- ❖ The basic applications for permanent magnet motors, especially in modern life, are covered in this chapter as well.
- ❖ Classification of permanent magnet motors according to the geometric shape of their rotors.
- ❖ Employment of machine frame transformations in analysing the operation of permanent motors and the process of rotor position estimation.
- ❖ Various techniques that are adopted in rotor position prediction.

CHAPTER THREE

LITERATURE REVIEW

3.1 Introduction

Since the middle of 80s of the last century, an increasing number in the efforts, which concern sensorless position estimation, has been reported. Especially at the years 1989 and 1990, where many approaches to implement the corresponding issue were proposed [56]. Kechiche, et al. (2011) summarised those methods of sensorless position techniques into two main categories [66]. Figure 3.1 shows this classification as given be [66]. The first category is called the fundamental models method which is applicable at medium and high motor speeds. It is further classified into three main approaches; back EMF observer, Kalman filter and flux modulation, which currently have an considerable importance [66]. In spite of the excellent performance and high reliability of this method, its essential weakness appears at the low rotor speeds. This is because it relies on the detection of the back electro-motive force EMF waveform (zero-crossing points in BDCM). So, it is related to the direct relation between speed of motor and the induced back EMF. Thereby, at low speeds, it leads to immeasurable back EMF waveform, impaired signal to noise ratio and consequently very hard ability to determine the zero crossing points. Moreover, at standstill there is no induced back EMF at all [67]. Therefore, this method is reliable at medium and high speed ranges only.

The second category is based on tracking the inherent machine feature of magnetic saliency. It has been performed through injecting a signal of high frequency in the stator circuitry [4],[5]. As long as the principle in this category is independent on rotor speed, it is confident in estimating the rotor position at low and zero speeds. It includes various approaches proposed over the past two decades. All of them are based on superimposing the high frequency signal on the fundamental stator frequency. Then, a heterodyne process has to be used to decouple the frequencies and extracting the rotor position angle. These approaches will highly be chronologically considered in the next sections.

Initially, this method encountered a main challenge, representing by the time variance of stator windings inductances with rotor position. This problem was solved later by adopting Park's and Clark's transformations, where two reference frames, rotor reference frame (dq - frame) and stator reference frame ($\alpha\beta$ - frame), are obtained respectively. These frames permit to deal with the stator inductances as independent variables on rotor position.

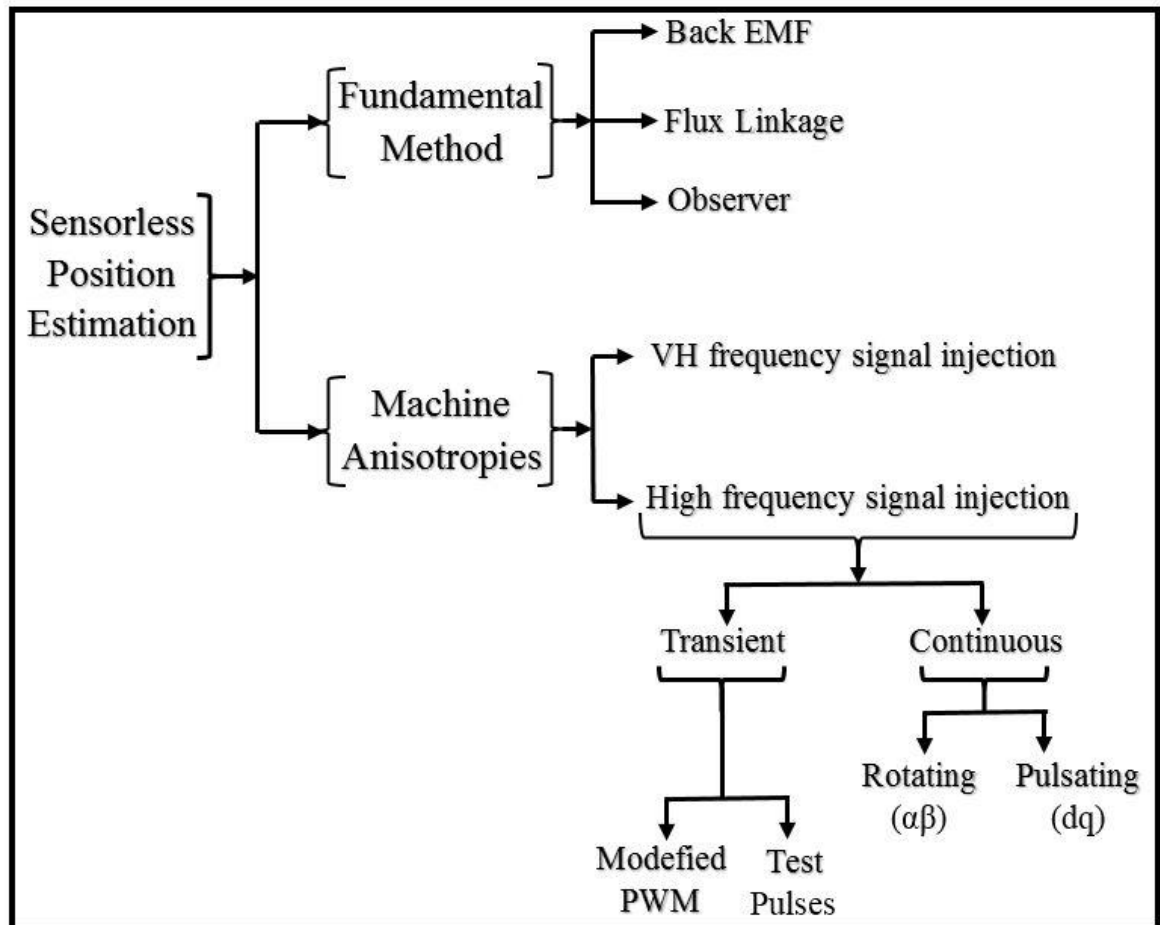


Fig. 3. 1, Method of sensorless position estimation

For any PM machine, an approximate limit of 3% of rated speed is critical in maintaining accurate sequence for the commutation process. This is because over that limit the fundamental model based estimation methods of rotor position, such as back EMF and Kalman filter, work properly, while under the specified limit, including the standstill, the accuracy of rotor position estimation is no longer acceptable and the active alternative method is the high frequency signal injection [68]. This method exploits the magnetic saliency, which is an inherent feature of the permanent magnet rotor. So, based

on the high frequency signal injection, several works have presented to investigate the machine saliency and to extract the rotor position information. Thereby, the estimation of rotor position at zero and low speeds has been implemented. From literature, the frequency of the injected signal has to be no less than ten times the fundamental frequency of motor and no more than one-tenth the inverter frequency. However, there is no certain limit to its voltage amplitude but it is important not to be too low to be detected, and not to be too high to avoid the effective torque ripple as it will be illustrated in detail later.

This chapter is going to be organized according to the adopted aspect in the estimation of rotor position. This will involve the;

- Modification in motor structure to be able to give information about the rotor position.
- Improving the rotor position estimation through improving the performance of motor driver.
- Reviewing the utilization of high frequency signal injection, HFSI, in the rotor position estimation during the full speed control running, especially, at the speed transit edges, hybrid operation.
- Reduction of the acoustic noise, which emerges as inherent feature to the injection of audible frequency.
- Filter drawbacks on the rotor position estimation and the trails of eliminating them.
- Attempts of realizing the rotor position through HFSI in the axes of the motor equivalent frames, Park and Clarke's frames.
- Application the HFSI technique to estimate the rotor position of nonpermanent magnet motors.
- Employing of the mathematical models and digital signal processors DSP in construction of the rotor position estimators.
- Adopting a square wave as injected signal, rather than the sinusoidal wave, to establish the HFSI estimator.
- Attempts to improve the performance of HFSI techniques.
- Usage of HFSI in different applications rather than the rotor position estimation.

Finally, an evaluation for the usage of HFSI technique in rotor position estimation, points of weakness and strength, has been presented.

3.2 Structure modification

Takashima, et al. (2002) proposed an approach to estimate the PM rotor position based on pasting nonmagnetic sheets on the rotor of BLDC motor. This is to cause inductance variations, depending on the relation between the stator winding inductances and the rotor magnetic flux. Then, a certain algorithm was built to investigate and analyses the eddy currents induced in those nonmagnetic sheets from which the rotor position was estimated [69]. Figure 3.2 illustrates the work concept as given by [69]. It was concluded that pasting a nonmagnetic material causes a shift in the rotor magnetization axis, from d_m to d_s , and change the saliency ratio from 1 to 1.12, as shown in Figure 3.2b. The above work might fail due to a substantial drawback, where masking parts of the rotor magnet surface by a nonmagnetic material could cause a distortion in the distribution of the rotor magnetic flux. This leads to increase the torque ripple, which causes a negative impact on the accuracy of rotor position estimation.

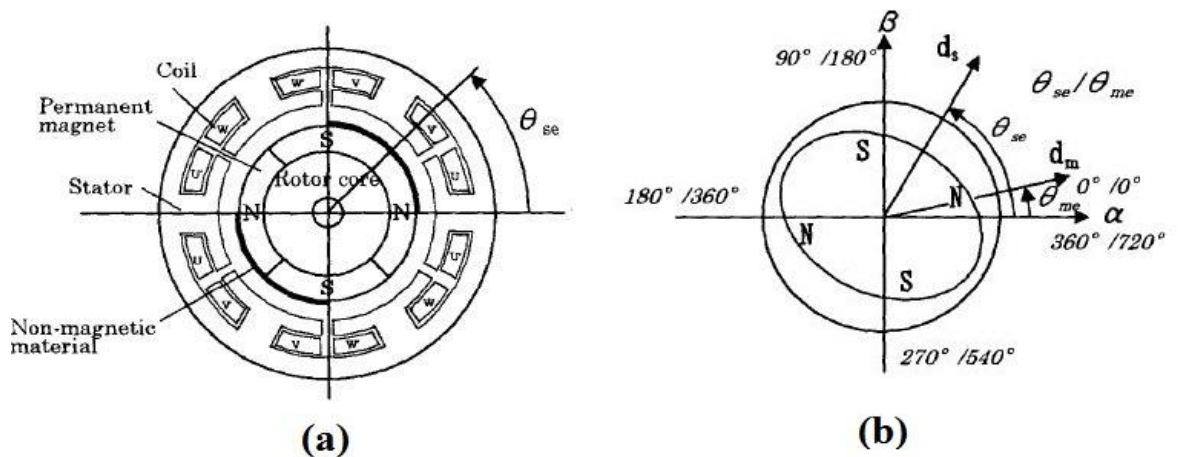


Fig. 3. 2(a) schematic for the motor structure with nonmagnetic materials (b) effect of nonmagnetic material on magnetization characteristics

More works about employing the motor structure modification in rotor position estimation will be reviewed later.

Hoon Jang, et al. (2003) controlled the rotor position of a surface mounted permanent magnet synchronous motor (SM-PMSM) by analysis of the high frequency impedance of the motor [70]. This was achieved after creating a magnetic salience in the stator of the motor through saturating the stator core. Then, an injection of a high frequency voltage permitted to obtain and analyse the difference in high frequency impedance. From this difference, the stator magnetic salience is detected and the information of low speed and standstill rotor position is extracted. Moreover, the researchers mentioned that this method is not only controlling the rotor position, but also the torque and speed [70]. This method was applied at low speed and it was not clarified if it is possible to be applied at medium and high speeds and what are the limitations against that. At the same year, the injection of carrier signal frequency was employed by S. Seman and J. Luomi to address the speed oscillation in estimating the speed and rotor position of PMSM at low speed domain. The carrier frequency component, i_c , which was involved in the motor current, was further analysed into positive sub-component, i_p , and negative sub-component, i_n . Then, it was given by the following equation:

$$i_c = i_p e^{i(\omega_c t + \varphi_p)} + i_n e^{i[(2\omega_r - \omega_c)t + \varphi_n]} \quad (3.1)$$

Accordingly, the rotor speed and position were obtained by low pass filtering the negative term of the above equation. The model, which was designed to satisfy this method, was simulated on a computer and the obtained results has proved that the low speed problem of the observer has been solved [71]. Originally, this method, of low speed position estimation, was proposed to work in conjunction with a high speed position estimation method. It was necessary to robust the work by suggestion the way of switching from low speed to high speed estimation methods, by which the position estimation is covered over a full range of speed operation.

Arias; et al. (2004) proposed to exploit the Matrix Converters to improve performance of low speed permanent magnet synchronous motor controller which based on the high frequency signal injection. The negative effects of the switching elements IGBTs, such as dead time and voltage drop, on rotor position estimation were investigated and it was proved that the Matrix Converters are able to reduce those effects [72]. Meanwhile, Hoon Jang; et al. (2004) tried again to present their view in high frequency signal injection and exploiting the analysis of the differences in HF

impedances, which was proposed in 2003. They tried to estimate the position and speed of a rotor in surface mounted PM machine through a high frequency fluctuating voltage. However, this time, a finite elements analysis procedure was employed in the impedances analysis, which were dealt as functions to rotor position estimation error. The corresponding results were compared with those obtained from an inverter system, based on pulse width modulation, which was tested for different injection conditions [73]. It is obviously clear that the authors worked in 2003 and 2004 were to catch the same aim. However, if the obtained results in 2004 were compared to thus of previous year, it will be noticed that this work represents a progress. This is because the drawbacks related to the saturation and nonlinearity of PWM inverter are overcome by this work. However, adopting the finite element analysis involves extremely high computational demands for real-time control, which may represent an obstacle in some applications.

In 2005, an approach to estimate the rotor position of a permanent magnet brushless DC motor PM-BDCM by injection a signal of a high frequency through the space voltage PWM inverter was proposed. This method tried to exploit the spatial saliency, even if it was very low, to detect the rotor position at low and zero speeds. The work introduced a simulated model for the motor and the control circuit. The given results proved the validity of the proposed approach [74]. Zhang; et al. proposed a method to investigate rotor position of a SM-PMSM at low speed or standstill. This paper presented a sensorless model based on park's transformations and the phase error between the synchronous reference frame and the estimated one. Moreover, it supposed a high frequency voltage should be injected in the estimated d-axis voltage. Then the required estimation for rotor position is detected from the estimated q-axis current through exploiting the magnetic saliency resultant from the saturation caused by the voltage injection [75].

In 2006, a group of researchers, from the Institute of Electrical Engineering Chinese Academy of Science, Beijing, presented a MATLAB model to estimate the rotor position of an interior permanent magnet synchronous machine IPMSM [76]. This work has included a novel format, which permits to test the IPMSM as a surface permanent magnet synchronous machine SM-PMSM. The simulation procedure used a carrier

signal injection to generate a rotating current vector in the presented model and to extract the position and polarity of the interior magnet. Some advantages are highlighted for this model such as its ability to estimate and start up the motor even for high initial torque, also the accuracy of estimation is independent on the motor speed. Other work was presented in 2006 by C. Ortega; et al. to propose a scheme of high frequency injected voltage for sensing rotor position at zero and low speed of a SM-PMSM whose driver type is Direct Torque Control (DTC) [77]. The adopted technique, DTC, permits to obtain the currents of the rotary reference frame, i_d and i_q . Then, the rotor angle, θ_r , was simply determined from the relation:

$$\theta_r = \frac{1}{2} \arctan \left(\frac{i_q}{i_d} \right) \quad (3.2)$$

In this work, a creative modification is positively indicated where no additional circuitry was required to generate the high frequency carrier, but it was generated from the fundamental frequency of the supplying voltage. It is worth to mention that the DTC has emerged at the end of 1990s as a second method, beside the vector control, to control driving of the sensorless PM motors. However, in 2006, this under discussion work was the first attempt, which discussed applying the DTC for driving the motor at zero and low speeds in addition to medium and high speeds.

3.3 Improving the performance of PMSM drive

The year 2007 witnessed an employing to the high frequency signal injection in field of dropping the technical problems, which represents essential threats to the PMSM ac drive, the three-phase inverter. Particularly, the zero current clamping (the distortion in current waveform due to the current clamping around the points of zero crossing) and distortion of carrier signal injection was encountered [78]–[80]. This obstacle was tackled by Choi and Seok (2007), where a compensation approach was presented to treat the problem of zero current clamping [81]. In this compensation method, the distortion factor related to the zero current clamping is found through a HF current and voltage injections. This permitted to determine the required compensation voltage to overcome the undertaking drawback of the inverter. A mathematical model was designed and tested on three-phase PWM inverter, which was driving a commercial PMSM. Figure

3.3 shows the results as given by [81], where there is an absolute improvement in the results of the proposed method.

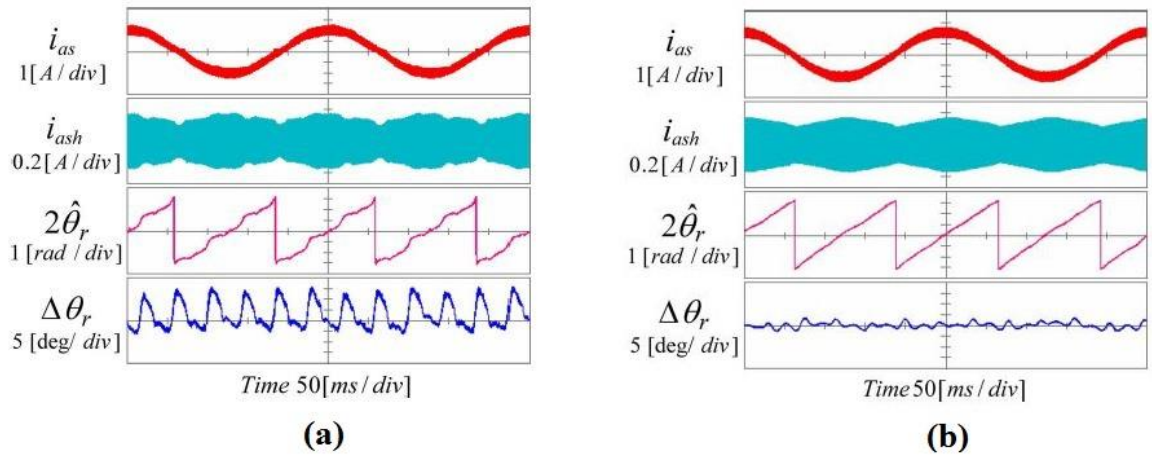


Fig. 3. 3, Effect of the treatment of zero current clamping on the accuracy of rotor position estimation (a) before (b) after

Moreover, 2007 also witnessed other researching activities in field of improvement the HF injection techniques by Ortega, Arias, and Carunua. They argued that the fundamental voltage of Matrix Converter are modified directly by an algorithm for high frequency signal injection. Thereby, informative signal is extracted from which the rotor position is detected [82]. While, another paper presented the view of Choi and Seok to reduce the position estimation error and the ripple in position/speed estimation which may occur due to the zero current clamping [83]. To achieve that, the researchers proposed injecting a HF pulsating signal to create an injection axis-switching scheme IAS to switch the frequency injection between the d and q axes. Figure 3.4 is a block diagram to show the basic idea of the proposed method as given by [83].

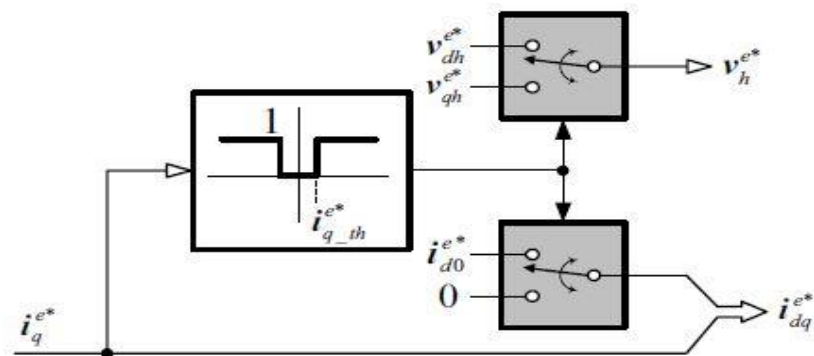


Fig. 3. 4, Basic idea of the injection axis-switch, IAS

The year 2007 also witnessed a work, which directly considered the high frequency signal injection in the motor at low speed operation. This work was presented by Shanshan, Yongdong and Xuejin to introduce a model by which two methods of high and low frequency signal injections to control low speed operation of permanent magnet motor were compared. The HF method was based on the idea of saliency and the corresponding difference between the L_d and L_q inductances. While the second method, LF, was based on the fundamental method where it analysed the ripple in the induced back EMF. According to the given conclusion, the former method presented more accurate results than the latter method [84]. This result of comparison had to be expected previously as long as the latter method was based on the back EMF and the domain of operation was at low speed. More works, which are interested in improving the inverter operation, will be noticed next.

3.4 HFSI in the hybrid operation of PMSM

The hybrid operation of PMSM is concerning the rotor position estimation over the full range of speed operation. Different estimation techniques are used at zero, low, medium and high speeds. The issue is to cover the overlap transition from one technique to another with minimum estimation error. In 2008, plenty efforts emphasized the importance of hybrid controlling system to run the PMSM over a full range of speed, from start up to high speed. Andreescu, et al. [37], presented a promising work by which the high frequency signal injection and flux observer were used to form a combined sensorless full speed range control system for IPMSM. The obtained results reflected an independency to the rotor position estimation from both the motor parameters and the inherent dc offset of stator current. At the end of 2008, another work was presented to improve the procedure of application of high frequency signal injection on PMSM hybrid operation. This improvement is based on Kalman filtering technique to be incorporated with system modelling technique to increase the accuracy of position estimation during the transit periods. A signal injection algorithm was used for zero/low speed estimation. Whereas, a direct scaling algorithm was used for medium/high speed estimation. Third algorithm of weighted coefficients was employed to perform the

estimation during the transition gap [85]. Figure 3.5 illustrates this concept as it was given by [85].

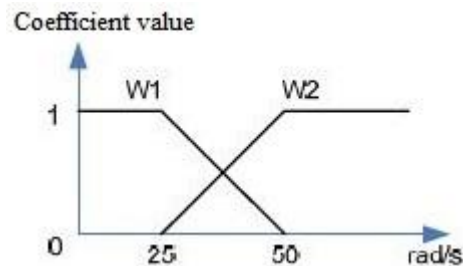


Fig. 3. 5, Schematic for estimation procedure by the weighted coefficients algorithm

Piippo, Salomäki and Luomi (2008) suggested supporting role to high frequency signal injection, which was combined with an observer of LC output filter. The aim of this combination is to form a proposed controller scheme to drive the PMSM over a wide speed of operation. The investigation of this scheme operation showed no negative effects to LC filter on signal injection process if the value of high frequency is properly chosen. Also the satisfied obtained experimental results reflected an encouraged success to this method [86]. Other studies, regarding the hybrid operation, will be discussed later.

3.5 The noise in HFSI

In 2009, the audible noise accompanied the use of high frequency signal injection was studied and some solutions were suggested. Reference [87] introduced a study, based on a neural network model, to investigate the relation among the high frequency injection, the expected audible noise and the error in position estimation was introduced. Accordingly, it was concluded that the proposed neural model was convenient in situations at which a trade-off should be done between the speed/position error and the noise [87]. This drawback of noise accompanying the use of HF signal injection was also tackled by reference [88] in 2009. It has aimed to achieve acceptable reduction in the audible noise of the electrical power steering which based on HF signal injection [88]. According to this work, the noticeable audible noise, because of the injection of high frequency, is encountered and dropped through adopting narrow band of high frequencies in injection process. These frequencies should be randomly distributed

around a central frequency. The problem of audible noise will be encountered in the next sections.

On the other hand, the problems threaten the operation of the three-phase inverters, which were widely discussed in 2007, returned to be restudied by QI Xin, et al. (2009). An extracting method to the involved information in the injected HF was proposed as an improvement to the original techniques. This improved method has the ability to block the inverter nonlinear distortion and to overcome the delay of the band-pass filter which are used to extract the HF current [89]. As long as this work has come as an improvement to previous one, it was more effective if the researchers mentioned that previous work and made a comparison between the results to show amount of improvement.

3.6 Eliminating the filtering process

In 2010, some claims emerged to eliminate utilizing of filters in construction of HFSI circuitries. The filtering represents an essential part in the conventional HF signal injection controllers. It is used in filtering the frequencies, which are modulated by the information of rotor position. The filtering process has a main disadvantage, which is represented by delaying the signal transfers among the controller blocks. This delay could lead to increase the controller response time and decrease its bandwidth. Therefore, many works have been done to compensate the presence of filters. Moreover, it has been found that the filtering action does not accomplish the rejection of undesired frequency components completely, where the frequencies out of the filter cut off frequency are attenuated rather than eliminated.

Nino, et al. (2010) presented a work to improve performance of HF signal injection controller through eliminating the filtering processes. The work concept based on adopting a transfer function to replace the filters in the structure of the injecting controllers. It was concluded that the proposed method yielded a significant progress in the dynamic operation of the controllers [90]. Figure 3.6 shows adopting the transfer functions to substitute the filter apertures as proposed by [90].

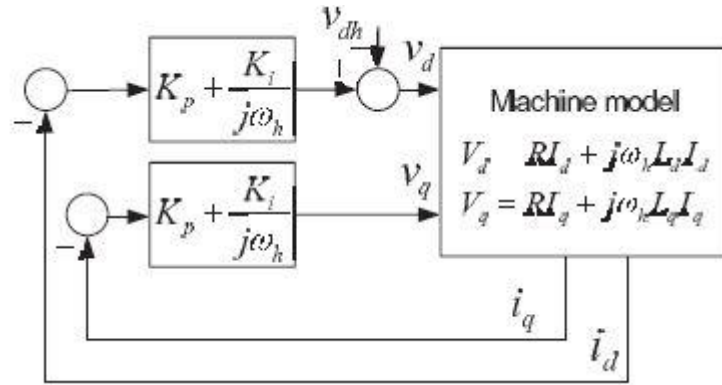


Fig. 3. 6, Method of substituting filters by transfer functions

A paper, of different trend, was also presented in 2010 by Wang et al. to compare the strategies of high frequency signal injection through the accuracy of rotor position estimation and amount of ripples accompanied the estimation process. To achieve this aim, a model of PMSM, which proposed early in 2010, was adopted again in this paper but in three different strategies for HF signal injection methods; rotating carrier, d-axis injection and α -axis injection. Then three criteria were determined to compare the efficiency of the tested injection strategies; torque ripple, drive efficiency and cost. The obtained results have shown that the first and third methods are more suitable to be used with IPMSM while the second is suitable for both IPMSM and SPMSM in spite of the high ripple accompanied the use of this method [91].

Yoon et al. reported in 2011 that most of the HF signal injection methods currently in use content filters, LPF and BPF, which cause limitation in bandwidth and delay in rotor position estimation process. Accordingly, the authors presented an approach to HFSI which eliminated the need to utilization of filters based on square waves should be injected in the d-axis of the rotor estimated reference frame. Then the rotor position angle was taken from the arc-cosine of the induced HF d-axis current [92]. In contrary, Kechiche et al. (2011) presented a model based on continuous signal injection on the d-axis of rotor reference frame of washing machine PMSM. In this work the error shift angle between the estimated and original rotor reference frames was measured and accordingly the rotor position angle was also measured [66]. The given results for this proposed have reflected an a precise estimation for rotor position at standstill and low

speed in spite of the utilization of two band pass filters which represent disagreement with the argument of Yoon aforementioned.

3.7 HFSI in the frame axes and saliency effect

Yu et al., (2011) presented promise view to control the operating of permanent magnet synchronous motor [93]. This is based on injecting a high frequency square wave in the q-axis of the estimated rotor reference frame. Then the rotor position can be extracted from the induced current. The promising thought in this work is the ability to apply it over the full speed range of motor running. The high frequency injection method provided good results of rotor position estimation under the inherent feature of IPMSM, which exhibits high inductive reactance. However, the authors presented the model for a certain type of motors, flux intensified permanent magnet synchronous motor FI-PMSM, which made it not possible to be generalized for any type of motors. In contrast an axes injection, either in the $\alpha\beta$ or in the dq frames, of different approach was suggested by Leidhold (2011) to estimate the rotor position at zero speed [94]. This approach based on utilizing the inherent HF component in the zero-sequence, which is always produced by the space vector PWM modulator. The estimation of rotor position by this method is highly affected by the magnetic saliency of rotor, so a good estimation is obtained at low saliency whereas a compensation for high saliency is required.

To estimate the rotor position at zero and low speeds apart from the saliency tracing, reference [5] proposed different approach to satisfy this aim. It based on the thought that the information of unknown machine saliency can be deduced by comparing its current responses with those of isotropic machine model. Thereby, the rotor position information can be obtained from the difference of both currents responses. It was determined that if a high frequency signal is added to the oriented controller output, then the existence of time derivative currents responses, in stator frame, is a sufficient condition to satisfy the estimation process successfully. To prove the validity of the proposed scheme, an experimental model, which included PMSM, was set up. Accordingly, the authors deduced that this procedure involves important advantages; the direct estimation provides high bandwidth estimator and dispensing the saliency tracking facilitates the estimation process in non-salient machines.

Reference [95] built a sensorless controller for an interior permanent magnet synchronous machine IPMSM based on PWM excitation whose current transient response was considered. Meanwhile, a relationship between inductance and current derivative, at one side, and the rotor position, at the other side, was established. The saliency error, which produces as a result to mutual inductances, was also considered to robust the corresponding mathematical model. It was concluded that the experiments, which were achieved on IPM based system, proved the validity of the proposed scheme.

In 2012, Murakami and et al. reported a method to detect rotor position at low speed based on injection high frequency square wave on the estimated d-axis of rotor reference frame. Then I_α and I_β are obtained from the envelopes of the high frequency component of the stator current as shown in figure 3.7 given below. Thereby, the rotor position is simply determined from the arc-tangent of (I_β / I_α) , assuming I_β is a sine waveform and I_α is a cosine waveform [45]. The weakness in this method is in this assumption because it is not valid unless the rotor saliency and the inductance of HF are both a sinusoidal function to rotor position in sufficient amount, which could only be verified by considering a certain IPM motor design. This is implemented by modifying the plane shape of the conventional IPM into V-shape in order to maximize the magnetic flux of IPM.

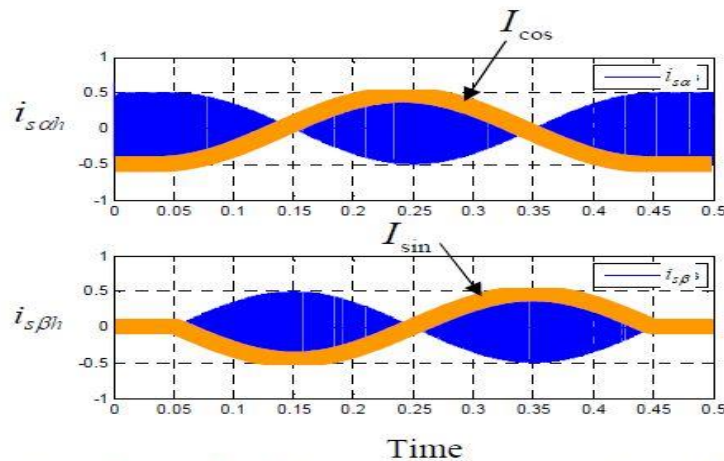


Fig. 3. 7, RP detection from envelopes of the stator current HF components

3.8 Addressing the drawbacks in HFSI

Osama's paper in (2012) was presented to tackle the noise and vibrations drawbacks accompanied the high frequency injection at low rotor speed of surface mounted permanent magnet synchronous machine SM-PMSM. It represented an improved employment for wavelet transformations by which it permitted to use a low amplitude voltage in injection process of motor stator windings to extract rotor position at low speed [96]. It gives the following current equations, at the rotor estimated reference frame, as responses to the injected high frequency wavelet:

$$\begin{bmatrix} i_{dh}^e \\ i_{qh}^e \end{bmatrix} = \begin{bmatrix} \frac{V_{inj} \cos(\omega_h t)}{Z_{dh} Z_{dq}} (Z_{av} - \frac{1}{2} Z_{dif} \cos(2\Delta\theta_r)) \\ \frac{V_{inj} \cos(\omega_h t)}{Z_{dh} Z_{dq}} (-\frac{1}{2} Z_{dif} \sin(2\Delta\theta_r)) \end{bmatrix} \quad (3.3)$$

where i_{dh}^e and i_{qh}^e are the estimated high frequency components in direct and quadrature directions of Park's reference frame respectively, V_{inj} is the voltage root mean square value of the high injected signal, ω_h is the injected high frequency in angular form, Z_{av} and Z_{dif} are the average and difference values for the maximum and minimum values of the high frequency impedances respectively and θ_r is the angle of rotor direct field in Park's reference frame.

By this equation, it is clear that the position information is involved with the impedance difference. As the target is the SM-PMSM rotor position, the difference term will be very small. Besides that, the injected signal is small too, wavelet. Therefore, it is a hard issue to deal with such current values. However, this work succeeded in presenting a model, which has full sensorless rotor position estimation, but the huge requirements of computations and data processing could form obstacle in many applications.

Jianmin and Jianwei tried in (2012) to implement some of basic thoughts on high frequency signal injection. They proposed a simulated model to measure the error in rotor position estimation at zero and low speeds of IPMSM due to the effect of back EMF and compare the results with the theoretical bases. The procedure was achieved by both continuous and pulsated HFSI, and the obtained results came as it is expected, there was very weak or no effect in the former while a certain amount of error was registered

in the latter under the influence of the high L_d/L_q ratio [97]. This is because the effective parameter in the study, EMF, is originally very weak or disappeared under the circumstances of study, zero or low speeds.

Whereas, the work presented by Cupertino, et al. (2012) addressed a more effective parameter on the performance of HFSI estimator, it was the delays in estimation process and its effect on accuracy of estimation [98]. The authors specified two sources for this delay, firstly, the algorithms used in estimation process and their digital implementation. Secondly, the filtering processes, which are necessary to extract the rotor position in many estimators. It is possible to argue that the results and conclusions of this work came to emphasis the previous thoughts about the delay drawbacks. A comprehensive rotor position estimation technology for surface mounted permanent magnet machine SM-PMSM was presented in 2012 by [99] to cover the whole range of operation from zero speed to high speed. The technology, which was fabricated on a single chip, involved HFSI scheme to estimate the rotor position at low speed. The work is combined with flux observer, based on the generated back EMF, for high-speed rotor position estimation. It specified the following transition process for the hybrid combining of low and high speeds controlling.

$$\theta_r = \alpha\theta_L + (1 - \alpha)\theta_H \quad (3.4)$$

$$\alpha = \begin{cases} 1 & \text{if } \omega_r \leq \omega_L \\ \frac{\omega_H - \omega_r}{\omega_H - \omega_L} & \text{if } \omega_L < \omega_r < \omega_H \\ 0 & \text{if } \omega_r \geq \omega_H \end{cases} \quad (3.5)$$

.where the subscripts r, L and H refer to the rotor estimated value, the estimated value at low speed and the estimated value at high speed respectively, and α is the transition factor.

The applied scheme of HFSI involved injection of high frequency voltage in the estimated d-axis of rotor reference frame and extracting the rotor position from the alternating current of the q-axis. Although the presented system was described as a full speed range, but the procedure for standstill was not illustrated in the work.

Utilizing of square wave in high frequency signal injection started emerging in 2012. This is to overcome two drawbacks threaten the estimator performance. Firstly, is to eliminate the use of filters in extracting the injected signal and thereby the rotor position angle. It is, as mentioned before, because the various types of filters (LPF, BPF, HPF and BSF), commonly inserted in injection circuitry, are responsible for narrowing the overall estimator bandwidth which cause in a certain delay in estimation process. Secondly, is to reduce the acoustic noise by employing a square wave in signal injection, rather than the conventional continuous sinusoidal signal injection, which was proved to have a significant contribution in reducing this noise.

To meet the above aims, Nae-Chun and Sang-Hoon proposed in 2013 an algorithm for sensorless control at start-up and low speed operation of interior permanent magnet motor based on employment of square wave in signal injection [38]. The algorithm relies on arithmetic operations to cause three significant reductions in time delays through filters eliminations in the system feedback route. Firstly, is the elimination of a low pass filter assigned to extract the fundamental frequency. Next, is the elimination of a high pass filter assigned to extract the high injected frequency. Finally, is the reduction of time delay in the demodulation process.

Reference [100] treated different drawback view related to the operation of high frequency signal injection. It considered the transient case during the load increase. It was stated that in case of sudden load increase, there should be a corresponding increase in amplitude of high frequency during the transient and it should back to the normal amplitude when the load back to steady state. This view came as an addressing to the resultant torque ripple due to the high frequency signal injection. To satisfy this aim, a high frequency signal, 500 to 2500Hz, and an adaptive amplitude was superimposed on the fundamental frequency in the $\alpha\beta$ stationary reference frame. Then a demodulation process based on the heterodyne principle was exploited to obtain the rotor position from the motor current responses.

Another work of different view was presented in 2013 to address the deviation which occurs in the estimation of rotor position of the PMSM due to the winding cross couplings that happen as a result to the winding asymmetries and saturation [101]. It based on a mathematical model, which involved an injection of HF current signal in d-

axis of the dq-reference frame. It was concluded that an accurate rotor position estimation was obtained from the practical model under test. Whereas, reference [102] has found that the accuracy and errors of rotor position estimation occurs in estimation process due to the variation in stator windings resistance and the delay times. It was concluded that a new approach, based on employment of the positive and negative sequences of terminal currents, was presented to detect and eliminate those errors. The weakness or lack of explicit rotor magnetic saliency was studied in reference [40]. This case is very clear in surface mounted PM motor, where the spatial saliency is distributed uniformly and it causes degrading in the ability of signal injection observer to extract accurately the rotor position at low speed. Accordingly, this reference proposed a different approach in extracting the rotor position estimation involved injection a square wave and exploiting the information on the envelope of the induced high frequency current component in the stationary reference frame. The proposed work is close to that which was presented by reference [45].

Returning to the acoustic noise, different scheme in extracting the rotor position estimation knowledge from the high frequency voltage injection current response was proposed in reference [103]. The work aimed to reduce the acoustic noise usually accompanied to the employment of high frequency voltage injection. It is based on sampling the stator measured currents through high frequency A/D followed by a statistical data manipulation of recursive least squares analysis. This led to inject high frequency voltage with a lower amplitude of factor 7 to 10 than the normal case. Although it causes a considerable elimination in acoustic noise, but it is expected to face the problem of delays and narrow bandwidth estimator as aforementioned in [38] due to the huge electronic and statistical manipulations for data.

3.9 HFSI in non-PMSM

Furthermore, the year 2013 witnessed emerging the applications of high frequency signal injection in purpose of estimation the rotor position of machines, which are different in type from the PMSM. Here are two of those applications, the first is the electrical energized synchronous motor ESM and the second is the doubly fed induction generator DFIG. The common feature for both of those applications is that the rotor is

electrically accessible, so there is an ability to control the rotor flux linkage during machine running. Moreover, the high frequency signal is injected in the rotor circuitry instead of the stator. All schemes of rotor position estimations of PMSM at low and high speed are applicable for ESM and DFIG. Accordingly, rotor position estimation of ESM was the subject of the study presented by reference [104]. The ESM is different from PMSM being its rotor is not designated using the rare earth permanent magnet. Instead, the rotor magnetic field is generated electrically, electromagnetic field. The injected high frequency was injected in the rotor windings, whereas the position of rotor was detected by sensing the terminal currents of both stator and rotor. Figure 3.8 shows a schematic modelling for this motor and the rotor injection process as it was represented by reference [104].

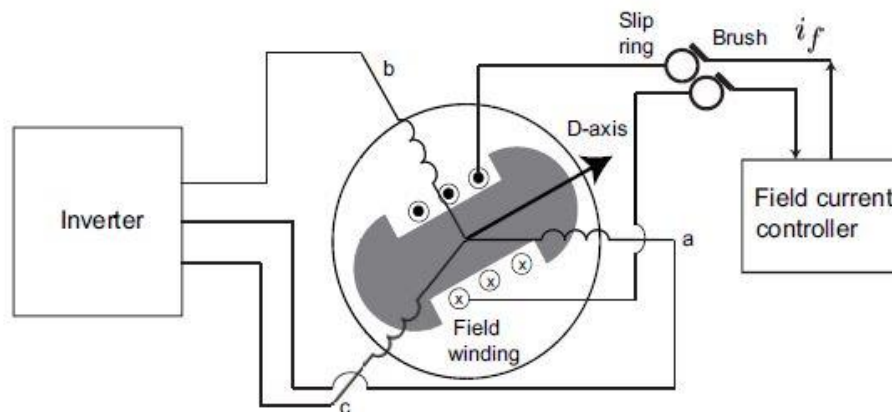


Fig. 3. 8, Schematic diagram for the electrically energized motor

Similarly, reference [105] injected a high frequency signal in the rotor winding of the doubly fed induction generator DFIG to estimate the rotor position by sensing the voltage terminals of stator windings which were connected to the grid. Other applications for HFSI on non-PMSM will be shown in the chronological review.

3.10 Mathematical models for HFSI

In 2014, the mathematical models were presented in implementing the HFSI. Yuanjun, et al. [106] employed the digital signal processing concepts and the high frequency voltage injection to present a view for initial PMSM rotor position estimation. It was based on utilizing an infinite impulse response IIR digital filter to make it possible

to manipulate the data of the terminals current response in the DSP controller. The given results showed that after 40msec of estimation running, the estimating curve went asymptotic to the line of real value which reflect good estimation process. Reference [107] presented a mathematical model to control a system for interior permanent magnet synchronous motor IPMSM over a full range of speed. High frequency signal injection scheme, based on tracking the machine saliency, was employed to achieve the low speed rotor position estimation. A scheme, based on the detected back EMF, was employed in medium and high speeds, and a hybrid controller organized the transaction of estimation between low and high speed schemes. With respect to low speed rotor position estimation, although there was a coincidence between the actual and estimated curves in majority points, but some points of 15° angle estimation error was also there which represent deterioration to the proposed observer.

Reference [64] (2014) criticised the direct injection of pulses in the stator windings to obtain the initial position estimation because they might cause an initial torque ripple. This torque ripple threatens the position estimation process at zero speed as it may cause to shift the rotor from its initial position. It proposed an alternative approach which was based on injection of a high frequency pulsating voltage in the d-axis of the rotor reference frame to obtain a primary estimation for rotor position. Then, the saturation, which is expected to be happened in the d-axis, should affect the d-axis current to give a second harmonic, which should carry the information about the magnet polarity. Combining the primary estimation with the polarity information led to detect the actual rotor position. Yi Chen, et al. (2014) used a mathematical algorithm to support the sensorless matrix-converter method, which was widely discussed in 2004, in estimation the rotor position of IPMSM [108]. The authors re-used this method in 2014 to create a significant reduction in the estimation error through selecting a virtual dc-bus voltage, from three levels, for the matrix-converter. Figure 3.9 shows the three levels, which were normalized to a V_{peak} ; low (up to 0.5), middle (up to 0.886) or high (up to 1) as given by [64]. This procedure was followed by an algorithm, given in reference [108], for duty cycle compensation.

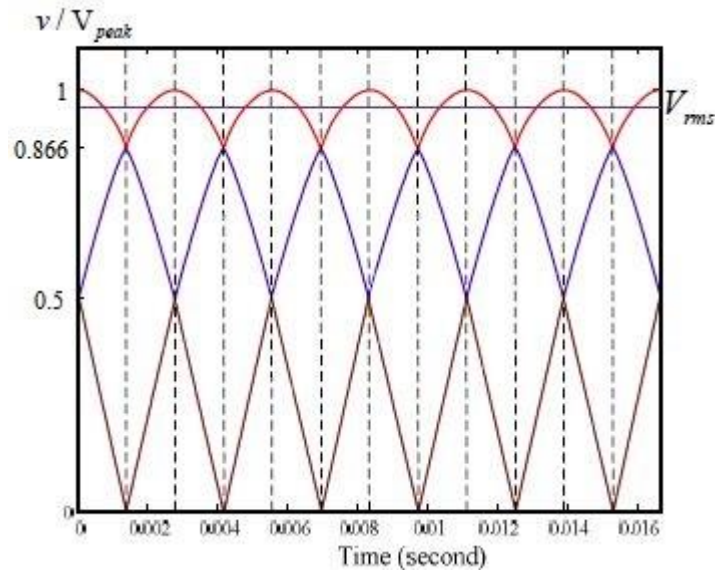


Fig. 3. 9, Method of three levels converter normalized voltages

Reference [109] proposed different approach for rotor position estimation based on utilizing a notch filter. According to this approach, the injection process of high frequency achieved as usual, but the process after sensing was different. A notch filter was employed to extract the rotor position angle, where the extremely narrow bandwidth of the filter permitted to obtain a single frequency which involved the rotor position information. Thereby, the LPF and BPF, which are already used in the convention HF injection estimator, were eliminated and this was the main aim of the paper to degrade the time delays those are always accompanied the filter usages.

Away from the PMSM, Toni Tuovinen and Marko Hinkkanen presented an adaptive full observer to drive a synchronous reluctance motor SyRM. The high frequency signal injection technique was used to estimate rotor position at zero and low speeds. No new scheme in signal injection was presented but the degrading of the cross saturation between d and q axes represented considerable improvement in estimation error correction. It was concluded that the proposed scheme suffered from the parameter error of the fundamental excitation model. This parameter might cause deterioration in the estimation accuracy if no extra improving arrangements are adopted [110]. The problem of audible noise, which rises with the usage of high frequency signal injection, re-studied in reference [111] to investigate the optimal injected signal amplitude to minimize this drawback. The proposed approach is based on the speed error of an IPMSM. The

amplitude of the injected current was reduced to a minimal, which did not deteriorate the estimation process. Reference [112] employed the high frequency signal injection to investigate the magnetic saliency of the permanent magnet synchronous machine PMSM. Then, an algorithm for enhanced rotor position estimation at low and zero speeds was presented to support operation of sliding mode controller SMC which was concluded as a new application.

Different thoughts to manage and control the high frequency signal injection was proposed in 2014. Alberti, et al. presented a finite element analysis procedure to define a strategy for predicting the response of HF signal injection in machines controlled by sensorless technique. The novelty in this paper was the proposed strategy which was to be created during the computational design of the machine to be inherently compatible with the machine parameters. The authors mentioned that the experimental results reflected high machine reliability which could make it as a promising tool for machine characterising [113]. Other different trend was suggested by Yang in reference [114] to estimate the rotor position at low speed by the aid of injection of a high frequency square wave. It was based on employment of a single current sensor to re-construct the three-phase currents of the motor. As the injected signal was at the same direction of the d-axis of the rotor, its voltage vector would be vertical on the fundamental voltage vector. Thereby, the saliency reflected current is extracted from the re-constructed dc-link current. This led to a significant reduction in re-construction error and a considerable improvement in sensorless estimation. The author mentioned that this approach was tested successfully on interior permanent magnet at speed of 60rpm.

Reference [115] exploited the high frequency signal injection technique in different manner, where the HF signal response employed to estimate the start-up rotor position of PMSM rather than the low speed rotor position. Two steps were adopted to implement this scheme. The primary rotor position was firstly estimated through sensorless two degree of freedom current control. Secondly, the evaluation of the d-axis inductance change, due to the change in the d-axis fundamental current, determined the rotor magnet polarity. It was concluded that this scheme inherently makes a compensation for error estimation which is a natural characteristic for all initial position estimation methods.

As mentioned before, not only the PMSM, but also other types of machines were controlled through the application of high frequency signal injection technique. In 2014, to implement the sensorless HFSI, reference [116] proposed a scheme to estimate the rotor speed of doubly fed induction motor DFIM. The HFS was superimposed with the stator windings voltage. Correspondingly, a high frequency current should induce into the bars of the rotor. The rotor position information was extracted from this HF induced current and accordingly the rotor speed was estimated. It was mentioned that the MATLAB model, which was designed for this purpose, showed an accurate speed estimation over the full range of motor speed running. Whereas reference [117] (2014) tried different style of high frequency signal injection to estimate the rotor position of concentrated windings surface mounting permanent magnet motor, cwSMPMSM. It was of multi-signal injection approach, where multiple signals, each had different frequency and amplitude, were injected in stator windings. Two main challenges were determined which stood strongly as obstacles against the sensorless control of the cwSMPMSM. First is the weak inductive saliency effect according to the smooth nature of the surface mounted PMSM which make it difficult to extract the rotor position information. Second is the nature of the cwSMPMSM which has multiple strong stator teeth saliencies causing in considerable cogging torque ripples. These ripples were strong enough to make the conventional sensorless control methods inapplicable. According to the literature, all the attempts of the sensorless control for the cwSPMSM were based on the principle of decoupling of the higher order saliencies from the fundamental one. New approach was adopted in [117] which employed multiple signals injection to estimate the rotor position through combining the responses of all injected signals.

The high frequency signal injection technique was also applied in 2014 by [118] to estimate the low speed rotor position of another type of motors called the switch reluctance motor SRM. The SRM are characterised by their high saliency ratio, so the high frequency injecting scheme is regarded as a successful way to estimate the rotor position at low and zero speeds. According to the required accuracy of estimation, the rotor position estimations of SRM can be classified into discrete and continuous methods. By the former, the speed of rotor is firstly estimated and thereby the rotor angle position is calculated. This type of SRM rotor position estimation produces low accuracy estimation. In contrast, the latter method gives a direct estimation for rotor position and

independent on the speed of rotor which makes it more accurate. This work, [118], injected high frequency sinusoidal signals in stator windings and by filtering the HF responses through BPF, the HF component was extracted. Then a series of coordinate transformations and signal filtering were achieved to obtain the currents and rotor position, which were given by the following equations:

$$i_{\alpha\beta} = ke^{j(\frac{\pi}{2}-\omega_r t)}$$

$$i_{\alpha} = k * \sin(\omega_r t) \quad , \quad i_{\beta} = k * \cos(\omega_r t) \quad (3.6)$$

$$\text{Rotor Position } \theta_r = \tan^{-1}(i_{\alpha}/i_{\beta})$$

In addition, there was an attempt in 2014 to control running of induction machine by sensorless estimator based on a high frequency signal injection. Regarding this aim, reference [119] presented a sensorless algorithm based on a square wave injection. It aimed to address two drawbacks which hardly affect the operation of induction machine estimator. They are the multiple saliencies and the deviations in salience orientation under the influence of loading. The former enhances the estimation error and increases the estimation difficulty, whereas the latter makes the error in the estimated position of rotor flux be varied with the speed and torque variations. It was found that injection of square wave type in the estimated synchronous reference frame dropped the error signal harmonics, whereas, the error in salience orientation was minimized when the wave was injected in the q-axis rather than the d-axis of the frame. Thereby, it was concluded that a significant improvement in rotor position estimation was achieved.

3.11 Square wave injection

The rotor position of PMSM at low speed was studied by reference [120] through injection of high frequency square wave into one coordinates of the stationary reference frame, $\alpha\beta$ frame. Then rotor position was retrieved by exploiting the oscillation of current responses which are modulated by the salience position dependence. The authors have determined three benefits for utilizing the square wave as injection signal rather than the sinusoidal. Firstly, the need for filters to decouple the fundamental and injected signals is avoided, and this could simplify the estimator structure. Secondly, elimination

of filters will lead to a significant decrease in estimator time delay which reflects a noticeable improvement in the estimator bandwidth and performance accordingly. Finally, the negative effect of windings resistance variations is considerably degraded.

The direct torque control DTC technique was re-used in 2014 within the high frequency signal injection for sensorless estimation of PMSM rotor position. Reference [121] presented an algorithm based on the DTC to create a SM-PMSM sensorless estimator. The algorithm should have light computational requirements to meet the basic condition of the DTC, short sampling period. In general, there are two advantages stand behind the predilection of DTC in certain applications, they are its relative simplicity and the high torque response. Whereas, there are two other factors which stand as obstacles against the wide usage of the DTC in sensorless estimation techniques. Firstly, it is possible to superimpose the HF into the control algorithm, but it is very hard to do that into DTC source inverter. Secondly, it is the condition of short implementation period for control algorithm which could not be satisfied readily. In spite of that, reference [121] succeeded in modifying the DTC algorithm based on a hysteresis current control to be able to accept an effective HF signal injection.

The inverter effects on the performance of the square wave injection estimator was studied in 2014 by reference [122]. It was mentioned that the inverter nonlinearity distorted the injected voltage and accordingly distorted the induced current which involved the information of rotor position angle. So the inverter distortion can cause a significant estimation error beside its impact on increasing the torque ripple. To tackle this problem, an adaptive signal injection magnitude, not fixed, was proposed by reference [122]. The varied amplitude of the injected voltage should insure a regulated ripple in the induced current. Thereby, a considerable decrease in error estimation and the torque ripple reduction should be noticeable. The authors concluded that an improvement of 17.9% in rotor position estimation at low rotor speed was achieved by adopting this method.

Finally, 2014 witnessed a study for the dynamic and static improvements for the performance of sensorless BLDM estimator at zero speed [123]. The high frequency signal injection technique was applied in this study to satisfy an accurate sensorless estimation for rotor position of BLDM at standstill. The concept is based on employment

of a three-phase HFSI into the stator windings. This is to influence the inherent machine saliency to discover the differences in phase current responses of the motor from which the rotor position is estimated. A simulated model was built to implement the study concept whose result showed a static performance improvement via an accurate rotor position estimation, less than 5° angle estimation error. Meanwhile, a minimum shift ripple torque was detected which reflected a considerable dynamic improvement. The study does not point out the method of magnet polarity detection or if the study tackled this problem.

In 2015, most of the researching efforts went toward the improvement of the HFSI techniques. The standstill rotor position estimation of brushless dc motor BLDM was studied by reference. [124] The stator winding inductances vary with the rotor position particularly in case of salient poles machines. This feature is regarded as a base to build a sensorless estimator to investigate the rotor position. Corresponding to this principle, this work established a scheme based on injection of three short duration pulses into the stator windings and analysis both voltage and current responses. The voltage responses were exploited to make comparisons between the inductances of stator windings and correspondingly divide the whole spatial angular space into six portions each of 30° angle width. Meanwhile, the current responses comparisons define obviously the polarity of rotor magnet. Thereby, the rotor position estimation for BLDM with 30° resolution was achieved within the half of the whole rotor space. Therefore, a technique is required to detect the rotor magnetic polarity and differentiate between the rotor angles in the two halves of the rotor space. Reference [125] presented a high frequency signal injection estimator of an adjustable amplitude injected voltage. The feature of adjustable voltage contributed in creating a significant position error reduction and lowering the torque ripple. The proposed estimator based on utilizing three types of filters; LPF, HPF and BPF. It may be worth to mention that, in the aforementioned literature, there was criticism to the presence of filters in the estimator configuration regarding them as the main reason for the estimation delay and lower estimator bandwidth.

Under the high frequency signal injection, the influence of inverter non-linearity and the proportional integral PI controller affect the accuracy of rotor position estimation. References [126], 2015, and [127], 2016, studied these effects on the IPMSM

and synchronous reluctance drive system respectively. Reference [126] proposed a procedure to cope with the drawback of the inverter non-linearity. Based on the injection of HF rotating voltage and the demodulated stator current, the component of rotor position is isolated from the component of high frequency. Then, the effect of inverter non-linearity was studied through the comparison of the estimated angle and the input command one. However, reference [127] replaced the PI controller, commonly used in construction of controllers, by an adaptive one which modifies its output according to the speed situation. The controller mathematical model was derived to give the amount of reduction in error estimation as a result of considering the effects of unequal mutual inductances and the motor speed influence. The experimental model, which was built around a digital signal processor, showed the superiority of the adaptive controller in the accuracy of rotor position estimation comparing to the conventional PI controller.

Vendula Muzikova and Tomas Glasberger proposed in 2015 a simulated model based on injection of high frequency signals to exploit the machine anisotropy to estimate both the rotor position and speed. The model involved two methods; sliding mode control, SMC and direct torque control, DTC. In field of electrical drives, the authors defined that the SMC and DTC have the advantages of; simplicity, fast torque and stator flux responses and efficient operation due to the short sampling period. Whereas the switching frequency, which is not constant during the stator period, is regarded as the main disadvantage of DTC. This is because it is a function of; rotor speed, load torque and the bandwidth of flux and torque hysteresis controllers. To meet their goals, the authors presented an algorithm for DTC mode through which the current was injected in the d-axis of the coordinate system, while for SMC, both d and q components of the stator current vector were controlled [128].

3.12 Improve the HFSI performance

The trend of researches in 2015 was still focusing on improvement of the sensroless drives of PMSMs at low speed through exploiting the high frequency signal injection. This trend can be explored via five works. Firstly, reference [129] presented a simulated MATLAB model to improve the speed estimation drive of PMSM at low speed. The proposed method worked according to comparing the desired input speed with the actual

motor speed to obtain speed error signal which was employed to produce a corresponding torque signal to run the motor. In the feedback loop, the rotor position estimation was extracted from the motor currents responses by aid of external signal injection. Meanwhile, reference [130] contributed in this trend of improvement through investigating the effect of inductance harmonics on the performance of the PMSM low speed rotor position estimators under the influence of high frequency signal injection. As it is known, the stator winding inductance of PMSM is strongly related to the rotor magnetic saliency. Accordingly, there will be a corresponding relation between this inductance and the accuracy of rotor position estimation. The effect of inductance harmonics was examined through both simulated model and practical experiment. They proved a significant reduction in position estimation error when those harmonics were considered.

Another concept for improvement of IPMSM rotor position estimation was proposed by reference [131]. The work concentrated on the drawbacks related to the presence of filters in the heterodyning process. The proposed method was to eliminate those filters from the estimator construction, and alternatively an algorithm was adopted. This algorithm was based on the differences between motor voltage and current equations in stationary reference frame. The rotor position then was deduced directly from the envelope of the obtained data. The same improvement, through coping the drawbacks of filters, was the aim of reference [132]. However, this reference did not eliminate the filters but compensated their delay effect. According to the analysis of main reason for this delay and an accurate determining to its magnitude, it was added to the input of the observer, whose outputs were both the speed and rotor position, to be taken into consideration. Finally, reference [133] presented an improvement based on different way in generating the high frequency injection signal, where it was proposed to achieve the generation through shifting the duty cycle between two adjacent switching intervals. This proposed technique allows to raise the value of injection frequency to half of the inverter switching frequency.

3.13 The HFSI in different applications

Different applications for high frequency voltage/current injection, which did not consider the rotor position estimation, emerged in 2015. Reference [134] achieved maximum torque per ampere MTPA for interior permanent magnet synchronous motor IPMSM by exploiting the high frequency signal injection. The estimation of magnet temperature in PM machines was the topic of reference [135]. It was satisfied through injection a high frequency pulsating current and then measuring the reflected high frequency resistance rising as a result of temperature effect on the permanent magnet. Whereas, Shih-Chin Yang employed the injection of high frequency pulsating voltage in two studies in domain of IPMSM stator windings fault [136], [137]. Firstly, in detection of the faults which occur in stator windings, and secondly, in evaluation of the fault detection performance in case of inverter fed PM machines. Differently, Fernandez, et al. also presented two studies to show the effects of high frequency signal injection on PMSM, but in field of estimation the magnetization state of IPMSM [138], [139]. The first was to study the variation in magnetization state of IPMSM in both cases standstill and running by injecting high frequency signal and estimating the magnetization in magnet type Samarium-Cobalt, SmCo, while the second was to estimate the magnetization state by investigation of the variation in high frequency stator resistance due to the injection of high frequency signal.

The year 2015 also witnessed a high frequency signal injection in sensorless control running of other motors rather than the PMSMs. The literature demonstrates the following three works which were achieved in 2015. A model for 9-phase concentrated wound IPM motor, which was undertaken in 2014 too, was presented to be controlled by injecting a high frequency into stator windings and estimating the rotor position and speed [140]. The rotor position sensorless vector control for doubly fed induction motor returned to be studied in 2015. The study this time was through the gate of comparison between stator and rotor currents without taking into consideration the machine parameters [141]. The switch reluctance motor SRM, whose rotor position estimation was analysed in 2014, was re-studied in 2015 according to the same principle of the previous year, coordinates transformations. However in this paper, a synchronisation

was to be done between the angular fundamental frequency of the 3ph inductance and the rotating speed of the space vector [142].

In contrast of the conventional HF signal injection methods, which is based on tracking the rotor position through the saliency investigation, reference [143] proposed (2016) a different method to estimate the rotor position. It was directly detected from the current response which comes as a result to a HF pulsating signal injection into the fixed-frequency estimated stationary reference frame. The current response which yields the rotor position should be followed by another procedure to detect the rotor magnet polarity through injection of another HF carrier voltage into the estimated rotor position. It was concluded that the proposed strategy showed a rotor position estimation of perfect steady state and dynamic performance. Whereas, Xu and Zhu exploited the zero-sequence voltage, resultant from the injection of carrier signal, to achieve sensorless control for PMSM based on the estimate reference frame. It was concluded that this proposed scheme was simpler, more reliable and robust than the conventional procedure [144].

3.14 Evaluation of HFSI estimation

The accurate sensorless rotor position estimation has an essential role in maintaining consistent running for PMSM. At medium and high speeds, this process is currently achieved with high accuracy according to sense the back EMF at motor terminals. Whereas, the issue at zero and low speeds is not completely resolved. However, the technique of high frequency signal injection HFSI is the more considerable in dealing with this problem right now. To make an evaluation to performance of this technique up to this point, it is important to highlight the strengths and weaknesses of this estimation method, which all concern the cost, complexity of hardware, range of speed, torque ripple and computational efforts.

The implementation of HFSI requires a complicated algorithm that has to be employed in order to control measuring and computing the necessary processes in the forward direction of the estimator. This algorithm always cause an intensive computational process. On the other hand, various types of filters are required to

implement the estimator feedback path, which is necessary to separate the injected and fundamental frequencies. These filters hardly affect the overall estimator performance through causing a delay time, where the estimator response time will be longer and correspondingly the estimator bandwidth will be narrower. Accordingly, the machine operating range will be narrower [90].

The other side of the estimation processing speed problem is represented by the time response of some electrical machine parameters. In spite of the delay time caused by the filters, some electrical machine parameters are still too slower in their response to follow the speed of HFSI process. So, it is necessary to test these machine parameters during the machine design stage so as to overcome this problem before putting the machine in the actual running case [113].

The position estimation error varies with the value of load condition, and it becomes more noticeable in case of heavy loads. This point has been highlighted by reference [45]. It has mentioned that, the heavily loaded motor shaft has an effect on the distribution of the HF inductance, which represents the response of stator windings to the injected HF. This compact comes as a reaction from the armature against the loading condition on the shaft. Therefore, the accuracy of rotor position estimation will highly drop. Reference [104] has mentioned this reason, which deteriorates the accuracy of HFSI estimation in case of heavy load, by another way when it referred to the saturation and cross coupling influence in stator windings at heavy load condition. Although there is no any referring in the literature to a certain effect for cogging torque on the accuracy of rotor position estimation at low speed, but it is strongly thought that this effect may be present in some form.

3.15 State-Of-Art

Practically, two main approaches are in use for zero speed rotor position estimation. The first depends on impulse response which is adopted in this thesis being cost effective [145][146] and simple to be implemented [124][147]. The following efforts in this approach are summarised:

1. In 2018, a paper has been published on the (IEEE TRANSACTIONS ON POWER ELECTRONICS) to estimate the rotor position at standstill and low speed. It was mentioned that the position error, resolution, is within 20 degrees [148].
2. In 2017, a group of researchers from (College of Electrical and Information Engineering, Hunan University, Changsha 410082, China) presented a paper (published on IEEE transaction on machines) to estimate the initial rotor position through injection of a voltage vectors. It was stated that the method has a good resolution but the work was done with 15° step between any two successive tests for rotor position estimation [149].
3. In 2015, three of researchers from (Cochin University of Science and Technology, India) presented a proposed method based on injection of three pulses in the stator windings and compare the current and voltage responses to obtain rotor position with resolution of 30° . The work did not include any other analysis but only the comparisons of current and voltage responses. The comparison results were summarised by the following table [124].

Table 3. 1: Comparisons results given by reference [124]

Phase Voltage Comparison	Inductance Comparison	Possible Initial Position	3 rd Injection	Peak Current	Initial Rotor Position
$V_{NB1} > V_{NA1}$ $V_{NC2} \geq V_{NA2}$ $V_{NB1} > V_{NC2}$	$L_B > L_C \geq L_A$	$0^\circ < \theta_0 < 30^\circ$ $180^\circ < \theta_0 < 210^\circ$	T_{C-}, T_{A-}	$I_2 > I_3$ $I_2 < I_3$	$0^\circ < \theta_0 < 30^\circ$ $180^\circ < \theta_0 < 210^\circ$
$V_{NB1} \geq V_{NA1}$ $V_{NC2} < V_{NA2}$ $V_{NB1} > V_{NC2}$	$L_B \geq L_A > L_C$	$30^\circ < \theta_0 < 60^\circ$ $210^\circ < \theta_0 < 240^\circ$	T_{C-}, T_{A-}	$I_2 > I_3$ $I_2 < I_3$	$30^\circ < \theta_0 < 60^\circ$ $210^\circ < \theta_0 < 240^\circ$
$V_{NB1} < V_{NA1}$ $V_{NC2} < V_{NA2}$ $V_{NB1} \geq V_{NC2}$	$L_A > L_B \geq L_C$	$60^\circ < \theta_0 < 90^\circ$ $240^\circ < \theta_0 < 270^\circ$	T_{C-}, T_{A-}	$I_2 > I_3$ $I_2 < I_3$	$60^\circ < \theta_0 < 90^\circ$ $240^\circ < \theta_0 < 270^\circ$
$V_{NB1} < V_{NA1}$ $V_{NC2} \leq V_{NA2}$ $V_{NB1} < V_{NC2}$	$L_A \geq L_C > L_B$	$90^\circ < \theta_0 < 120^\circ$ $270^\circ < \theta_0 < 300^\circ$	T_{B-}, T_{A-}	$I_3 > I_1$ $I_3 < I_1$	$90^\circ < \theta_0 < 120^\circ$ $270^\circ < \theta_0 < 300^\circ$
$V_{NB1} \leq V_{NA1}$ $V_{NC2} > V_{NA2}$ $V_{NB1} < V_{NC2}$	$L_C > L_A \geq L_B$	$120^\circ < \theta_0 < 150^\circ$ $300^\circ < \theta_0 < 330^\circ$	T_{B-}, T_{A-}	$I_3 > I_1$ $I_3 < I_1$	$120^\circ < \theta_0 < 150^\circ$ $300^\circ < \theta_0 < 330^\circ$
$V_{NB1} > V_{NA1}$ $V_{NC2} > V_{NA2}$ $V_{NB1} \leq V_{NC2}$	$L_A > L_B \geq L_C$	$150^\circ < \theta_0 < 180^\circ$ $330^\circ < \theta_0 < 360^\circ$	T_{B-}, T_{A-}	$I_3 > I_1$ $I_3 < I_1$	$150^\circ < \theta_0 < 180^\circ$ $330^\circ < \theta_0 < 360^\circ$

Moreover, this paper summarises the rotor position estimation for relevant works by the following:

- ◆ In 2003, Chinese researchers published a paper on considering (Initial Position Detection Technique for Three-Phase Brushless DC Motor without Position and Current Sensors). A resolution of 60° was achieved [145].
 - ◆ In 2002, three researchers (from China) published a paper on IEE focusing on position detection and start-up of BDCM. A resolution of 60° was achieved [150].
 - ◆ In 1997, researchers from (Rockwell Automation, Advanced Technology Labs, United States) published a paper on IEEE Industry Applications Society considering the zero speed rotor position estimation. Accordingly. A resolution of 22.5° was achieved [147].
4. In 2015, researchers from (the School of Electrical Engineering, Southeast University, China) presented a paper at (the Conference of Electrical Machines and Systems, Thailand) to estimate the zero speed rotor position through pulse injection. The achieved resolution was not mentioned, but from the given results one may deduce it is 1 degree [151].
 5. In 2007, researchers from the (National Electronics and Computer Technology Center, Thailand) presented an approach to estimate the initial rotor position of SRM. A resolution of 15° was achieved [146].

In the above works, the estimation process was achieved depending mainly on the comparisons among the motor responses to predict the domain, sector, of the rotor position. In this thesis, an extra analysis was added within each domain. This addition focused on the mille-volt variations in motor responses within each domain. Thereby, it becomes possible to improve the domain resolution to approach the unity.

The second approach bases on continuous injection of HF carrier signal and the following efforts are summarised:

1. In 2015, researchers from the “Research Center for Motion Control of MOE, Southeast University, Nanjing, China” presents a paper [152]. The paper method based on injecting high frequency low voltage pulses. The proposed method divided

the whole rotor space into 12 sectors each of 30° . A technique was employed to detect rotor polarity. The given results showed an estimation resolution of 1° with an error up to 5° in each estimated position. Following, is the graph of the paper results.

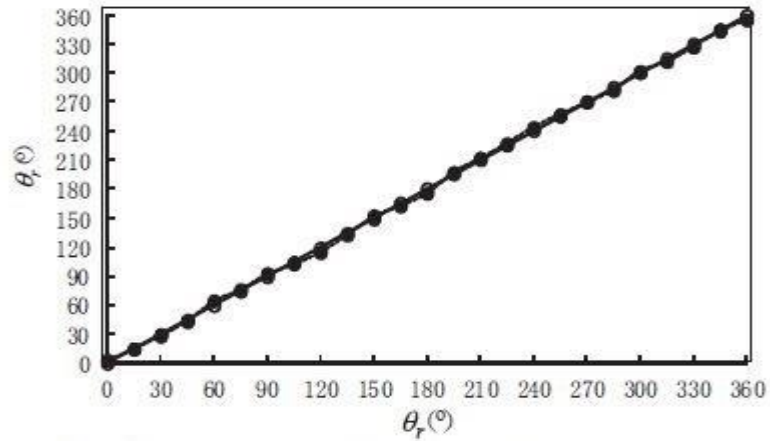


Fig. 3. 10, Estimation results given by reference [152]

- In 2010, researchers from “School of Electrical Engineering and Automation, Harbin Institute of Technology, Harbin, China” presented method for initial rotor position estimation which was based on injecting a high-frequency rotating voltage signal into stator winding to obtain the rotor pole position. In order to identify magnet polarity, two voltage signals are injected. The given results showed an estimation resolution of 1° with an error up to $\pm 4.2^\circ$ in each estimated position. Following, is the graph of the paper results [153].

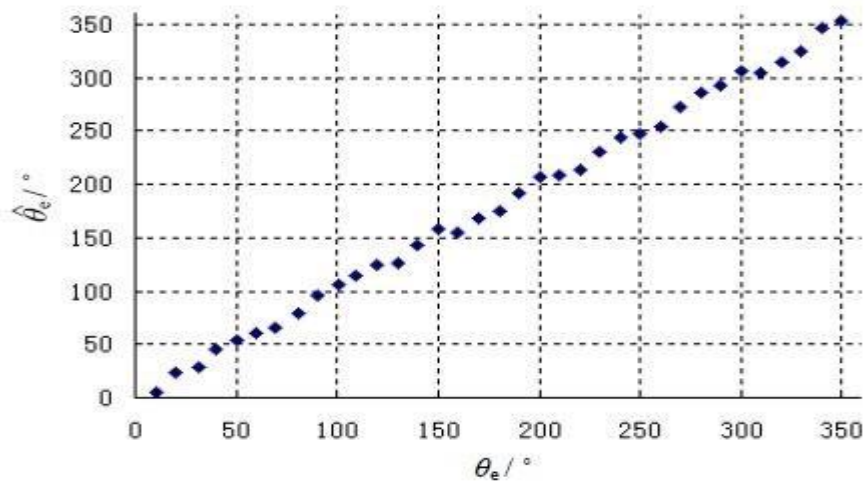


Fig. 3. 11, Estimation results given by reference [153]

3. In 2014, researchers from “Automation College of Science and Engineering, South China University of Technology” presented a paper for zero-speed rotor position estimation based on injecting a rotating voltage of 500 Hz/430 V. No technique for magnet polarity detection was required. The given results showed an estimation resolution of 1° with an error up to $\pm 2.8^\circ$ in each estimated position. Following is the graph of the paper results [154].

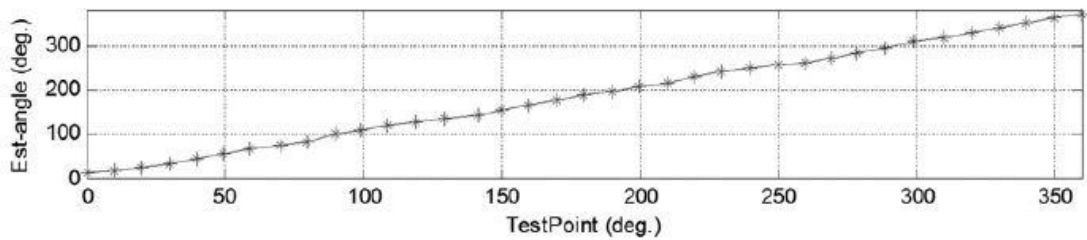


Fig. 3. 12, Estimation results given by reference [154]

4. In 2017, researchers from the College of Electrical and Information Engineering, Hunan University, Changsha 410082, China proposed a method bases on continuous injection of square pulses in stator windings to estimate the rotor position at zero-speed. The obtained results presented a resolution of 1° with estimation error up to 3° varies with each position [155].
5. In 2018, researchers from Northwestern Polytechnical University presented a work for Initial Rotor Position Estimation based on injection of a square wave. A position resolution of 3° was obtained [156].

3.16 Summary

This chapter presents a survey for estimating the rotor position of PMSM at zero and low speeds through four main frames.

- ❖ Firstly, **rotor position**, a demonstration is presented for the points that are related to; the importance of rotor position estimation to achieve a safe and high performance running strategy for PM motor, the obstacles that are related to the

implementation of this topic and a classification for the currently adopted methods in this field of study.

- ❖ Secondly, **chronological review**, a historical timeline for the researching attempts to solve the various problems, which are related to estimate the rotor position of PMSM at zero and low speeds, is explored. It is found that, the previous works tried to address the key point of rotor position estimation through exploiting different approaches, which are related to; machine inherent features, modifying the machine structure, utilizing different estimator control strategies ... etc. Therefore, this chronological review is also previewed hereby accordingly.
- ❖ Thirdly, **high frequency signal injection**, a wide domain of reviewing is assigned in this chapter to explore the earlier works, which adopted the technique of high frequency signal injection to build the estimators of prediction the rotor position at zero and low speeds of motor running conditions. This is because this technique has currently a wide-range of applications in this field.
- ❖ Fourthly, **addressing the drawbacks**, this chapter has also explored the researching efforts to improve the performance of rotor position estimators at zero and low speeds through tackling the drawbacks that are accompanying the applied estimating strategies. The main points, which were targeted by the researchers, are related to; noise reduction, filtering processes minimisation and avoiding the huge mathematical computations.
- ❖ Fifthly, HFSI in different applications, rather than rotor position estimation, has been reviewed, as well, in this chapter.
- ❖ Sixthly, an evaluation for the accuracy of currently adopted methods, in field of rotor position estimation at zero and low speeds, has been presented.
- ❖ Finally, **assessment**, a brief evaluation for the technique of high frequency signal injection is presented, by this chapter, through exploring its strength and weakness points.

CHAPTER FOUR

INVESTIGATION OF ZERO-SPEED ROTOR POSITION

THROUGH MODELLING SYSTEM

4.1 Introduction

Over the past two decades, the permanent magnet synchronous motors PMSMs have become in a considerable position among the motor applications. This comes from the characteristically brilliant features of the PMSMs in spite of being more expensive application than the conventional motors, like the induction machines. For instance, the environment pollution and climate changes are currently an enormous challenge around the world. The diesel-powered engines have an essential contribution in this trouble situation [157]. Gradually, the friendly environment electric vehicles, EV, based on PMSM engines have proceeded to substitute the CO₂ contaminated vehicles. This is because of the promising features of the PMSM in this type of applications, which is summarized by the best fuel consumption, no pollution of CO₂ emissions, higher reliability, higher size to power ratio and faster speed response [19], [158]–[162]. However, the general essential properties of PMSMs, which has opened wide application areas towards these motors, are the high efficiency of power consumption, flexible controlling, non-noisy and robust operation, small size, ... etc. [73], [125], [139], [160]–[163].

These features of the PMSMs are highly related to the timing sequence of the commutation process by which the excitation of the stator windings should be performed. However, the commutation circuitry needs an accurate information about the rotor position angle as a prior condition to work properly. Therefore, as the commutation process is the key term in optimum operation of PMSM, consequently, the accurate rotor position estimation is regarded as a crucial element to maintain best running for this motor. The required position information is provided, with high precision, by adopting one form of sensing techniques, which are given in section 2.9 of chapter 2. However,

the adoption of sensors has remarkable drawbacks such as their high cost, unreliable usage, large size... etc. [57]. To overcome the sensor usage obstacles, the majority of researching attentions has turned toward the sensorless techniques [57], [73], [164].

4.2 The problem of rotor position estimation at zero-speed

At medium and high motor speeds, the sensorless techniques for rotor position estimation are dependent upon detection of the induced back electromotive force, back EMF (the zero-crossing points at BDCM). However, at low speed, a problem emerges due to the weakness in the back EMF that makes it immeasurable and cannot be employed in position estimation. Moreover, the back EMF totally disappears at zero motor speed. These hard situations, at zero and low speed, are a consequence for the direct relation between the induced back EMF and motor speed. Therefore, the efforts of sensorless rotor position detection at zero and low speed have focused on exploiting the machine magnetic saliency as an alternative solution [10].

Another problem has emerged at zero and low speed rotor position estimation. The problem is related to the rotor magnetic isotropy, it is called the magnet polarity. To illustrate this topic, let us suppose that it is required to estimate the rotor position of a PM motor whose rotor has one pole-pair. This means the rotor has one North Pole and one South Pole. Then the rotor magnetic cycle will repeat frequently every 180° . Therefore, it might not possible to distinguish between the angle (x) and the angle ($x+180^\circ$) because they are under the same magnetic effect. The situation becomes worst as the pole-pairs increases. Reference [165] studied the magnetic polarity on rotor position estimation. It exploited the stator core saturation effect to determine the position of the North-pole. Figure 4.1, as given by reference [165], demonstrates the magnetic polarity and concept of core saturation.

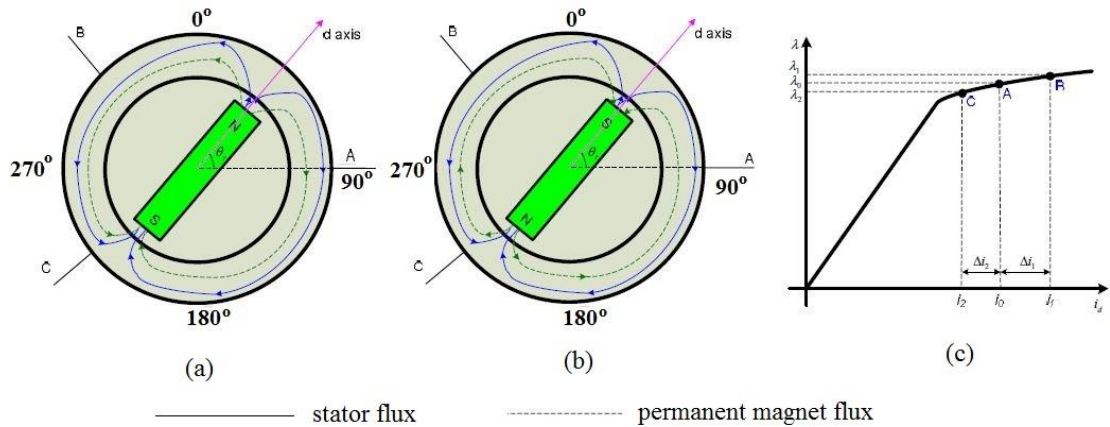


Fig. 4. 1, Concept of magnetic polarity and its saturation effect

Accordingly, the methodology of zero and low speed rotor position estimation includes two steps. The rotor position should be primarily detected and next the rotor magnetic polarity is found out. The results of these two steps are added to decide the final rotor position estimation method.

4.3 Mathematical model of PMSM

Modelling is the science or art of extracting the characteristics of a corresponding real-world system. This happens through representing an actual hardware system into a mathematical computerized model. Thereby, the actual system behaviour is facilitated and a better understanding for its operation is visualized. By modelling, it becomes easy to optimize or improve the system behaviour through the soft modification of the modelled system parameters and testing its new performance. In general, the models are either statics or dynamic. Any model, which is not time variant, is classified as a static model, i.e. the system steady-state condition [166].

The following assumptions were taken into consideration in modelling the PMSM in this topic:

- a) The following symbols represent the modeled PMSM parameters:
 - R_s represents the stator phase resistance.
 - L_d , the equivalent stator phase direct inductance in rotor reference frame, d-axis direction, which responsible for generation the field current I_d , (see figure 2.28 for more details).

- L_q , the equivalent stator phase quadrature inductance in rotor reference frame, q-axis direction, which responsible for generation the torque current I_q , (see figure 2.28 for more details).
 - λ_m is the rotor flux linkage.
 - λ_d and λ_q are the flux linkages in d and q directions respectively.
 - p is the rotor pole-pair number.
 - V is the voltage value of the 3-phase input source.
 - f is the input voltage frequency.
 - J is moment of inertia. Kg.m^2 .
 - B is viscous damping N.m.s .
 - T_L and T_d are the applied load and the drive torque respectively.
- b) Values of motor parameters are loaded via an m-file.
 - c) The saturation effect, eddy currents and hysteresis losses are neglected.
 - d) Back EMF is sinusoidal to satisfy the PMSM modelling.

Then, the following necessary blocks were modelled:

4.3.1 Transformation of stator variables to stationary reference frame

The following matrix form relation could achieve the transformations of the stator variables to the stationary reference frame, according to Clarke transformation. The stator voltages, V_a , V_b , and V_c , were taken as a base for this transformation [59].

$$\begin{bmatrix} V_\alpha \\ V_\beta \end{bmatrix} = \frac{2}{3} \begin{bmatrix} 1 & \frac{-1}{2} & \frac{-1}{2} \\ 0 & \frac{\sqrt{3}}{2} & \frac{-\sqrt{3}}{2} \end{bmatrix} \begin{bmatrix} V_a \\ V_b \\ V_c \end{bmatrix} \quad (4.1)$$

4.3.2 Transformation between stationary and rotary reference frames

4.3.2.1 Stationary to rotary reference frame

The following matrix is employed to achieve the modelling for this transformation.

$$\begin{bmatrix} V_d \\ V_q \end{bmatrix} = \begin{bmatrix} \cos(\theta) & \sin(\theta) \\ -\sin(\theta) & \cos(\theta) \end{bmatrix} \begin{bmatrix} V_\alpha \\ V_\beta \end{bmatrix} \quad (4.2)$$

4.3.2.2 Rotary to stationary reference frames

This modelling is satisfied by exploiting the following transformation matrix

$$\begin{bmatrix} V_\alpha \\ V_\beta \end{bmatrix} = \begin{bmatrix} \cos(\theta) & -\sin(\theta) \\ \sin(\theta) & \cos(\theta) \end{bmatrix} \begin{bmatrix} V_d \\ V_q \end{bmatrix} \quad (4.3)$$

4.3.3 Modelling the motor fields λ_d and λ_q

Generation of the currents of rotor reference frame is obtained from the motor fundamental equations. Reference referred to the PMSM equations is achieved by the following matrix [167]:

$$\begin{bmatrix} V_q \\ V_d \end{bmatrix} = \begin{bmatrix} R_s & 0 \\ 0 & R_s \end{bmatrix} \begin{bmatrix} I_q \\ I_d \end{bmatrix} + \begin{bmatrix} \frac{d}{dt} & \omega_r \\ -\omega_r & \frac{d}{dt} \end{bmatrix} \begin{bmatrix} \lambda_q \\ \lambda_d \end{bmatrix} \quad (4.4)$$

where λ_d is the total linkage flux in the direct axis, which is derived from eq.(4.4) as:

$$\lambda_d = \int (V_d - R_s * I_d + \omega_r * \lambda_q) \quad (4.5)$$

Similarly, the total linkage flux in the quadratic direction, q, is given by:

$$\lambda_q = \int (V_q - R_s * I_q - \omega_r * \lambda_d) \quad (4.6)$$

These two equations of linkage fluxes are modelled as shown in figure 4.

It should be noticed that, up to this point, the currents I_d and I_q are not generated yet. They will be calculated in the next modelling block and feedback to the inputs of this model.

4.3.4 Modelling the stator currents in the rotor reference frame

The total magnetic field in the direct axis, d-axis, is the combination of the d component of the stator field and the rotor magnet field. This is mathematically expressed by:

$$\lambda_d = L_d I_d + \lambda_m \quad (4.7)$$

From which yields:

$$I_d = \frac{\lambda_d - \lambda_m}{L_d} \quad (4.8)$$

Whereas, the magnetic field in the quadratic direction, q-axis, is solely given by the q-component of the stator field, which mathematically is given by:

$$\lambda_q = L_q I_q \quad (4.9)$$

Thereby:

$$I_q = \frac{\lambda_q}{L_q} \quad (4.10)$$

4.3.5 Modelling the motor outputs

Three of the motor outputs will be considered here. They are the electromagnetic torque T_e , the angular speed ω_r and the rotor position angle θ . Recalling the electromagnetic torque equation, which is expected to be generated by the modelled PMSM, as it is given in chapter 2, yields:

$$T_e = \frac{3}{2} \frac{P}{2} \{(L_q - L_d)I_q I_d + \lambda_m I_q\} \quad (4.11)$$

This torque equation is corresponding to motor parameters. Whereas, the dynamic electromagnetic torque equation of the PMSM, as given by reference [168], is shown below:

$$T_e = T_L + B * \omega_m + J \frac{d(\omega_m)}{dt} \quad (4.12)$$

Integration of this equation yields the motor angular speed ω_r , rad/s:

$$\omega_r = \frac{1}{J} \int (T_e - T_L - B * \omega_r) dt \quad (4.13)$$

Then, integration the motor angular speed produces the mechanical rotor position angle, θ , in radian:

$$\theta = \int \omega_r dt \quad (4.14)$$

Accordingly, the PMSM is modelled according to the above equations as shown below by figure 4.2.

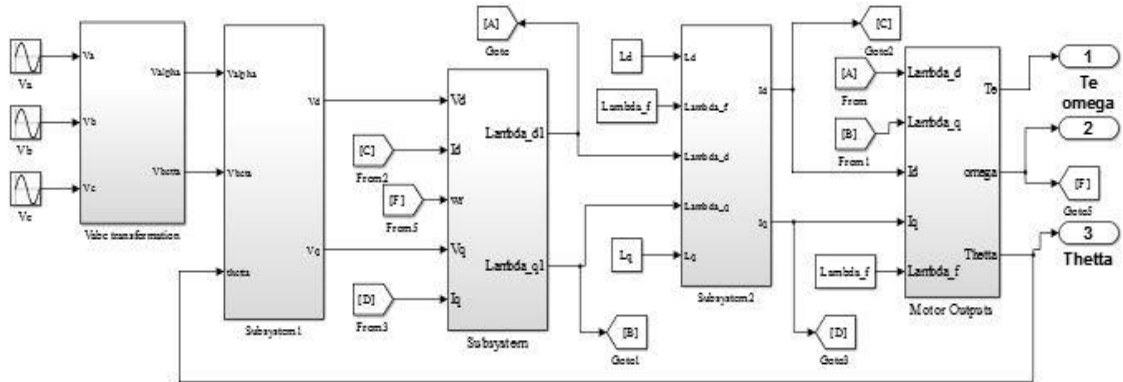


Fig. 4. 2, The complete modelling system for PMSM

4.4 The proposed method for modelling the ZSRPE

4.4.1 Basic concept

In order to simulate the zero-speed rotor position estimation ZSRPE, a “MATLAB” model has been built. This model will be used, in the next chapter, as a base to implement the practical platform. The “MATLAB” simulated model was based on injection of high frequency pulses into the stator windings. This was to make the machine saliency to be more measurable parameter, which would cause in a considerable sinusoidal oscillation in the stator winding inductances with rotor position. Then, the model tracked the inductance variations to obtain the required estimation for rotor position of the PMSM at standstill.

The proposed model injects a sequence of square pulses into the stator coils of the motor. Each pulse has a total period of $300\mu\text{sec}$, 50% duty cycle. This period, which was also used by other researchers [124], should be chosen to be smaller than the time constant of the motor windings so as to avoid the rotor response during pulse injection. Figure 4.3 illustrates the shape of the injected pulses.

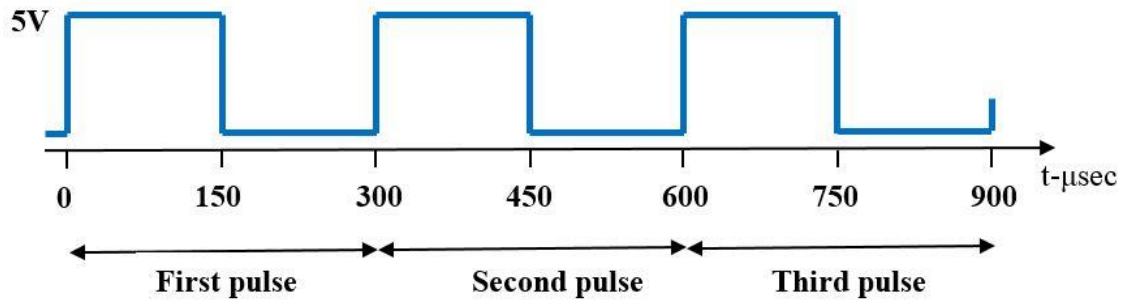


Fig. 4. 3, Sketch of the injected pulses

The model should measure either the motor terminal voltages and currents or the voltages only. Then, the measurements are analysed to extract two numbers which are used as address lines to access a memory structure, or a 2D lookup table structure. The value of the corresponding rotor position angles are stored in the internal cells of that structure of memory or lookup table. Figure 4.4 demonstrates the proposed idea.

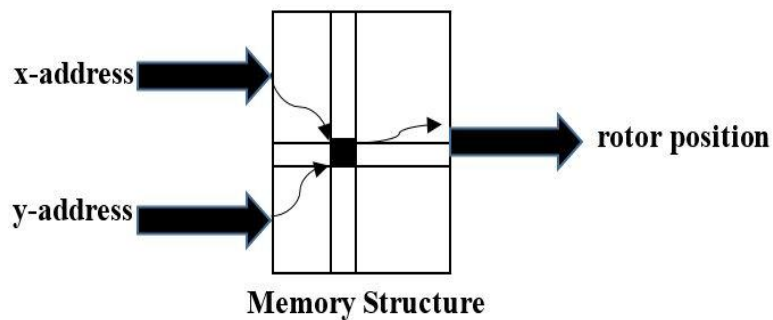


Fig. 4. 4, The proposed memory structure for picking up the rotor position

Figure (4.5) is a block diagram to illustrate the basic implementation view for concept of the proposed method which depends upon the pulse injections to estimate the rotor position of PMSM.

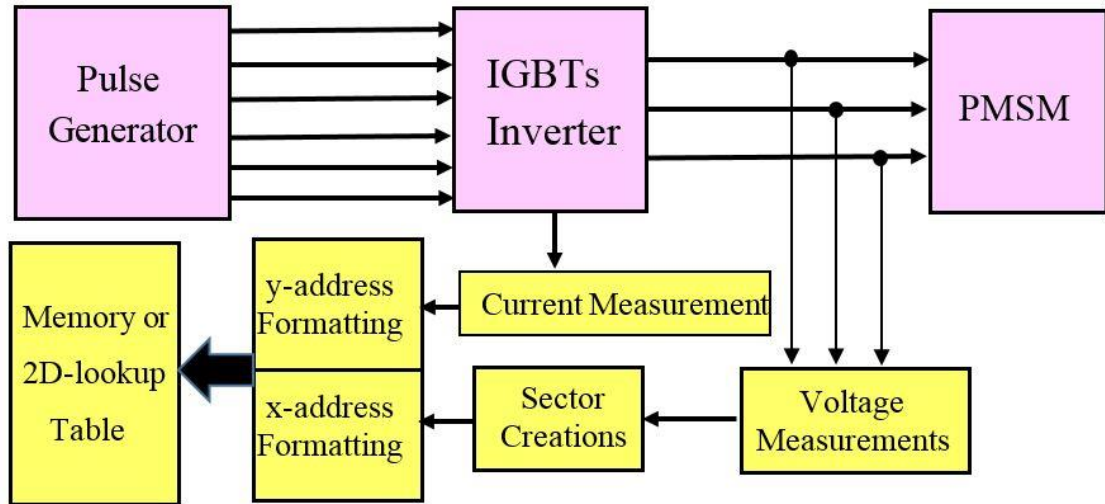


Fig. 4. 5, Pulse injection in the zero speed “MATLAB” model

4.4.2 Formatting the x-address from the voltage measurements

This formatting was achieved through employing the voltage and current measurements to create two address lines, x and y lines as illustrate below. These voltages and currents appeared as responses to pulse injections.

4.4.2.1 Voltage waveform formations

Each pulse injection generates two waveforms, so six waveforms were obtained from the injection of three pulses. Here, it is going to discuss the methodology of generation four waveforms from injection of two pulses. At zero-speed, any two coils of the stator windings of a 3-ph permanent magnet synchronous motor can be excited in series through some form of excitation voltage. The third non-excited coil may be exploited to observe the voltage drops across the two other excited coils. Figure (4.6) illustrates the adopted method, in this work, for applying a pulse voltage, of 150 μ sec duration time, between the terminals of coils A and B. This is the first pulse, which was applied in the work. The corresponding current (I_{on}) is shown by a solid line, passing through the coils.

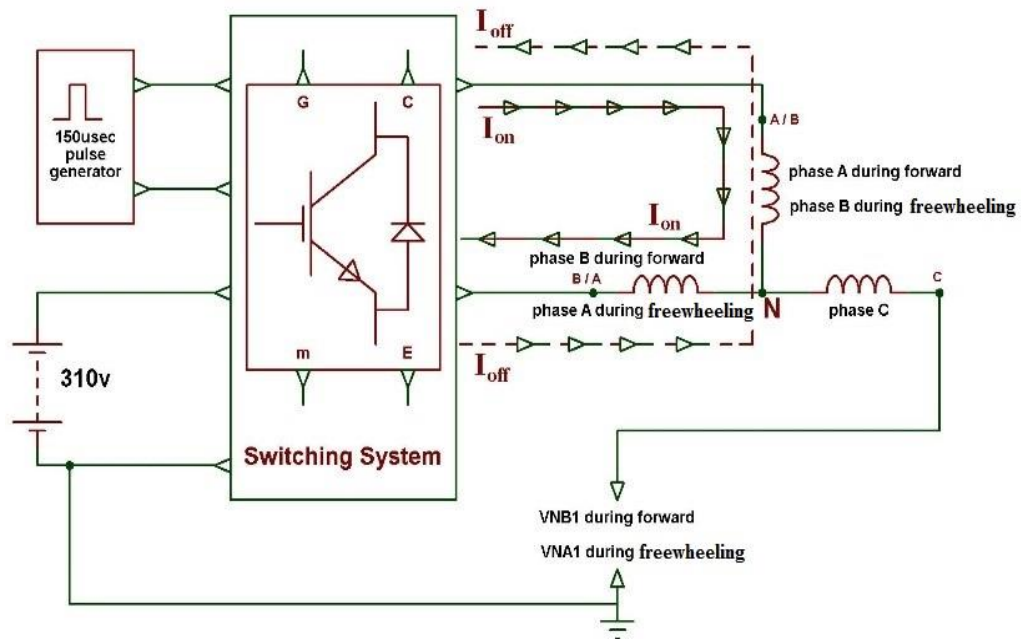


Fig. 4. 6, Excitation of coils A and B by the first pulse and the freewheeling reaction

Then, the measured voltage, between the free terminal of coil C and the ground, indicated the value of voltage between the neutral point N and the other terminal of coil B, so this voltage is labelled as V_{NB1} where the subscript '1' refers to the measured voltage due to the injection of first pulse. After 150µsec, the excitation pulse disappeared and the connection of coils A and B was reversed under the action of a freewheeling process via the inverter elements, IGBTs. This process allowed to flow the freewheeling current (I_{off}), which is illustrated in figure (4.12) by a dashed line. So, another voltage at the terminal of the free coil, coil C, was sensed which represented the voltage drop across coil A and therefore it is labelled as V_{NA1} . Thereby, the voltage waveforms V_{NB1} and V_{NA1} are formed.

Same events repeated to form the voltage waveforms V_{NC2} and V_{NA2} when the second pulse excited the windings A and C, as shown in figure (4.7), where the two voltages V_{NC2} and V_{NA2} were obtained at the free terminal of the third non-excited coil, coil B. Again, the subscript '2' refers to the voltages measured after applying the second pulse with same duration of 150µsec. Similarly, the voltages V_{NB3} and V_{NC3} were measured at the free terminal of coil A when a third pulse was injected into the series coils B and C.

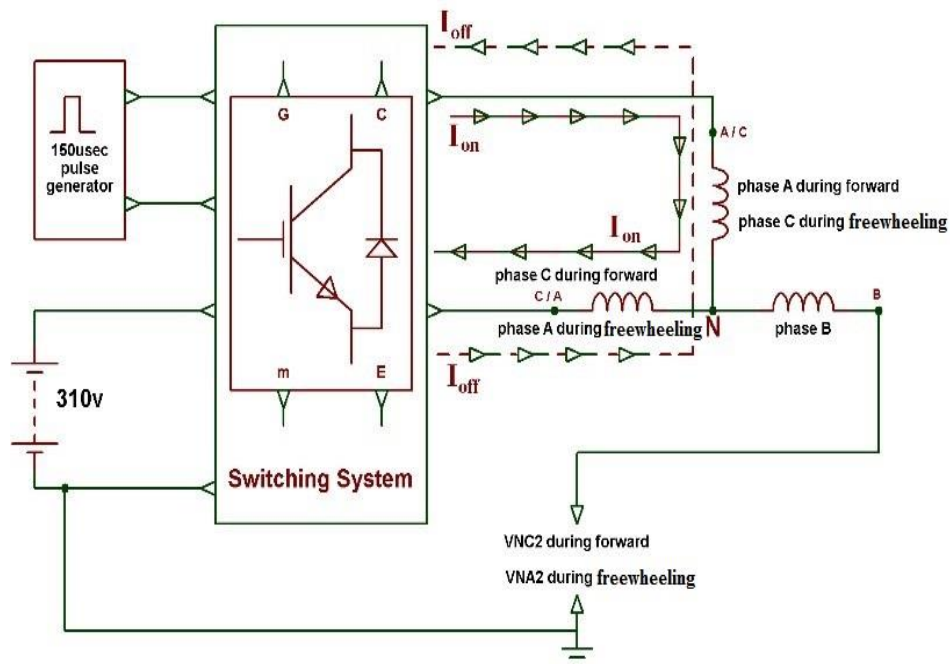


Fig. 4. 7, Excitation of coils A and C by the second pulse and the freewheeling reaction

4.4.2.2 Defining a specific value for each waveform

The voltages waveforms V_{NB1} , V_{NA1} , V_{NC2} and V_{NA2} are shown in figures 4.8(a) and 4.8(b) as they appeared in the simulation results. Next, to define a specific value for each waveform, the voltage at the middle of each period was picked up. This was achieved through employing four narrow pulses, very short duty cycle 10 µsec, which were centered at the middle of each waveform. The proposed model generated these pulses and they are shown in figure 4.8(c). Finally, the waveforms and the narrow pulses were multiplied. Thereby, the voltage value at the middle of each waveform was obtained. These four values are shown in figure 4.8(d). Therefore, figure 4.8 illustrates the modelling procedure for measuring the voltages V_{NB1} , V_{NA1} , V_{NC2} and V_{NA2} when the rotor was at position 45°.

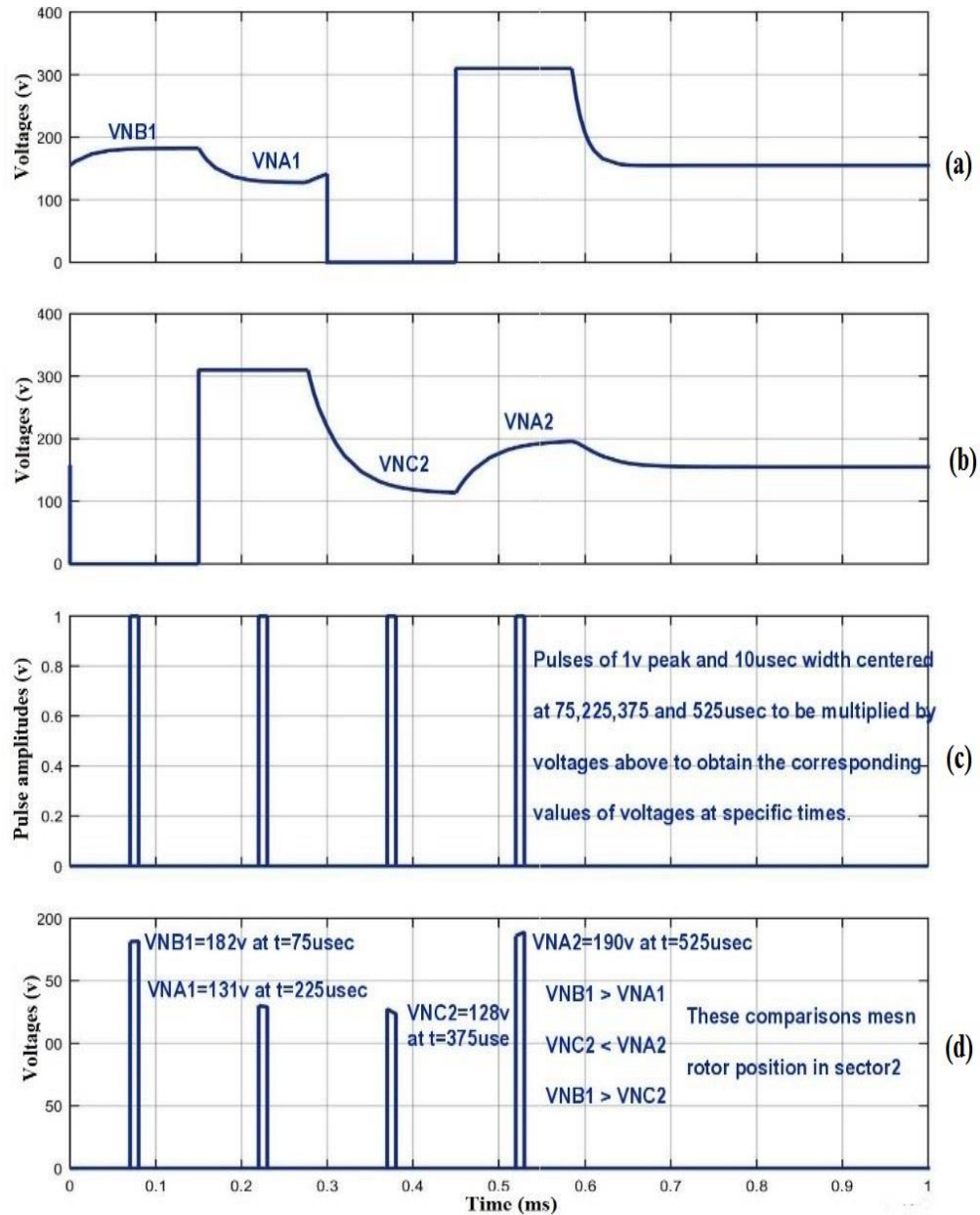


Fig. 4. 8, The zero-speed voltage measurements of PMSM at rotor positions 45°

This measuring procedure was repeated for rotor position varying from 0° to 360° and the corresponding four voltages shapes, V_{NB1} , V_{NA1} , V_{NC2} and V_{NA2} , over the whole rotor spatial space were obtained as given in figure (4.10).

4.4.2.3 Rotor space sectors and x-address creation

Three considerable comparisons between the voltage values; V_{NB1} , V_{NA1} , V_{NC2} and V_{NA2} , over the whole rotor space, can be achieved. These comparisons lead to divide the whole rotor angular spatial space into six sectors each of 30° angular width

approximately. The block diagram given in figure (4.9) illustrates the steps of performing this part, where the motor terminal voltages are measured, compared, decoded and finally the x-address line is obtained.

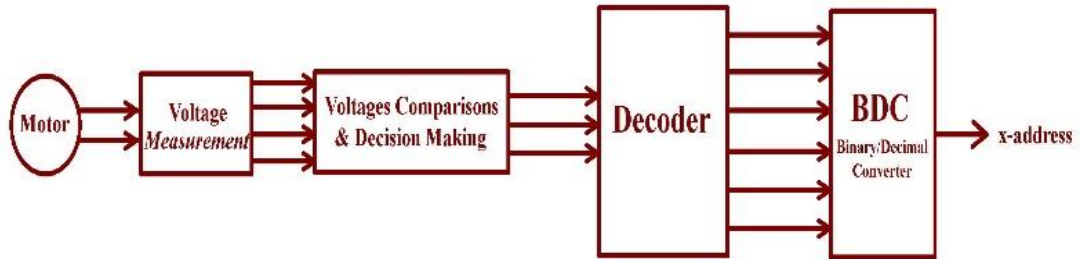


Fig. 4. 9, Block diagram for voltage comparisons and x-address creation

The manner of the rotor space division into sectors differs according to the number of rotor pole-pairs. Table 4.1 summarizes the voltage comparisons and the corresponding divisions of the spatial space of a rotor, which has one pole-pair. It should be noticed that due to the magnetic similarity, this voltage comparison and sector divisions will be repeated every 180°. So, table 4.1 represents the sector data between (0° and 180°) or (180° to 360°). These sector numbers are employed later to form a memory address line, x-address.

Table 4. 1: Division of the rotor spatial space into sectors and x-address creation

Voltages comparisons	Logic states of sectors:					
	1	2	3	4	5	6
$V_{NB1} \geq V_{NA1}$	1	1	0	0	0	1
$V_{NC2} \geq V_{NA2}$	1	0	0	0	1	1
$V_{NB1} \geq V_{NC2}$	1	1	1	0	0	0
$(x\text{-address})_2$	111	101	001	000	010	110
$(x\text{-address})_{10}$	7	5	1	0	2	6

Figure 4.10 represents the voltage waveforms with a projection for the sector divisions according to the comparison results among them.

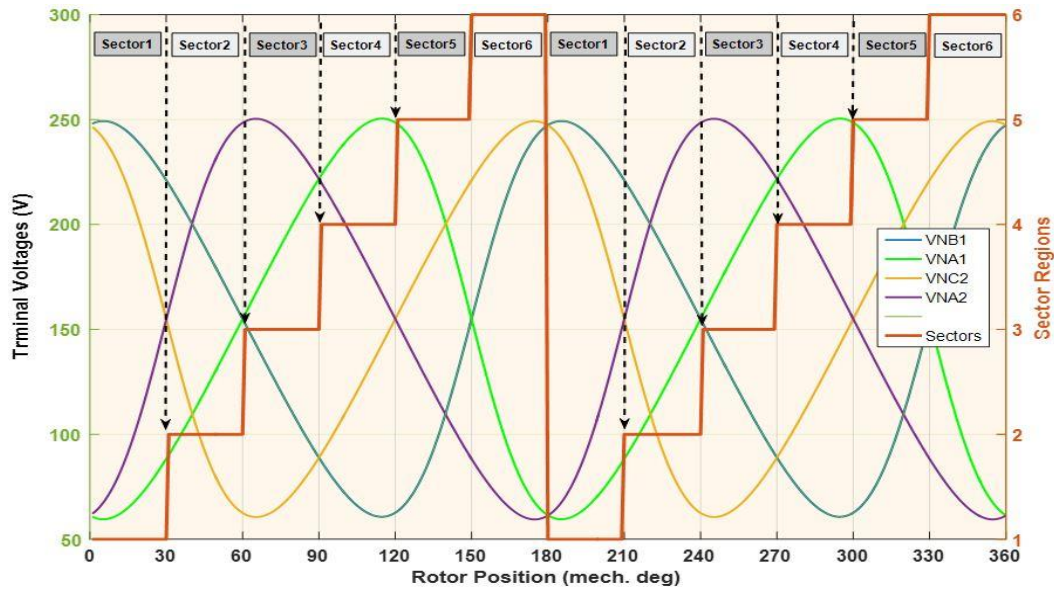


Fig. 4. 10, The stator voltage waveforms and division of rotor space into sectors

With respect to the results in table 4.1, the x-address is formatted from decoding the voltage comparisons. Therefore, the x-address line has six values, which divide the memory cells into six groups. Each group contains sixty of the rotor position mechanical angles.

4.4.3 Formatting the y-address

The y-address is either formatted depending upon the current responses or considering the mille-volt variations in one of the voltage responses. The former is a conventional and mostly adopted in PMSM controlling schemes, while the latter is a proposed method by this work. The employment of voltage response permits to dispense the use of current sensors (only in the estimator not on the overall control driving system) that makes the position estimator remarkably less dependent on sensing elements and correspondingly cost effective. Anyhow, modelling of both approaches are going to be discussed through the next sections.

4.4.3.1 Formatting the y-address through current responses

Each of the injected pulses fired shortly a pair of the inverter elements, IGBTs, one from the upper and one from the lower sides. Thereby, a short duration current produced

and passed in a pair of stator coils in the forward direction, I_{on} , as indicated by the solid lines in figures 4.6 and 4.7. After elapsing the high period of the injected pulse, the current I_{on} disappeared and a freewheeling current started to flow in the reverse direction, I_{off} , as illustrated by the dashed lines in the above figures. The following equations gives the mathematical representation for that current:

$$i(t)_{ON} = \frac{V}{R} \left(1 - e^{-\frac{R}{L}t}\right) \quad (4.15)$$

$$i(t)_{off} = \frac{V}{R} \left(e^{-\frac{R}{L}t}\right) \quad (4.16)$$

where V is the source voltage, R is the sum of resistances of both phase-pair, assume A and B (R_A+R_B), L is the sum of inductances in that phase-pair, L_A+L_B . Figure (4.11) shows the two pulses and the corresponding two currents, I_1 and I_2 .

The first pulse caused the voltage drop V_{NB1} that is expressed by:

$$V_{NB1} = i * R_B + L_B \frac{di}{dt} \quad (4.17)$$

The range of time variant was within the pulse width, 150usec. Therefore, the full range for current growth did not appear. Instead, only the portion of linear variation was noticeable as illustrated in figure 4.11. This portion is described by the known straight line equation $y=mx+c$, where “ m ” is the slope and “ c ” is a constant. Thereby, the variation of current di/dt will equal to the slope “ m ”, which allows to rewrite the equation (4.17) as a formula for the current:

$$i = \frac{V_{NB1}-m*L_B}{R_B} \quad (4.18)$$

All the terms on the right hand side of (4.18) are constants with respect to rotor position except the voltage V_{NB1} . This means that the value of current will be a function to the rotor position. The choosing of short duration current has made it possible to run this model for a wide range of motor rating currents where this short duration, 150µsec, represents very small fraction of the current time constant (L/R) of any motor. Figure 4.11 illustrates the two applied pulses, each of 300µsec period and 150µsec duration time, and the corresponding shapes .of current responses, where the peak of second current I_2 was exploited to create the y-address of the memory.

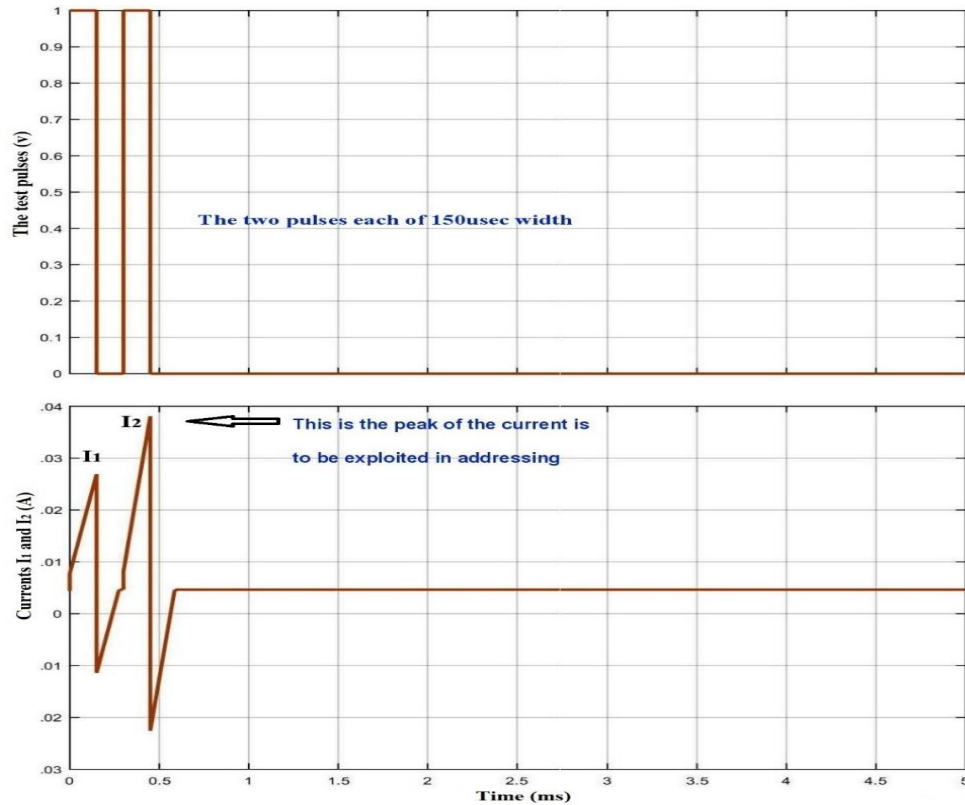


Fig. 4. 11, Two injected pulses and the corresponding current responses

The modelling structure, which can implement the y-address formatting through the current sinusoidal variation, is highlighted by figure 4.12. It is clarified as follow; after sensing and measuring the peak value of the current I_2 , the modification and amplification block takes the action to cancel the first common three digits of the current reading and to amplify and reform the residuals. The residuals cannot be adopted directly in y-addressing because they are too close to each other. So, a certain deviation between the residual values should be create. This is done by the deviation algorithm block. At this stage, the problem is represented by some of the current residuals at the output of the algorithm block, which still have very closed values, so certain numbers stored in the shift memory block were added to these residuals to create the required shift, more details about this will be given in the next section.

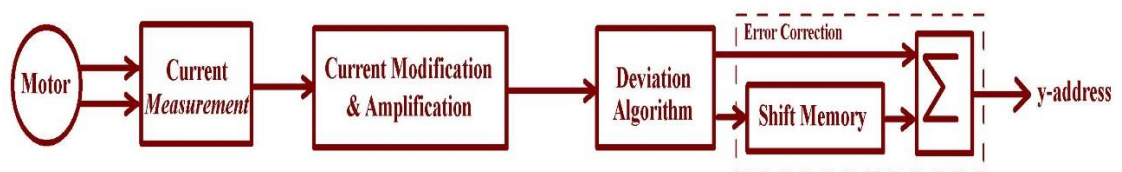


Fig. 4. 12, Block diagram for the circuitry of y-address extraction

4.4.3.2 Formatting the y-address from a voltage measurement

One of the voltage responses, which were employed to format the x-address, is exploited in creating the y-address. As it was proved, the inductances of stator windings are sinusoidal variables with rotor position. This reflects on the terminal voltages making them oscillate sinusoidally with position of rotor. This point was exploited in this work to obtain a full sensorless rotor position estimation at zero-speed.

If the voltage V_{NB1} is taken as an example for voltage analysis, then, by figure 4.12, it is written as follow:

$$V_{NB1} = V_{dc} \frac{Z_B}{Z_A + Z_B} \quad (4.19)$$

where V_{dc} is the dc link voltage and Z_A , Z_B are the impedances of windings A and B respectively.

In complex form, (4.19) can be expressed as:

$$V_{NB1} = V_{dc} \frac{R_B + j\omega L_B}{(R_A + R_B) + j\omega(L_A + L_B)} \quad (4.20)$$

where ‘ ω ’ is an angular frequency and, in (4.20), it is equivalent to the switching speed of the IGBT which is determined by the frequency of the firing injected pulses. Accordingly, the resistive component in both numerator and denominator of (4.20) is omitted comparing to the corresponding high inductive component. Therefore, (4.20) is rewritten as:

$$V_{NB1} = V_{dc} \frac{L_B}{L_A + L_B} \quad (4.21)$$

This equation expresses the measured voltage V_{NB1} as a function to the values of the winding inductances L_A and L_B . As the inductances are functions of rotor position by the effect of rotor magnet saliency, so, indirectly, the measured voltage will be a function of rotor position as well and it will fluctuate highly as there is a remarkable saliency in the rotor spatial space. To implement formatting the y-address from the voltage response, the modelling structure given in figure 4.13 was adopted.

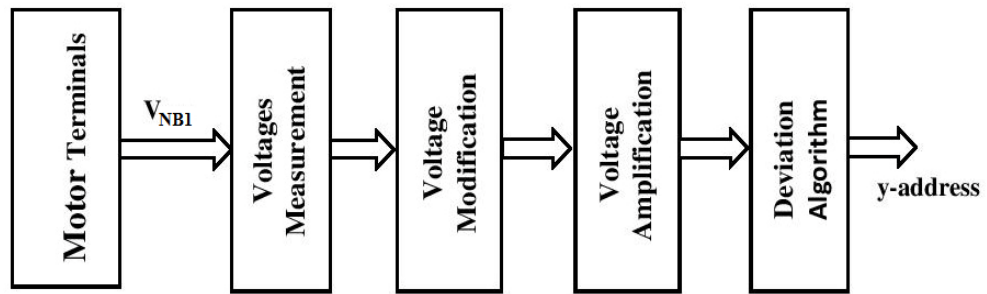


Fig. 4. 13, Block diagram for y-address implementation through voltage response

4.4.4 Modelling blocks for deviation algorithm

By revising the modelling results, it was found there is a problem related to the presence of very closed current or voltage readings. This problem is clarified by figure 4. 14 where the hard readings are circled.

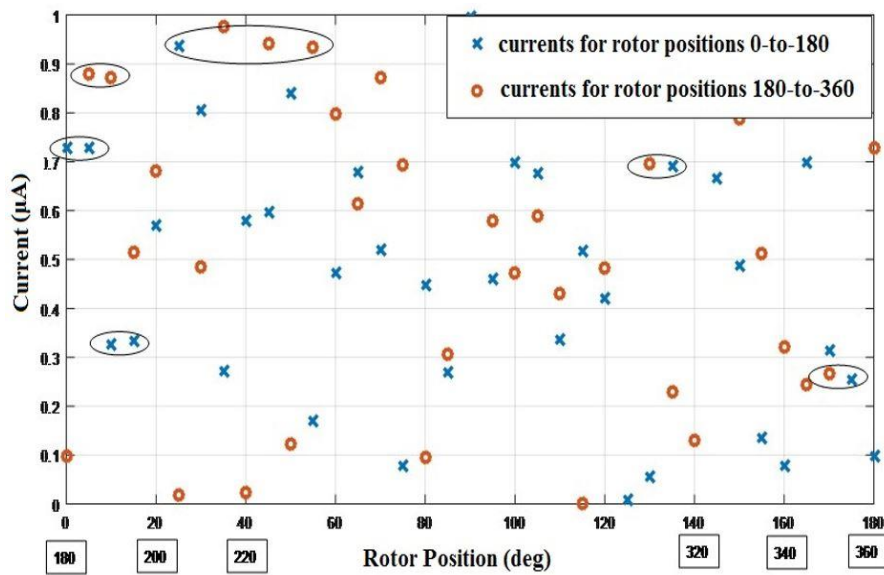


Fig. 4. 14, The readings of current peaks in ZSRPE modelling

Therefore, it became very hard task for the estimator to distinguish among them. This problem was tackled in this modelling work by suggesting an algorithm whose applying could make a certain deviations among those very closed readings. Thereby, the errors in position estimations is avoided.

The proposed algorithm is based on a simple arithmetic exponential function. In a certain domain, the exponential function becomes sensitive to any variance in the

exponential index [169]. Thereby, a small index change causes a larger change in the value of the exponential function. So, the current, or voltage, values were regarded as the indices in the algorithm in order to maximise the differences among them. In spite of that, some current peaks were very hard to make significant differences among them by the proposed algorithm and they caused a mistakable addressing. For this reason, an error correction block has been added to the model given within the figures 4.15 to manipulate these values as possible. However, there were still odd values from the current peaks, or voltages, that could not be separated neither by the algorithm nor by the error correction and they caused some rate of error.

4.5 Implementation of the proposed method for modelling the ZSRPE

The main blocks to implement the ZSRPE are illustrated below:

- I. The pulse generator, this block was created through employing the step function model.
- II. The inverter, this block was built through exploiting six switching elements, IGBTs.
- III. The PMSM, this block was implemented by adopting the model described in 4.3 above.
- IV. The decoder, this block was introduced by the user function tool.
- V. The memory, this block was implemented by a 2D-lookup table.
- VI. The other different blocks were combined by various modelling tools.

4.5.1 ZSRPE for IPMSM

The concepts of zero-speed rotor position estimation, ZSRPE, were simulated and run by the “MATLAB/Simulink” environment according to the idea shown in figure (4.4). The work aims to implement rotor position estimation of 1° resolution. To meet this goal, the exact angular positions, from 0° to 360° , of the permanent magnet rotor under test were stored in the cells of the memory block given in the figure. The location of each memory cell is accessed via two address buses, x and y, whose methods of formatting were discussed above. Figure 4.15 gives an implementation for the y-address formatting according to the measurement of the dc link current. Appendix C.8 gives details for modelling the IGBT switching block which is shown in this figure.

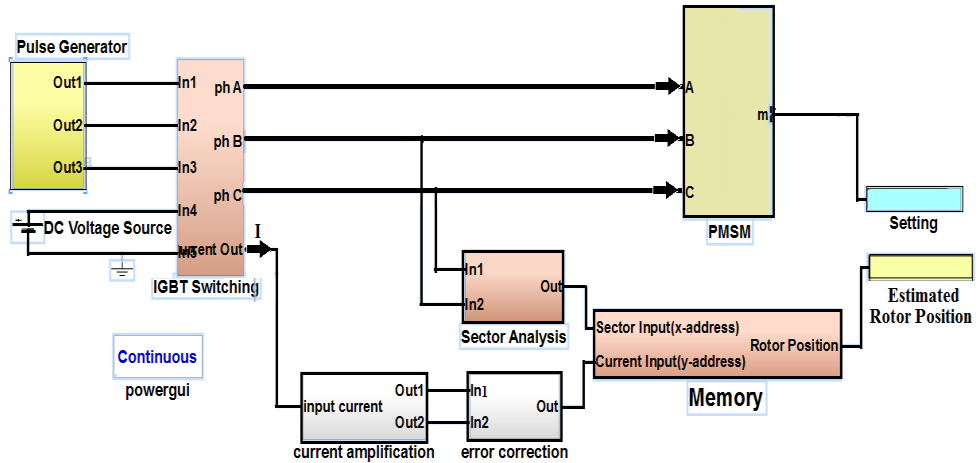


Fig. 4. 15, Modelling the ZSRPE by employing the motor output voltages and current

Table 4.2 shows the parameters of IPMSM under the modelling test for zero-speed rotor position estimation.

Table 4. 2: Parameters of the modelled IPMSM

Parameter	Value	Unit
No. of phases	3	-
Rotor Type	Salient	-
No. of poles	2	-
Stator Phase Resistance	2 Ohms	Ω
Stator Inductance	$L_d = 0.75, L_q = 1.25$	mH
Flux Linkage	0.285757	V.s
Inertia , Viscous damping	$0.621417(g.m^2), 0.303448$	mN.m.s
DC Link Voltage	310	V

4.5.2 ZSRPE for SM-PMSM

Most of the proposed works for the PMSM zero speed rotor position estimation, ZSRPE, are based on the detection of the rotor magnetic salience. Therefore, the standstill and low speed rotor position estimation in SM-PMSM becomes more difficult, complicated and still represent a difficult challenge [21]. This trend has been confirmed

by [22], which mentioned that the absence of remarkable level of saliency in SM-PMSM produces equal inductances at the rotor reference frame L_q , the quadrature inductance, and L_d , the direct inductance, which makes the saliency tracking methods for initial rotor position estimation useless. Reference [23] mentioned that many approaches for zero-speed rotor position estimation are found to be inefficient in non-salient rotor motors because they are based on the rotor magnetic saliency, which may be unnoticeable in surface mounted PMSMs. This saliency weakness will be analysed in detail in the next section.

To tackle this problem, a simulated model has been proposed which is based on injection of three high frequency pulses into the stator coils of a SM-PMSM. Then, the millivolt variations at the motor terminals have been measured and exploited to predict the rotor position. Thereby, no current measurement was required as it the case with the method of estimation the rotor position of the IPMSM given above in 4.4.1. Depending only on the measured voltages, without the needing to any form of current measurements and current sensors, represents a significant improvement because it makes the estimator be a full sensorless.

The six obtained voltages were compared with each other and the result of these comparisons was dividing the rotor spatial space into main and sub-sectors as illustrated in table 4.3.

Table 4. 3: Distribution of rotor position angles on main sectors and subsectors

S_1	S_{11}	S_{12}	S_{13}	S_{14}	S_{15}	S_{16}
	$1^\circ - to - 10^\circ$	$11^\circ - to - 20^\circ$	$21^\circ - to - 30^\circ$	$31^\circ - to - 40^\circ$	$41^\circ - to - 50^\circ$	$51^\circ - to - 60^\circ$
S_2	S_{21}	S_{22}	S_{23}	S_{24}	S_{25}	S_{26}
	$61^\circ - to - 70^\circ$	$71^\circ - to - 80^\circ$	$81^\circ - to - 90^\circ$	$91^\circ - to - 100^\circ$	$101^\circ - to - 110^\circ$	$111^\circ - to - 120^\circ$
S_3	S_{31}	S_{32}	S_{33}	S_{34}	S_{35}	S_{36}
	$121^\circ - to - 130^\circ$	$131^\circ - to - 140^\circ$	$141^\circ - to - 150^\circ$	$151^\circ - to - 160^\circ$	$161^\circ - to - 170^\circ$	$171^\circ - to - 180^\circ$
S_4	S_{41}	S_{42}	S_{43}	S_{44}	S_{45}	S_{46}
	$181^\circ - to - 190^\circ$	$191^\circ - to - 200^\circ$	$201^\circ - to - 210^\circ$	$211^\circ - to - 220^\circ$	$221^\circ - to - 230^\circ$	$231^\circ - to - 240^\circ$
S_5	S_{51}	S_{52}	S_{53}	S_{54}	S_{55}	S_{56}
	$241^\circ - to - 250^\circ$	$251^\circ - to - 260^\circ$	$261^\circ - to - 270^\circ$	$271^\circ - to - 280^\circ$	$281^\circ - to - 290^\circ$	$291^\circ - to - 300^\circ$
S_6	S_{61}	S_{62}	S_{63}	S_{64}	S_{65}	S_{66}
	$301^\circ - to - 310^\circ$	$311^\circ - to - 320^\circ$	$321^\circ - to - 330^\circ$	$331^\circ - to - 340^\circ$	$341^\circ - to - 350^\circ$	$351^\circ - to - 360^\circ$

Figure 4.16 shows the modelling of rotor position estimation for SM-PMSM at zero speed by adopting only the motor terminal voltages and decoding the comparison results into sixteen values.

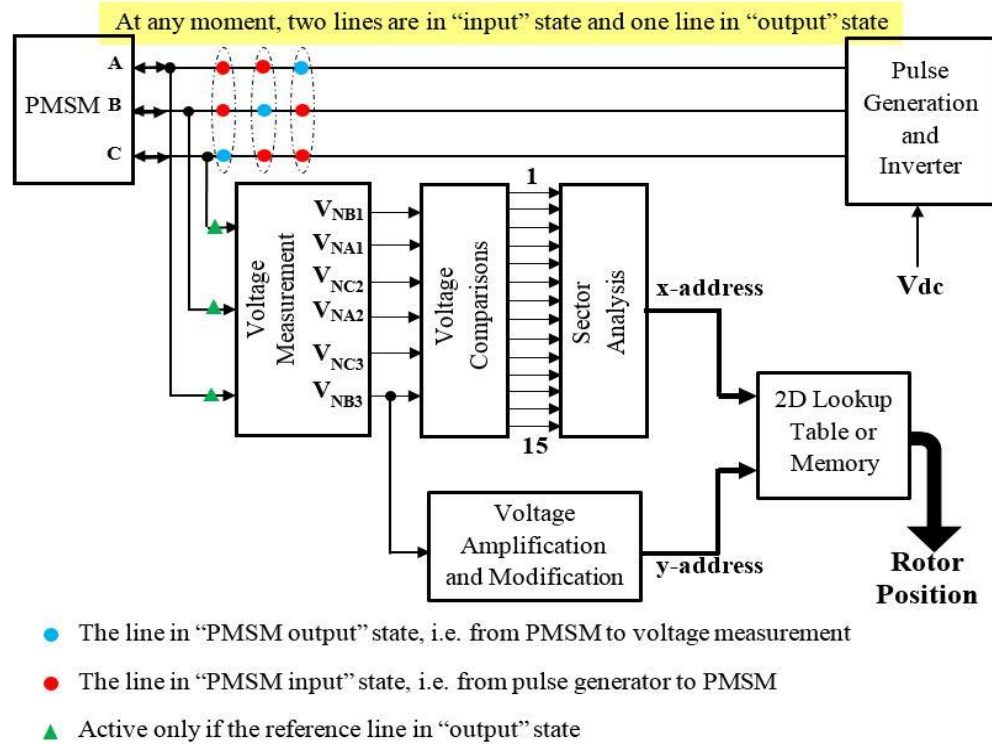


Fig. 4. 16, Modelling the ZSRPE by exploiting only the motor terminal voltages

Table 4.4 gives the parameters of SM-PMSM under the modelling test to estimate the zero-speed rotor position. The parameters of resistance, inductance and power rating are adopted according to those of the commercial motor M0200-104-00.

Table 4. 4: The modelled SM-PMSM parameters

Parameter	Value	Unit
No. of phases	3	-
Rotor Type	Round	-
No. of poles	6	-
Stator Phase Resistance	0.6	Ω
Stator Inductance	1.7	mH
Flux Linkage	0.064322	V.s
Inertia	0.2700	g.m ²
DC Link Voltage	310	V
Viscous damping	0.4924	mN.m.s
Rated power	200	W

4.6 Modelling the effect of saliency weakness on RPE

The magnitude of magnetic saliency in PMSMs differs according to the method of fixing the permanent magnets on, or into, the rotor body. Accordingly, the variation level of the stator winding inductances with rotor position will increase or decrease in direct relation with saliency amount. Therefore, there will be a remarkable change in the amount of the sinusoidal oscillation at the motor terminal voltages. Consequently, it may become hard task for rotor position modelling estimator to achieve the voltage comparisons due to that weak oscillation. This topic was verified by modelling two motors terminal voltages. The first motor is type interior permanent magnet, IPM, which characterized by its high saliency. Whereas, the second motor is type surface mounted magnet, SPM, which has a uniform magnetic field distribution and, accordingly, very weak saliency. Figure 4.17 shows the modelling results for the oscillation magnitudes in terminal voltages of both motors, V_{NB1} , with rotor position variation.

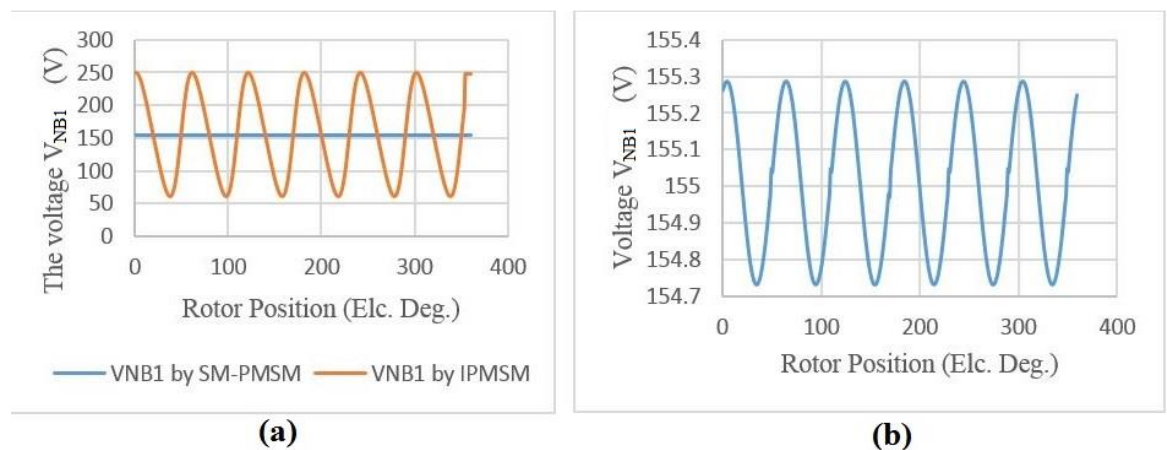


Fig. 4. 17, Saliency effect on voltage oscillation in (a) IPM and SPM (b) SPM

As it is noticed by the figure, the oscillation of the voltage V_{NB1} with rotor position variation, in the interior type, is more than the corresponding voltage oscillation in the surface mounted PMSM ($V_{p,p}$ for surface mounted = 0.5V whereas 205V for interior). Figure 4.18 presents a statistic view for the comparison between the voltage oscillations at the terminals of both motors. In this figure, the standard deviations for IPMSM and SMPMSM are 65.85 and 0.1967 respectively. Moreover, the range of variation is 188.7 in the IPMSM against 0.5559 in the SMPMSM. These statistical results emphasize the effect of saliency strength on the amount of oscillation in the motor terminal voltages.

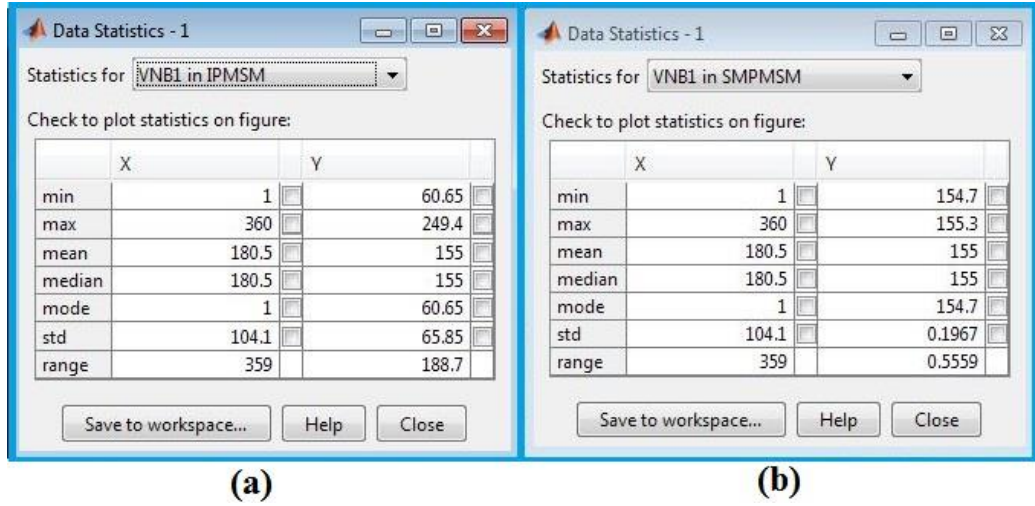


Fig. 4. 18, Statistic analysis for the voltage at the terminals of (a) IPMSM (b) SMPMSM

This modelling result reflects the considerable difference in the amount of saliency and its impact on inductance variation in both types of machines, and highlights the fact that the SM-PMSM is characterised by having a weak saliency in contrast to the IPMSM. This modelling results tell that more consideration should be taken in designing of the RP estimator of SM-PMSM.

4.7 Mathematical modelling view

Let us define a row vector, S , of dimensions $(m \times 1)$ to represent the sector vector where the index ‘ m ’ refers to the expected number of sectors in the rotor spatial. In this work $m=6$ because the rotor spatial space has six sectors, so:

$$[S]_{6,1} = [S_1 \ S_2 \ S_3 \ S_4 \ S_5 \ S_6]^T \quad (4. 22)$$

The vector S is a binary vector which means that each element in S , S_1 to S_6 , has a binary value, either 0 or 1, which is defined as follow:

$$S_i = \begin{cases} 1, & \text{if } i = \text{sector reading} \\ 0, & \text{otherwise} \end{cases} \quad i = 1,2, \dots,6 \quad (4. 23)$$

As a result, at any moment of time, a unique element in S will be at logic ‘1’ while all other will be at logic ‘0’ because at any given moment, the rotor position is at a unique sector.

Similarly, a binary variables matrix, I , of dimensions (n x m) can be defined to refer to a current readings matrix, where “n” represents the number of current readings within a specific sector “m”, and can be determined by:

$$n = \text{number of sub-sectors} \times \text{number of angles per sub-sector} \quad (4.24)$$

In this work n equals 60, and I is given by:

$$I_{ixj} = \begin{bmatrix} I_{1,1} & I_{1,2} & I_{1,3} & I_{1,4} & I_{1,5} & I_{1,6} \\ I_{2,1} & I_{2,2} & I_{2,3} & I_{2,4} & I_{2,5} & I_{2,6} \\ I_{3,1} & I_{3,2} & I_{3,3} & I_{3,4} & I_{3,5} & I_{3,6} \\ \vdots & \vdots & \vdots & \vdots & \vdots & \vdots \\ \vdots & \vdots & \vdots & \vdots & \vdots & \vdots \\ I_{60,1} & I_{60,2} & I_{60,3} & I_{60,4} & I_{60,5} & I_{60,6} \end{bmatrix} \quad (4.25)$$

where j refers to sector number and i refers to the score of the current reading within the j^{th} sector. The binary value of each element in this matrix is defined by:

$$I_{i,j} = \begin{cases} 1, & \text{if } I_{i,j} = I_r \pm 10\%I_r \\ 0, & \text{otherwise} \end{cases} \quad I_r: \text{current reading} \quad (4.26)$$

Whereas, the matrix θ gives all the possible rotor position angles distributed on the rows according to sector number, e.g., row number one includes all the sixty angles involved in sector1. This matrix is given by:

$$\theta_{m,q} = \begin{bmatrix} \theta_{1,1} & \theta_{1,2} & \cdots & \cdots & \cdots & \theta_{1,60} \\ \theta_{2,1} & \theta_{2,1} & \cdots & \cdots & \cdots & \theta_{2,60} \\ \vdots & \vdots & \vdots & \vdots & \vdots & \vdots \\ \vdots & \vdots & \vdots & \vdots & \vdots & \vdots \\ \theta_{6,1} & \theta_{6,2} & \cdots & \cdots & \cdots & \theta_{6,60} \end{bmatrix}^T \quad (4.27)$$

where ‘m’ represents the sector number and ‘q’ the angles in the m^{th} sector.

Then, the multiplication of the three matrices, defined above, yields the rotor position:

$$\text{Rotor Position} = [[\theta] \times [S]]^T \times [[I] \times [S]] \quad (4.28)$$

Figure 4. 19 illustrates the modelling of the arithmetic approach for rotor position estimation. The SM-PMSM, whose parameters are given in table 4.3, was tested in this modelling scheme. While figure 4.22, in the results section, shows an application for the model when the rotor at position 25°.

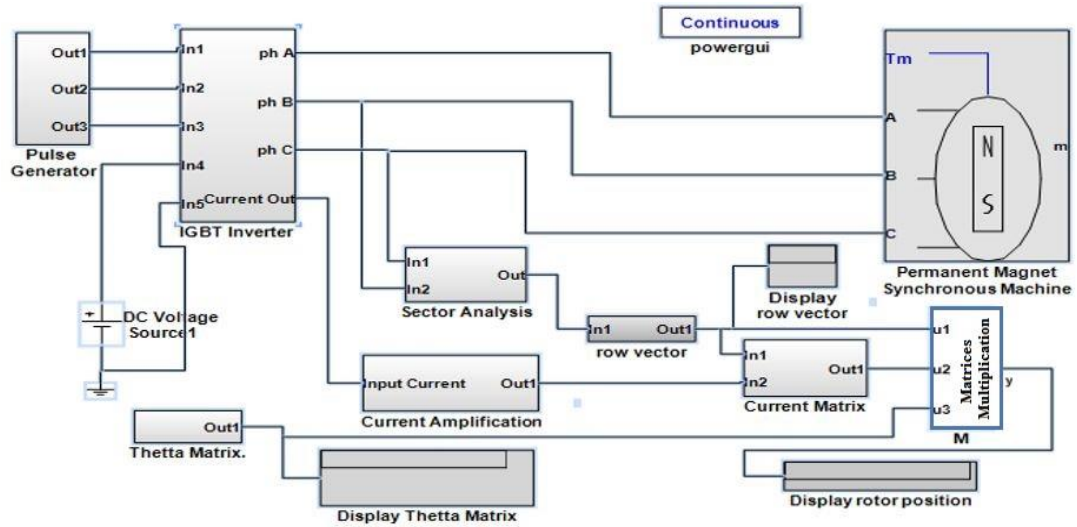


Fig. 4. 19, Mathematical “Simulink” model view for rotor position estimation

4.8 Simulation results

Figure 4.20 shows a snap for the oscilloscope screen in the “MATLAB/Simulink” environment. This oscilloscope was used to display the three injected pulses and the motor terminal voltages responses.

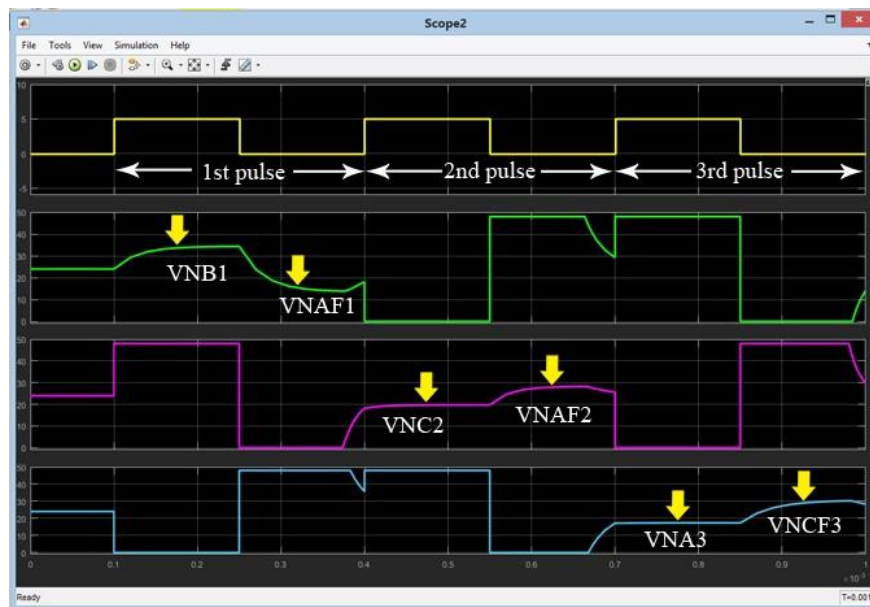


Fig. 4. 20, The injected pulses and the corresponding voltage responses in the modelling system

Figures 4.21(a) and 4.21(b) illustrate the modelling graphical results, which were obtained through a “MATLAB/Simulink” environment dynamic models, for both types of motors IPMSM and SM-PMSM respectively. The plots give the estimated rotor position against the actual position. The ramp straight lines is for the correct estimations, while the peaks, $e_1, e_2 \dots$ etc., are the errors in the estimation process. It is noticeable that the interior type has five estimating errors, out of 360 total estimations, against 8 for the SM-PMSM. Therefore the IPMSM has a lower rate of error than the surface mounted due to the improvement in the estimator performance under the influence of higher rotor saliency in IPMSM. This higher saliency makes the stator inductances to be more affected by the variation in rotor position. This leads to a higher voltage oscillation at the rotor terminals and a corresponding improvement in the estimating process.

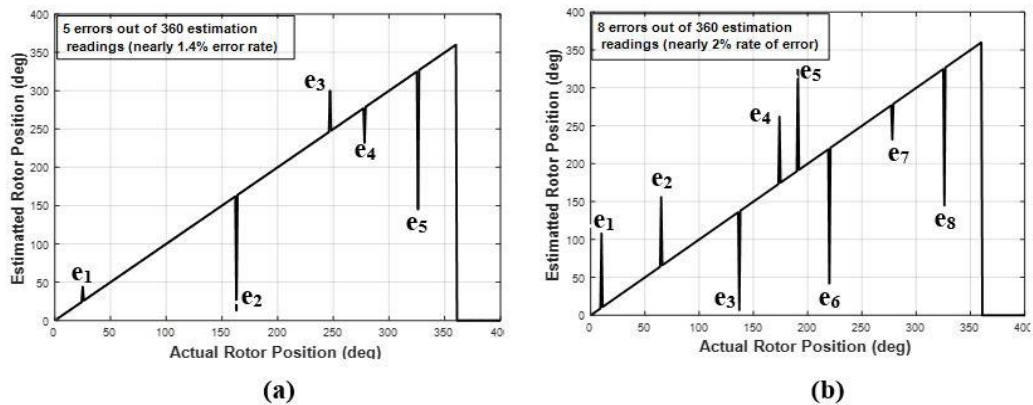


Fig. 4. 21, Results of modelling the ZSRPE for (a) IPMSM (b) SM_PMSM

Figure 4.22 shows an example for rotor position according to the arithmetic model. The figure shows portions of the; theta matrix, current matrix, sector column vector and binary indicator of the current column. The estimation was achieved when the setting rotor position was 25° . The estimator successfully estimated the rotor position at 25° by applying the equation (4.28).

the under test motor. These dimensions are exploited to access a memory structure, or a 2D-lookup table, where the corresponding values of the rotor positions are stored.

This chapter also presents a mathematical simulation model for the rotor position estimation. This based on creating row and column vectors related to rotor position. A matrix, which represents the all-possible measured values of the terminal voltages or currents, at different rotor positions, is also created. Then multiplication of the row vector, column vector and the matrix gives the predicted value for the rotor position of permanent magnet synchronous motor.

The proposed “MATLAB” models were applied on two types of the permanent magnet motors, the interior magnet, IPMSM, and the surface mounted, SM-PMSM. Although it was found there is no large difference in the accuracy of the rotor position estimation in both cases, however, the estimation approach for interior motor was more accurate and softer. The reason is attributed to the fact that this type of motor, inherently, has larger amount of saliency, which the models were built according to its value, comparing to the surface mounted type.

CHAPTER FIVE

PRACTICAL SET-UP AND VERIFICATION FOR ZERO-SPEED ROTOR POSITION ESTIMATION

5.1 Introduction

The work, in this chapter, illustrates the details of designing and implementing a platform, which should be employed to achieve the practical estimation for rotor position of a surface mounted permanent magnet synchronous motor, SM-PMSM. The strategy of performing this estimation was built on injection of three high frequency pulses in the stator windings and exploiting the voltage responses at the motor terminals. The setting-up of the platform is based on two main parts. First is a microcontroller type “ATmega328” which is supported by a C language programming software. Second is a three-phase voltage inverter, which has been built in the Cardiff University School of Engineering laboratory. The platform also includes some analogue components, such as operational amplifiers, have been involved to support the operation of the microcontroller and the inverter. In addition, the platform includes a pointer for the indication of standstill rotor position. Two commercial permanent magnet motors, types “M0200-104-4-000” and “ACM2n320-4/2-3”, have been tested, by the designated platform, to estimate their zero speed rotor position.

This chapter is going to be organized into seven main sections. Section 1 presents an introduction to the chapter subject. Section 2 introduces the main in the practical platform and gives a discussion for each of them. Section 3 describes the real world implementations for the modelling of the zero-speed rotor position estimation in addition to the principle of operation. Section 4 highlights the strategy, which was adopted in the work in exciting the motor windings. Section five demonstrates exciting the motor winding by the injected pulses and formation of the voltage responses. Section six presents the obtained results for zero-speed rotor position estimation and gives

comparisons with both the modelling results of chapter four and the results, which were obtained by applying different rotor position strategies. Eventually, section seven summarizes the chapter contents

5.2 Construction of the practical platform for ZSRPE

Figure (5.1) shows a block diagram for the essential parts that required in designing the ZSRPE platform and the method of connection between them. In addition, the figure include an indication for the flow of the practical zero-speed rotor position estimation according to the proposed method in this work

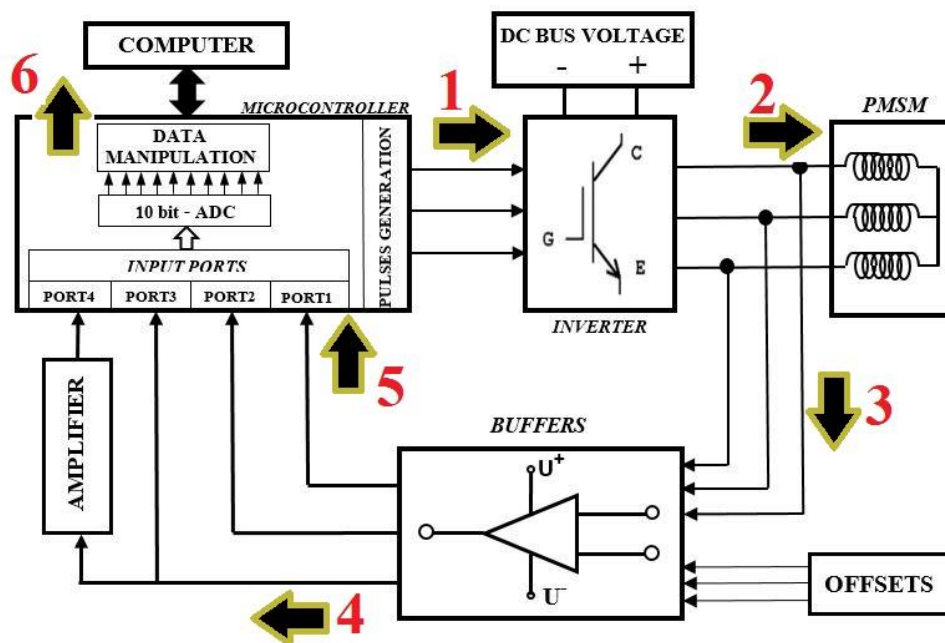


Fig. 5. 1, Block diagram for practical platform of ZSRPE

Briefly, it is performed as follow:

- 1) Firstly, the microcontroller generates pulses and fires the inverter switching elements.
- 2) The inverter converts the pulses into a higher level and injects them into the motor windings.
- 3) The motor voltage responses are fed to a buffer circuit, which works as offset as well.
- 4) One of the buffer outputs is amplified.

- 5) The buffer outputs, amplified and non-amplified, are fed to the microcontroller.
- 6) The microcontroller analyses the signals, estimates the motor rotor position, and finally transfers the estimation to the peripheral computer to be displayed.

These steps will be discussed in detail later.

Next are definitions for the various units of the practical platform shown in Figure 5.1.

5.2.1 The microcontroller

Currently, the electronic control schemes, which are convenient to be used with PMSM drive, are either MCU, microcontroller unit, or DSP, digital signal processor, depending on the application requirements [170]. In this work, a microcontroller type “AVR ATmega328” was employed to manage the overall operations of the estimation process. This is an 8-bit, CMOS, low-power microcontroller. It is designated to be able to execute powerful instruction per a single clock cycle at rate 1 MIPS. It is programmed either through the assembly code or the C language code. Figures 5.2 illustrates this microcontroller pin configurations [171].

This microcontroller has been manufactured to provide the following main features, which were used in constructing the designing scheme:

- 32 kbyte flash memory.
- 1kbytes EEPROM and 2kbytes SRAM
- 32 general-purpose registers.
- Capability to drive PWM signals (6 channels).
- 10-bit ADC with programmable gain.
- 6 analogue input ports and 13 digital input/output ports.
- SPI serial port

In this work, the “ATmega328” was employed to achieve the following tasks:

- Generates 5V, 3 kHz injection pulses at its output port.
- Receives the motor terminal voltages.
- Performs the A/D conversion.
- Performs the comparisons between the measured motor terminal voltages.
- Prepares the peripheral connection with the PC.

- Performs the calculations for the standstill rotor position estimation.

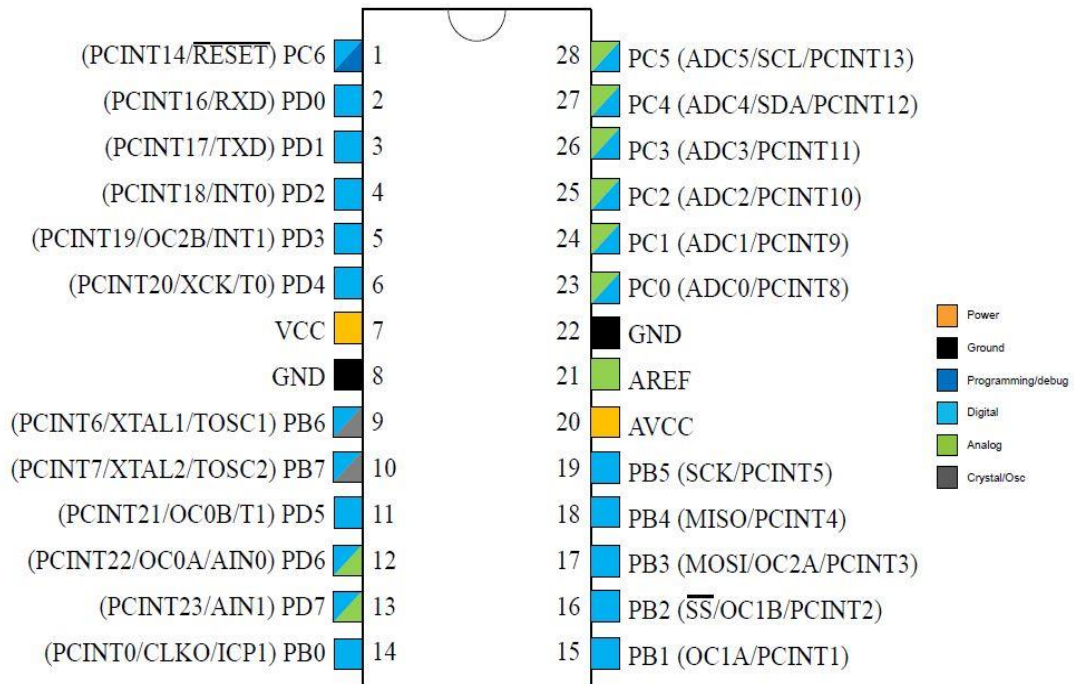


Fig. 5. 2, Pin configurations for the microcontroller “ATmega328”

A functional description for the employed microcontroller is given in appendix B.4.

5.2.1.1 The microcontroller hardware and software integration

It is meant by the hardware and the software integration that, the hardware tasks are solved and achieved via the software programming and vice versa. Reference [172] reported an academic project to implement the hardware laboratory instrumentations through the microcontroller software. These microcontroller facilities were exploited in this project to overcome some problems in the practical platform, or to simplify its hardware design. For instance, the electronic circuit which was required to implement the comparisons between the measured terminal voltages was substituted, through the C programming of the microcontroller, by an ‘if statement loop’. Thereby, fifteen comparison results, which were labeled by the letters A through P, were obtained. Similarly, the required electronic circuit for conversion the word from binary form into decimal form, to obtain the sector number, was substituted by the following equation, which was achieved by the C programming too.

$$sector\ number = 15 * A + 14 * B + \dots + 1 * P \quad (5.1)$$

5.2.2 Inverter

The inverter in the hardware structure of motor driving system has the role of 3-phase power supply. It achieves the task through inverting the dc link voltage into three-phase ac power. This is done through firing a set of electronic switching elements by pulses of width modulation, PWM. The switching elements are either MOSFETs or IGBTs. Two electrical circuits are connected in parallel to each switching element. The first is an embedded freewheel diode whose role is to return the power from the machine coils to the DC bus when the switching element transits from ON to OFF condition. This is to avoid the switching element damage due to the high voltage peaks generated by the inductive motor current during the ON period. The second is a snubber circuit, which works to damp the oscillations between the switching element terminals when they are fired by high frequency pulses. Moreover, the stray capacitances between the printed circuit tracks is able to be avoided if laminar bus-bars are used. Figure 5.3 is a schematic diagram to illustrate the basic component of the 3-ph bridge inverter in application of PMSM driver [173].

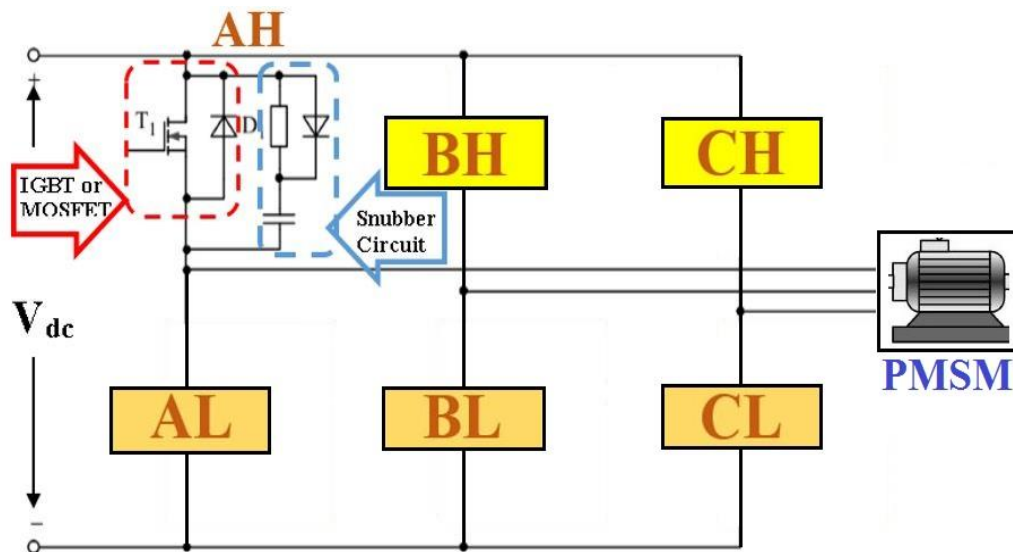


Fig. 5. 3, Basic structure of the 3-ph bridge inverter

5.2.3 The PMSMs under test

The surface mounted permanent magnet synchronous motors, SM-PMSMs, have been widely used in many fields of applications. Therefore, in the practical work, two types of commercial permanent magnet synchronous motors, type surface mounted,

were driven under the test of rotor position estimation. This is to verify the validity of the proposed practical sensorless zero-speed rotor position estimator. The models of the under-test PMSMs are “AcM2n0320-4/2-3” and “M0200-104-4-000” and they were produced by “EUROTHERM SSD Drive GmbH” [174] and “Applied Motion” [175] respectively. The brief electromechanical specifications of those permanent magnet motors are given in table 5.1. While The detail specifications of these motors are shown in the appendices C.1.5 and C.1.6 as given by the manufacturers [174], [175].

Table 5. 1, Specification parameters of the PMSMs in the ZSRPE practical platform

Parameter	Value		Unit
	ACM2n320-4/2-3	M0200-104-000	
No. of phases	3	3	-
Rotor Type	Round	Round	-
No. of pole-pairs	3	4	-
Stator Phase Resistance	1	0.6	Ω
Stator Inductance	4.2	1.7	mH
Rated Power	1340	200	W
Moment of Inertia	2.4	0.00706154	kg.cm ²
Rated Voltage	325	48	V
Rated current	6.4	6.4	A
Rated torque	3.2	0.64	Nm
Rated speed	4000	3000	rpm
Magnetic Material	NdFeB	---	-

Figures 5.4 (a) and (b) show the servo motor “AC M2n0320-4/2-3” and the code abbreviation meaning respectively as given by [174].

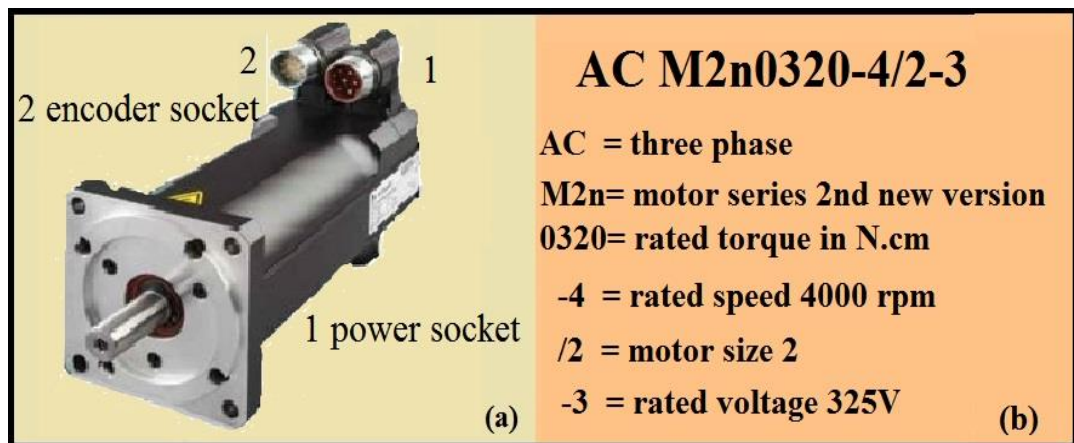


Fig. 5. 4, PM motor “Ac M2n0320-4/2-3” and its abbreviation code

Figures 5.5 (a) and (b) show the servo motor M0200-104-000 and the code abbreviation meaning respectively as given by [175].

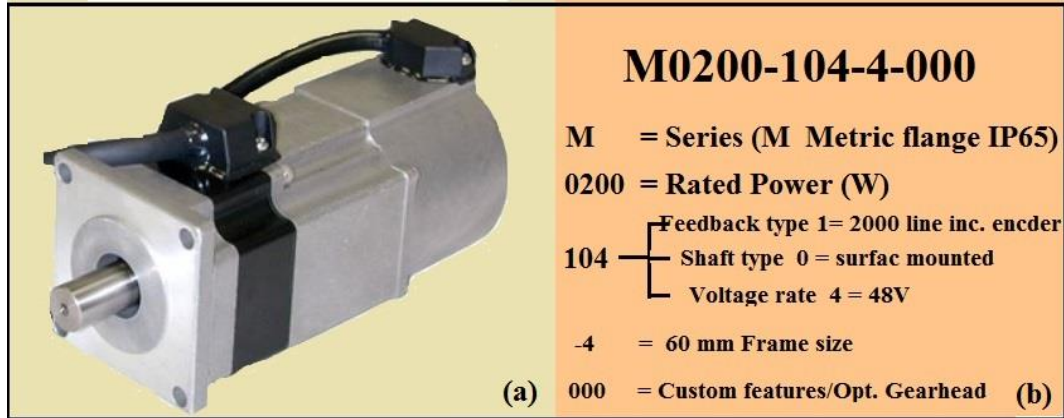


Fig. 5. 5, PM motor “M0200-104-4-000” and its abbreviation code

5.3 Describing the practical model

The practical works for ZSRPE were carried out by employing two SM-PMSMs types “M0200-104-4-000” and “ACM2n320-4/2-3” as drive servo motors which are explored above in section 5.2.3. The “MATLAB” models, which were discussed in chapter four, were taken as a base to implement the experimental platform. Figure 5.6 gives a demonstration for the steps of the creating the x, y, and memory addresses.

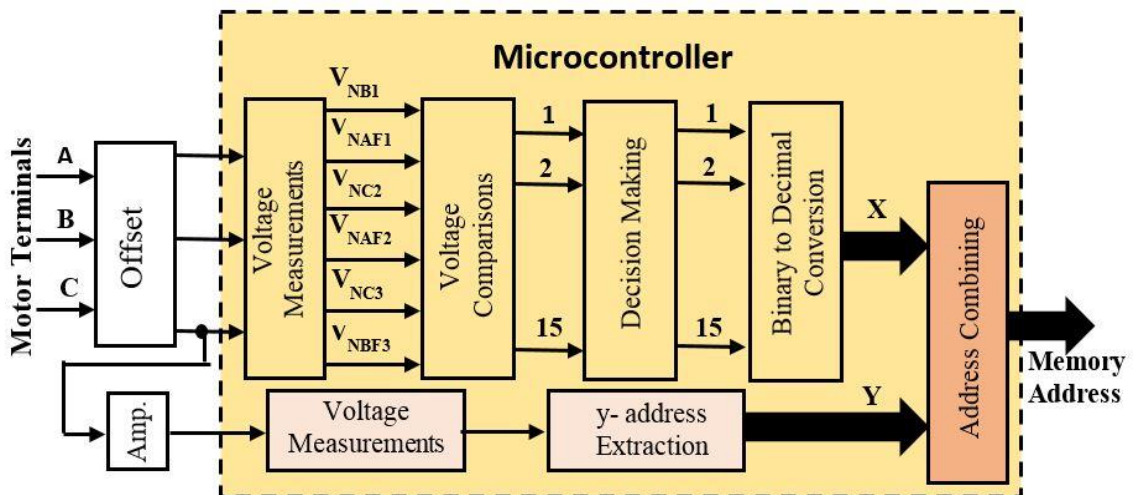


Fig. 5. 6, Memory address formatting in ZSRPE practical platform

The main blocks in the modelling view, which were discussed in chapter four, were satisfied in the practical model as shown below:

- 1) The look-up table in the modelling system is implemented in the practical model by a 1kbyte-EEPROM, which is embedded in the structure of the microcontroller.
- 2) The x and y dimensions were generated by the same procedures which were adopted in the modelling system. Then, they were combined to form the memory address.
- 3) The switching devices in the modelling inverter were satisfied by the IGBT electronic components type “FGH40N60SMDF-ND”, see appendix C.1.1. These switching devices were supported by a series RC snubber circuit.
- 4) The modelling blocks for measuring the motor terminal voltages were measured through the analogue input ports of the microcontroller, which are pins 23 through 28 as shown in figure 5.3.
- 5) The comparing and the binary to BCD modelling blocks were substituted by software codes, C language programming, available by the microcontroller.
- 6) The repetitive injection of pulses led to accumulated rotor position shifts which formed finally a noticeable rotor position difference from the initial standstill setting. Therefore, an arbitrary light load was applied to the rotor shaft just to damp the rotor response to the injected pulses.

The following sections functionally demonstrates the other major practical implementations.

5.3.1 Generating of the triggering signals by software implementation

Figure 5.7 shows the shape, peak, and periods of the high frequency pulses, which were used to trigger the switching elements. These pulses are either generated through a hardware pulse generator or exploiting the software facilities provided by an embedded microcontroller, or a digital signal processor. The latter was adopted in this work to implement the pulse generations of the practical platform. Briefly, the microcontroller generate the pulses through a high activation for one of its digital output ports, pin NO.3 in figure 5.2. This activation should continue until it satisfy the ON time period, 150 μ sec. Then, the microcontroller reset that port to zero for a timing period of 150 μ sec

too. Thereby, a full pulse is generated, and the microcontroller repeats the same procedure twice to generate the other two pulses.

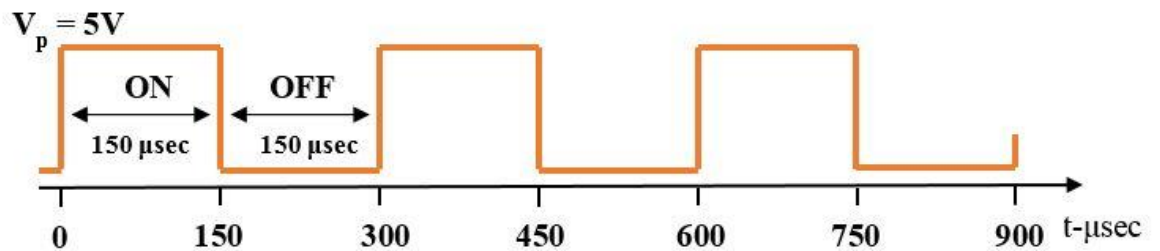


Fig. 5. 7, The practical model injected pulses

5.3.2 Triggering the inverter elements

Figure 5.8 illustrates an implementation for each leg within the inverter circuitry, which are given in figure 5.3, as given by reference [176]. The process of firing the upper switching elements, IGBTs, does not occur as simple as the firing of the lower switching elements. This happens due to the lack of a low electrical reference voltage at the drains of the upper IGBTs. This problem was solved through creating a high voltage pulses at the gates of those elements to be able to force the IGBTs to switch to ON condition. Therefore, class C amplifiers were connected to the IGBT gates to drive the PWM pulses of the upper switching elements [176]. This approach is a convenient firing process for applying in zero-speed estimators. However, at low and high speeds rotor position estimations different techniques should be adopted, such as the bootstraps, which will be discussed in the next chapters.

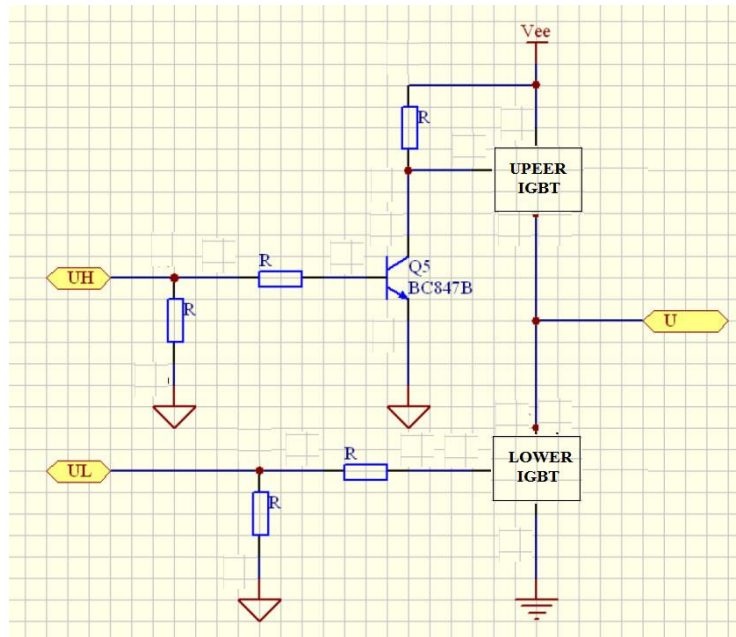


Fig. 5. 8, Implementation of switching elements

5.3.3 Voltage offsets

The measured motor terminal voltages need to be offset before they are measured by the microcontroller. This is to filter the voltage shift due to the biasing voltages of the active electronic component in the platform. Furthermore, for accurate formatting the y-address, the voltage, which is driven to port4 in figure 5.1, should be amplified to fit the voltage range of the microcontroller, 0 to 5V. To achieve those two tasks, an offset and amplification circuit was built around a set of op-amplifiers.

5.3.4 Analogue to digital conversion

A high resolution A/D, supported by the software facilities, is provided by the microcontroller. The embedded A/D converter has a 10-bit resolution, which permits to differentiate among 2^{10} (1024) different levels in the 5V analogue input. This resolution, 0.9 mV per digit, was employed to tackle the problem of weak oscillation at the motor voltage responses. Without this high A/D resolution, it becomes difficult for the estimator to differentiate between the motor voltages at different rotor positions. Moreover, it is possible to interface a higher resolution A/D converter with the microcontroller.

5.4 Sequence of triggering the inverter switching elements

At low and high speeds, the switching elements are triggered continuously according to a certain sequence provided by a commutation circuit. At zero speed, the situation is different. They are triggered for a short time just to detect the position of the rotor. In this work, to achieve the ZSRPE, three high frequency pulses, 3 kHz, were injected into the stator windings of the motor through sequentially firing the switching elements. Referring to figure 5.3, the sequence in this proposed platform is (AH + BL) \rightarrow (BH + CL) \rightarrow (CH + AL) was adopted in firing the IGBTs. Triggering the switching devices has no certain pattern. However, two triggering mistakes must be avoided. First, firing two switching devices, which lies on the same leg because it cause a short circuit between the supply terminals through the switching devices. Such mistake could damage the inverter electronic circuit. Second, firing two switching elements, which lies at the same level, upper or lower, because it is meaningless.

Figure (5.9) gives a picture to the actual platform, which was used to implement the zero-speed process of rotor position estimation.

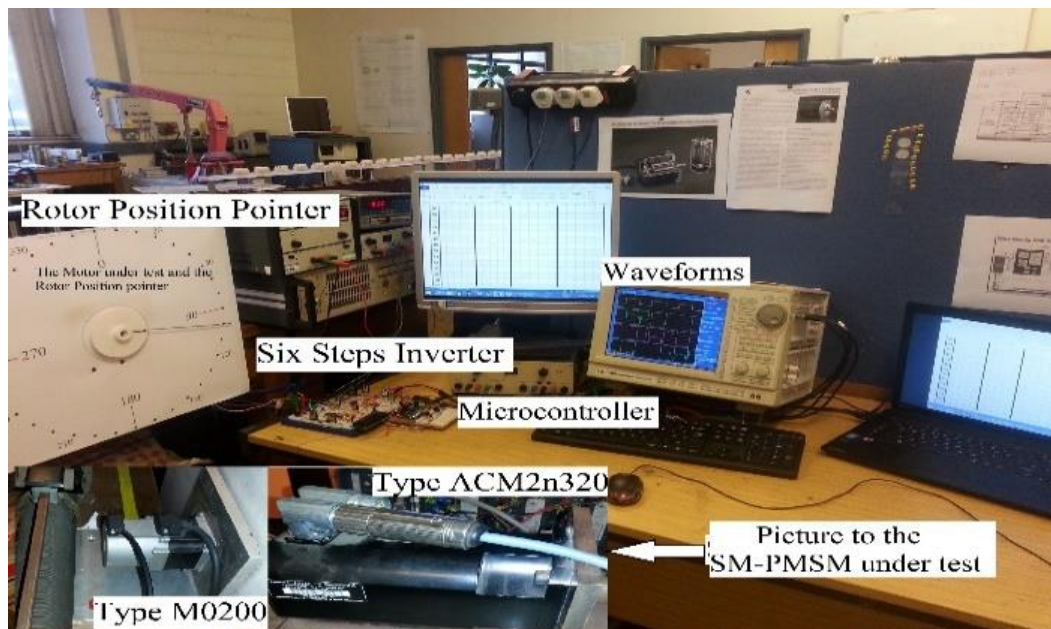


Fig. 5. 9, Details of the practical platform

5.5 Exciting the stator windings

Each injected pulse fires two of the six IGBTs formed the inverter. Accordingly, two of stator winding will be excited as two series inductors. For instance, the first injected signal fires the IGBTs AL and BL, as illustrated in the inverter drawing in figure 5.3. So coils A and B are in a series connection whereas the non-excited coil, C, is a free terminal. Thereby, it was employed to measure the voltages at the excited coils with respect to the neutral point N. This case is illustrated in figure 4.12 in chapter 4. Therefore, the voltages V_{NB1} and V_{NA1} are obtained during the forward and freewheel periods of the first injected signal. According to the excitation sequence means, discussed in section 5.4, the stator coils C, A and B were the free coils, non-excited, during the 1st, 2nd and 3rd injected pulses respectively. Therefore, the voltages V_{NB1} , V_{NC2} and V_{NA3} were obtained during the forward period of the three injected pulses, while, the voltages V_{NAF1} , V_{NBF2} and V_{NCF3} were obtained during the freewheeling period of the three injected signals respectively. The steps of injecting the pulses, measuring the motor terminal voltages, comparing the measured voltages, formatting the memory address and extracting the rotor position is illustrated by the flow chart shown in figure (5.10).

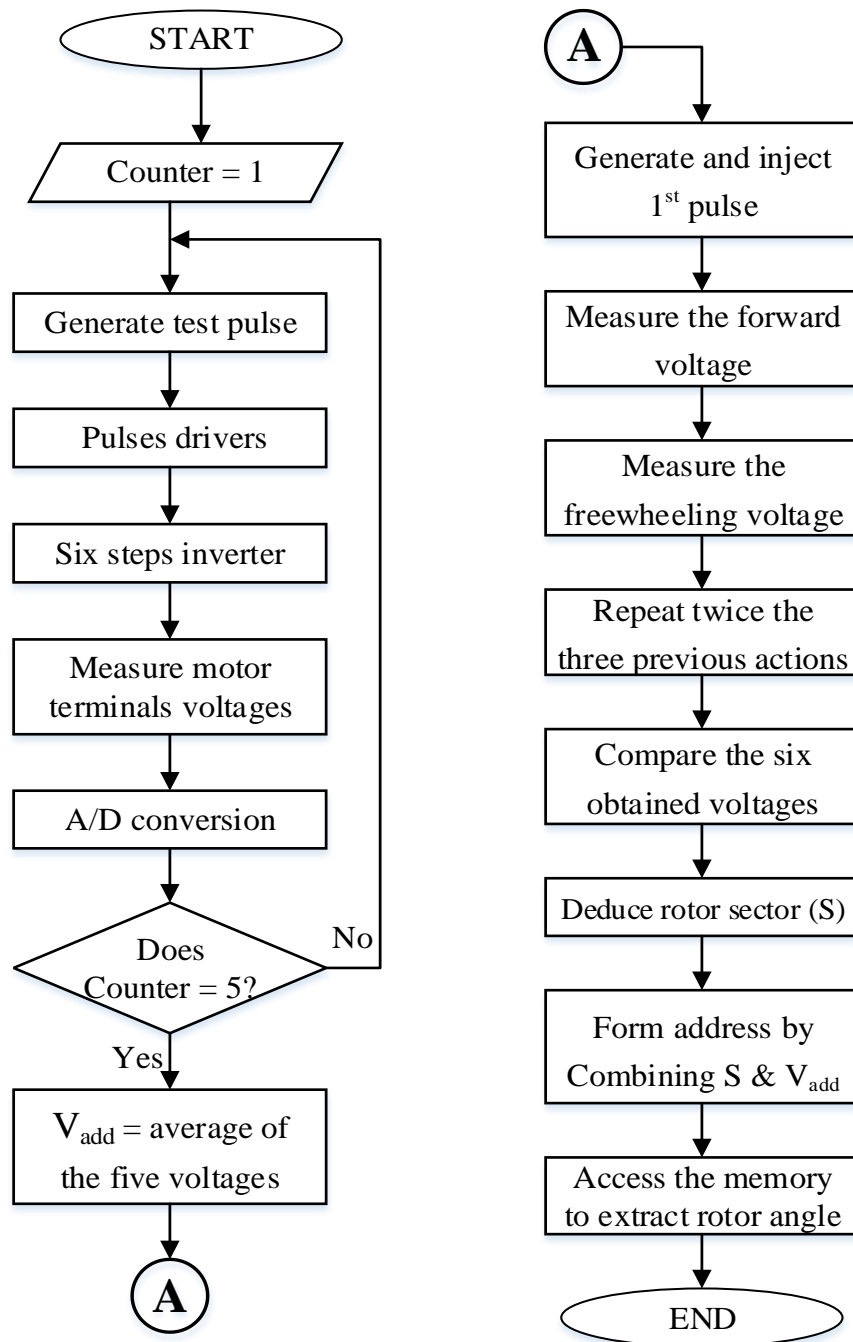


Fig. 5. 10, Flowchart for the procedure of ZSRPE by the practical platform

5.6 Results

5.6.1 Results of the proposed practical platform

Figure (5.11) shows a snap for the screen of the oscilloscope, which was employed in the practical platform. The snap illustrates the three injected pulses and the corresponding resultant voltage waveforms at the motor terminals after the buffer and offset blocks shown in figure 5.1. The green waveform is for the voltages measured at the terminal of coil C. The magenta waveform is for the voltages measured at the terminal of coil A. whereas, the blue waveform is for the voltages measured at the terminal of coil B.

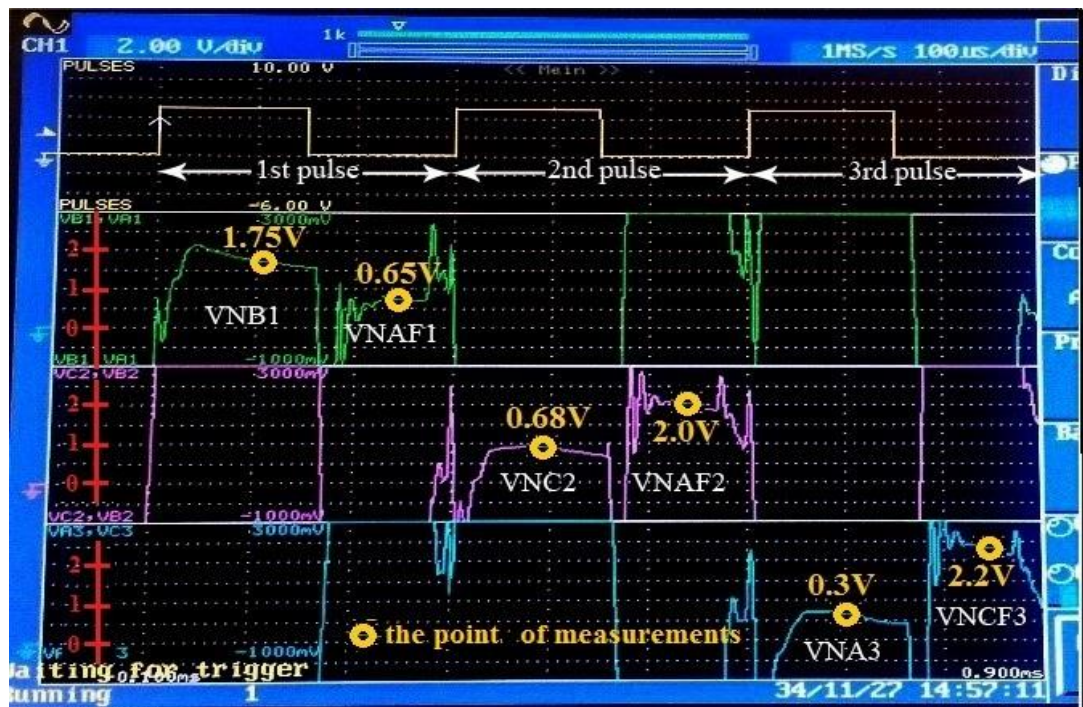


Fig. 5. 11, Injected pulses and waveform responses in ZSRPE practical platform

5.6.2 Processing the motor terminal voltages

These waveforms of the motor terminal voltages were processed by the microcontroller to extract the rotor position. The obtained estimation results for rotor position estimation are represented graphically in figure (5.12). The procedure of obtaining these results is illustrated by the following highlighting points and the flowchart shown in figure (5.10).

- ❖ Figure 5.11 includes four plots, the first for the injected signals, the other for the voltages, which were measured at the terminal of coils C, A, and B respectively from the second to the fourth plot.
- ❖ The microcontroller was programmed to take the voltage readings exactly at the points, which are indicated in the figure by small yellow circles. This is to avoid the oscillations, which appears at the waveform transition edges.
- ❖ During the period of the first pulse, the terminal of coil C was free. So, it sensed the terminal voltage of coil B during the period of high level of 1st pulse and, therefore, the controller is ordered to measure the voltage V_{NB1} . While, during the low level of 1st pulse, the free coil, C, sensed the terminal voltage of coil A and, therefore, the controller is ordered to measure the voltage V_{NA1} .
- ❖ Same events of first pulse repeated during the period of second and third pulses. Thereby, the microcontroller recorded the voltages V_{NC2} , V_{NA2} , V_{NC3} , and V_{NB3} .
- ❖ At this moment, the microcontroller started comparing the voltage values to determine the logic state for the variables A through P, which are mentioned previously in section 5.2.1.1.
- ❖ The variables A through P are binary variables. Their values, 1 or 0, are determined according to the true or false of comparison statements.
- ❖ Table 5.2 illustrates the comparison statements, which was adopted in the microcontroller programming.

Table 5. 2, Comparison statements in calculating the x-address

	Variables															
	A	B	C	D	E	F	G	H	I	J	K	L	M	N	P	
Comparison Statement	$V_{NB1} \geq V_{NA1}$	$V_{NB1} \geq V_{NC2}$	$V_{NB1} \geq V_{NA2}$	$V_{NB1} \geq V_{NC3}$	$V_{NB1} \geq V_{NB3}$	$V_{NA1} \geq V_{NC2}$	$V_{NA1} \geq V_{NA2}$	$V_{NA1} \geq V_{NC3}$	$V_{NA1} \geq V_{NB3}$	$V_{NC2} \geq V_{NA2}$	$V_{NC2} \geq V_{NC3}$	$V_{NC2} \geq V_{NB3}$	$V_{NA2} \geq V_{NC3}$	$V_{NA2} \geq V_{NB3}$	$V_{NC3} \geq V_{NB3}$	

- ❖ The microcontroller used the equation (5.1) to calculate the sector number, which represent the x-address.
- ❖ The microcontroller was programmed to take multiple measurements for one of the motor terminal voltages and use an algorithm to average it. This to improve the accuracy of y-address formatting.
- ❖ The microcontroller also ordered to use the millivolt variations to format the y-address and combine it to the x-address to form the memory address.
- ❖ The microcontroller used the memory address to access the memory and obtain the results of estimation.

The obtained estimation results for rotor position are shown graphically in figure (5.11). The graph of results includes two parts. First is a straight line between the actual and the estimated positions. This part represents the correct result of estimations. The second is a set of peaks. These peaks represent the errors in the estimation process. For instance, when the rotor is at actual position 40° , the proposed estimator estimates it wrongly by the peak e_2 which means 130° as an estimated rotor position.

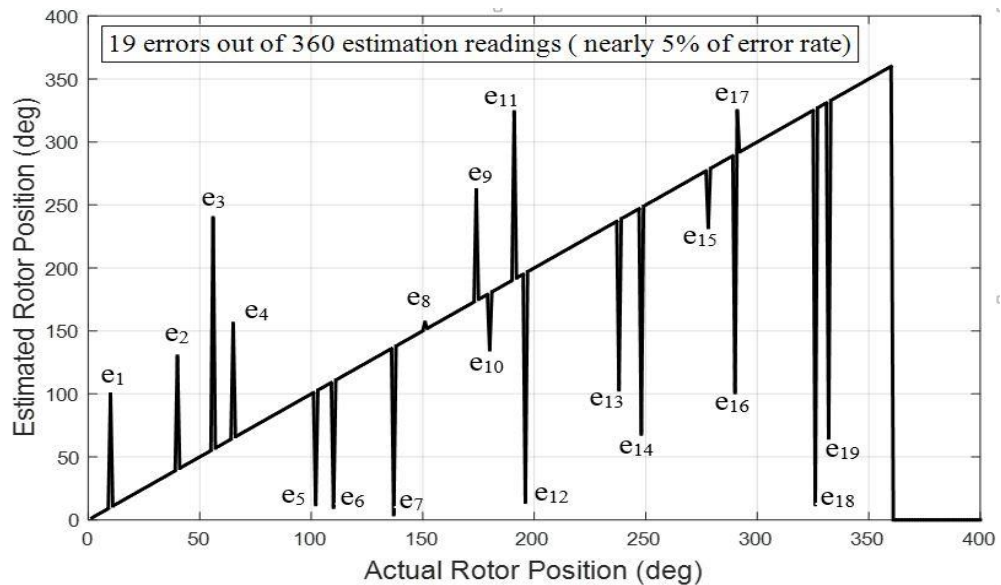


Fig. 5. 12, Graphical representation for obtained ZSRPEs from the practical platform

Table 5.2 gives a summary for the error estimations via the actual positions in the practical process of ZSRPE.

Table 5. 3, Summary of errors in ZSRPE for the practical platform

Actual	14	40	56	65	100	110	137	151	174	180	191	195	238	248	278	290	291	326	332
Estimated	100	130	240	156	10	6	4	157	262	135	324	9	103	168	232	101	325	12	65
Error NO.	e ₁	e ₂	e ₃	e ₄	e ₅	e ₆	e ₇	e ₈	e ₉	e ₀	e ₁₁	e ₁₂	e ₁₃	e ₁₄	e ₁₅	e ₁₆	e ₁₇	e ₁₈	e ₁₉

Then the error rate has been calculated as the percentage ratio of the total error estimations,19, to the total number of rotor position estimations,360, which has been found to be approximately equal to 5% . If the error is regarded as the difference between the estimated and actual positions, then Fig. (5.13) is obtained.

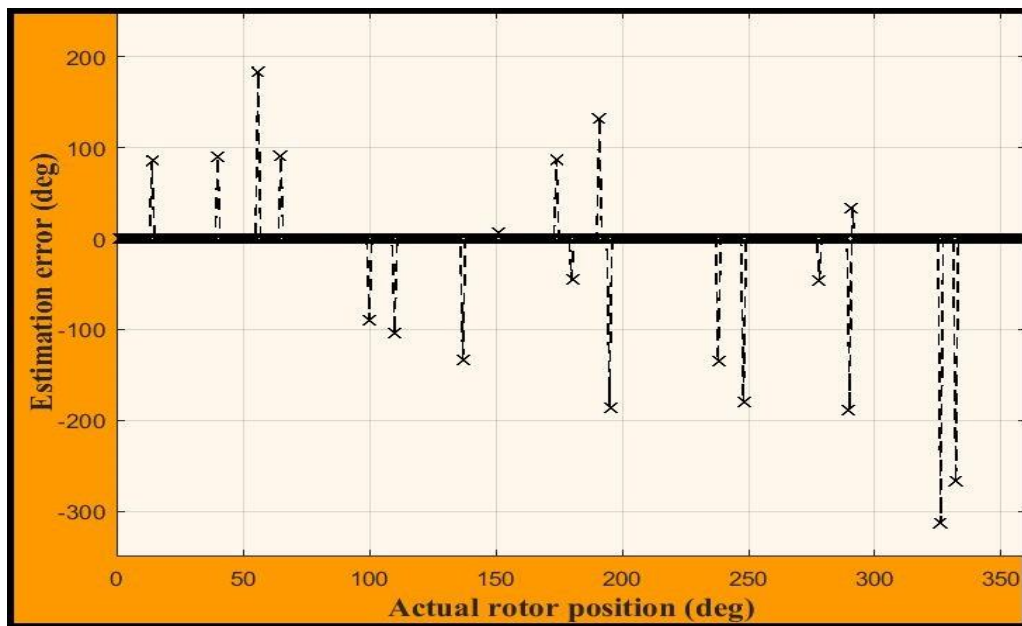


Fig. 5. 13, Estimation errors as difference between the estimated and actual positions

5.6.3 Comparison between the “MATLAB” and practical model results

Comparing figure 5.11 in the practical platform with the relevant figure 4.26 in the modelling system shows the high oscillation at the regions of pulse transitions. This indicates that the snubber circuits in the inverter of the practical model could not

suppress completely the oscillations at the collectors of the switching devices (IGBTs), which emerge due to the high rate of switching on the gates.

The comparison between the results of the modelling system, given in chapter four, and the results of the practical platform model are achieved through comparing the figures 4.27b and 5.11. It seems that real world platform has succeeded to follow the simulation “MATLAB/Simulink” environment model in estimating the zero-speed rotor position. However, the rate of error of the real world is 5% comparing with 2% for the modelling system. This difference is due to:

- 1) The noise, transient conditions, high switching effects, component contacts ... etc. which always accompanied the practical platforms.
- 2) The practical platform suffer from some of the inherent features of the motors under test, such as the saturation effects, secondary magnetic saliencies, rotor magnet polarity ... etc. These factors negatively affect on the estimation accuracy whatever the designer does to avoid them.
- 3) In contrast, the modelling calculations are based on a set of differential equations algorithm so they are immunised against the negative effects mentioned above.

5.6.4 Comparing the proposed estimator with other relevant works

Comparing with other relevant techniques, the proposed method is characterised by its simplicity, fast estimation and high resolution. The dispensing of magnetic polarity requirement and adopting only the voltage measurements are the major contributions in the simplicity of the presented technique. The exclusive voltage measurements reduce the complexity of current measurements and making the model full sensorless through dispensing the current sensors. No large computing processes are required so that the estimated results are obtained within a short time, 1.3 msec, and no microcontroller or digital signal processor of high specifications is required. The aforementioned features make the proposed work to be cost effective. However, the main limitation, weakness, in this zero-speed position estimation method is the uncontrolled uncertainty in distinguishing the voltage millivolt variations, which was adopted in formatting the y-

address. Table 5.4 presents a brief comparison with other relevant works [124] [145] [147] [150] which were based on the same principle of impulse response.

Table 5. 4, Comparing `performance of the propose estimator with other works

	Method given by reference				
	[124]	[145]	[147]	[150]	proposed
Resolution	30 degree	22.5 degree	60 degree	60 degree	1 degree
Magnet polarity	Yes	Yes	Yes	NO	No
Current sensors	1/dc-link current	3/phase current	1/dc-link current	1/dc-link current	No
Voltage certainty	good	good	good	good	Weak
Error rate	Not given	Varies with the rotor position	Not given	Not given	5%

For the purpose of comparison, figure 5.14 shows the graphical results of both the modelling scheme and the experimental platform.

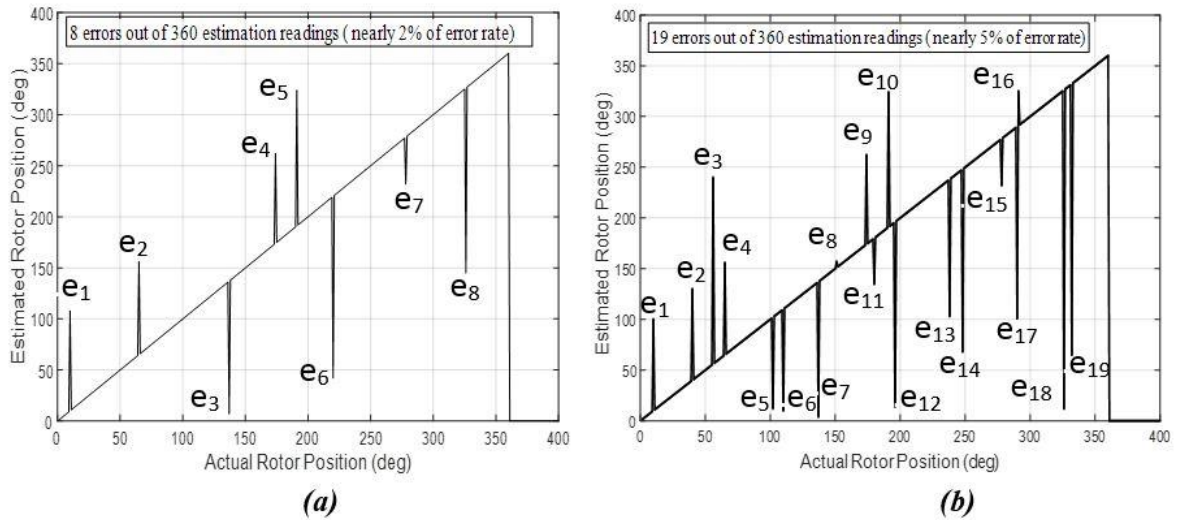


Fig. 5. 14, Comparing the estimation results (a) modelling (b) experimental

5.7 Summary

This chapter presents details of the practical implementation thought for sensorless position estimation of the permanent magnet motor at zero speed condition. The chapter topic is verified through a practical platform, which is built around a microcontroller.

The aspect of the proposed method for ZSRPE is achieved through employing the microcontroller as a pulse generator to excite the motor stator windings with three successive pulses. Each pulse is type return zero, RZ, of amplitude 5V and full period of 300 μ sec and 50% duty cycle. The pulses are fed to the motor windings through an inverter structure after being amplified. The voltage responses at the motor terminals are measured through the microcontroller analogue input channels. The responses are converted into digital forms to be ready for mathematical processing by the C-language programming library of the microcontroller. Two models of commercial surface mounted permanent magnet motors are tested by the built practical estimator. Accordingly, the obtained results for the rotor position estimation at zero speed, for resolution 1 degree of rotor angle, showed an approximate error rate of 5%, where the estimator has given estimation failure in 19 rotor positions out of 360.

CHAPTER 6

SIMULATION ANALYSIS FOR ROTOR POSITION ESTIMATION OF SM-PMSM AT LOW SPEED

6.1 Introduction

It becomes as a fact that the simulation and modelling approaches are effective procedures to study the various conditions of real-world systems and to ensure that any suggested model could verify the expected results as close as possible to the real time model. This give prior thoughts about the vision for the hardware implementation of the modelled system, the system behaviour under various test conditions and the expected results to be obtained.

Reference [177] mentioned that the modelling schemes provide a good environment for the researchers for repetitive conducting and analysing to the mathematical problems, which are involved in the actual problems, to reach the optimum condition. Moreover, it concluded that it is very beneficial to have a group of mathematical models with their results and feedbacks which all represent a guide for solving a certain problem. Reference [178] reported that the concept of mathematical modelling started in Germany in the 19th century when the mathematicians were employed in the assurance companies. Since that time, the modelling and simulation technique have started to win more reliability and to gain more of research focusing. Currently, it becomes a scientific true that the simulation and modelling processes help the engineers and scientists in saving time and cost during designing a certain project [179].

Within the environment of simulation and modelling, the “MATLAB/Simulink” program currently stands as a distinguished computing environment which provides full-featured modelling schemes. Various versions of “MATLAB/Simulink” have been designated to provide a convenient and attractive mathematical approaches to represent the real word problems and optimize their solutions [180]. During the early design

phases, the “MATLAB” simulation and modelling aspect project a spot of light on those conditions, which are difficult or highly cost effective to be studied on real time prototypes. Base on the aforementioned, the “MATLAB/Simulink” environment was employed in this work to model and simulate the rotor position estimation of permanent magnet motors when they are supposed to be run at low speed.

The low-speed rotor position estimation (LSRPE) represents a challenge for the researchers due to the weak induced back EMF, generated in the stator windings, within this range of motor speed. This is due to the direct relation between the motor speed and the induced EMF, whose zero crossing points are always used as base in rotor position detection at medium and high speeds. The back EMF weakness drops the signal to noise ratio (S/N) and makes it difficult to detect the points of zero crossing in the back EMF waveform. Therefore, the implementation of LSRPE by exploiting the back EMF becomes inapplicable choice [181]. The alternative method is by influencing the machine inherent feature of magnetic saliency through injection a high frequency signal into the stator windings. The saliency impact will be involved as a sinusoidal variations on the amplitude of the high frequency. Therefore, extracting this frequency, in a separate control loop, provides an opportunity to extract the information related to the rotor position [182].

This chapter verifies the employment of modelling and simulation approaches in establishment of rotor position estimator at low speed spinning. This modelling verification is achieved through a “MATLAB/Simulink” environment version 2015b. The outlines of this chapter include three key points. Firstly, section 6.2 illustrates the general principles which are adopted in modelling the low-speed rotor position estimation, LSRPE. Secondly, section 6.3 explains the proposed method in modelling the LSRPE. Finally, section 6.3 explores the obtained results by the proposed model.

6.2 General scheme for modelling the LSRPE

The general modelling scheme highlights the outlines for modelling the low-speed rotor position estimation. The rotor position estimation circuitry is always involved as a part of the complete scheme of controlling the PM motor running. The control systems

for driving the PMSM are brought to control motor speed, torque or both. Anyhow, they are normally closed loop control systems of one or more of feedback loop, or loops.

Therefore, the modelling approach for estimating the rotor position of PMSMs is a closed loop control system of double loops. First loop, forward path, is to control the motor terminal voltages or currents in order to manage the power transfer, or delivery, to the targeted motor. While the second loop, feedback loop, is to provide the first loop with the necessary control parameters. For example, controlling the operation of the PMSM through a servo system requires a forward path to supply the motor with the necessary power and two feedback paths to support the forward operations. The first feedback path provides the forward path with two important control parameters, first is the actual speed to be compared with the setting speed, while the second feedback path is to report the forward path the rotor position estimation in order to maintain an optimum overall operation for the control system [183].

6.2.1 Modelling the forward path

In the proposed modelling scheme, the motor was driven directly from the inverter output whose input was controlled by some form of pulse width modulation, PWM. Generally, the PWM is driven either via voltage comparisons or via current comparisons. Accordingly, two main methods are available to satisfy the generation of PWM, thereby controlling the forward path power and motor driving. These methods are highlighted below.

6.2.1.1 Forward path with PWM via voltage comparison

This configuration of PWM is always achieved by exploiting the space vector pulse width modulation, SVPWM, technique. Two voltage components are responsible for controlling the SVPWM performance. They are a horizontal component V_α and a vertical component V_β that both form the stationary reference frame. According to the modelling control scheme shown in figure 6.1, the forward path is functionally divided into two sub-paths, the quadrature and direct sub-paths. Therefore, formatting of V_β and V_α are achieved through the quadrature and direct sub-paths respectively. This method was adopted in this work in setting-up the practical model as it will be mentioned in the

next chapter. The methodology of this method in formatting V_β and V_α is shortly given below:

6.2.1.1.1 Modelling procedure for generating the voltage V_β

Firstly, the reference setting speed is compared with the estimated speed to obtain a speed error signal, e_s ³. Then, a proportional integration for this error, PI controller, gives an output reference current, i_{qr} . This current component is compared with the similar component that actually estimated from motor current, coming via the feedback loop, i_{qe} . The comparison result produces the final quadratic current error signal ei_q . This component is equivalent to the torque component in the total motor current. The error signal ei_q is passed through a third proportional integral PI to produce a voltage component which represents the quadrature voltage V_q in the rotary reference frame. Finally, a modelling block is required to convert this quadrature voltage component V_q into its equivalent form in stationary reference frame V_β .

6.2.1.1.2 Modelling procedure for generating the voltage V_α

This voltage component is modelled via the direct sub-path within the forward path. Considering the principle of field oriented control method, the main hypothesis in this widely used method is based on creating a quadrature relation between the rotor flux and stator current. This hypothesis is adopted to ensure producing of a maximum torque during rotor spinning [184]. To simulate this method, firstly, the direct component of stator current i_d is set to zero through resetting a constant modelling block. This zero current component, $i_d = 0$, is compared with the similar component that actually estimated from motor current, coming via the feedback loop, i_{de} . The obtained error signal, ei_d , is passed through a proportional integral to produce a reference direct current component i_{dr} . A comparison between i_{dr} and the high frequency injected signal, IF, is achieved to produce the direct voltage component V_d after a proportional integral operation. Finally, the same modelling block, which was exploited to produce V_q , is used

³ In this work, the subscript “e” refer either to “error”, if it comes at the beginning of any abbreviation, or to “estimate” if it comes at the end of any abbreviation.

to convert the direct voltage component V_d into its equivalent form in the stationary reference frame V_α .

6.2.1.2 Forward path with PWM via current comparisons

By this method, the speed comparison is employed to create the quadrature component, i_q , which is combined with the zero direct current component, i_d , to form a dq-reference frame. Then, the currents of this frame, i_q and i_d , are converted to the stator side to obtain three motor reference currents $i_{abc-ref}$. These reference currents are compared with the actual motor currents and the results of comparisons are used to drive a sine PWM technique. This technique was adopted in this work to achieve the modelling of low-speed rotor position estimation.

Theoretically and by modelling verification, the comparison between the performance of current and voltage PWM methods, to show the benefit of each method, has pointed out that the former is simpler in implementation while the latter is more efficient in consideration of power inverting, from dc to ac, by an inverter model [185].

6.2.2 Modelling the feedback path

Referring to figure 6.1, the feedback path has three main contributions; detection and estimating the motor currents in the estimated rotary reference frame i_{de} and i_{qe} , extracting and estimating the rotor position angle θ_e and finally, estimating the actual motor angular speed ω_e . The modelling implementation of these contributions is illustrated below:

6.2.2.1 Modelling detection and estimation of motor currents

This is achieved through simulating the direct measuring of stator phase currents i_a , i_b and i_c . Then, they are transformed to the rotary reference frame passing through the stationary reference frame. Thereby, the direct and quadrature estimated currents i_{de} and i_{qe} are obtained and fed to the forward path.

6.2.2.2 Modelling the estimation of rotor position and angular speed

The rotor position information is obtained by either sensor technique, encoder or solver, or by a sensorless technique, which are implemented by different methods. If a high frequency was injected in forward path, then the rotor position information will appear as a sinusoidal variations at the peaks of that high frequency. Therefore, this frequency should be filtered out in the feedback path to extract the rotor position information. So, the estimated rotor position angle, θ_e , is detected. By the fact that the rotor angular speed is time variant of the rotor angle, then differentiating the rotor position angle with respect to modelling time gives the value of the estimated speed, ω_e . This modelling procedure will be discussed later in more details in the proposed model.

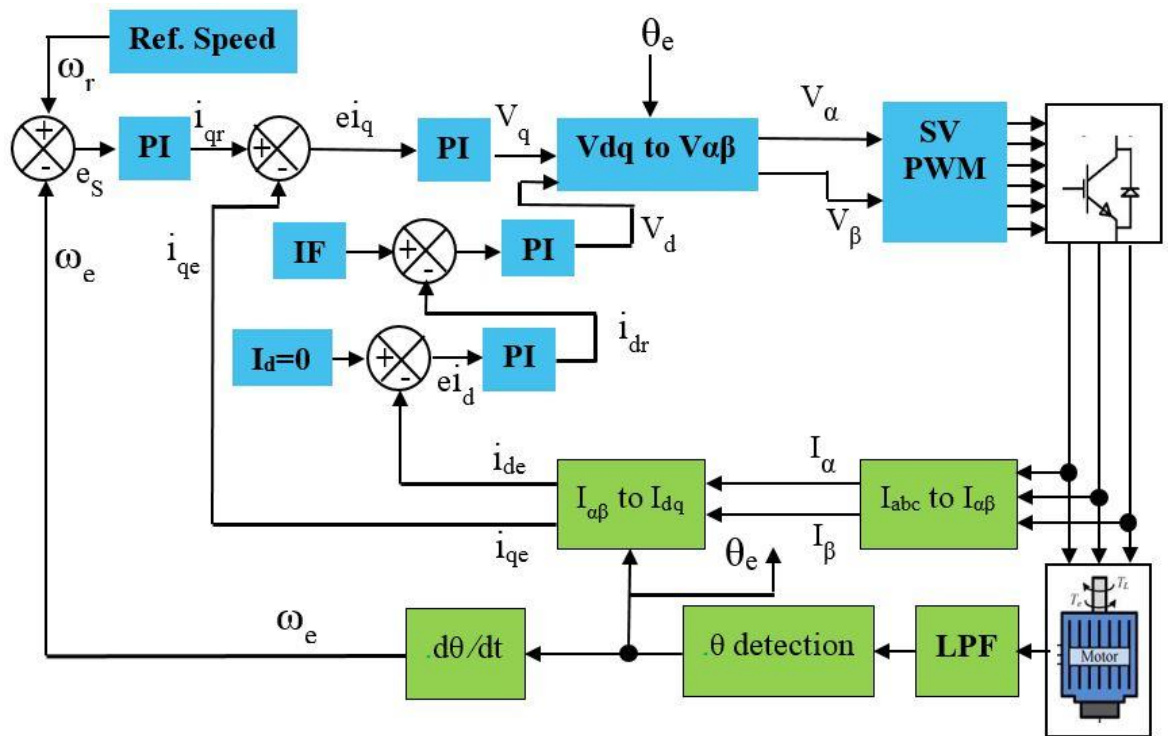


Fig. 6. 1, Overall scheme for modelling the LSRPE with voltage PWM

6.3 Proposed modelling scheme for LSRPE

The proposed modelling method focused on an approach which extracts the rotor position angle in the feedback loop. However, figure 6.2 demonstrates the proposed “MATLAB/Simulink” environment modelling scheme to estimate the rotor position at low speed. The model is presented in blocks form, where the yellow blocks represent the forward path and the cyan blocks are presented to form the feedback path. In the forward path, each line at the left of the block represents an input and at the right represents an output. This direction of signal is reversed in the feedback path. The modelling was built considering the assumption that the simulated motor was running under the field oriented control.

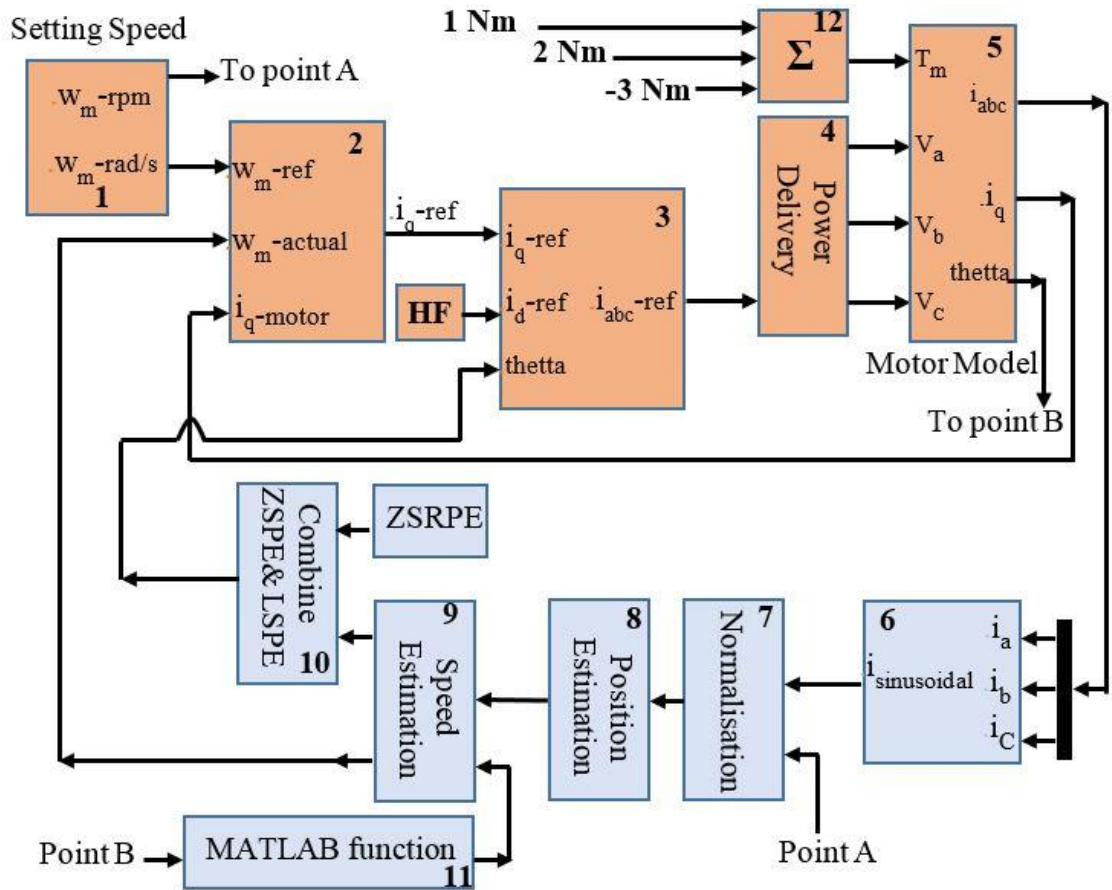


Fig. 6. 2, Modelling scheme for low speed position estimation

Table 6.1 gives a functional definition for the block numbering which is shown in this figure.

Table 6. 1: Index for blocks numbering in figure 6.2

1	Setting speed	5	PM motor model	9	Speed estimation
2	Reference torque current	6	Magnetic saliency detection		
3	I_{abc} reference current	7	Unity peak normalization	11	Position recovery
4	Power management	8	Position estimation	12	Applied torque
10	Combining initial position with low speed rotor position estimator				

Next is a brief explanation of each block involved in figure 6.2. For the purpose of simple reviewing, the blocks are going to be explored according to their presence in forward or feedback paths.

6.3.1 Blocks of forward path

Figure 6.3 demonstrates the main blocks that were used to realize the forward path in the given LSRPE model. Their title definitions are as highlighted in table 6.1. They are briefly illustrated as given below:

6.3.1.1 Setting speed Block

This block, which is labelled by number 1 in figures 6.2 and 6.3, includes a modelling facility to set the desired mechanical reference speed, ω_m , in rpm. It also includes simple mathematical expressions for conversion the mechanical speed from rpm to rad/sec and electrical speed, ω_e , in rpm. Therefore, it has three outputs to represent these three speed forms.

$$\omega_m(rad/sec) = \frac{\pi}{30} \cdot \omega_m (rpm) \quad (6.1)$$

$$\omega_e = p \cdot \omega_m \quad p: \text{number of rotor pole} - \text{pair} \quad (6.2)$$

6.3.1.2 Block of reference torque quadrature current

This block, which is labelled by number 2 in figures 6.2 and 6.3, is to extract the quadrature current, i_q , which could adjust the output torque. The block was designed to include two main parts. The first part is to compare the motor actual speed, ω_{m_actual} with the setting reference speed, ω_{m_ref} , to produce a speed error signal, e_{speed} :

$$e_{speed} = \omega_{m_ref} - \omega_{m_actual} \quad (6.3)$$

This error was passed through a proportional-integral speed controller to convert the error into torque component, from which an error quadrature current component, i_{qe} , was extracted. The electromagnetic torque which always produces by the SM-PMSM is given by [183] as follow:

$$T_e = k \cdot i_q \quad , \quad \text{where } k = \frac{3p}{2} \lambda_m \quad (6.4)$$

The goal of the proportional-integral speed controller is to produce a reference torque component T_{ref} according to the following equation:

$$T_{ref} = K_p \cdot e_{speed} + K_i \cdot \int_0^t e_{speed} dt \quad (6.5)$$

Combining (6.4) and (6.5) yields i_{qe} :

$$i_{qe} = \frac{T_{ref}}{k} = \frac{K_p \cdot e_{speed} + K_i \cdot \int_0^t e_{speed} dt}{k} \quad (6.6)$$

In the underlying LSRPE model, the PI parameters K_p and K_i , were adjusted to reach the acceptable output responses from the motor model. The adjusting procedure of the PI parameters was based on a manner similar to that adopted by bi-section method in numerical analysis [186].

The second part is to obtain a reference quadrature current i_{q_ref} from two current components. They are the error quadrature current and the actual quadrature component motor current i_{q_motor} . Thereby, the i_{q_ref} was obtained through comparing these two current components and passing the yielded error signal through a current proportional-integral controller.

6.3.1.3 Reference current Block

This block, which is labelled by number 3 in figures 6.2 and 6.3, is to obtain a reference for the three-phase motor currents, i_{abc_ref} . To conduct this, a reference direct current component, i_{d_ref} , was obtained from combining the high frequency injected signal with the direct current component which was assumed to be zero. At this point, there are two options to continue. First is by monitoring the current variations. Therefore, the i_{q_ref} and i_{d_ref} should be converted from the rotary reference frame to the three variables machine frame I_{abc_ref} by an embedded user defined function based on recalling the following matrix from chapter 2:

$$\begin{bmatrix} I_a \\ I_b \\ I_c \end{bmatrix} = \begin{bmatrix} \cos(\theta) & \sin(\theta) \\ \cos(\theta - 120) & \sin(\theta - 120) \\ \cos(\theta + 120) & \sin(\theta + 120) \end{bmatrix} \begin{bmatrix} I_d \\ I_q \end{bmatrix} \quad (6.7)$$

The second is by monitoring the voltage variations. Therefore, the i_{q_ref} and i_{d_ref} should be converted into the corresponding voltages V_{q_ref} and V_{d_ref} . By this option the control modelling scheme should continue as illustrated in figure 6.1. In this work, the first option was adopted just to cover all the possible controlling implementations.

As it is clear from the conversion matrix in equation (6.7), rotor position information is an essential term to achieve the task. Therefore, the estimated position angle, in the feedback path, was fed through this block input which is labelled by “theta”.

6.3.1.4 Power management Block

This block, which is labelled by number 4 in figures 6.2 and 6.3, was constructed by two main blocks, a model for sine pulse width modulation SPWM and a model for power inverter. Two inputs exist in this block, the first is for the actual motor currents, I_{abc} , and the second is the reference currents, I_{abc_ref} . The corresponding currents in the two inputs were compared with each other. The differences were used to produce the pulse width modulation signals. The last were exploited to drive the inverter, which accordingly provided their phase sinusoidal voltages to the next block, motor model. Figure 6.9 illustrates the current waveforms at the input terminals of this block and the resultant PWM signals.

6.3.1.5 PM motor model

This motor model is represented by block number 5 in figures 6.2 and 6.3. Basically, the motor model, which was designated in chapter 4, was employed in this modelling scheme. Some modifications and additions were made to meet the requirements of the LSRPE modelling scheme.

6.3.1.6 Applied torque Block

This block is labelled by number 12 in figures 6.2 and 6.3, To verify the capability of the proposed model to deal safely with the load variations, three levels for the applied torque were chosen, Three step function models were embedded to generate the required step levels at different specified times. These levels simulated three torque values 1, -3 and 2 Nm as shown in figure 6.4 which are labelled by T1, T2, and T3 respectively. Then, the applied torque was obtained from the summation of torque levels T1, T2 and T3. This applied torque, which has transitions 0-1-3-0, is represented in figure 6.4 by label (Σ). The torque levels T1, T2 and T3 were satisfied through three step function models whose parameters were set to verify the amplitude and timing of torque application.

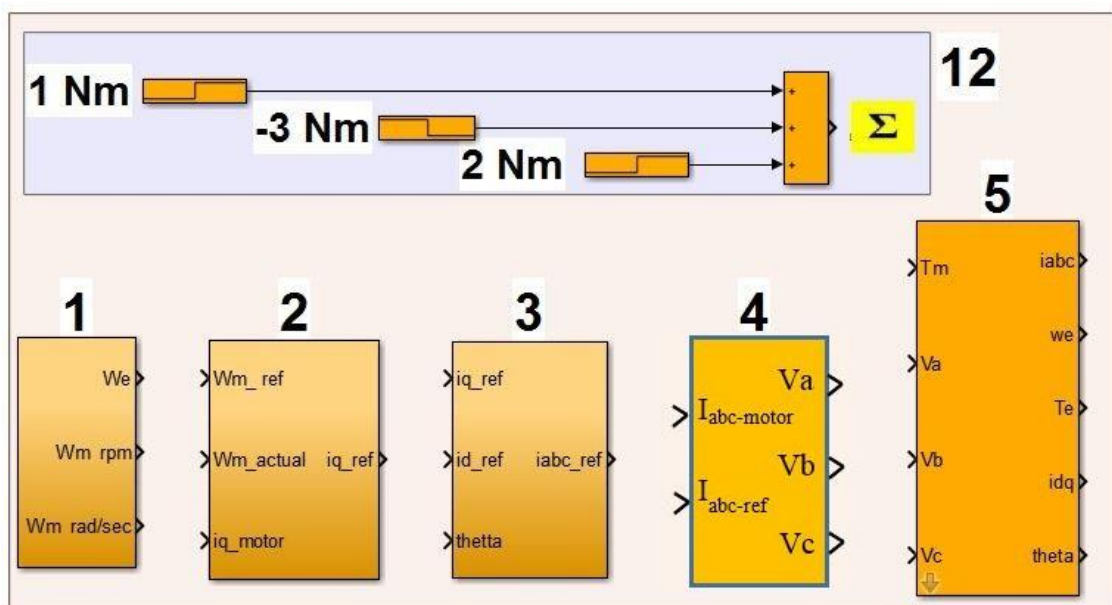


Fig. 6. 3, Forward path main blocks for LSRPE modelling scheme

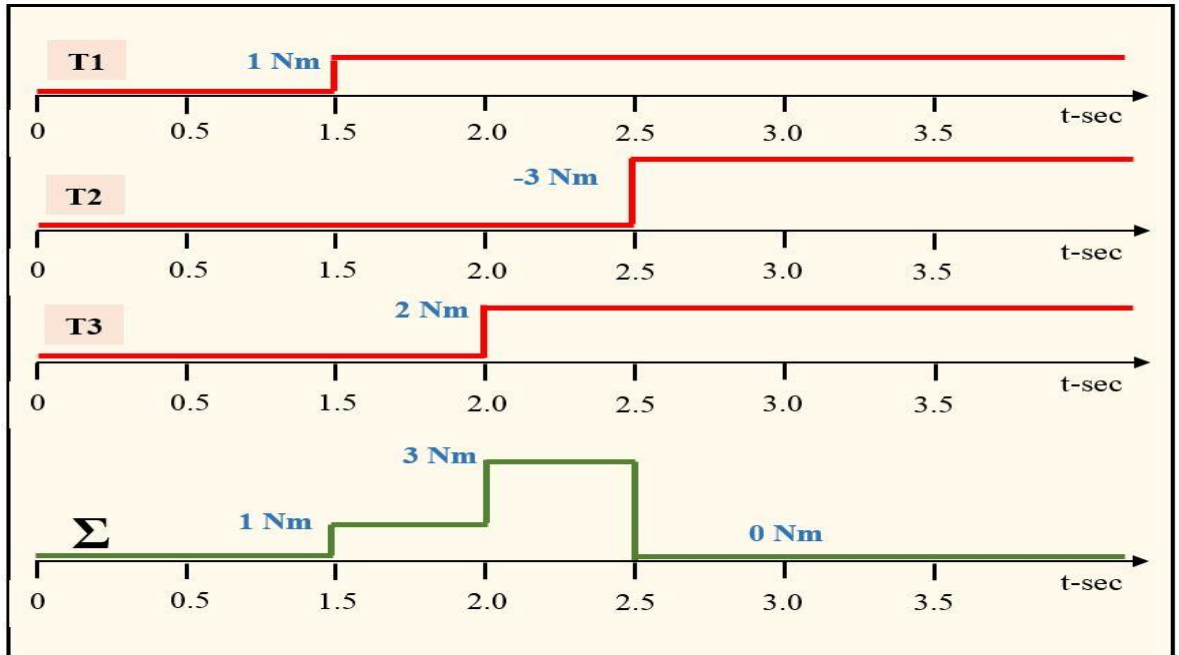


Fig. 6. 4, Variation of the applied torque load in the LSRPE modelling system

6.3.2 Blocks of feedback path

Figure 6.5 demonstrates the main blocks that were used to realize the feedback path in the given LSRPE model. Their numbering definitions are as highlighted in table 6.1.

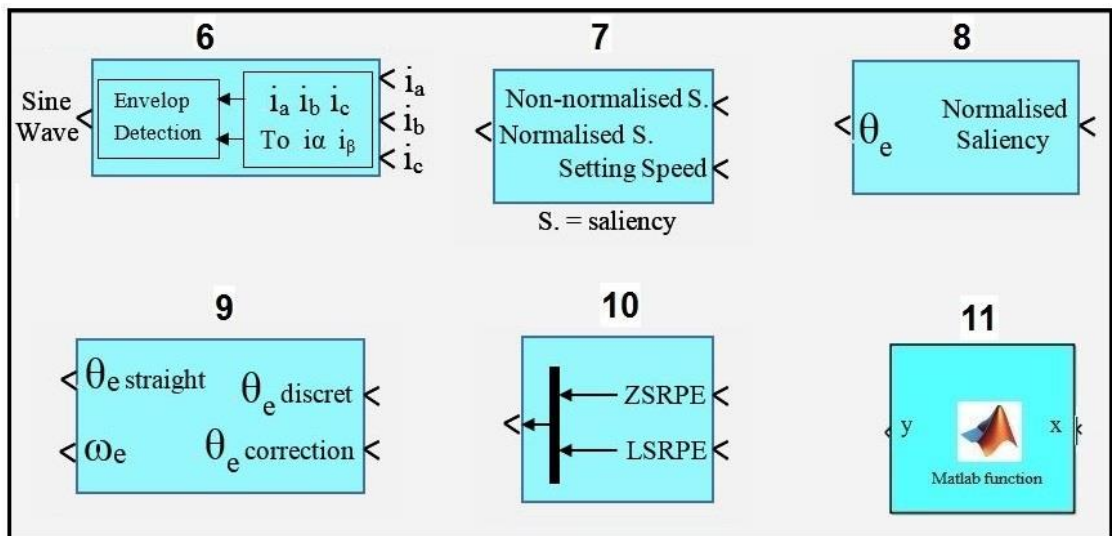


FIG. 6. 5, FEEDBACK PATH MAIN BLOCKS FOR LSRPE MODELLING SCHEME

These feedback blocks are briefly illustrated as given below:

6.3.2.1 Block of magnetic saliency detection

This block, which is labelled by number 6 in figures 6.2 and 6.5, was designated to input the motor stator currents, i_{abc} , and to use the mathematical relation of converting the stator variables into the two dimensions stationary reference frame i_α and i_β . Thereby, the i_{abc} currents were converted into the $\alpha\beta$ - reference frame by employing the following matrix transferring function:

$$\begin{bmatrix} i_\alpha \\ i_\beta \\ i_o \end{bmatrix} = \frac{2}{3} \begin{bmatrix} 1 & -\frac{1}{2} & -\frac{1}{2} \\ 0 & \frac{\sqrt{3}}{2} & -\frac{\sqrt{3}}{2} \\ \frac{1}{2} & \frac{1}{2} & \frac{1}{2} \end{bmatrix} \cdot \begin{bmatrix} i_a \\ i_b \\ i_c \end{bmatrix} \quad (6.8)$$

As the key function of this block is to track the machine magnetic saliency, so one of these two component was band-pass filtered, i_β , and processed through a heterodyning process to extract the envelop of the current component, i_α , whose envelope variation determined the amount of machine salience. The result for this saliency detection is shown in figure 6.11.

6.3.2.2 Unity peak normalization Block

This block is labelled by number 7 in figures 6.2 and 6.5. Its main function is to normalize the value of input current so as to provide an output oscillated between +1A and -1A. Figure 6.11, in the modelling results section, 6.4, demonstrates the required function, to be conducted by this block, through showing its input and output signals. This block function was achieved through three mathematical operations. Firstly, the input was offset to remove the dc component and thereby the input waveform sinusoidally vibrated between positive and negative parts. Secondly, the peak of each part was individually detected, as it will be illustrated in the next paragraph, because it was found that the saliency effect does not yield a pure sinusoidal waveform, $|I_p^+| \neq |I_p^-|$. Eventually, the positive and negative parts of the saliency effect impact were divided by the positive and negative peaks respectively. Figure 6.6 highlights this proposed concept.

The first input, in this block, is to input the sinusoidal waveform of the saliency detection which has to be normalized. While, the second input reads the motor setting speed, ω_m . The frequency value (f) of the second input signal and the speed value (ω_m) of the first input relate to each other by the fundamental equation of the synchronous motors, which is given by:

$$\omega_m = 60 * \frac{f}{p} \tag{6.9}$$

Therefore, this block uses the first input value to determine the expected frequency value of the saliency signal at first input. From which, the block could calculate the time-value of one fourth of the full wave period ($T/4$) of the sinusoidal saliency waveform. Fundamentally, the ($T/4$) value is corresponding to the peak value of any sinusoidal waveform. Thereby, the block detects the peak current (I_p) of the first input through employing this ($T/4$) time-value.

Figure 6.6 presents an illustrative a block diagram for the concept of implementation for this block function.

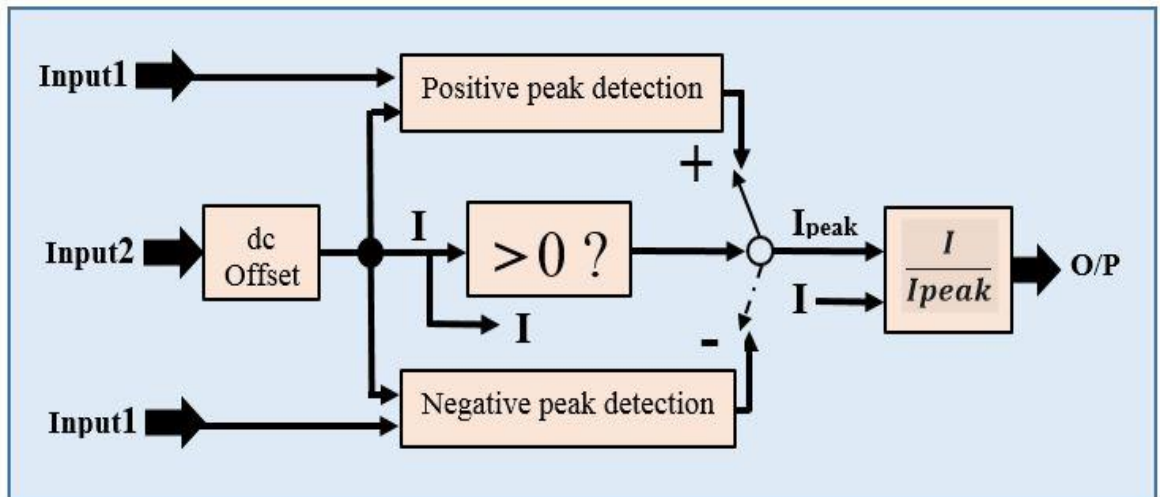


Fig. 6. 6, Structure of the unity peak normalization block

6.3.2.3 Position estimation Block, θ_e

This block, which is labelled by number 8 in figures 6.2 and 6.5, has a single input by which it receives the output of the unity peak normalized block, and a single output, which represents the estimated value of the rotor position at low speed. This block achieved its task by simply applying the inverse trigonometric sine function, arcsine, for the input signal. As the range of the MATLAB function (`asin`) is -90° to 90° , so the rotor positions in the second and third quarters will not be detected. Therefore, a certain algorithm was designated and embedded in this block to overcome this obstacle. The proposed algorithm was based on detecting the positive and negative slope ranges of the input signal, from which it had to determine the right quarter of the rotor position.

6.3.2.4 Block of speed estimation, ω_e

This block, which is labelled by number 9 in figures 6.2 and 6.5. The basic method to determine the mechanical speed is by dividing the difference between two cascaded angular rotor positions by the time interval between the readings of these positions [187]. This is mathematically expressed by:

$$\omega_{rm} = \frac{\theta_{t2} - \theta_{t1}}{\Delta t} \quad (6.10)$$

A main drawback involved by applying this method is a noticeable vibration that appears on the speed curve. To tackle this problem, a smooth speed is obtained by adopting a process of low pass filtering for the instantaneous changes in rotor position. The transfer function $F(s)$ of this filter has been determined by reference [187] as given below:

$$F(s) = \frac{s}{\tau*s+1} \quad (6.11)$$

where τ is an adjustable interval which is chosen by try and error. Anyhow, reference [187] has mentioned that this interval is a trade-off between the introduced lag and the noise of filtering process.

In this work, the proposed speed estimator was based on equation (6.10) with an addition of a smoothing sub-block to reduce the drawback of speed vibration. Figure 6.7 demonstrates a block diagram for the speed estimation block.

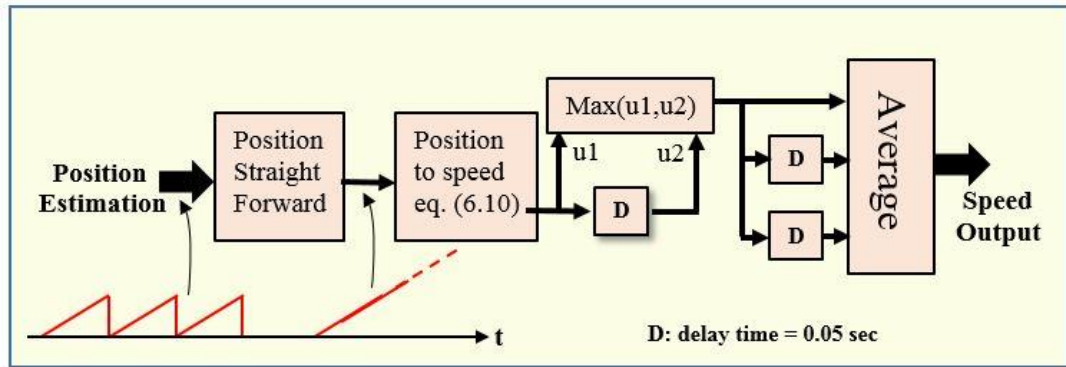


Fig. 6. 7, Block diagram for speed estimation

6.3.2.5 Position recovery Block

This block, which is labelled by number 11 in figures 6.2 and 6.5, is continuously observes the change in rotor position estimation. The general trend for position estimation is an increment in the value of rotor position detections. Therefore, this block was designated to detect and recover any drop in the present reading for position estimation comparing with the previous reading. If this condition occurs, the recovery block ignores the present false reading and estimates the existing position by incrementing the previous position by one degree.

6.3.2.6 Block of Combining the initial and low speed positions

At start-up period, the model of low-speed rotor position estimation was designated to read the initial rotor position from the zero speed estimator. The start-up period was roughly estimated to be 0.05 second. Figure 6.8 is a block diagram to illustrate the concept of this block, which is labelled by number 10 in figures 6.2 and 6.5.

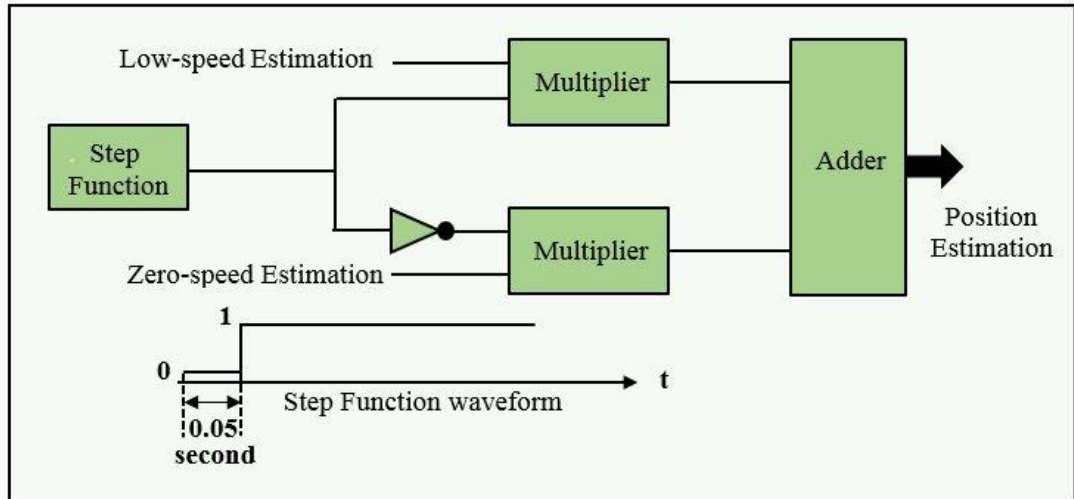


Fig. 6. 8, Block of combining the zero and low speeds rotor positions

6.4 Modelling results of the LSRPE

The following graphical results for the low-speed rotor position estimation model were obtained. The simulation time was one second except at the load test it was three seconds. While, the mechanical reference speed was set to 250 rpm.

Figure 6.9 illustrates three plots for variables in the forward path. The first is for the winding currents which were drawn by the PMSM model. The second is for the reference currents that were obtained at the output of the reference currents block. The third is for the PWM signals that were obtained according the comparison results of the motor currents and reference currents which were achieved by the power management block. All the three plots in this figure are zoom-in within the time interval between 1.45 to 2.11 second.

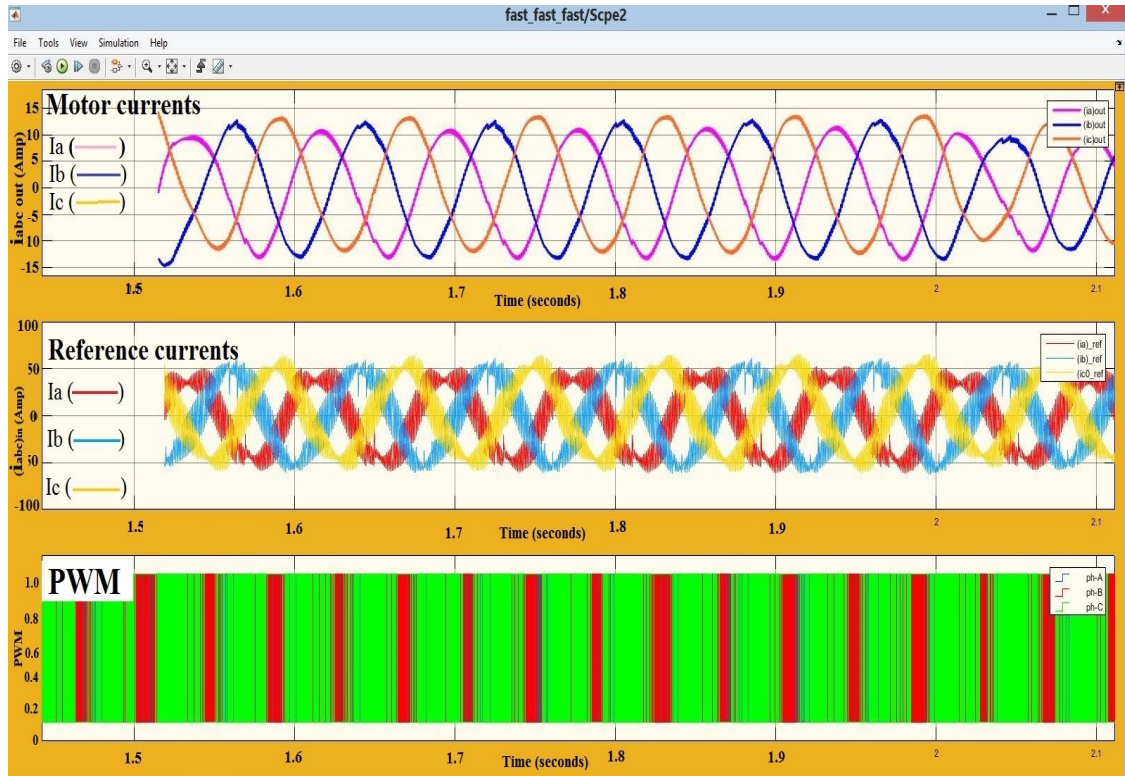


Fig. 6. 9, Motor currents, reference currents, and PWM

Figure 6.10 demonstrate three modelling graphical results a, b, and c. All of them were scoped in the feedback path. Graph (a) is for the i_{β} , i_{β} , which was obtained from a Clarke transformation for the motor currents. Graph (b) is for the high frequency component that was extracted through a band-pass filtering process for i_{β} . Graph (c) is for the upper envelope detection of the high frequency component, which supposed to be representing the machine saliency impact. Therefore, this graph should include the rotor position information.

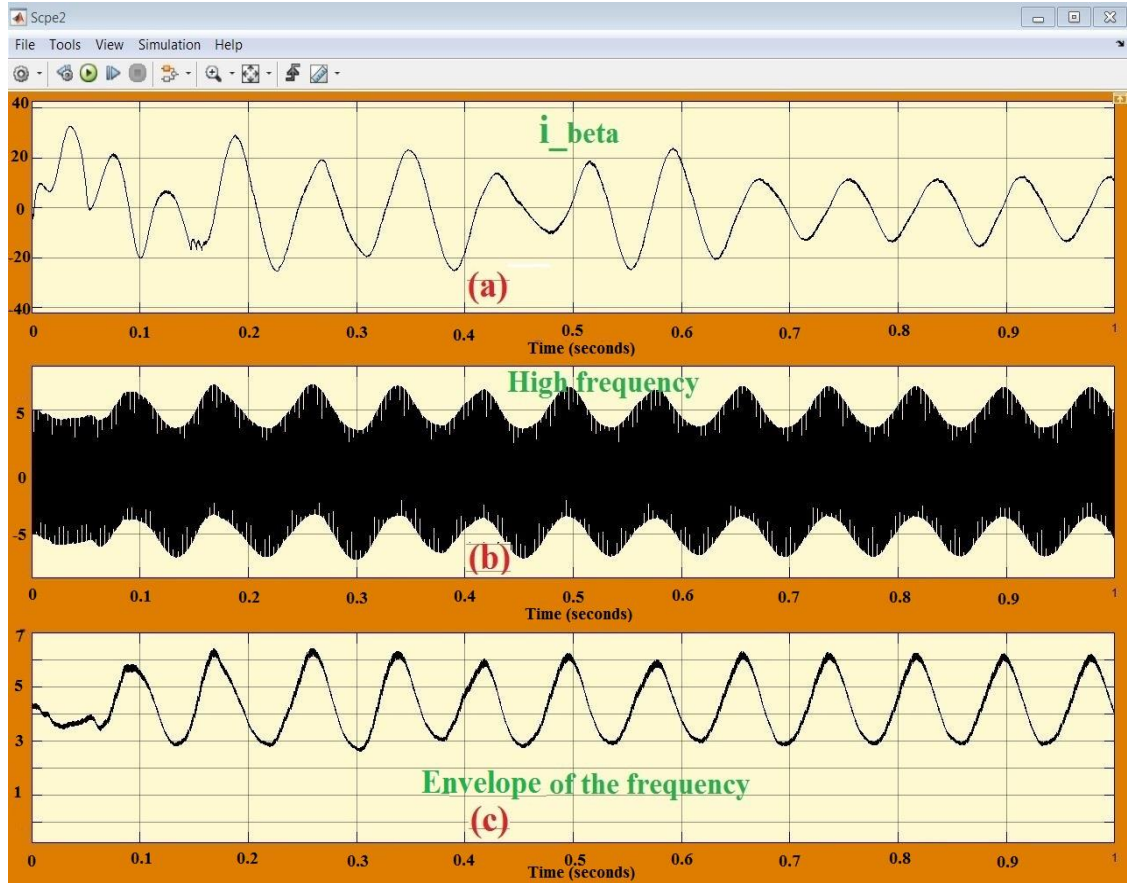


Fig. 6. 10, Waveforms at three output points in the saliency detection block

Figure 6.11 presents the waveforms at the input and output of the unity peak normalize block. As it was mentioned in section 6.3.2.2, the function of this block is to normalize the input signal, machine saliency, to be oscillated between upper and lower peaks at the output. From the graphic result, the block succeeded in achieving the task.

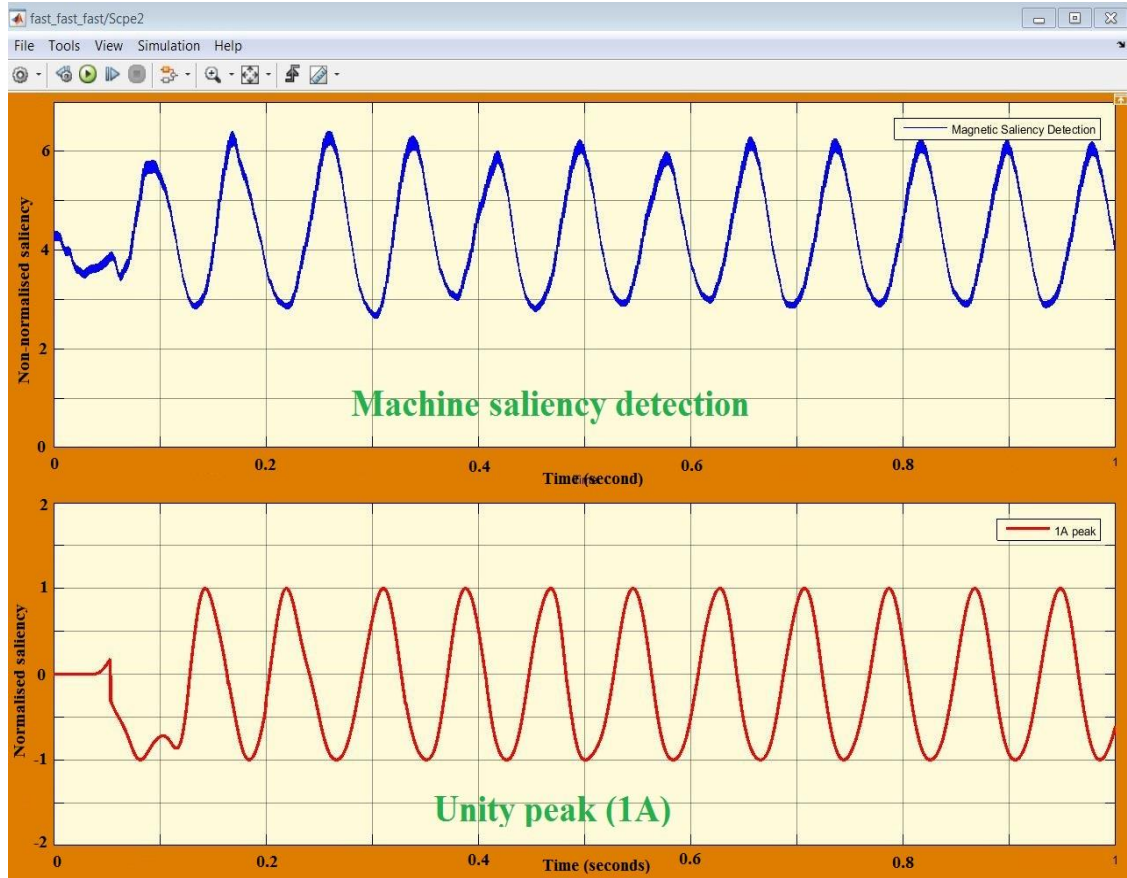


Fig. 6. 11, Input and output of unity peak normalisation block

Figure 6.12 shows three graphical results at the outputs of two blocks in the feedback path, the unity peak normalization block and the position estimation block. First plot highlighted the formatting of the saliency detection waveform, envelope of the high frequency, into a unity peak sin-waveform. It is noticed that the position estimation has some points of distortions due to the non-pure sine waveform of the saliency detection. Whereas the second plot presents a graphical representation for the result of calculating the electrical rotor position angle through sine inverse of the first plot. Third plot is a re-representation for the second plot in form of a continuous position estimation angle rather than repetitive every 360 degrees.

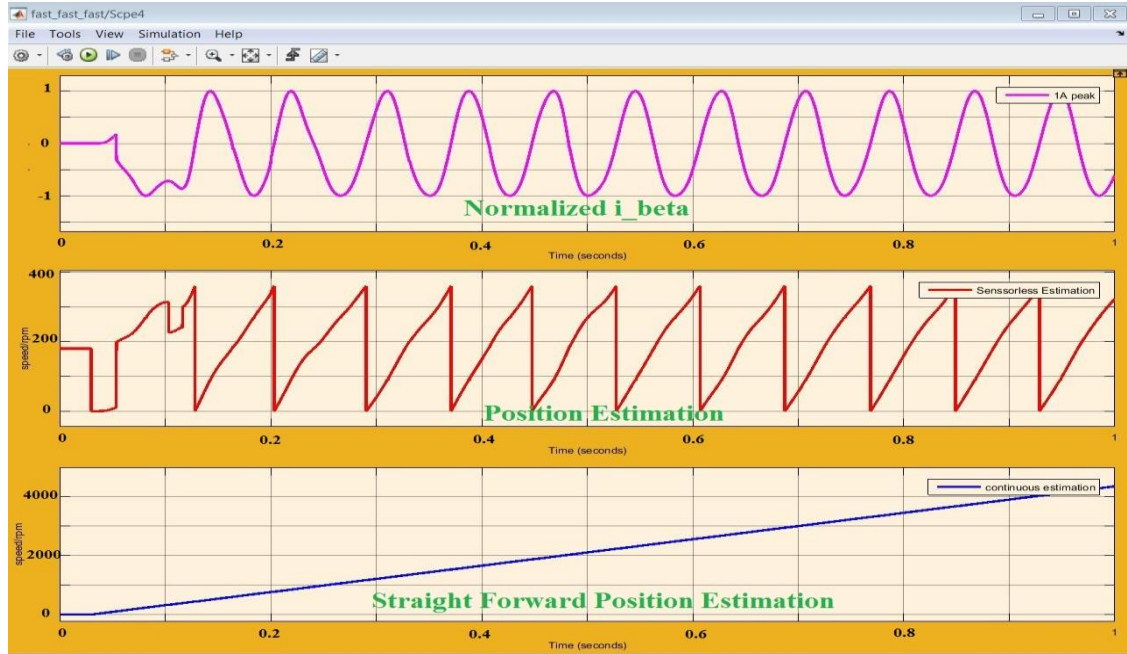


Fig. 6. 12, Outputs of blocks unity peak normalization and position estimation

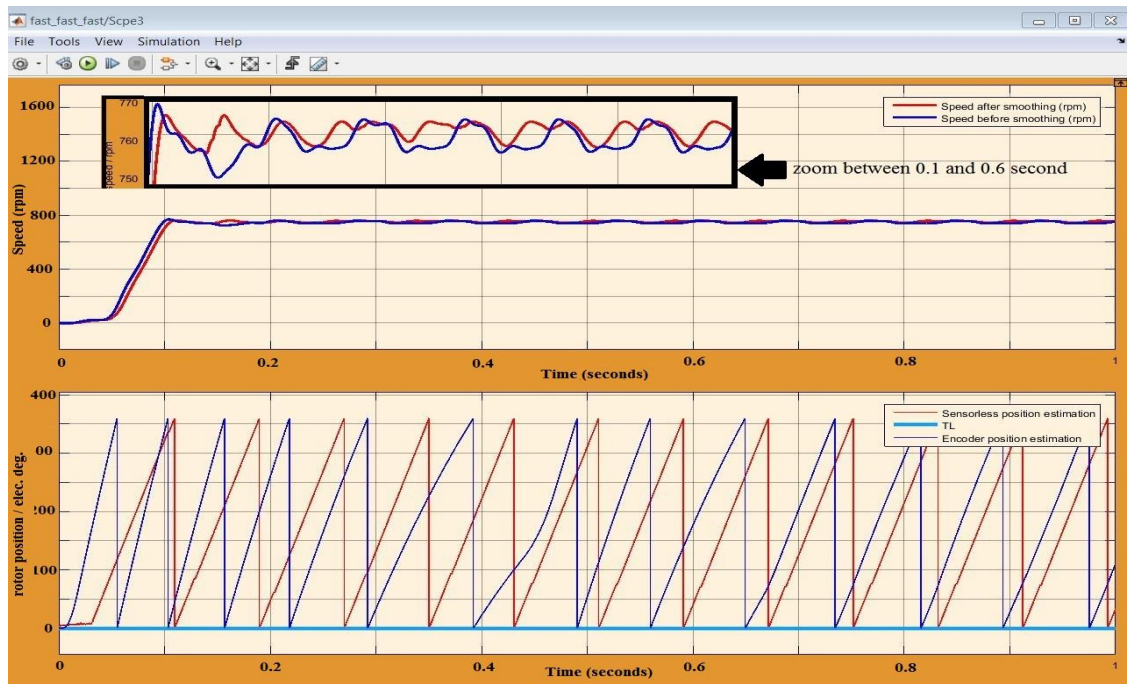


Fig. 6. 13, Speed and position estimation curves by LSRPE modelling

Another graphical result within the feedback path is introduced in figure 6.13. This figure presents curves for modelling the speed estimating with and without smoothing process. The zoom window shows that the speed smoothing has a weak effect. In

addition, the second plot in the figure shows the sensorless rotor position estimation from which the speed, given in the first plot, was derivative. It also provides the encoder position estimation curve to be compared with the corresponding curve of the proposed sensorless technique.

Figures 6.14 and 6.15 demonstrate group of graphical results, which describe performance of the simulated PMSM in the model of low-speed rotor position estimation, at no-load and load conditions respectively. The load condition is described by sudden change in the applied torque, both up and down.

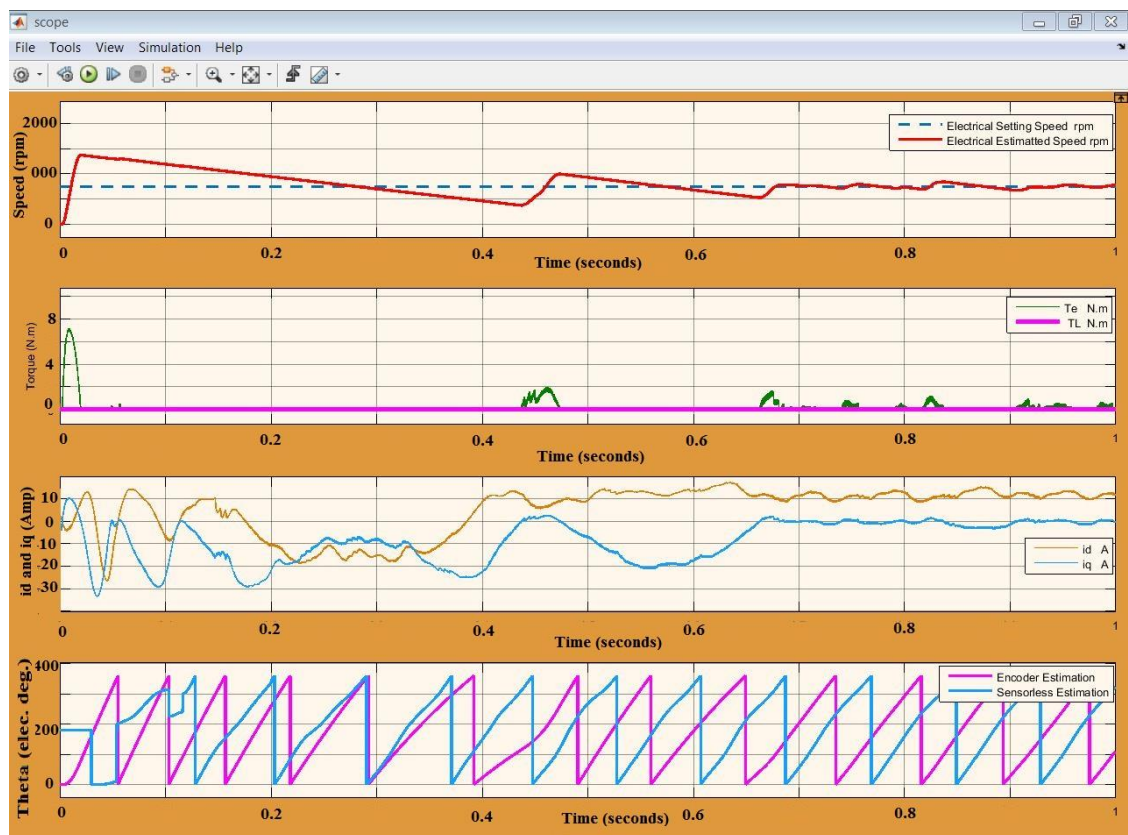


Fig. 6. 14, PMSM output curves by modelling system (at no-load)

As shown in the load test figure, figure 6.15, at time $t=1.5\text{sec}$, the applied torque changes from zero to 1Nm . This sudden change in load condition affected the level of speed ripple which recovered later under the influence of PI speed controller. Same events repeated when the applied torque jumped to a level of 3Nm . A more noticeable speed oscillation happened when the rotor released form the applied load. It took longer time to recover by the speed PI controller because it cannot generate a negative torque to

suppress the sudden overshoot which occurred in the motor speed with load change. However, the figure shows less effect of load condition changes on the direct and quadrature currents and so on rotor position estimation.

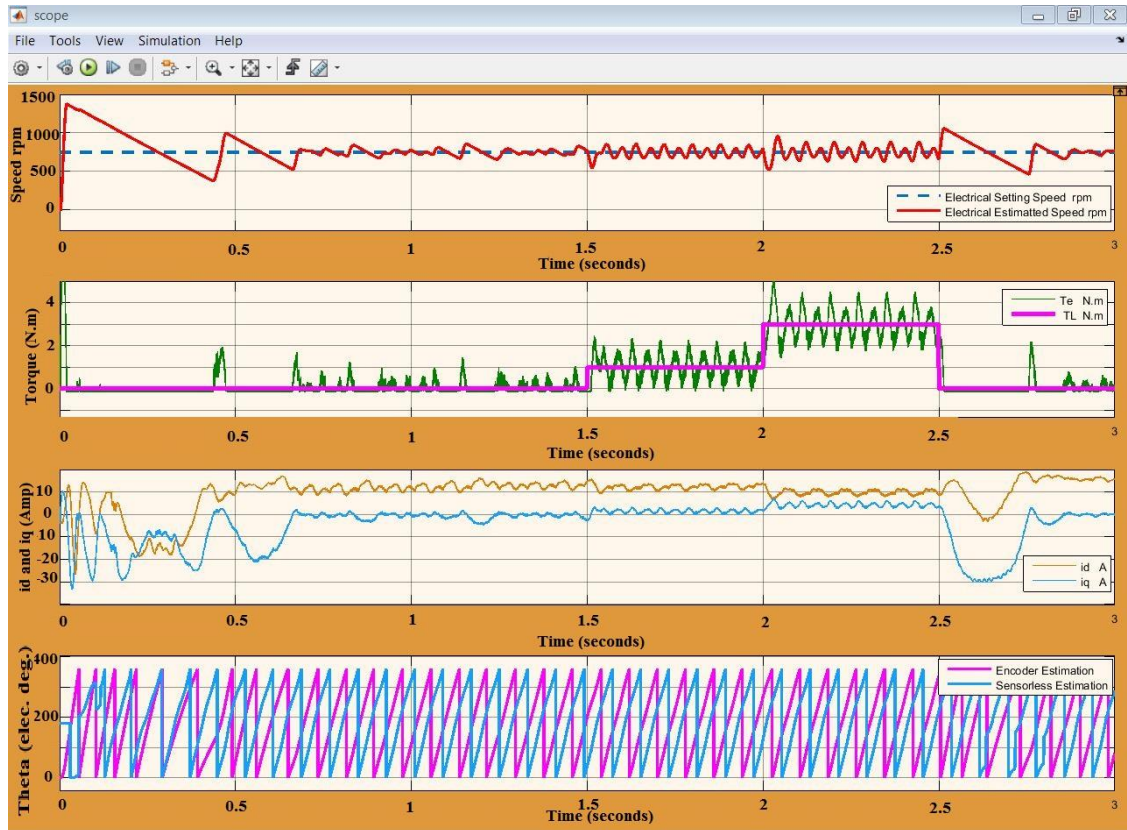


Fig. 6. 15, PMSM output curves by modelling system (under load test)

6.5 Summary

The main points in this chapter are summarised below:

- ◆ First the chapter presents a short introduction through which the importance of simulation and modelling are discussed. The MATLAB program, as a technical modelling language and simulation environment, is considered to implement the topic of this chapter.
- ◆ Through this chapter, the general trend in modelling the control system for running the permanent magnet motors, PMSM, is also discussed. As the PMSM is classified as a servo motor, the presented modelling scheme is designed according to this direction. The model of control scheme is introduced to be a

closed loop system which consists of a forward path to control the supplying of power to the modelled motor and a feedback path which should estimate both the motor rotor position and speed.

- ◆ The strategy for the modelling low speed rotor position estimation is built, in this chapter, depending on injecting a high frequency in the forward path. Then, this high frequency, which should be modulated with the information of the rotor position, is extracted in the feedback path. Finally, a heterodyning process is applied on the high frequency, within the feedback path, to demodulate the required rotor position estimation from the amplitude envelope of the high frequency.
- ◆ In addition, this chapter demonstrates the various obtained results from running the simulation program. The results point out the capability of proposed modelling system to give a continuous estimating track for the simultaneous variation in rotor position when the motor is running at low speed. Moreover, the results show a good response by the proposed modelling scheme to recover the rotor position estimation from any change due to a corresponding change in the value of applied load.

CHAPTER SEVEN

REAL-TIME EXPERIMENTAL SET-UP TO PREDICTE ROTOR POSITION OF SM-PMSM AT LOW SPEED

7.1 Introduction

This chapter has been planned to address this topic through twelve sections, which are outlined as follow. Section one presents a summary for this chapter. Section two introduces to the development in real time implementations and verification of rotor position estimation. Whereas section three gives a description for the adopted practical test bed, in this work, to satisfy the rotor position estimation at low motor speed running. Moreover, it discusses the theoretical base of test bed implementation and explores the various microcontroller peripherals, which are necessary to support the speed operation and rotor position estimation processes. Sections four and four introduce type of motors and encoders, which are employed in the test bed implementations, respectively. Binary converter that converts the encoder pulses into digital word, is introduced in section six. While section seven explains details of a magnetic brake load that to be used in motor load tests. Section eight discusses the strategy that was used to startup the motors under test. Whereas section nine highlights the method which is adopted in harmonics analysis. Section ten discusses some obstacles which emerge due to the employment of microcontrollers as cores in test bed implementations. Moreover, it suggest solutions which may be suitable to solve those obstacles. The obtained practical results are explored in section eleven and, finally, a summary for this chapter is presented in section twelve.

7.2 Development in real-time implementation

Real-time implementation has recently witnessed a remarkable improvement due to the significant progress on its verification methods and the continuous development in

software and hardware industry of signal processing systems. The leading impact in this field belongs to the essential development in power electronic, microelectronics and software engineering technologies since the middle of the 80s in the last century. The high quality electronic components and devices of low size, low weight, efficient power consumption, low cost ... etc. are the promising results for that development which has led to the production of high performance microcontrollers and digital signal processors development systems. These productions have been efficiently employed in manufacturing the integrated development systems for machines driving and control [188].

Meanwhile, the synchronize development in production of permanent magnet materials has positively accelerated the trends toward permanent magnet machine applications. Therefore, potential efforts have been noticed within the past two decades focusing on improving the operation environment for these machines. Consequently, the parameters, which directly affect the machine running and controlling process have been highly considered. Among these parameters, the accurate prediction for rotor position has found to be have a crucial impact in achieving this issue.

The difficulty in estimating the rotor position depends upon two obstacles. First is the motor speed at which the rotor angle estimation is demanded. While this point is regarded to be solved at medium and high rotating speeds, it still need some improvements and studies at low and zero speeds. Second is the machine itself, whether it was of surface mounted magnetic rotor or other types. For the surface mounted permanent magnet machines, it is more complicated to estimate the rotor position than the other types. This is because the surface mounted PM machine has a uniform rotor field distribution which causes in a weak magnetic saliency by which the estimation principle, at zero and low speeds, is totally dependent upon [189]–[191].

7.3 Description of the low-speed test bed

The main function for the practical test bed is, firstly, to provide the power to the under test permanent magnet motor and, secondly, is to estimate the motor rotor position

at low speed running. The basic descriptive structure for the proposed low-speed practical test bed is shown in figure 7.1 through functional block diagrams. The figure includes two main paths, forward and feedback, in which two microcontrollers, master and slave, are employed respectively to work as the core in each path. In addition, a set of peripheral devices is appended to each path to support the microcontroller actions.

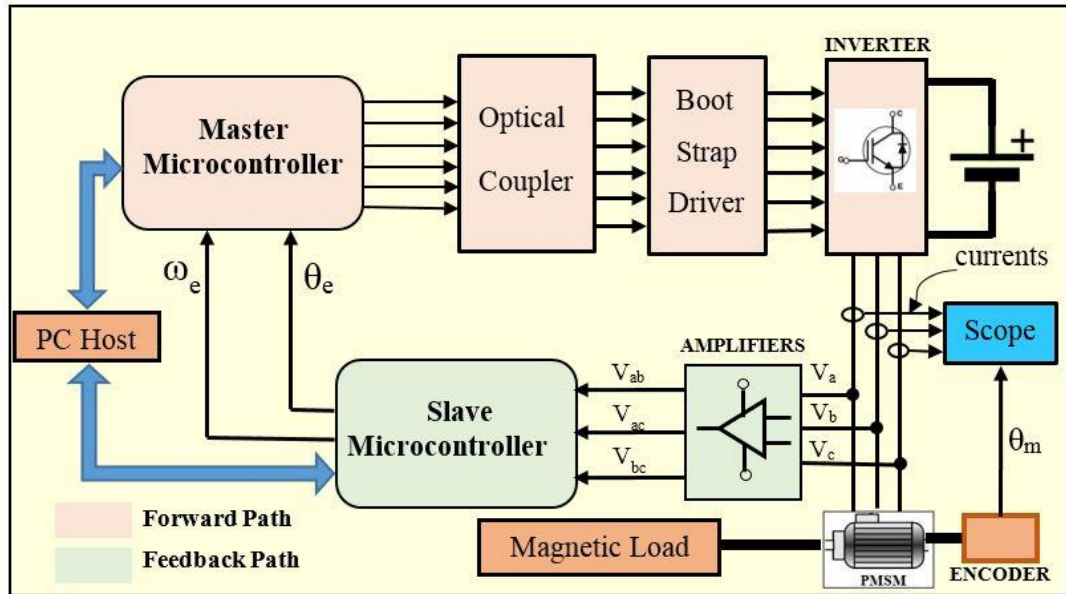


Fig. 7. 1, Block diagram for the practical test bed

Accordingly, the test bed is described with respect to the various operations, which are achieved by each path, as follow:

7.3.1 Forward path operations

The operations in this path are performed through four main blocks; master microcontroller, optocoupler, bootstrap driver and power inverter. A brief explanation for each of these blocks is given next.

7.3.1.1 Master microcontroller

The key topic for this microcontroller is to manage providing the necessary power outputs to energize the under test PMSM through a voltage source inverter, VSI, according to the space vector principle of operation. In this test bed, the goal of the master microcontroller is planned to be achieved through a proposed speed control

scheme. Therefore, the inputs to this microcontroller are limited by three values; the setting speed value, the estimated speed value and the rotor position value. While its outputs represent the standard six PWM switching sequences to drive the switching devices, IGBTs, of an inverter structure.

Figure 7.2 shows a functional block diagram for the different tasks, which are to be conducted by the master microcontroller through the C-language software programming in order to startup the PMSM. In addition, the figure also outlines the concept of the proposed method to control the motor speed. Detail information about the principle of operation for each block, in this figure, will be highlighted in the next sections.

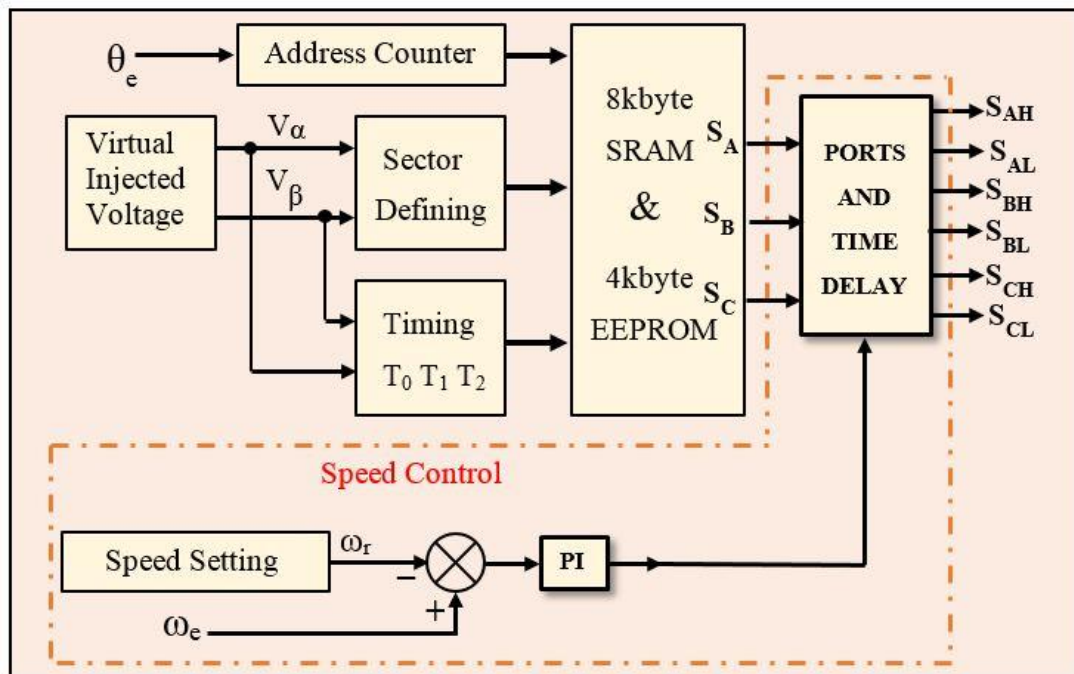


Fig. 7. 2, Functional block diagram for the master controller tasks in practical LSRPE

The figure blocks were implemented by a microcontroller development board, which is built around the chip “ATMEGA2560”. Figure 7.3(a) shows the physical structures of this master microcontroller, chip, and figure 7.3(b) shows the microcontroller development board [171]. A functional pins configuration for the employed master microcontroller is given in appendix B.5.

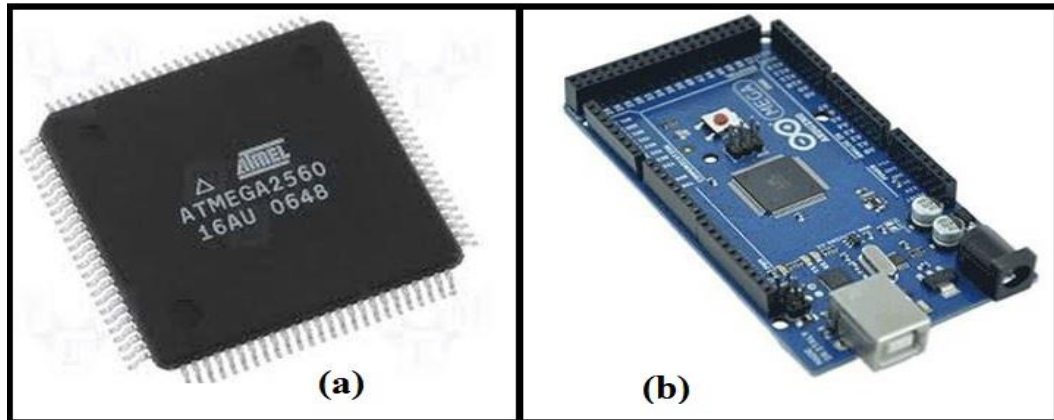


Fig. 7. 3, Micro-computer 2560 (a) chip (b) development board

This microcontroller has been manufactured to provide the following main features, which were used in this block implementation.

- 256kbyte flash memory
- 4kbytes EEPROM and 8kbytes SRAM
- 32 general purpose registers
- 54 digital input/output ports , 15 of them capable to drive PWM signals
- 16 ports for analogue inputs
- 10 bit A/D with a programmable gain facility
- 16MHz crystal oscillator

A certain limitation is present in utilizing this microcontroller and accordingly the proposed method, where after progressing in utilizing the underlying microcontrollers, it has been found that their PWM output channels have different switching frequencies. Therefore it becomes impossible to employ it in implementing the standard form of SVPWM. To save the cost, time and efforts of learning new programming language, the decision was not to replace this microcontroller by a new one and to continue in utilizing this microcontroller and trying to program it to be able to overcome this obstacle. Although this problem looks as a created problem, its proposed solution has provided an opportunity to enrich the thesis by adding a contribution through presenting a new approach in field of SVPWM implementation. This approach is well introduced in chapter seven.

The specified microcontroller was employed within the practical test bed to achieve the following six tasks, sections 7.3.1.1.1 to 7.3.1.1.6, through a C-language software programming.

7.3.1.1.1 Generating virtual injected voltages

It was supposed that the optimum 3-ph sinusoidal waveforms (V_a , V_b , and V_c) were noticed at the motor terminals and then they were transformed into the $\alpha\beta$ -reference frame. They are given by the fundamental equations:

$$V_a = V_{max} \cdot \sin \omega t \quad (7.1)$$

$$V_b = V_{max} \cdot \sin \left(\omega t - \frac{2\pi}{3} \right) \quad (7.2)$$

$$V_c = V_{max} \cdot \sin \left(\omega t + \frac{2\pi}{3} \right) \quad (7.3)$$

These voltages are always exploited in generating the two components V_α and V_β which are used to drive the space vector pulse width modulation scheme, SVPWM. The transformation process to the $\alpha\beta$ - reference frame is achieved through:

$$\begin{bmatrix} V_\alpha \\ V_\beta \end{bmatrix} = \frac{2}{3} \begin{bmatrix} 1 & -0.5 & -0.5 \\ 0 & 0.866 & -0.866 \end{bmatrix} \begin{bmatrix} V_a \\ V_b \\ V_c \end{bmatrix} \quad (7.4)$$

Thereby, the C-language programming tool of the master microcontroller was employed to virtually generate the components V_α and V_β which were injected in the space vector technique. Appendix C.1.7 presents a graphical representation for the virtual voltages, which were used to drive the motor “M0200”, with their transformations to the components V_α and V_β .

7.3.1.1.2 Sector determination

In the complex plane, the voltage components V_α and V_β form a revolving vector over a complete variable round angle, ϕ , from 0 to 2π . In the space vector theory, this round angle is divided into six divisions, or sectors, each of angular width equals to $\pi/3$. The trigonometric relation ($\arctan(V_\beta/V_\alpha)$) defines the sector position number, 1 through 6, of the revolving vector at any moment. This concept is highlighted in figure 7.4. In this figure, the revolving vector is pointed out as V_{ref} and this to be discussed later.

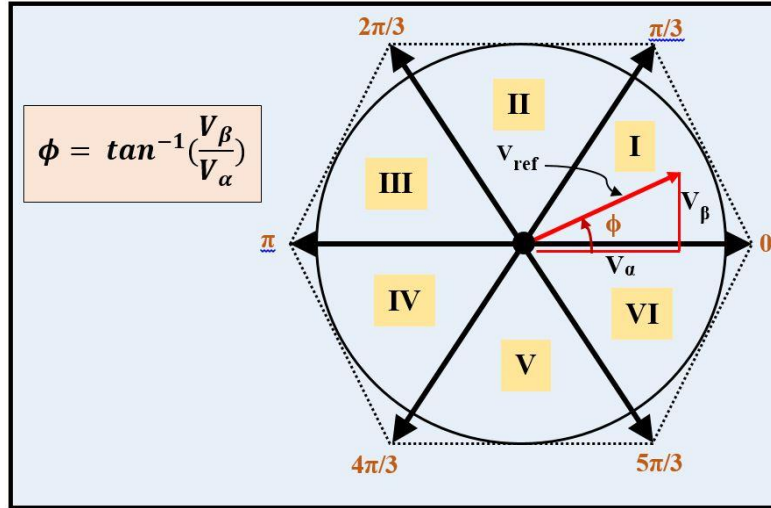


Fig. 7. 4, Sector divisions of the space vector

This sector determination was achieved by the master microcontroller through its facilities by the function (inverse tan) given in the C-language mathematical library. It may be worth to mention that the C-language library applies the inverse tan function (atan) in quarters one and four only. Therefore, the instantaneous values of V_α and V_β were exploited to determine the space vector angles in the second and third quarters. Alternatively, the instruction (atan2) verifies the inverse tan function in all quarters.

7.3.1.1.3 Timing of motor excitation

This section is explained through the space vector, SV, theory. According to this theory, the management of power transfer from a power supply unit to a PMSM, via a 3-ph inverter, is achieved through three essential steps.

Firstly, the revolving vector, which was earlier mentioned in section 7.3.1.1.2, revolves at an angular speed (ω_s) where the subscript “s” refers to the sampling rate frequency. Analysis of the revolving vector to its two basic components V_α and V_β , at each point within the complex plane, yields two timing intervals T_1 and T_2 according to the following equations:

$$T_1 = \frac{2}{\sqrt{3}} \cdot m \cdot T_s \left\{ \sin\left(\frac{\pi \cdot S}{3}\right) \cdot \cos(\phi) - \cos\left(\frac{\pi \cdot S}{3}\right) \cdot \sin(\phi) \right\} \quad (7.5)$$

$$T_2 = \frac{2}{\sqrt{3}} \cdot m \cdot T_s \left\{ -\cos(\phi) \cdot \sin\left(\frac{\pi \cdot (S-1)}{3}\right) + \sin(\phi) \cdot \cos\left(\frac{\pi \cdot (S-1)}{3}\right) \right\} \quad (7.6)$$

where “m” is called the SV modulation index. This index plays an essential role in defining the amount of applied voltage to the motor. It is defined as the ratio between the used voltage length of the revolving vector, V_{ref} , to the maximum allowed voltage length, which equals to 0.866 of the dc bus voltage V_{dc} .

$$V_{ref} = \sqrt{V_{\alpha}^2 + V_{\beta}^2} \quad (7.7)$$

$$m = \frac{V_{ref}}{0.866V_{dc}} \quad (7.8)$$

The intervals T_1 and T_2 are partial intervals from the total switching period T_s , and they represent the activation times for each of the two active vectors in a specified sector. Classification of space vectors into active and non-active vectors will be illustrated in section 7.3.1.1.5.

Secondly, subtraction the intervals T_1 and T_2 from the total sampling period T_s yields the timing interval T_0 which represents the working period of the non-active vectors. Therefore, the given four periods, T_s , T_1 , T_2 and T_0 , are related by the following equation:

$$T_s = T_1 + T_2 + T_0 \quad (7.9)$$

Thirdly, the values of intervals T_1 , T_2 , and T_0 vary with the vector revolving and the inverting process is performed through firing the inverter switching elements along the initially calculated intervals T_1 , T_2 , and T_0 .

Therefore, the inverter output voltages will be in form of pulses whose widths vary with the variations of the intervals T_1 , T_2 , and T_0 and, thereby, the motor is driven through the pulse width modulated, PWM, voltages of the inverter output.

The accurate calculations for the motor exciting times T_1 and T_2 ensures a correct running for the driven motor. This topic is illustrated as follow. Refer to figure 7.4, the circle area, whose radius is defined by the rotating vector V_{ref} , points out the output voltage derived to the motor, the larger circle area the greater output voltage. The maximum acceptable radius length is that of the circle which forms the inner tangent of

the hexagon sides. With respect to the hexagon area, the zone inside the maximum circle and its circumference are the zones of under modulation and full modulations respectively. In contrast, the region between the circumference and the hexagon sides is the over modulation zone. The last region is a forbidden operation region because the operation of motor under the over modulation could lead to make the summation of T_1 and T_2 greater than the total sampling period T_s and this yields a negative timing period T_o . Such values for timing intervals cause in losing the correct excitation sequence of stator coils and failing in the motor running.

In this test bed, and base on the above theoretical illustrations, the following operations were conducted through the software programming of the master microcontroller by employing the given above equations:

- Determining the modulation index according to a pre-setting value.
- Revolving the vector V_{ref} according to a predefined sampling rate N_s which defines the number of iteration upon one complete revolution in the space vector plane. Higher sampling rate lead to lower torque ripples and lower upper speed limit, and vice versa.
- Calculate T_1 , T_2 , and T_o according to the values of V_α and V_β and a predefined value of switching period T_s .
- Maintaining the value of modulation index to be less than the over modulation limit. It does so through comparing the input value for modulation index with an upper permitted limit which should be defined previously.

7.3.1.1.4 Address counter

This is a software codes implementation to create counting states to be used in addressing the EEPROM memory structure, which will be discussed next. With respect to SV thought, these counting states were used in this work to implement two significant concepts. Firstly, the time required for full counting period determines the motor full rotation period and correspondingly the motor maximum low-speed limit. Secondly, the total number of counting states determines the step width in the space vector pattern, and this is the meaning of sampling rate N_s . For example, if the total number of counting

states was 1000, then the SV width step is $360^\circ/1000=0.36$ degree. The step width plays an important role in harmonic reduction, the small step width the less harmonic effect.

Therefore, the counting states and sampling rate divide the whole space vector angular width, 360 degrees, into small angle divisions through a simple mathematical process. This process is reversely achieved through supposing the angle division is primarily known and the corresponding counting state is required. Thereby, the counting states are modified during accessing the memory cell according to the value of the estimated rotor position, θ_e . This makes it possible to jump from one location to another inside the standard SV pattern, rather than proceeding sequentially. Thereby, the estimator corrects the sequence of exciting the stator windings according to the estimated rotor position.

In the employed test bed, the master microcontroller managed the operations in this section through its C-language software by:

- Generating the counting states through iteration loop starts from a lower value and proceeds up to the value of sampling rate.
- Using these counting states to derive the embedded EEPROM memory structure which will be explained next.
- Modify the counting states according to the value of rotor position estimation as it is demonstrated above.

7.3.1.1.5 SVPWM and Memory

These two points are discussed within one section hereby because the space vector is at first briefly analysed, then its standard patterns are determined, stored in and executed through a memory structure, in conjunction with the timing intervals T_1 , T_2 , and T_o as it will be discussed next.

SVPWM: According to the SVPWM theory, there are eight switching states, S_0 to S_7 . In binary form, they are 000, 100, 110, 010, 011, 001, 101 and 111. The binary bit 1 returns to the corresponding inverter-switching device in the upper legs is switched ON. In contrast, the binary bit 0 returns to the corresponding inverter-switching device in the lower legs is switched ON. Six of the eight switching states, S_1 to S_6 , cause current flow

in the motor windings, so they are called as active vectors. In contrast, two switching states, S_0 and S_7 , are null, non-active vectors. Consequently, no current flows from the source to the stator coils during these two states and the applied voltage drops between motor terminals are zero.

Figure 7.5 highlights these active and non-active vectors represented in the complex plane of space vector. In addition to the essential eight space vectors, sub-vectors between each two successive main sectors can be created according to the values of the two components of the $\alpha\beta$ -frame, V_α and V_β . Correspondingly, the timing intervals of each main sector, T_1 and T_2 with respect to the total sampling time T_s , are generated according to the horizontal and vertical analysis for these sub-sectors.

In this test bed, the master microcontroller applied the concept of space vectors through the C-language software programming to:

- ❖ Define the space vector zones, sectors 1 through 6, according to the calculations of space vector angle by utilizing the two components V_α and V_β .
- ❖ Create the standard space vector patterns for each sector as they are defined by the space vector theory. Appendix C.1.8 shows those standard space vector patterns together with the corresponding switching states for the inverter devices, IGBTs.
- ❖ Load the SV patterns in conjunction with their corresponding timing intervals in the memory EEPROM cells, which will be discussed later, using the counting states, which are discussed above, in addressing the memory cells.

For instance, if the microcontroller has defined the space vector zone to be in sector1, then it should start creating and storing the standard space vector pattern as in the following eight steps:

- ◆ Start with the null vector S_0 , store, in the addressed EEPROM cells, $S_A=0$, $S_B=0$, $S_C=0$, and interval= $T_0/4$.
- ◆ Increment counting state and store the active vector S_1 as $S_A=1$, $S_B=0$, $S_C=0$, and interval= $T_1/2$.

- ◆ Increment counting state and store the active vector S_2 as $S_A=1, S_B=1, S_C=0$, and interval= $T_2/2$.
- ◆ Increment counting state and store the null vector S_7 as $S_A=1, S_B=1, S_C=1$, and interval= $T_0/2$.
- ◆ Increment counting state and store the active vector S_2 as $S_A=1, S_B=1, S_C=0$, and interval= $T_2/2$.
- ◆ Increment counting state and store the active vector S_1 as $S_A=1, S_B=0, S_C=0$, and interval= $T_1/2$.
- ◆ Finally, increment counting state and store the null vector S_0 as $S_A=0, S_B=0, S_C=0$, and interval= $T_0/4$.

The standard SV sequences with the corresponding IGBTs switching conditions, voltage at the stator winding terminals, and the phase currents through the defined six sectors are shown in Table 7.1. It is important to notice that there is only one bit alert with each switching state transition from a given sector to the next successive sector [5] [7].

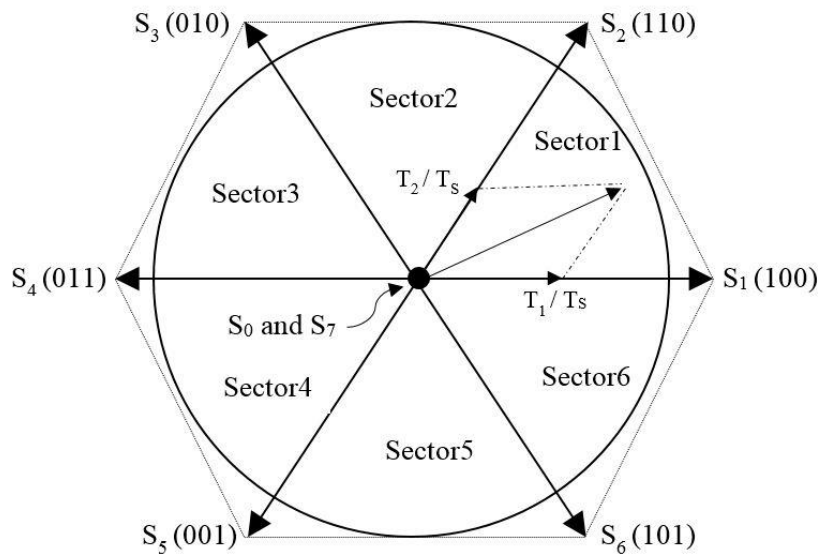


Fig. 7. 5, Space vectors representation in complex plane

Table 7. 1: Summary of SV voltages and currents analysis

SW. State	Binary			Switching Conditions						Winding Voltages			Current Flow
	S _A	S _B	S _C	A ^U	A ^L	B ^U	B ^L	C ^U	C ^L	V _{AN}	V _{BN}	V _{CN}	
S ₀	0	0	0	OFF	ON	OFF	ON	OFF	ON	0	0	0	0
S ₁	1	0	0	ON	OFF	OFF	ON	OFF	ON	V	-V	-V	i _a
S ₂	1	1	0	ON	OFF	ON	OFF	OFF	ON	V	V	-V	i _a +i _b
S ₃	0	1	0	OFF	ON	ON	OFF	OFF	ON	V	V	-V	i _b
S ₄	0	1	1	OFF	ON	ON	OFF	ON	OFF	-V	V	V	i _b +i _c
S ₅	0	0	1	OFF	ON	OFF	ON	ON	OFF	V	-V	V	i _c
S ₆	1	0	1	ON	OFF	OFF	ON	ON	OFF	-V	V	V	i _a +i _c
S ₇	1	1	1	ON	OFF	ON	OFF	ON	OFF	0	0	0	0

$V = V_{dc}/2$

As an example, figure 7.6 presents an illustrative diagram for the stator winding configurations with the progress of the SV sequence execution in sector 6 in which the space vector sequentially transits through the sequences S₀, S₁, S₆, S₇, S₇, S₆, S₁ and S₀ as illustrated in figure 7.5, shown above, and the sixth drawing in appendix C.1.9. Each configuration should wait for a delay time interval, t₀, t₁, or t₂ as illustrated in figure 7.7 shown below.

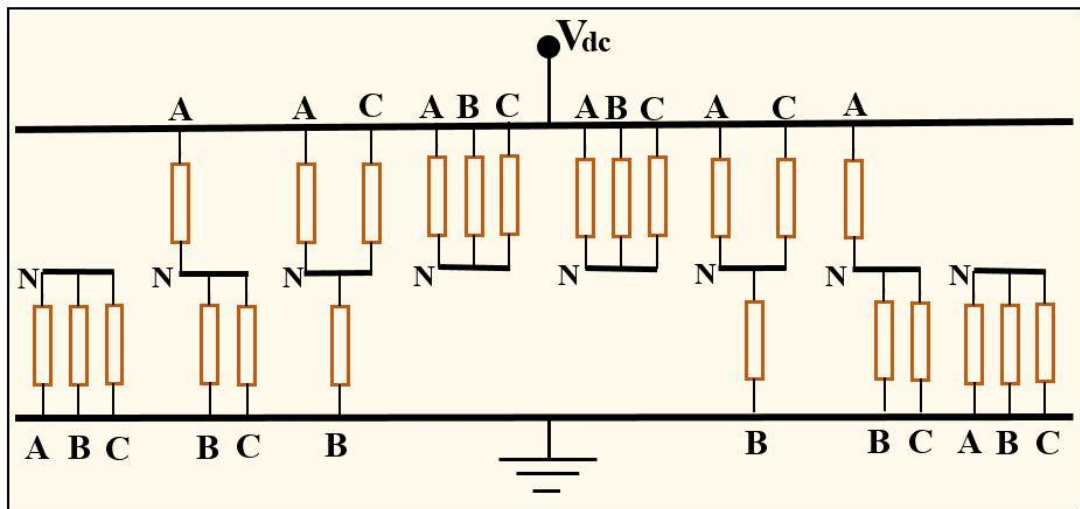


Fig. 7. 6, Sequence of motor winding connections in sector 6

According to table 7.1, the software programming of the microcontroller should report the inverter switching elements, IGBTs, how and how long to be switched ON or OFF. According to this procedure, the phase voltage of each coil, V_{ph} , and the phase-phase voltages are derived to yield the following matrix forms [192]:

$$\begin{bmatrix} V_{AN} \\ V_{BN} \\ V_{CN} \end{bmatrix} = \frac{V_{dc}}{3} \begin{bmatrix} 2 & -1 & -1 \\ -1 & 2 & -1 \\ -1 & -1 & 2 \end{bmatrix} \begin{bmatrix} S_a \\ S_b \\ S_c \end{bmatrix} \quad (7.10)$$

$$\begin{bmatrix} V_{AB} \\ V_{BC} \\ V_{CA} \end{bmatrix} = V_{dc} \begin{bmatrix} 1 & -1 & 0 \\ 0 & 1 & -1 \\ -1 & 0 & 1 \end{bmatrix} \begin{bmatrix} S_a \\ S_b \\ S_c \end{bmatrix} \quad (7.11)$$

For the considerations of harmonic reductions, the microcontroller programming should be able to avoid the next two space vector conditions:

- The ordinary case of switching intervals T_1 , T_2 , and T_0 is the switching interval of the non-active vectors, switching states S_0 and S_7 , T_0 , is significantly smaller than those of the active vectors T_1 and T_2 . Therefore, it is necessary to ensure that the non-active switching interval T_0 not to be smaller than the rated switching time of the employed inverter switching device, IGBTs.
- For purposes of improving the quality of the produced PWM, which is the target of the SV technique, it is necessary for the rotating vector to cross over the edges, which are relatively close to the active vectors. This is because one of the active timing intervals, T_1 or T_2 , may encounter the same switching problem of T_0 which is discussed above.

Therefore, forbidden regions will appear in the complex plane of the space vector. These regions are shown in figure 7.7 as it was given by reference [193]. In this work, the master microcontroller was programmed to detect and avoid these forbidden regions.

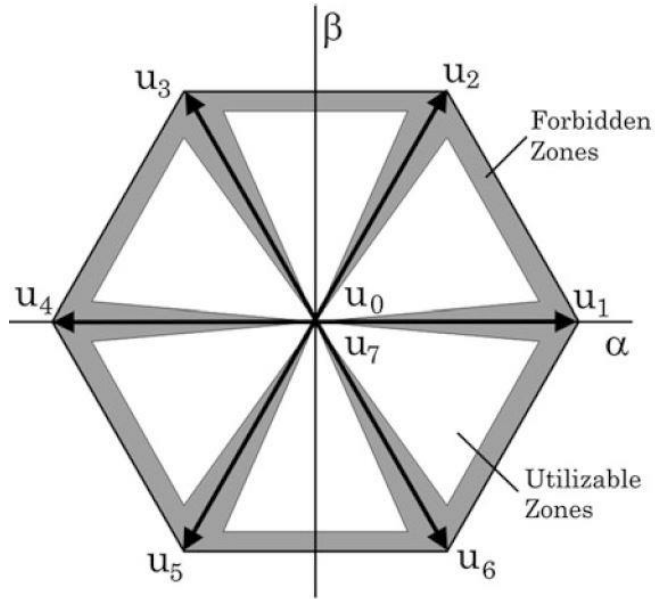


Fig. 7. 7, Prohibited regions in SV technique

EEPROM: The SV sequence is shown in figure 7.8. This sequence determines the period of firing and commutation the upper switching devices, IGBTs, of the inverter.

		T _s							
		t ₀	t ₁	t ₂	t ₀	t ₀	t ₂	t ₁	t ₀
S1	AH	0	1	1	1	1	1	1	0
	BH	0	0	1	1	1	1	0	0
	CH	0	0	0	1	1	0	0	0
S3	AH	0	0	0	1	1	0	0	0
	BH	0	1	1	1	1	1	1	0
	CH	0	0	1	1	1	1	0	0
S5	AH	0	0	1	1	1	1	0	0
	BH	0	0	0	1	1	0	0	0
	CH	0	1	1	1	1	1	1	0
S2	AH	0	0	1	1	1	1	0	0
	BH	0	1	1	1	1	1	1	0
	CH	0	0	0	1	1	0	0	0
S4	AH	0	0	0	1	1	0	0	0
	BH	0	0	1	1	1	1	0	0
	CH	0	1	1	1	1	1	1	0
S6	AH	0	1	1	1	1	1	1	0
	BH	0	0	0	1	1	0	0	0
	CH	0	0	1	1	1	1	0	0

T_s: sampling period t₀ = T₀/4 t₁ = T₁/2 t₂ = T₂/2 0: Low 1: High

Fig. 7. 8, Standard space vector firing sequence

While the condition states of the lower switching devices are in reverse of the upper. The sequence is to be stored in the internal memory of the microcontroller. This memory

is a 4kbyte x 8bits memory type EEPROM which is embedded within the hardware master structure of the microcontroller. It was employed in the set-up of the test bed for estimating the rotor position estimation of PMSM at low speed.

SRAM: This is a volatile 8kbytes x 8bits built-in static memory of random access. It was employed to store the codes of software programming routines. If the routine includes arrays or look-up tables, which require a wide memory space, then this will represent a programming problem which should be addressed through programming skills. For example, if it was possible to program the entries of a look-up table to be type “byte” rather than “integer”, then the required SRAM space to verify this table will drop down to half. This is because the “byte” variable is of length 8bits while that of “integer” is of 16bits.

It should be noticed that the SRAM is a volatile memory, so the codes data will be lost after turning off the power. Therefore the data should be either reloaded after each turning off or transferred to a flash memory after being have their final program form, because the flash memory is another built-in memory but it is of type non-volatile.

7.3.1.1.6 Speed control

In this test bed, the strategy of running the underlying motor at low speed was designated according to a proposed speed control concept. The speed control scheme was verified by the master microcontroller through the C-language software programming. It includes:

- **Setting speed ω_s :** Which was implemented via a variable external dc voltage, 0 to 5V via a potential divide resistor. Then it was fed to the microcontroller, μC , through one of its analogue inputs, and the μC mapped it within a speed range from 0 to 500 rpm.
- **Estimated speed ω_e :** This was fed to the master microcontroller, through another analogue input port, directly from the estimated speed output of the slave microcontroller. It was also mapped from 0 to 500 rpm to match the setting speed range. The mapping process hereby was based on that which was adopted by the slave-microcontroller to convert the speed into voltage, 0 to 5V variation.

- **PI controller:** Library of the master microcontroller provides a software application for PID controller. In this test bed implementation, the available software PID was used as a proportional integrator PI. Generally, this controller was employed to perform the speed controlling task through adjusting the actual speed to a value which is close, or equal, to the setting speed. In the undertaken practical model, the PI controller has been implemented through the available C-language software programming.

The setting and estimated speeds formed the input parameters of the software PI statement {PID (Input, Output, Setpoint, K_p , K_i , K_d , Direction)}[194]. The values of K_p and K_i parameters were primarily set according to those of the modelling scheme. Then, they were adjusted by adopting the same procedure given in the modelling scheme. While the value of K_d parameter was set to zero.

The speed controlling, in this test bed, depends upon a principle of controlling the execution period of motor energizing program. Therefore, the output of PI statement was taken as an added delay time to the timing intervals, T_1 , T_2 , and T_o of the SV codes, which are read from the stored timing data in the EEPROM of the microcontroller. This added delay time will increase in the full period of the PWM signals at the inverter output terminals. Thereby, the frequency of those signals will decrease and the motor speed will also decrease accordingly. Accordingly, the maximum verified output frequency was nearly 22.5 Hz.

7.3.1.2 Optocoupler

This coupler is type “HCPL2531” dual channel integrated circuit coupler. In this coupler, embedded photo detection transistors, at the output terminals, are optically coupled to embedded LEDs at the input terminals. It was exploited as an interface unit to provide an isolation for the master microcontroller outputs from the bootstrap inputs. Figure 7.9 shows a schematic diagram for the interconnections of the undertaken optocoupler according to its data sheet [195].

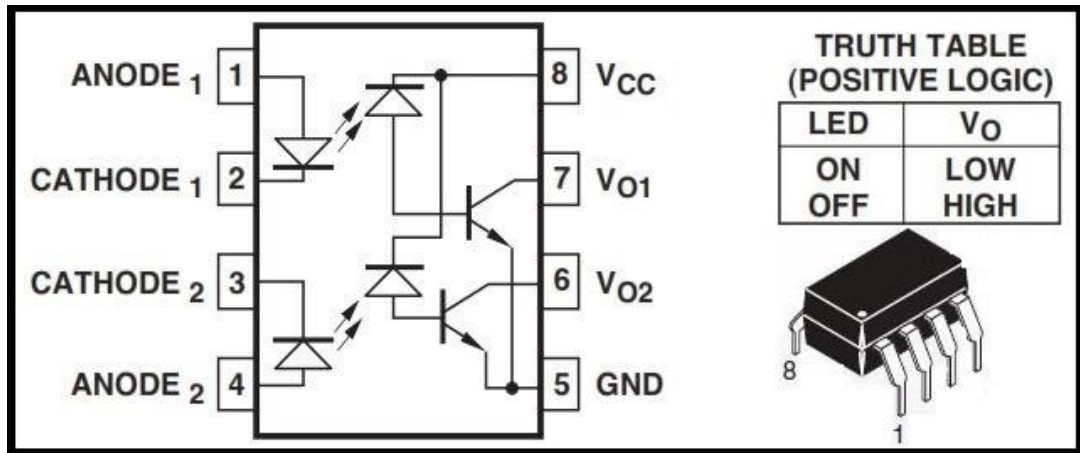


Fig. 7. 9, Optocoupler HCPL2531

7.3.1.3 Bootstrap gate drive

In high voltage and high frequency switching electronic inverter circuitries, two problems should be tackled, the losses due to the high frequency switching process and the switching action of the upper switching devices. One of the widely adopted method, to overcome these problems in this field of application, is the bootstrap driver. The principle of supporting the switching process of the upper devices, as shown in figure 7.10, is based on charging the boot capacitor C_{boot} of the upper inverter device during the period at which the lower complement element is switched ON. When the lower element is switched OFF and the upper is demanded to be switched ON by triggering its gate, the C_{boot} provides a negative charge on the source, or the emitter, of the upper device which will help in achieving the switching ON action [196]. This bootstrapping concept is highlighted by Figure 7.10 as it was given by reference [196].

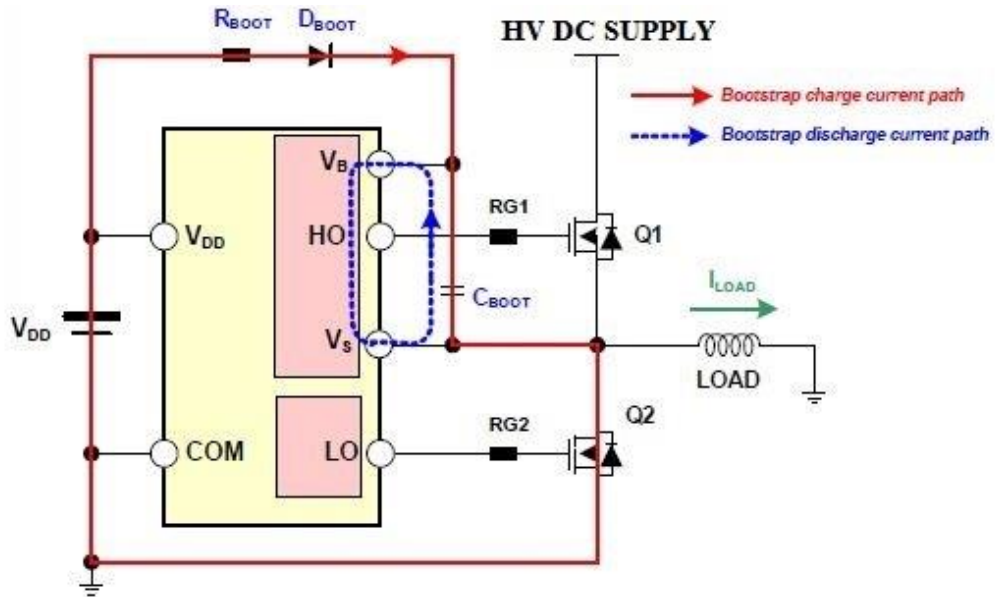


Fig. 7. 10, Principle of bootstrap operation

In this work, an integrated circuit of bootstrap driver, “L6388E”, was employed. This driver provides two outputs, HVG and LVG, to trigger the gates of the upper and lower complementary switching devices respectively. The most important feature for this driver is that it provides a protection against the simultaneous firing of the upper and lower switching devices which, are laid on the same inverter leg and thereby it solves the problem of dead time. Figure 7.11, demonstrates the details of this driver and the method of load connection [197].

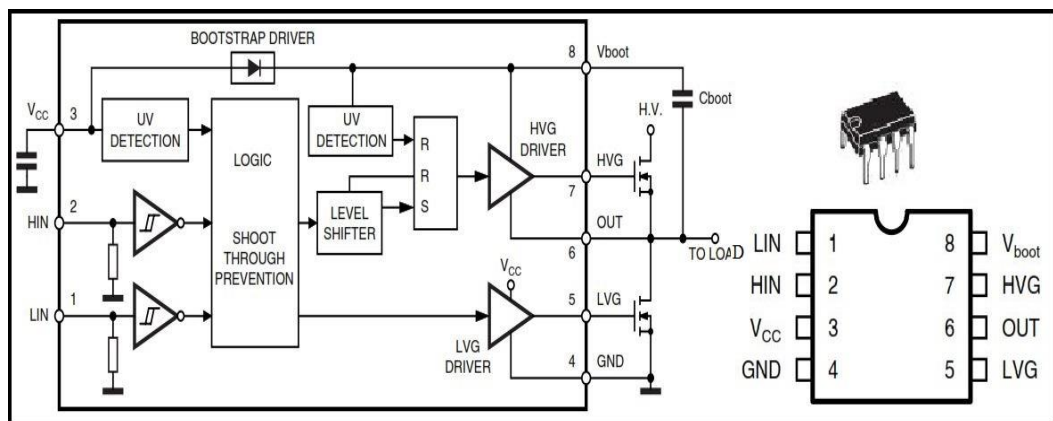


Fig. 7. 11, Bootstrap driver type L6338E

7.3.1.4 Inverter

The inverter is the technique of converting the dc input voltage into an ac voltage of variable magnitude and frequency. Therefore, it represents the more adopted method for constructing variable speed driving, VSD, electronic structure. There are two main principles to implement the power inverting process, voltage source inverter, VSI, and current source inverter, CSI. The former was used to implement the inverter circuitry in this test bed. Thereby, the proposed inverter, in this work, is shown in figure 7.12.

Switching devices, IGBTs, type “FGH40T100SMD” were used in the inverter synthesis. It is able to drive 40A and 1000V voltage supply. More information about this IGBT are given, in form of a brief data sheet in appendix C.1.2. A snubber circuit, type RCD, was connected between the high and low voltage terminals of each IGBT to absorb the voltage transient spikes at ON and OFF high frequency and high voltage switching processes. All the electronic components of this inverter, together with the bootstrap integrated circuits, are assembled and fitted on a printed circuit board which drawing details are given in appendix C.6.

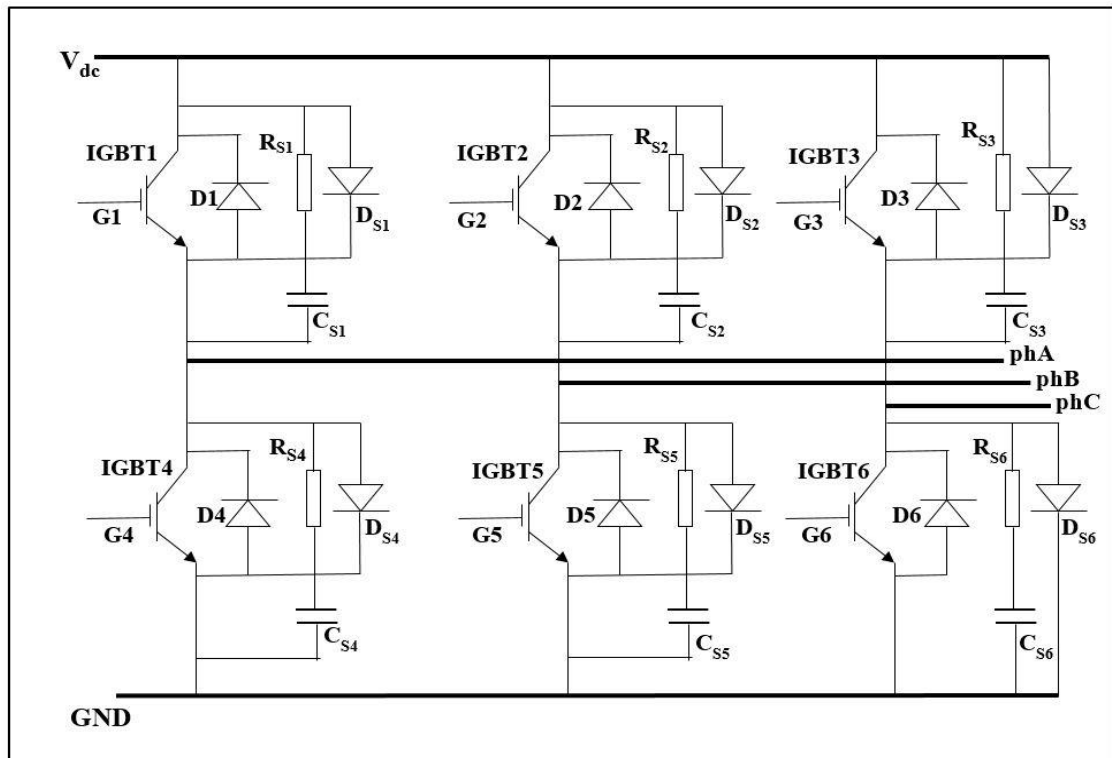


Fig. 7. 12, Schematic for the used in the practical test bed

7.3.2 The feedback path operations

The main tasks to be achieved by the operations in the feedback path are the estimating of rotor position and speed for the permanent magnet motor under test. To conduct these tasks, the same strategy, which was adopted in the modelling scheme given in chapter six, was re-adopted in the feedback path of this practical test bed. A significant difference between the modelling and practical schemes is that the practical feedback processing depended upon measuring of the motor terminal voltages rather than the currents. Although the currents in this practical scheme were also measured, these measurements were just for monitoring the system performance.

In this practical test bed, all the feedback processing operations were achieved by the slave microcontroller by the aid of some necessary peripherals. Therefore, the feedback path are discussed through two main parts, which are illustrated below.

7.3.2.1 Amplifiers

The main function of the amplifier unit in the feedback path was to convert the motor phase voltages into line voltage. This was done by stepping down values of the phase voltages via potential dividers, then passing them to operational amplifier subtraction circuits. Figure 7.13 illustrates this procedure for obtaining V_{ab} . The voltage amplitudes should be limited within the microcontroller range 0 to 5V.

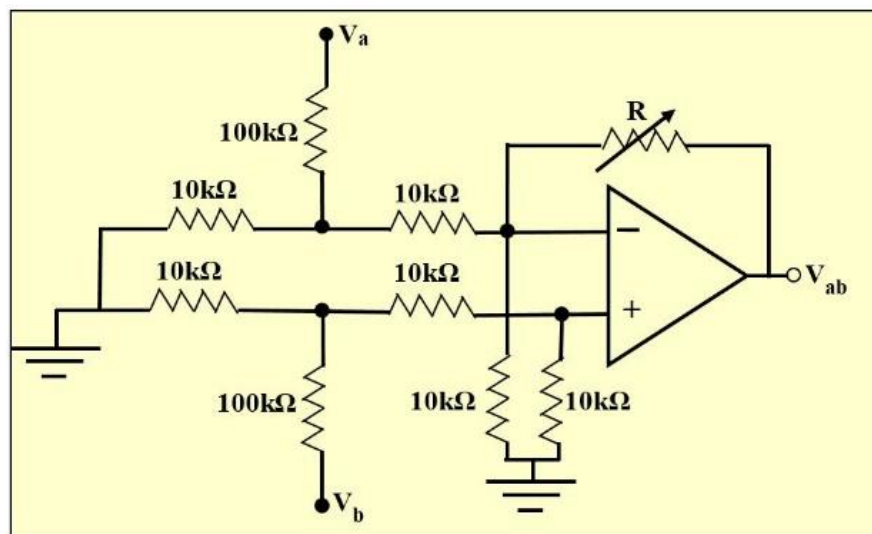


Fig. 7. 13, Converting V_a and V_b into V_{ab}

7.3.2.2 Slave microcontroller

This microcontroller is type “ATmega328”, which was used in the practical model for estimation the zero speed rotor position. Figure 7.14 demonstrates a functional block diagram for its employment to manage the main operations in the feedback path of the low speed rotor position estimation, LSRPE.

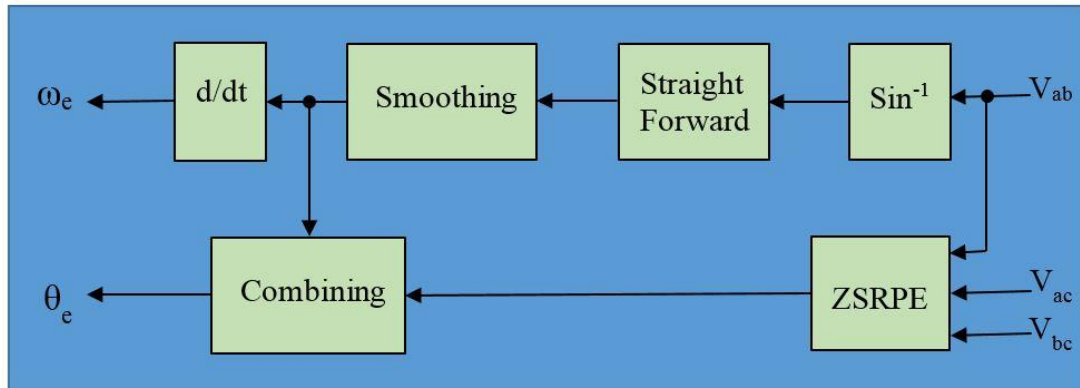


Fig. 7. 14, Functional block diagram for the slave micro-controller in LSRPE

The blocks, which are given in this figure, are mainly the same block which were used in the modelling scheme of chapter six. Therefore, implementation of each block function, in this practical scheme, was achieved depending on the same principles of verification which were adopted in the modelling system in chapter six. Therefore, these principles of implementations are not going to be re-explained by this field. It is sufficient to mention that, the block implementations were done through employing the C-language programming of the slave microcontroller.

The main function for the slave microcontroller is to exploit the voltage variations at motor terminals to provide a continuous estimation for rotor position and speed upon motor low speed running. Therefore, the inputs to this microcontroller are limited by the motor line voltages as shown in figure 7.14. While its two outputs are represented by a ramp function for the instantaneous rotor position estimation and a continuous recording for the rotor estimated speed.

7.4 PMSMs under test

Two surface mounted permanent magnet synchronous motors SM-PMSMs were put under test in this practical test bed. Their models are “M0200-104-000” and “ACM2n320-4/2-3”. These motors are the same models, which were tested, in the practical platform of the zero speed rotor position estimation, which is presented in chapter five. Therefore, the data about their parameters is not re-mentioned here, it is sufficient their specifications which are given in table 5.1 and the two appendices C.1.3 and C.1.4.

7.5 Encoders

As it is known that the encoder is a sensor technique to translate the motor shaft revolving movement into electrical signals for the purposes of controlling and counting the motor rotations per time unit. Two types of encoders were employed in implementing this practical test bed for low speed running and rotor position estimation. Therefore, each of the two under test motors has an encoder mechanically coupled to its shaft. The encoder of the motor M0200-104-000 is housed internally within the motor frame. This encoder provides 8000 counts per a mechanical revolution through its cable which is pointed out in figure 7.15. More details about this encoder are given in appendix B.1.

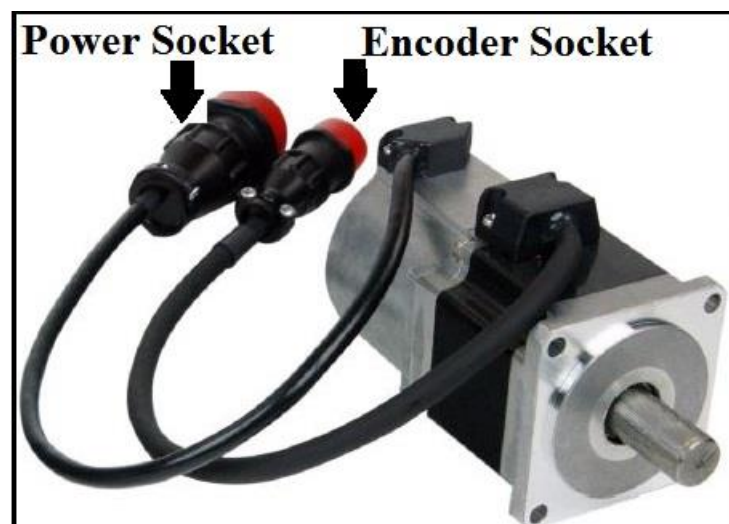


Fig. 7. 15, Encoder connection in the motor M0200-104-000

Whereas, the encoder that couples to the motor “AC M2n320-4/2-3” is model “755HS” from BRITISH ENCODER [198]. This encoder is externally coupled to the motor shaft. More technical information is found in appendix B.2.

7.6 Binary converter and DAC

Generally, the binary converter is a digital electronic device which counts the received counting states that comes as square pulses, and output a digital number in form of a Binary Coded Decimal, BCD. This number should represents the number of received pulses within a certain time interval. In this test bed, the employed binary converter is named ECOUNT from US DIGITAL, which counts the input counting states, the encoder is the source of these counting states, upon a complete motor mechanical revolution. This binary converter has an output of 24bits, so it counts up to 2^{24} counts/revolution. More details about this encoder are given in appendix B.3 according to the product datasheet [199].

Meanwhile, a digital to analogue converter, DAC, type “AD767JN” was used to convert the digital output of the binary converter, varied BCD number, into an equivalent analogue form. So, a ramp voltage function, 0 to 5V, was obtained at the output of this DAC which represented a graphical representation for the encoder rotor position estimation from 0 to 360 degrees. A brief datasheet for the employed DAC is given in appendix C.1.3.

Figure 7.16 demonstrate the employed strategy to achieve the encoder rotor position estimation at low speed running.

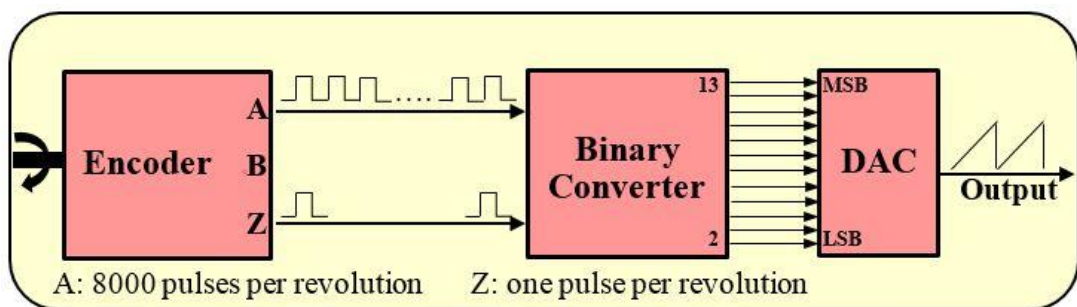


Fig. 7. 16, Encoder rotor position estimation

7.7 Magnetic brake load

This magnetic brake was designed and fabricated by “IS LEROY SOMER” to be used as a load for motors under test. Fundamentally, it works depending on the general principle of the braking systems through converting the mechanical output power of the motor under test into a thermal radiation. This brake works in conjunction with a mechanical measurement module which facilitates the measurements of power, speed and torque of the motor to be tested. In addition, the applied torque by this brake is controlled manually through adjusting the torque/dc volt knob on the front panel of this module [200]. This brake load includes the following main parts:

- Powder brake to apply variable load torque on the underlying motor.
- Tachogenerator to transfer the motor shaft speed into an analogue voltage.
- Mechanical measurements module to display the torque, speed and power readings, in addition to controlling the adjustable applied torque.
- Load cell to measure the brake applied force.

Figure 7.17 illustrates details of this magnetic load brake. It is also implicitly shown within figure 7.19.

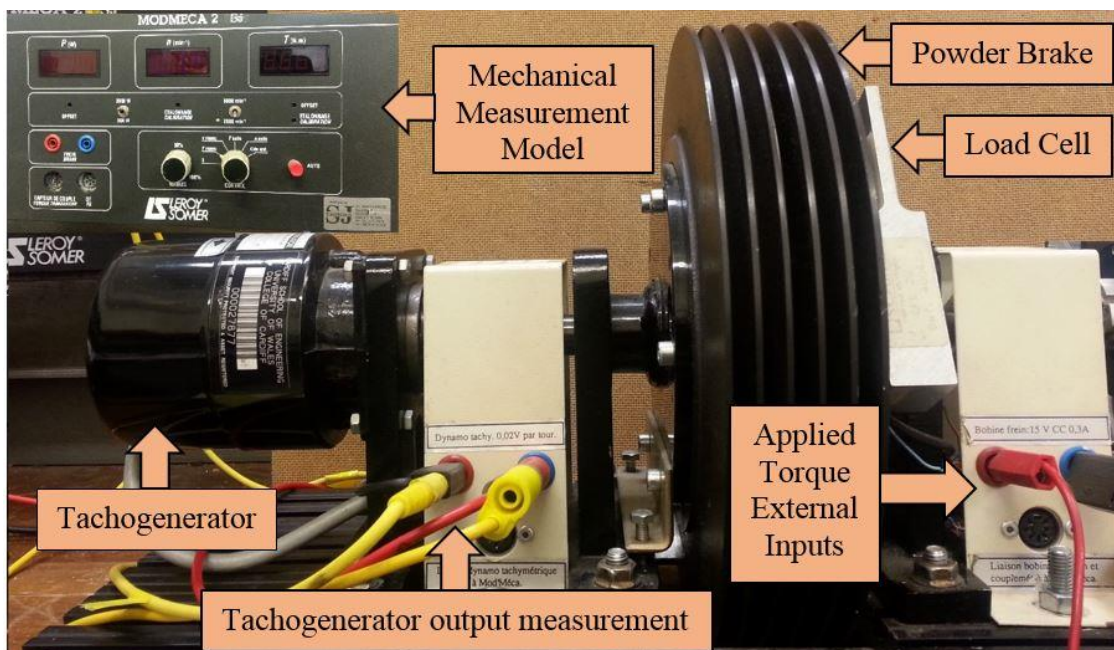


Fig. 7. 17, Details of the magnetic brake

7.8 Startup strategy

In this work, the adopted startup strategy was built based on the ramp up method. In origin, this method was presented by reference [201] to startup a brushless dc motor, BDCM. It is hereby re-employed to startup the PMSM, and is highlighted as follow. For proper startup of any PMSM, the initial rotor position should be known previously. In this practical work, this condition was provided via the zero speed estimator, which was discussed in chapters four and five. Then, one complete cycle of the standard space vector code for energizing the inverter switching elements were stored in the dynamic memory of the master microcontroller. A time-period, along which the inverter switching devices would be fired, was defined. It should be known that the time-period is directly proportional to the applied load condition.

At this moment, the master microcontroller starts the commutation process according to the stored sequence, in its memory, and the value of the time-period. It achieves the process through several repetitive iterations. When the motor starts running, the microcontroller gradually drops down the pre-defined time-period by a pre-defined step with each new iteration. As the iterations proceeds, the motor speed gradually increased. This manner of commutation continues until the value of the time-period becomes zero. At this point, the motor should has a certain level of speed which is sufficient to permit the microcontroller to leave the startup strategy and transfer to the commutation process of the low speed controlling scheme. The following figure, 7.18, may help in understanding this strategy.

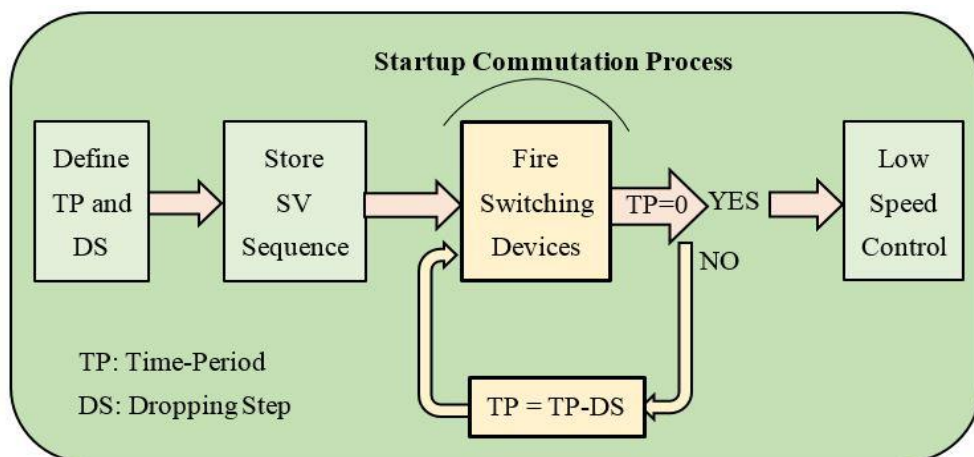


Fig. 7. 18, Startup strategy

7.9 Harmonic calculations

The practical harmonic calculations were done through a MATLAB programming package file. This package achieves the harmonic analysis through finding the Fourier Fast Transformation, FFT, for the variables data to be analysed. Accordingly, the obtained sequences S_A , S_B , and S_C , for the practical space vector, to fire the inverter switching devices, were used as matrix elements in a MATLAB m-file. This m-file exploited the given matrix to calculate the expected voltages at the inverter outputs according to equation (7.10). Finally, these voltages were fed to the MATLAB harmonic package to achieve the harmonics analysis, and showed the harmonic results in form of a graphical representation, which is shown within the practical results.

7.10 Avoiding microcontroller limitations

Generally, the real-time control schemes are designed based on the closed loop controlling theory and synthesized around a microcontroller, μC , or a digital signal processor, DSP. They are characterized by having a limit timing domain to collect data of the system to be controlled. This point should be carefully considered when depending upon the microcontrollers as a base to build a real-time control system, otherwise, a deteriorated control performance is resultant [11]. The preferred method to overcome this problem is by avoiding the software processes which includes a huge computing time demands.

According to the work in software designing for this test bed, it has been noticed that the repetitive calculation for a certain operation consumes much processing time. The better way to address this drawback is through representing, those frequent computations, via a look-up table technique. This concept was applied in this work to reduce the programming stress on the master microcontroller and it is noticed by the presence of look-up tables in the programming codes which are given in appendix A.2. Moreover, at certain programming situations, it is beneficial to make a trade-off between the software and hardware implementations for a certain process. For example, it becomes clear now that the logic states of the control signals of the lower switching devices in the inverter circuitry, S_{AL} , S_{BL} , and S_{CL} are inverse of those of the upper

switching devices S_{AH} , S_{BH} , and S_{CH} . For this reason, it may represent an inefficient programming skill to compute the controlling signals of the lower switching devices rather than simply verifying them through a simple hardware inverting implementation.

Design of the microcontroller programming codes should also take into consideration the limited available space for the embedded memories in the microcontroller chip. This especially considered in adopting the look-up tables and in writing the C-language codes. Reference [202] has mentioned that the unlimited use of expressions in ATmega328, like codes for strings or look-up tables, leads to a failure and halt in program execution even if it was successfully uploaded.

In this work, the above points were highly considered in designing the various software C-language programs, which were adopted to activate the master and slave microcontrollers in order to be able to manage the practical controlling scheme for low speed operation and position estimation. Details for these C-language programs, programming codes, are given in appendix A.2.

7.11 Practical Results

Figure 7.19 illustrates a snap for the actual practical test bed including the magnetic break. It points out the various parts that were used to establish the low speed control system excluding the microcontrollers board, which are given individually with their peripherals, in figure 7.20.

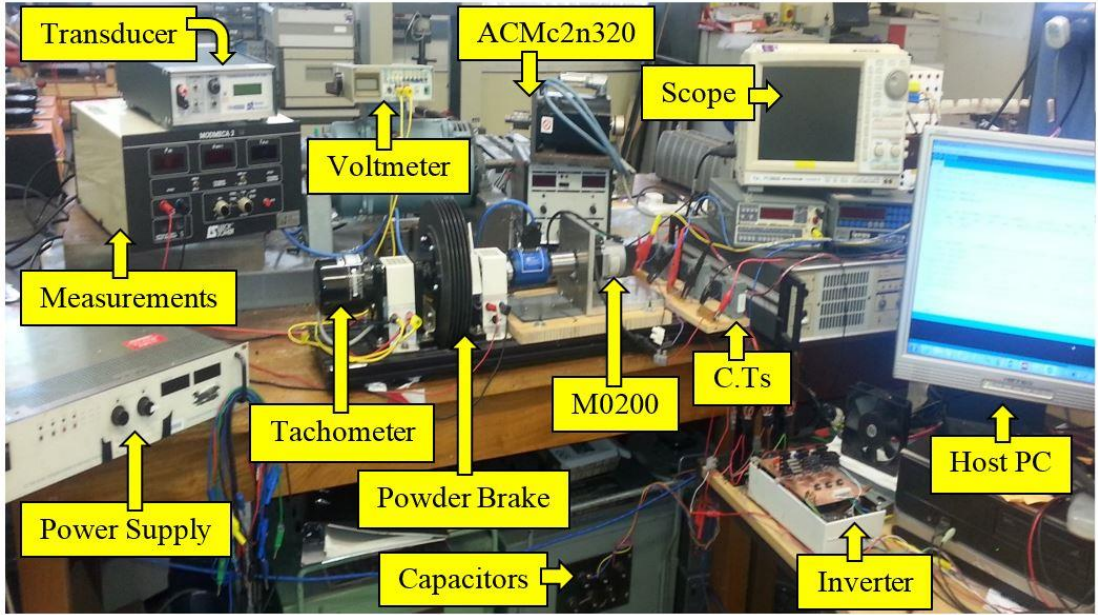


Fig. 7. 19, A snap for the practical test bed

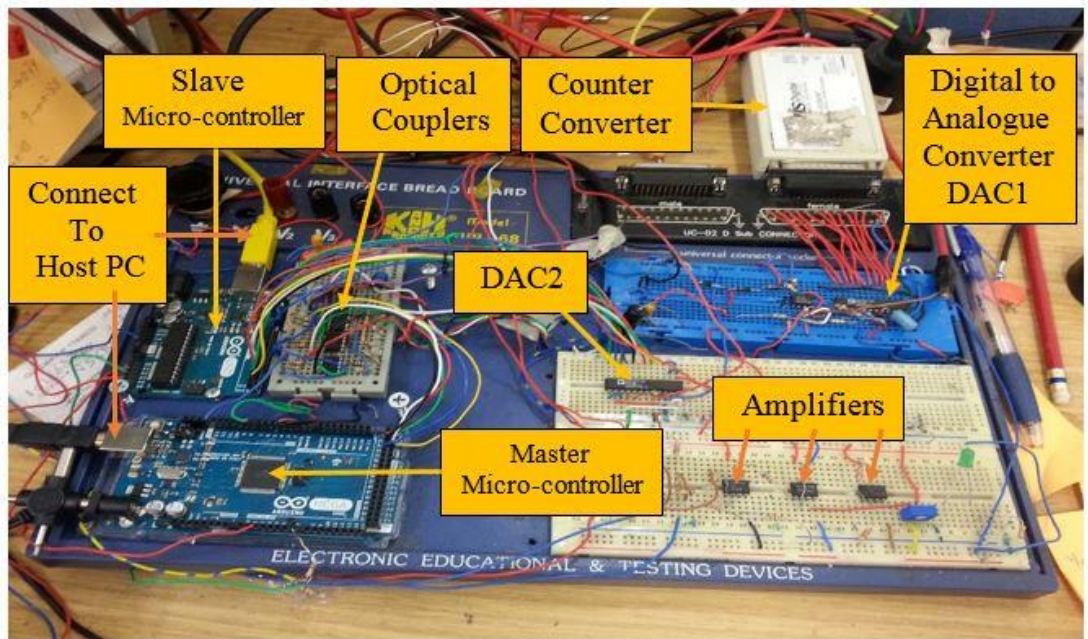


Fig. 7. 20, Real view for master and slave microcontrollers and their peripherals

The practical results of low speed operations will almost be explored in graphical forms according to the recordings of the microcontrollers. Some of graphs will be explored in form of snaps, while the others will be viewed in form Microsoft excel graph. This facility is available because the USB connection between the microcontrollers and the host PC facilitate this operation of exploring the microcontroller recordings on excel screen.

In this results review, the results will be explored through three groups; firstly, results of the low speed rotor position estimation, secondly, results of applying the startup proposed method and, finally, results of power delivery to the both tested motors, under load and no load conditions.

7.11.1 Results of rotor position estimation at low speed

A snap for the graphical results, which were obtained by the process of rotor position estimation for the motor “M2n0320”, is given in figure 7.21. Figure 7.21 (a) shows the encoder (sensor) and senseless rotor position estimation at low-speed, LSRPE, for the motor “M2n0320”. While figure 7.21 (b) shows the detected sinusoidal track of machine saliency form which the sensorless estimation was obtained. It should be known that:

- This sinusoidal variation of saliency track was normalized by the slave microcontroller to be having 1V peak voltage.
- This normalization is to prepare the saliency sinusoidal variation for extracting the simultaneous rotor position estimation by the arithmetic library of the slave microcontroller through a sine inverse trigonometric function.
- Frequency of this sinusoidal saliency variations is directly related to motor speed.
- Therefore, the estimated motor speed was calculated from the derivation of the estimated rotor position graph.

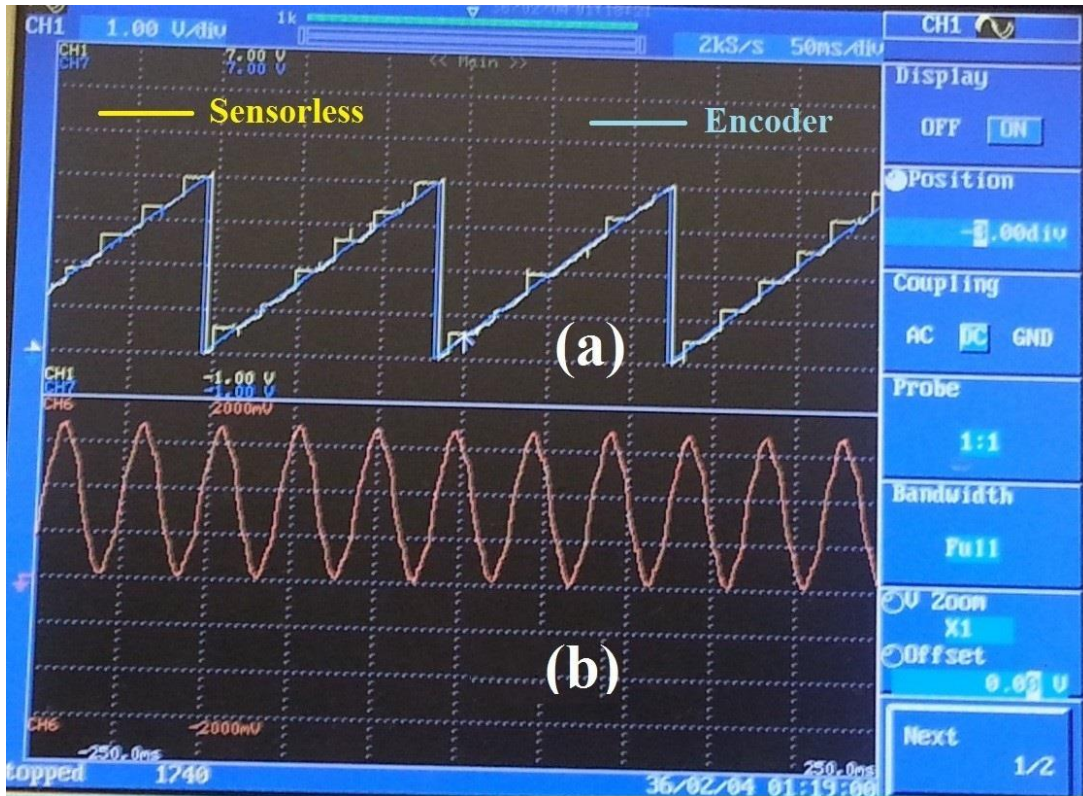


Fig. 7. 21, LSRPE for the motor M2n0320 (a) encoder and sensorless (b) saliency track

By this figure, It is noticed that the encoder (sensor) estimation is going smooth ramp graph, while the sensorless estimation has some breaks which appear due to the non-pure sinusoidal saliency variations from which this sensorless estimation was obtained, especially at the regions of distortion in the saliency track.

Figure 7.22 illustrates an excel graphical representation for the results of rotor position mechanical estimation at low speed running for the PM motor “M2n0320”. The shown graphs were obtained according the results which was recorded by the slave microcontroller and transferred to the excel window in the host computer. Comparing this graph result with that given in figure 7.21, it seems that transferring the estimation data from the microcontroller to excel has caused a nonlinearity in the encoder position estimation. While figure 7.23 shows the sensorless estimation error regarding the encoder readings as reference values. Peaks of high values are appeared in this figure because of the phase difference between the sensorless and encoder estimations

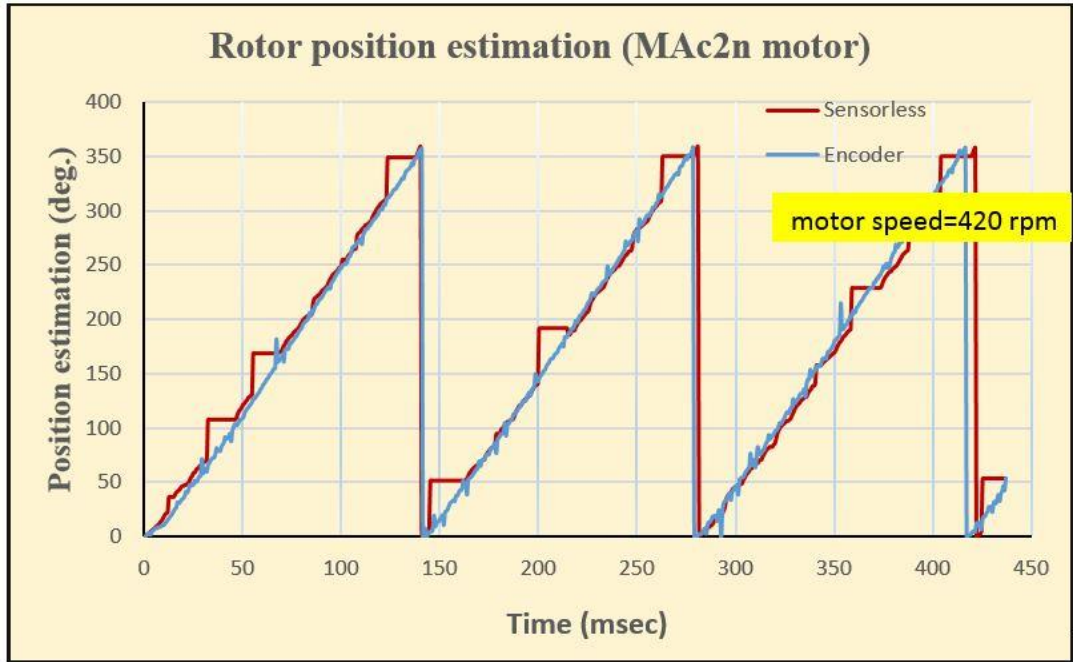


Fig. 7. 22, LSRPE for the motor M2n0320 encoder and sensorless

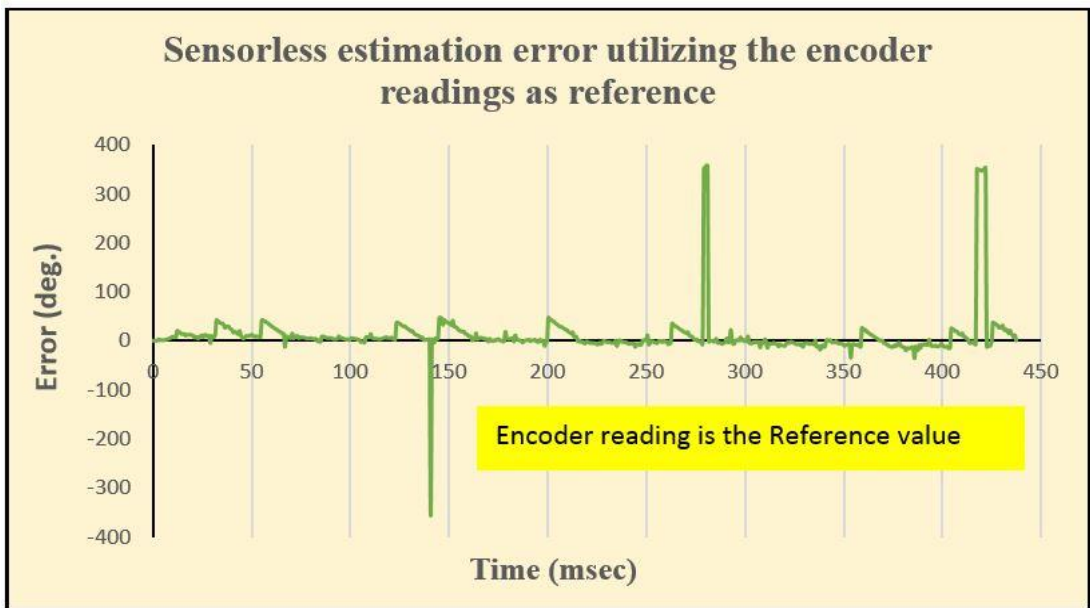


Fig. 7. 23, Error between sensorless and encoder RP estimations for M2n0320

Similarly, figures 7-24 and 7-25 show the same graphical results, but for the low speed rotor mechanical position estimation applied on the motor M0200.



Fig. 7. 24, LSRPE for motor M0200 encoder and sensorless

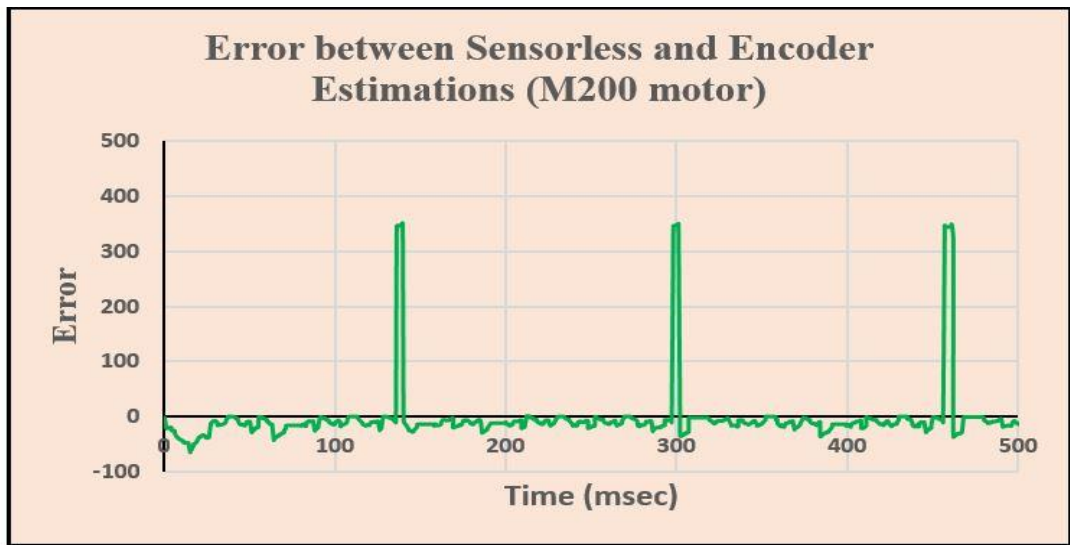


Fig. 7. 25, Error between sensorless and encoder RP estimations for M0200

7.11.2 Results of startup strategy and harmonic analysis

Figure 7.26 shows an oscilloscope snap for the no load start-up stator winding currents in the motor M0200. The current readings were measured as voltage readings across 1Ω resistor at the secondary coil of 40/5 current transformer. It is noticed that, upon the startup period, the current of each phase oscillates between positive and

negative peaks because the variation in SV sequence change the phase winding from source of current to drain and vice versa.

Whereas, figure 7.27 demonstrates the running currents for the same motor at modulation index $m=0.3$. The given phase currents have the basic sinusoidal variation with phase difference 120° . It is clear that this current waveforms possess the pure sinusoidal fundamental frequency with remarkable side frequencies which create the harmonic negative effect on torque ripple and speed fluctuations at the shaft mechanical output.

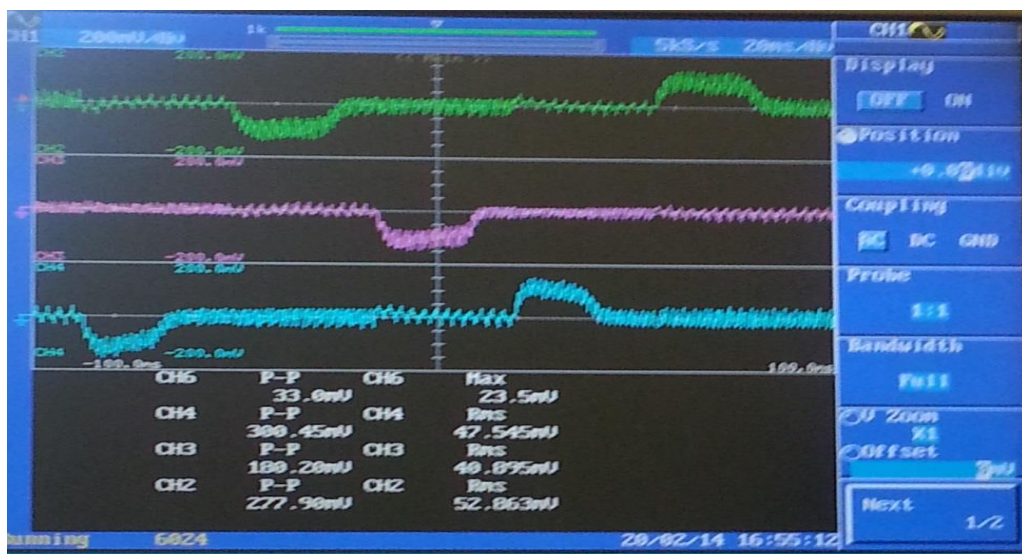


Fig. 7. 26, Start-up currents for the motor M0200

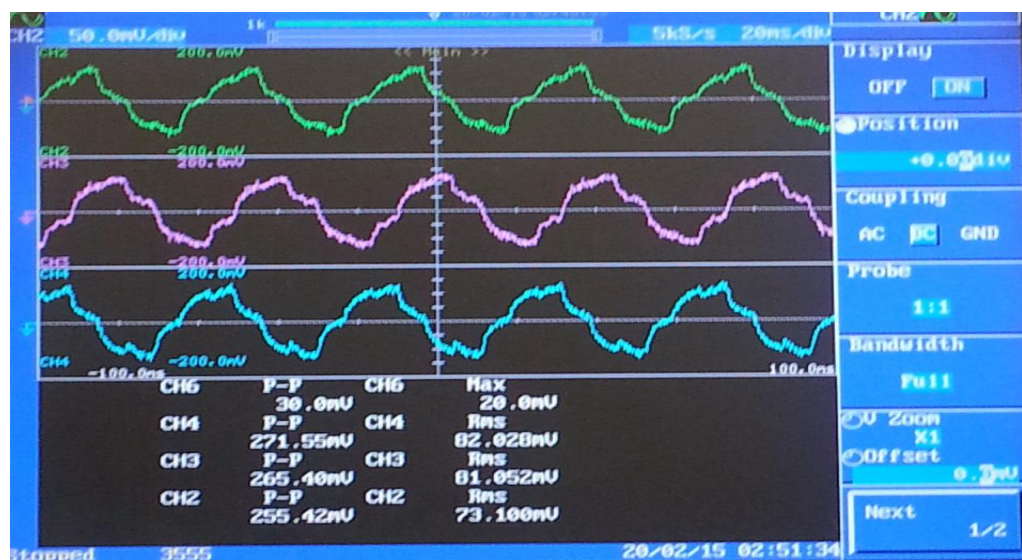


Fig. 7. 27, No load currents of the motor M0200

Figure 7.28 demonstrates the variation in values of startup times as a function of dropping steps, in load condition, for both motors under test, “M0200” and “M2n0320” as they were recorded by the slave microcontroller. The microcontroller was programmed to calculate the startup time from starting the motor energisation till the rotor reached the setting speed.

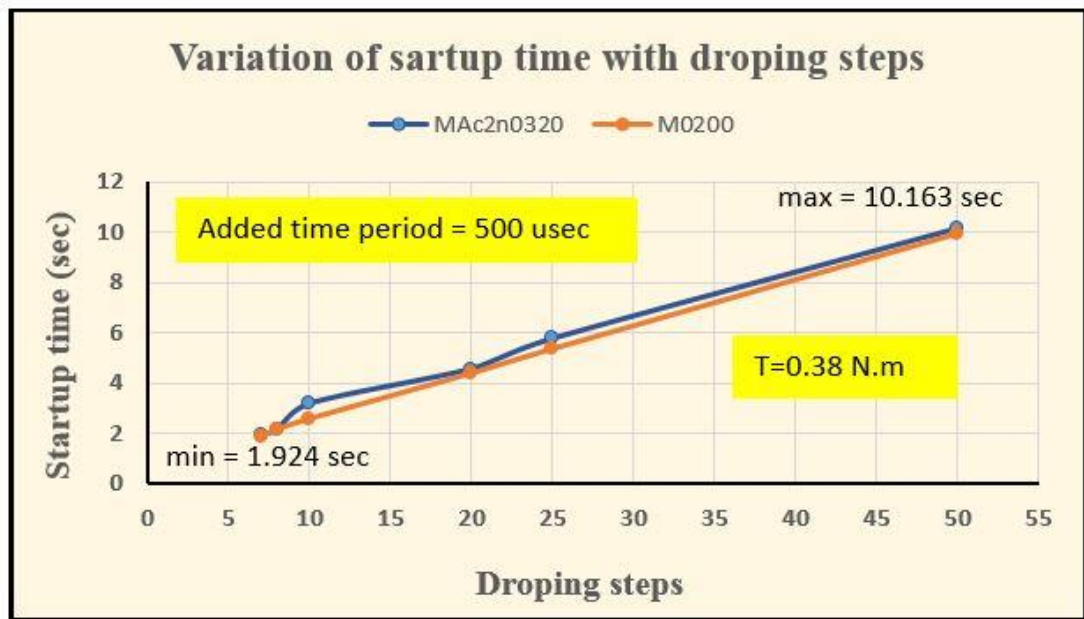


Fig. 7. 28, Start-up time for the motors M0200 and M2n0320

As it shown in the figure, a significant increase in startup time occurs as the number of dropping steps increases. It is expected that the increase in startup time may reduce the corresponding ripple and the matter becomes a trade-off between the startup time and amount of output mechanical ripple.

The harmonic analysis for the inverter output voltage, when the motor was running at a mechanical speed 250 rpm, is given in figure 7.29. The desired harmonic is shown in the figure by the blue bar, which appears at frequency 12.5Hz. The undesired harmonics, which have high frequencies, were easily drained by an output bandpass filter, but it caused in an extra currents of a considerable values to be drawn through the IGBT switching elements. This was led to a harmful thermal effect which was tackled through a ventilation process. However, the undesired harmonics at low frequencies

were hard to be completely removed, so they were responsible for the noticeable ripple at the output speed.

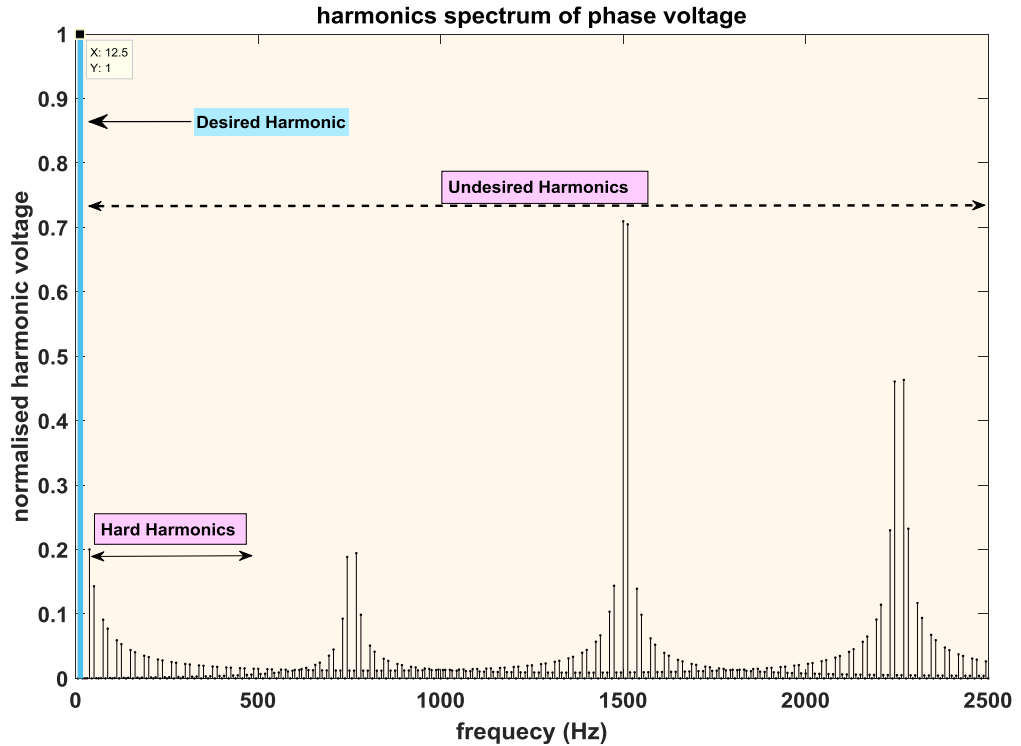


Fig. 7. 29, Harmonics analysis for the practical inverter output by a MATLAB view

7.11.3 Results related to motors power delivering

The motors, which were targeted by the power delivery through this low speed test bed, were supplied from the inverter output terminals. Figure 7.30 shows the inverter output line voltage, V_L , when the inverter switching devices were fired by the PWM switching signals S_A , S_B , and S_C , after passing through the bootstrap driver. These switching signals are also shown in the figure given below.

It should be noticed that:

- Amplitude of this PWM inverter output voltage is determined by the value of the direct voltage that is applied on the inverter input.
- Frequency of this output voltage is determined by the speed of fetching the space vector sequence from the EEPROM of the master microcontroller.
 - Speed of fetching is controlled through the added delay time.

- Speed of fetching is directly related to the desired motor speed which is defined by the pre-setting speed.

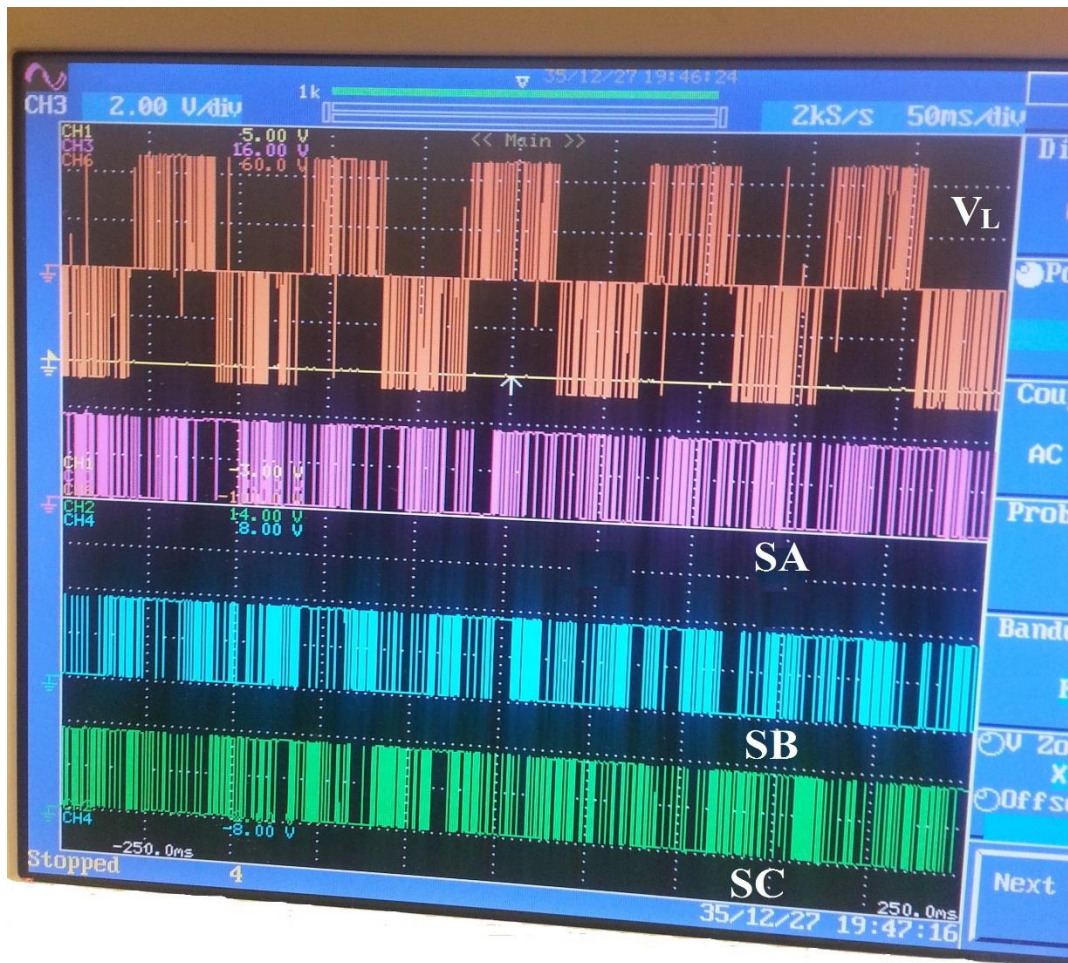


Fig. 7. 30, Line voltage V_{ab} and PWM switching signals S_A , S_B , and S_C

Figures 7.31 and 7.32 represent the excel graphical view for the inverter output phase and line voltages V_{an} and V_{ab} respectively. These voltage drawings were obtained from applying the above switching sequence S_A , S_B , and S_C , as they were given by the master microcontroller, in equations (7.10) and (7.11).

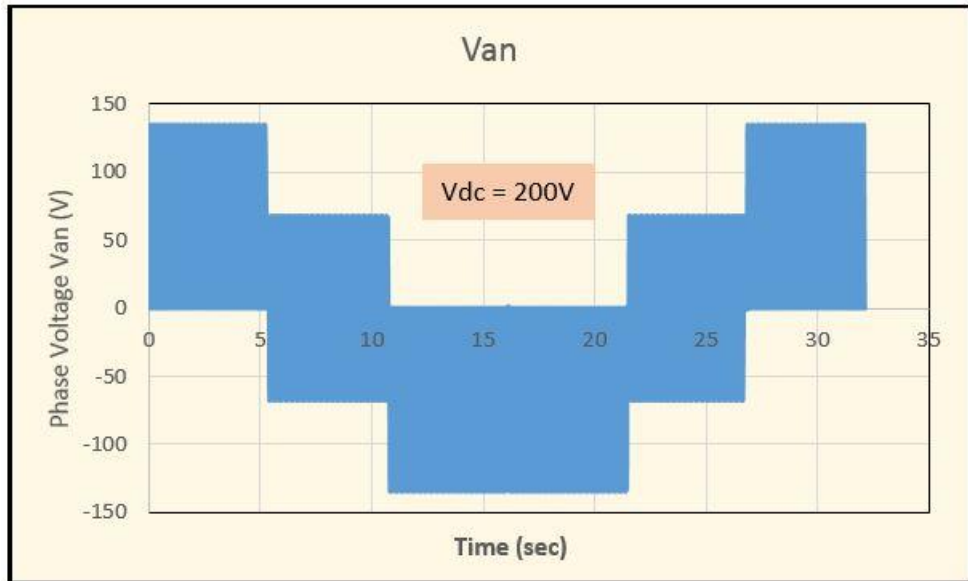


Fig. 7. 31, Variation of the output phase voltage V_{an}

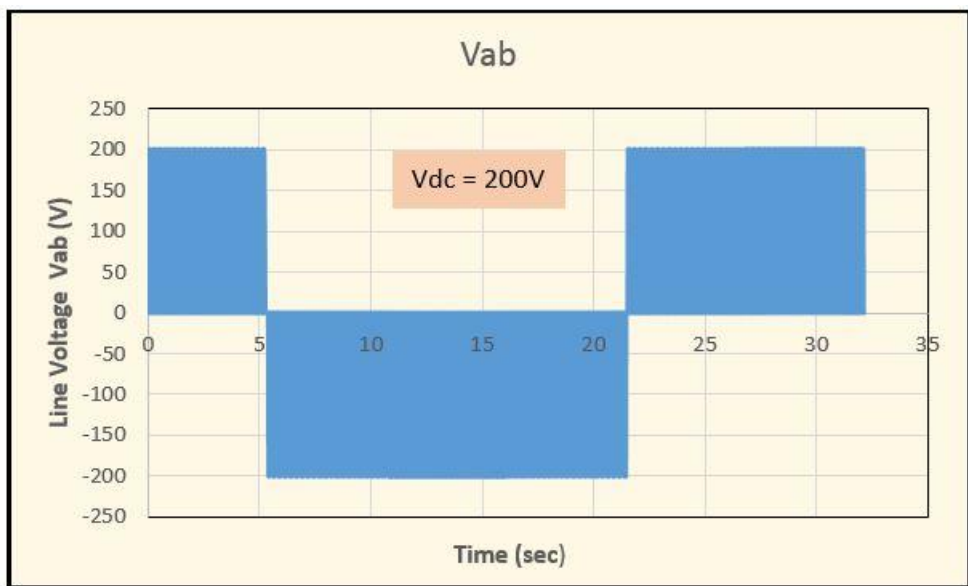


Fig. 7. 32, Variation of the output line voltage V_{ab}

Figure 7.33 shows the slave microcontroller observations for the actual torque variations of the motor “M2n0320” when it was running at speed 374rpm. This was done through feeding the analogue torque output, of the transducer “E302”, to the slave microcontroller via one of its analogue inputs. Thereby, the μC reads and record the instantaneous values of torque with approximately 150 sample/sec predefined sampling rate. It is clear the effect of harmonics, which could not be filtered as it was explained above in figure 7.29, caused torque ripple.

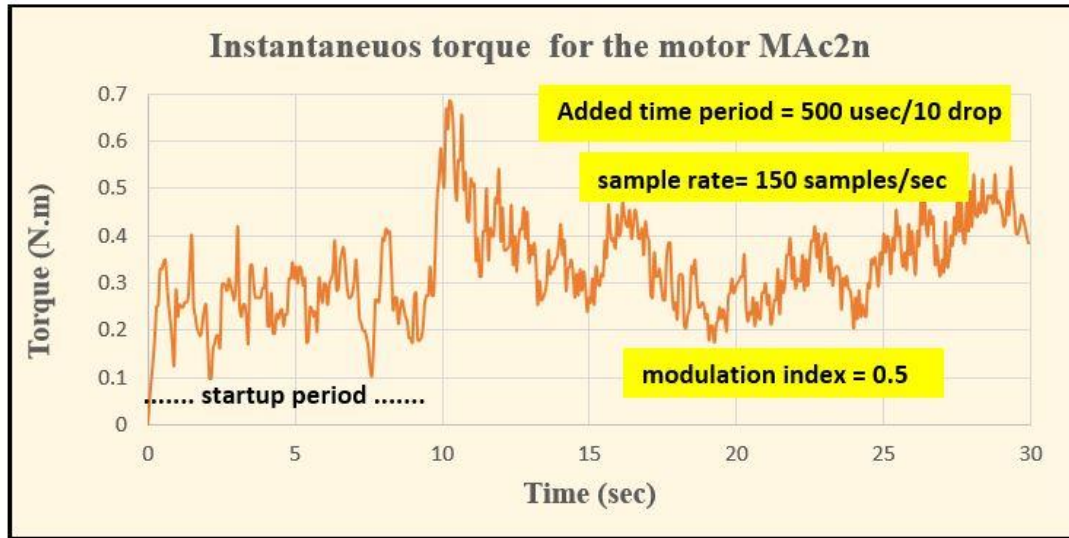


Fig. 7. 33, Instantaneous torque produced by the motor “M2n0320”

Figures 7.34 and 7.35 track the speed growths for the two motors “M2n0320” and “M0200” at different values for modulation index. Increasing the modulation index reflects in increasing the motor power. With a constant applied torque, this should reflect in corresponding increase in motor speed. The motor “M0200” was running at its rated voltage while the “M2n0320” motor was running at half of its rated voltage. The given graphical speed representation are smoothed through a microcontroller software. This smoothing process has led to lost noticing the over shot in speed growth. From other side of view, the startup time has determined the value of speed rise time.

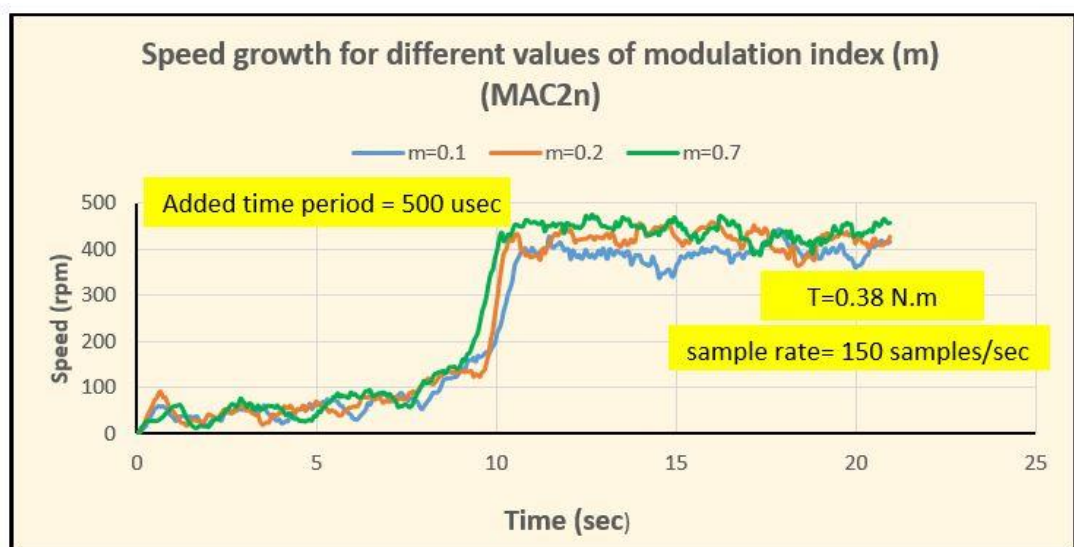


Fig. 7. 34, Speed growth of the motor M2n0320 for different modulation index

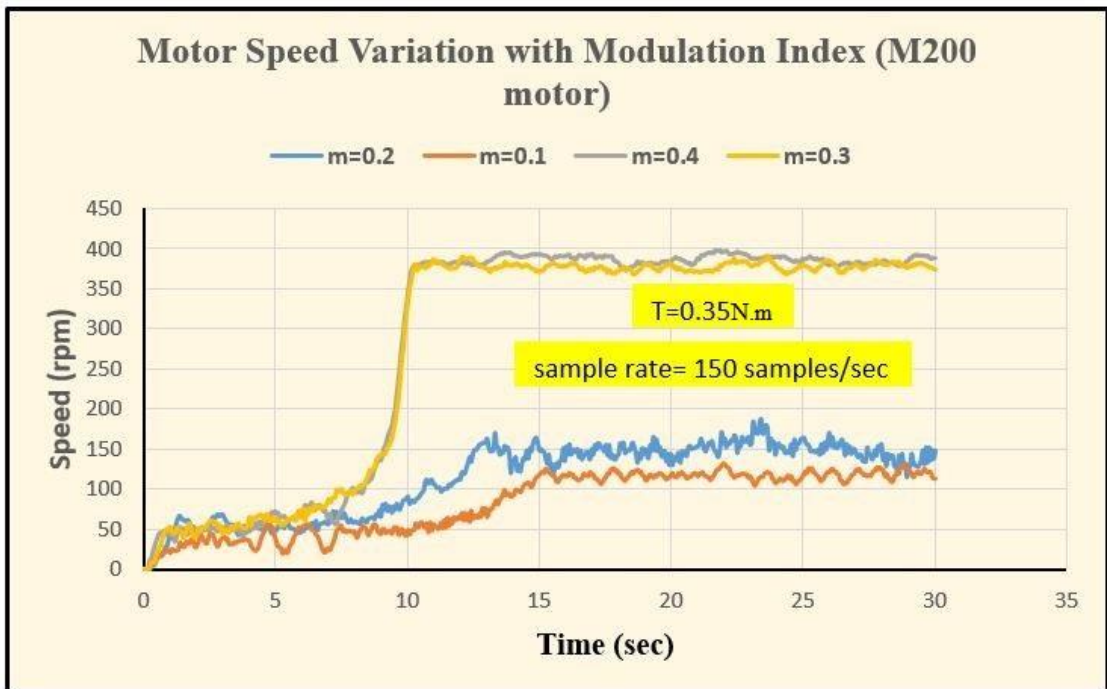


Fig. 7. 35, Speed growth of the motor M0200 for different modulation index

Figure 7.36 highlights the effect of speed smoothing on reducing the speed ripples. It shows the actual and smoothed speeds for the motor “M2n0320”. Smoothing process was achieved by the slave microcontroller through averaging each ten speed readings. The given standard deviation is for the actual speed.

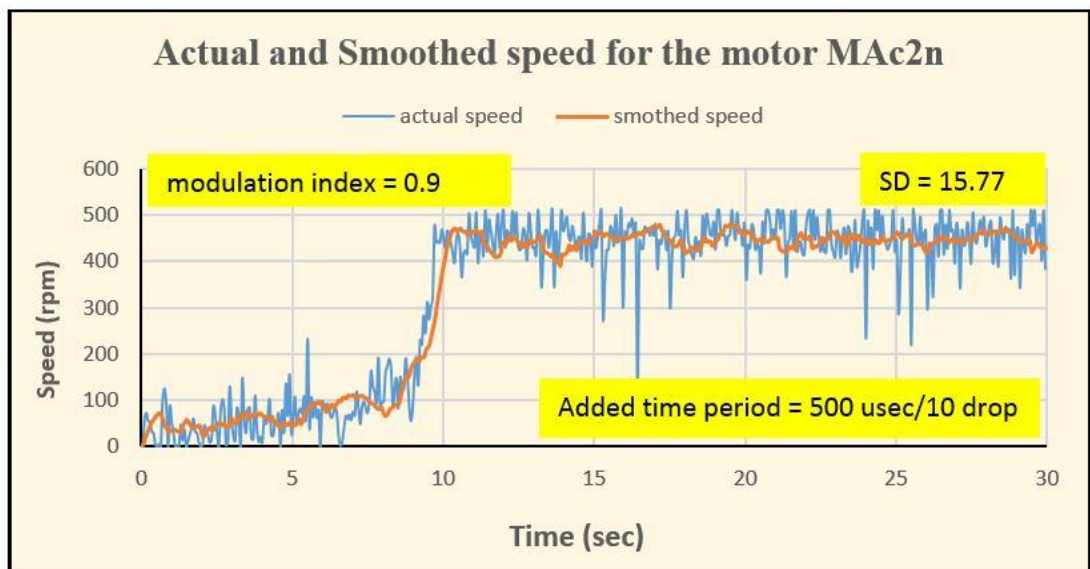


Fig. 7. 36, Actual and smoothed speed curves for the motor M2n0320

Figures 7.37 and 7.38 show the growth of speed for the two motors at different applied torques by the magnetic brake load. The figures highlight the maximum torque that is applied on both motors before failures. More details about the failure boundary are given in table 7.2.

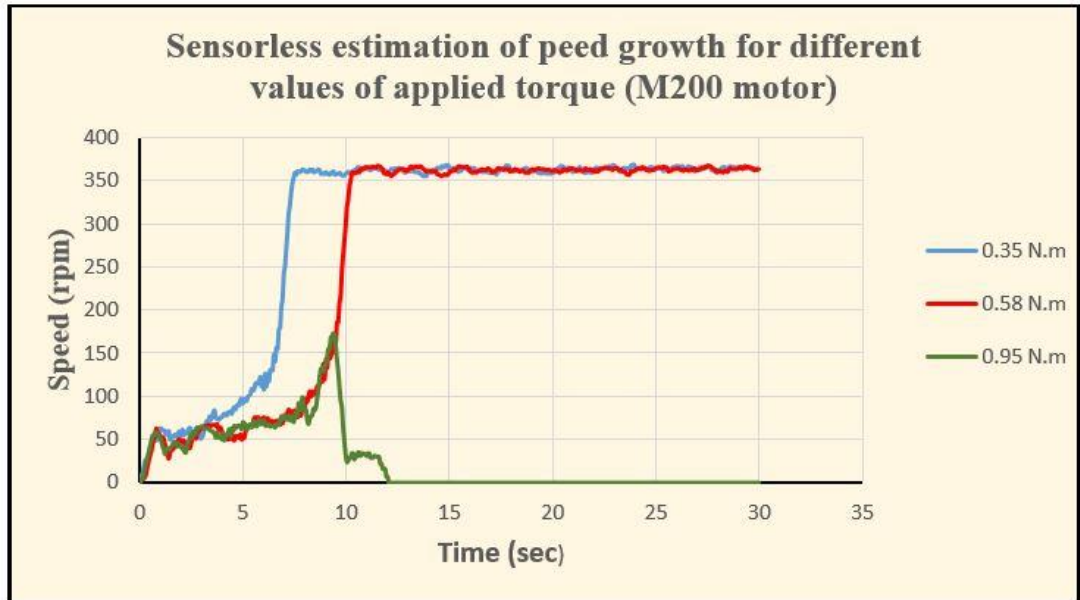


Fig. 7. 37, Speed growth of the motor M0200 for different levels of applied torque

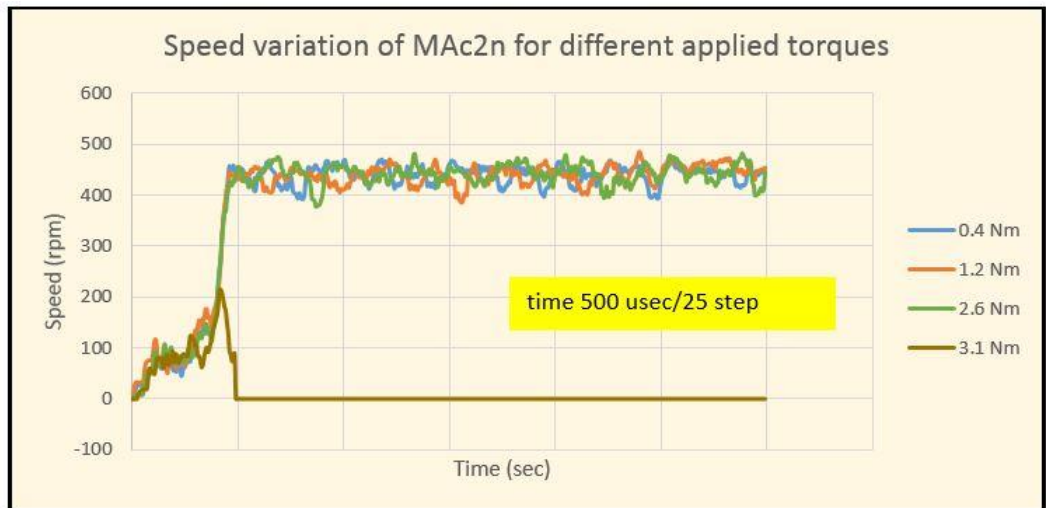


Fig. 7. 38, Speed growth of the motor M2n0320 for different levels of applied torque

Figure 7.39 presents growth of estimated speed of the motor “M0200” as it was actually plotted, by the slave microcontroller “Atmega328”, on the screen of host personal computer via a USB serial communication port. Note that the independent variable, on the horizontal axis, represents the microcontroller readings. This is according to the view of plotting strategy which is provided by the microcontroller manufacturer [203]. Each reading in this figure is corresponding to (0.0066 second) according to the given sampling rate. So, the overall length of the horizontal axis, in timing scale, is approximately 30 seconds with sub-divisions 6, 12, 18 and 24 seconds.

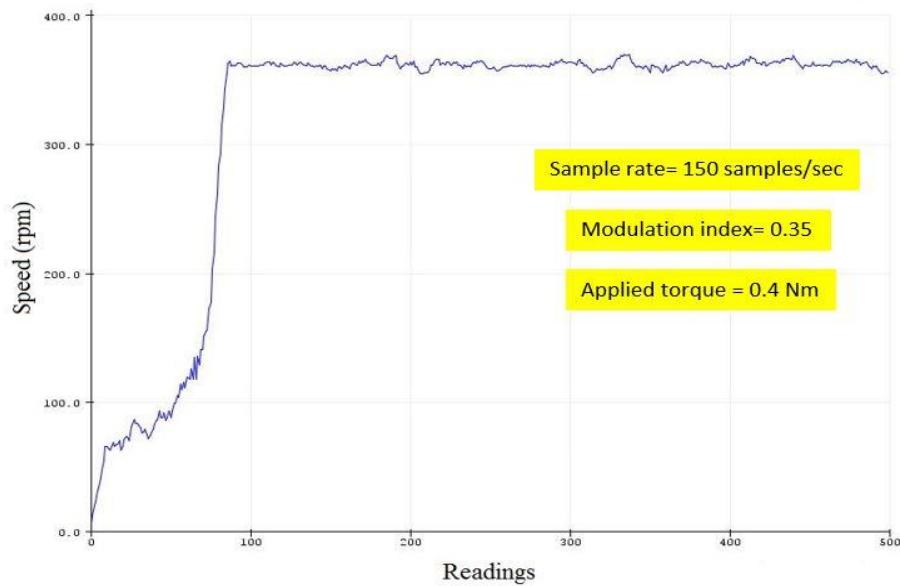


Fig. 7. 39, Speed growth of the motor M200 by the microcontroller plotter

Table 7.2 shows the recordings of speed and power for different values of the applied torque. The findings in this table were obtained at startup conditions of 500 μ sec total added period and 25 μ sec step period. Appendix C.3 includes snaps for these recordings as they appeared on the transducer display “E302” [204]. It is noticed that the linearity of the power to torque ratio is approximately valid for both motors.

Table 7. 2: Load test for both powered motors

Motor M2n0320					Motor M0200				
Break Voltage (V)	T (Nm)	ω_m (rpm)	P (W)	P/T	P/T	T Nm	ω_m (rpm)	P (W)	Break Voltage (V)
0	0.40	442	18.52	46.3	34.03	0.30	325	10.21	0
0.2	0.60	429	26.97	44.95	34.47	0.32	329	11.03	0.1
0.4	0.66	422	29.29	44.38	32.33	0.36	325	11.60	0.2
0.6	0.90	440	41.53	46.14	31.63	0.38	318	12.02	0.3
0.8	1.06	426	47.38	44.70	34.24	0.46	327	15.75	0.4
1.0	1.34	442	62.10	46.34	33.63	0.60	321	20.18	0.5
1.2	1.50	411	69.39	46.26	34.03	0.64	325	21.78	0.6
1.4	1.98	427	88.65	44.73	33.91	0.68	323	23.06	0.7
1.6	2.82	435	128.5	45.57	34.43	0.74	328	25.48	0.8
1.7	2.86	444	133.2	46.57	32.93	0.9	314	29.64	0.9
1.8	3.6	---	---	-----		0.9	---	---	1.0

7.12 Summary

This chapter concerns the real-time implementation for the test bed which should control power supplying, speed controlling and rotor position estimating for the underlying motor according to the proposed method to achieve each of these tasks. Therefore, it presents the following main points:

- 1) It was found that the results for low speed position estimations follows through a ramp function graph the encoder readings successfully.

- 2) Although the effect of harmonics was explicit, the startup strategy succeeded in driving the underlying motors properly.
- 3) Results of changing the parameters of the used SV technique and their effects on the speed of motors under test were observed and presented in graphical forms.
- 4) A brief introduction to clarify the progress in implementations of the real-time control system
- 5) Demonstrating to the details of design scheme for the practical test bed to be used to estimate the rotor position for the employed permanent magnet motors when they are running at low speed.
- 6) Pointing out verification of the feedback path function, which aims to implement a proposed method to detect the rotor position for the motor under tests through tracking the rotor magnetic saliency. This is achieved by observing the sinusoidal voltage variations on one of the motor line voltages rather than observing the three phase voltages at the motor terminals.
- 7) This chapter explores the main tools, microcontrollers, which are used to achieve the goals of motor power energizing and rotor position estimation. In addition, it points out the necessary peripherals to support the microcontroller operations and to facilitate obtaining the required results.
- 8) Finally, this chapter review the results of rotor position estimations in the feedback path, and the results concerning the power delivery through the space vector processing in the forward path.

CHAPTER EIGHT

CONCLUSION, FUTURE WORKS AND NOVELTY

This chapter will focus on; the main thoughts which are concluded from this work, the essential contributions that have been verified through presenting this thesis, the key points which are considered as novelties for the presenting work and finally exploring a group of suggestions to future works that is possible to be achieved depending upon the results of this thesis.

8.1 Main conclusion points

1. Considering the reasonable findings, it is concluded that this thesis presents an improved investigation for the sensorless rotor position estimations verified practically on two types of surface mounted permanent magnet synchronous motors, SM-PMSMs. The estimations are conducted when the tested motors at two different speed conditions, zero speed and low speed running. Two modified methods are adopted to verify the aspects of, firstly, zero speed and low speed rotor position estimations, and secondly the excitation control of the PMSM stator windings at low speed operation. Verification of each method is firstly modelled through a “MATLAB/Simulink” environment modelling scheme and then through a real world test bench. Therefore, this thesis has been documented with four worked chapters, chapters four through seven.
2. A detailed “MATLAB/Simulink” model for SM-PMSMs to estimate the zero speed rotor position has been developed. “MATLAB/Simulink” environment is characterised by having a high mathematical modelling performance, high flexibility, and a wide simulation library. These are the main reasons to choose this software-programming tool, in this thesis, to establish the modelling schemes for the rotor position estimation at zero speed and low speed SM-PMSM operation conditions. An innovative procedure based on sensorless

sensing solely the motor terminal voltages is adopted, in this thesis, to estimate the standstill rotor position. At motor stationary condition, terminal voltages of the PMSM model are influenced, through a simulation process, by injecting high frequency pulses into the motor stator windings. Being these windings are supposed to be under an effect of a strong magnetic field, coming from the modelled permanent magnet rotor, it is deduced that their voltage responses should sinusoidally oscillate with variations of the simulated rotor position angles.

3. Based on the implementation results of the zero-speed modelling scheme, a real world platform is constructed to predict the rotor position of SM-PMSM at rest condition. The platform is built around a microcontroller of 16MHz crystal oscillator, 8bit word length, wide library of arithmetic functions, 32 general purpose registers, and a USB connection with a host computer for efficient C-language programming and data exchange. In addition, this microcontroller includes an embedded high sensitivity analogue to digital convertor, (1/1024) V per bit, which is employed for the purposes of sensing the mille-volt variations at the motor terminal voltages. Two commercial surface mounted permanent magnet motors are examined by the experimental platform for detecting their standstill rotor positions. Therefore, it is concluded that this proposed estimator is able to distinguish voltage variations of 0.9766 mV, at less, at motor terminals.
4. Accordingly, three main contributions are satisfied through adopting the suggested method in estimating the zero speed rotor position. Firstly, being the method is based solely on the sensorless measuring for the terminal voltages, without needing for any form of current measurements through current sensors, C.Ts. This makes the proposed method being a sensorless approach regarding only the approach of zero speed estimation. Secondly, a high discrimination for rotor position estimating is achieved depending upon exploiting the mille-volt variations of terminal voltages. Finally, the proposed method permits to satisfy the task without any technique for rotor polarity detection.
5. Comparing the results of the standstill rotor position prediction in both cases, modelling scheme and real time test bench, confirms that both of them could

successfully estimate the rotor positions of the surface mounted permanent magnet motors under test. Both estimators, modelling and experimental, are examined to obtain an estimation of 1-degree resolution. The modelling estimator has failed in estimating eight positions out of 360, while the experimental estimator has given a failure in 19 positions out of 360. In percentage error, the modelling scheme satisfied an estimation accuracy of 98% against 95% for the practical test bench. According to the recording of the employed microcontroller, the practical platform takes 1.3 msec to give a reading for each rotor position estimation. While, in the modelling scheme, setting the simulation time at 1 msec is sufficient to estimate any rotor position angle at the zero speed.

6. For the low speed works, 15% of rated speed of the underlying motor is approximately determined as an upper limit for the low speed running. A model of closed loop controlling scheme is simulated to estimate the rotor position of SM-PMSM under that speed limit. The forward path of this model is designated based on a standard method, field oriented control, to simulate energizing the modelled motor. While, the feedback route includes a promising proposed approach for investigating and detecting the low speed variations in rotor position angles. Corresponding to the obtained results by the proposed method, it is concluded that the sinusoidal variation in a single line voltage on motor terminals, rather than variations of the three phases, is sufficient to extract the information of rotor position angles at low speed operation.
7. In this thesis, verification of rotor position estimation at low speed by a real world test bench is achieved through a closed loop system. It is implemented by employing two microcontrollers, one in each of the two bench paths. Each microcontroller is of; a 16MHz clock cycle, multi input and output ports, an effective C-language programming through USB interfacing with a personal computer as well as RAM and EEPROM embedded memory structures of few kbytes capacities. The two commercial surface mounted PMSMs, which are tested in the zero speed practical estimation, are also employed in this examination of low speed position estimation. Correspondingly, one deduces

that the microcontrollers, in spite of being have limited capabilities comparing with those of digital signal processors, they are employed in establishing an embedded controllers in PMSM high performance drive systems.

8. While the feedback path in the low speed test bed has witnessed a practical implementation for the promising modelling proposed method for extracting the rotor position information, the experimental forward path also has witnessed an implementation for a proposed technique to generate the space vector patterns PWM sequences. Originally, this was attended to process the shortcoming of the microcontroller in field of SVM technique. It has been based on pre-storing the standard SVPWM sequence in a memory structure, which is 4kbytes EEPROM embedded in the microcontroller of the forward path. The registered results from this test bench have showed a successful rotor position estimation at low speed in addition to a good performance in driving the PM motors under test with fast dynamic response for load variation. Base on the aforementioned, it is concluded that the complicated space vector process has a chance to be implemented through sequential executions for a brief and simple predefined patterns which give a comprehensive description for SV process.
9. The thesis has provided an opportunity to comparing the power delivering graphical results at low speed motor running results, which are obtained by the modelling scheme and the experimental test bench, has appeared that the proposed method is of an effective performance for generating the sequence of space vector technique and driving the inverter, in the practical forward path. Accordingly, a deduction is reported that the proposed practical power delivering method is equivalent to the performance of the applied standard method in the modelling scheme.
10. Moreover, the results of both, the modelling and experimental approaches, shows that the estimators successfully estimate the low speed rotor positions of the underlying motors through the thought of exploiting the oscillations in the motor line voltage. At this point, it is concluded that the successful implementation of this thought, through the feedback path of both approaches, and the

corresponding obtained results have been satisfied the validity of the proposed method for low speed rotor position estimation.

11. Two main obstacles are exists in estimating the rotor position at zero and low speed operation. For the zero speed, depending upon the voltage variations only may suffer from a weak certainty in the mille-volt variation, which is tackled through adopting an analogue to digital converter of highest resolution as possible. For the low speed, there are an inherent low frequency harmonics at the inverter outputs, which threaten the stability of rotor position estimation. Therefore, it should be tackled through a high performance filtering process.
12. Utilizing the microcontroller technique as an intelligent core to implement the practical test bed has some limitations in regarding the speed of software execution, SVM implementation and the available space of memory. Accordingly, it is concluded that if these limitations do not carefully considered, they might deteriorate the dynamic response of the control system. This problem is emerged at low speed controlling implementation more than that of zero speed because of the multi functions that should be managed by the microcontroller at low speed processing.
13. At this point, it becomes clear the importance role for accurate rotor position estimation in ensuring soft and robust running for PMSM. However, the error in the position estimation may occur at any moment and for different reasons. According to the observations upon this thesis working, it is concluded that the worst error in position estimation is that which predicts the rotor angle at different sector. Such error deteriorates the space vector sequence of power delivering and leads to motor failure running. Whereas the error within the sector, although it still represent an error and should be avoided, it appears in form of a temporary change in motor output speed or torque. The same situations happen (or the motor start running in reverse direction) in case of error in zero speed rotor position estimation.
14. Although the decision of wrong estimation at zero speed is explicit to be taken, it is more complicated to be sensed at low speed as it suddenly and temporarily

happens while the estimation process is going continuously with motor spinning. However, it is noticed through the proper presence of failure in motor running or the increased ripple in output speed and torque. Based on this, it is concluded that the correct motor performance at low speed operation is regarded as a criterion for the successful employed strategy for sensorless rotor position estimation.

15. The low cost and simplicity of the proposed method has been referenced by four added references on page 69. Reference [145] mentioned that “This method does not require any current or position sensor, thereby it is significantly cost effective”. Reference [146] mentioned that “This method is a simple method to determine the standstill rotor position. It is implemented without any form of position or current sensors, so it is suitable for low cost applications”. Whereas, both references [124] and [147] emphasised that this method is characterised by having a simple implementation for estimation process.

8.2 Main contributions

The main contributions, which are verified by this thesis, through the rotor position estimation at zero and low speeds, is summarised by the following six points:

- **Impulse response:** firstly, this thesis contributes in highlighting the ability of the impulse response method, which is applied here, in successfully achieving the rotor position estimation of the PMSMs at zero speed.
- **Advantage:** it also contributes in pointing out the advantage of adopting this method in the concerned field of application being it has a simple and cost effective implementation.
- **No saliency problem:** an additional contribution is given by demonstrating the difficulty of investigating the rotor position of surface mounted PMSM and has proved it graphically. The thesis has interpreted that being all the adopted

methods, to estimate the zero speed rotor position, have based on tracking the machine saliency, which is very weak in the SM-PMSM. Moreover, it has contributed in establishing zero speed estimator for the rotor position of the surface mounted PMSM based on sensing the mille-volt variations at motor terminals.

- **Power electronic and PM materials:** the thesis has succeeded in projecting a spot of light on the relationship between the wide spreading of PMSM and the progress in both power electronic applications and permanent magnet material discoveries.
- **SVPWM:** through addressing the limitation of microcontroller in implementing the SVM, this thesis has a successful contribution in field of SVPWM through presenting a modified techniques for implementing the theory of space vector pulse width modulation and running the targeted motor accordingly. This technique is characterised by a simple verification and no huge competing operations are required.
- **DSP and microcontroller:** finally, comparing the digital signal processor and microcontroller technologies, the former is more efficient in managing the controlling process while the latter is of lower cost, simple to use, and more suitable for embedded controlling systems. While the dedicated digital signal processors are mostly adopted in controlling the operation of PMSM, this thesis has contributed in showing the ability of modern microcontrollers in substituting those digital signal processors so as to establish cheaper and embedded control schemes.

8.3 Novelty

The verified novelty through this thesis is summarised by the following points which are categorised according to the zero and low speed works.

Zero speed

The novelties, which is noticed to be verified by this thesis through the rotor position estimation at zero speed, is summarised by the following three points:

- ❖ **Sensorless implementation:** this thesis shows the possibility of implementing a sensorless estimator through adopting solely the voltage variations at motor terminals and eliminating sensing of motor currents through current sensors, usually current transformers (only through zero speed estimation).
- ❖ **Magnet polarity:** adopting the mille-voltage variations at the motor terminals has permitted to show that it is possible to decline the techniques of magnet polarity detection in implementing the estimators of zero speed rotor position estimators.
- ❖ **High resolution:** the proposed zero speed estimator, by this thesis, is characterized by having a high resolution, 1 degree, for rotor position discrimination.

Low speed

Whereas the novelties for low speed rotor position estimation and motor running is summarised by the following two points:

- ❖ **Single phase voltage variations:** the rotor position at low speed is estimated based on investigating the voltage variations on a single line voltage rather than the motor three phase voltage variations. Thereby, a considerable reduction in cost and complexity of hardware/software implementations is verified.
- ❖ **Standard SV pattern:** a space vector technique, based on exploiting the standard pattern of space vector sequences, is experimented in this thesis to drive the power to the underlying motor, through an inverter scheme, in the proposed test bed control system for low speed running.
- ❖ **Speed control:** a promised strategy for controlling motor speed has been hereby presented. Briefly, it is adopted on modifying the inverter output frequency through adjusting its full period by additive delay times. In this thesis, the proposed speed control strategy is performed by the master microcontroller.

According to the crystal oscillator in this controller, 16MHz, a fundamental frequency, at the inverter output, of nearly 22Hz is verified and it is dropped down through the additive delay time. This value for fundamental frequency is corresponding to a higher low speed limit of 450 rpm for a targeted motor of three pole-pairs. The value of the fundamental frequency is increased, and consequently the upper limit of low speed will increase too, through adopting a master microcontroller of higher crystal oscillator. Thereby, a higher range of speed control is verified.

8.4 Suggestions for future works

Through working on this thesis, it has been noticed that the following points, which are related to the PMSM rotor position estimation or motor running, are either not fully covered or they are not mentioned through the literature. Therefore, they are an important subject of study in future works.

- 1 **Temperature effect:** rising the ambient temperature of PMSM, over a certain limit, damage the permanent magnet material through either weaken the strength of its magnetic field or even losing its magnetic properties. Such temperature rising may come from the environmental circumstances at which the PMSM works, or from a continuous running of PMSM over a long period. Anyhow, happening of such thing causes in deteriorating the accuracy of zero and low speeds rotor position estimation because all the adopted techniques, for rotor position estimation at zero and low speeds, are dependent upon tracking the magnetic properties of the PMSM rotor. Therefore, it is important to deeply investigate the proper effects of temperature rising on rotor position estimation, and how it is tackled. It may worth to mention that the literature might not has a mention for effect of temperature rising on sensorless rotor position estimation.
- 2 **Cogging torque:** it is well known that the cogging torque has a negative effect on the ripple performance of the PMSM. This impact should has a certain amount of drawback on the accuracy of the rotor position estimation at zero and low

speed. In spite of that, a survey for the relevant literature lead to the fact that this subject is not searched sufficiently.

- 3 **Secondary saliency:** under the effect of strong magnetic field provided by the rotor permanent magnet, a difference appears between the values of direct inductance L_d and the quadrature inductance L_q . This deference is expressed by the machine saliency or the primary saliency and it has found a useful application in field of rotor position estimation at zero and low speeds. There is another type of saliency, which called the secondary saliency, emerges either from effect of the physical design of the driver system, such as the inverter dead time or nonlinearity and the harmonics generated by the high frequency switching process, or from the physical design of the rotor permanent magnet itself. Consequently, this secondary saliency could cause undesired harmonics, which have a negative effect on rotor position estimation at zero and low speeds if it is not properly suppressed. According to the literature, there is a little general attention on the issue of secondary saliency, but not specifically on its effect on rotor position estimation.
- 4 **The resolution of A/D:** as the mille-volts variations at the motor terminal voltage is considered as a base for detection the zero speed rotor position, then a good distinguishing among the mille-volt variations will be a crucial factor in determining the accuracy of rotor position estimation. As the motor analogue voltages are primarily converted into digital form by means of A/D converter, therefore, this proposed work for zero speed rotor position estimation is possibl to be re-achieved by adopting an A/D of higher resolution. This improvement may help in overcoming the problem of voltage uncertainty.
- 5 **Fault diagnosing:** When the estimator is accurately able to detect the angle of rotor position at zero speed, then any error may occur later in position estimation is properly comes due to unexpected change in the standard PMSM parameters. This mostly happens when a physical damage has taken place in the motor structure. Therefore, a PMSM fault diagnostic system is built around this thought.

References

- [1] S. Bistak and S. Kim, “AC Induction Motors vs. Permanent Magnet Synchronous Motors,” *Fuji Electric Corp of America*, 2017. [Online]. Available: <http://empoweringpumps.com/ac-induction-motors-versus-permanent-magnet-synchronous-motors-fuji/>.
- [2] NXP Freescale Semiconductor Inc., “Sensorless PMSM Field-Oriented Control,” Document Number: DRM148, Design Reference Manual, US, 2016.
- [3] John Chandler, “PMSM Technology in High Performance Variable Speed Applications,” Technical Report, Infranor Inter AG Company, Switzerland, 2005.
- [4] D. Bae and Y. Park, “Sensorless Drive for Interior Permanent Magnet Brushless DC motors,” in *IEEE International Conference on Electric Machines and Drives, USA*, 1997, pp. 5–7.
- [5] D. Paulus, P. Landsmann, and R. Kennel, “Sensorless Field Oriented Control for Permanent Magnet Synchronous Machines with an Arbitrary Injection Scheme and Direct Angle Calculation,” in *IEEE, Symposium on Sensorless Control for Electrical Drives, UK*, 2011, pp. 41–46.
- [6] G.-J. Su and J. W. McKeever, “Low-cost Sensorless Control of Brushless DC Motors with Improved Speed Range,” *IEEE Trans. Power Electron.*, vol. 19, no. 2, pp. 296–302, 2004.
- [7] R. W. Hejny and R. D. Lorenz, “Evaluating the Practical Low-speed Limits for Back-EMF Tracking-based Sensorless Speed Control Using Drive Stiffness as a Key Metric,” *IEEE Trans. Ind. Appl.*, vol. 47, no. 3, pp. 1337–1343, 2011.
- [8] Y. D. Yoon, S. K. Sul, S. Morimoto, and K. Ide, “High Bandwidth Sensorless Algorithm for AC Machines Based on Square-wave Type Voltage Injection,” *2009 IEEE Energy Convers. Congr. Expo. ECCE 2009*, pp. 2123–2130, 2009.

- [9] SIEMENS, “Synchronous and Asynchronous Servo Motors for SIMOVERT MASTERDRIVES,” Catalog DA 65.3 • 2004, 2004.
- [10] A. I. Haitham Abu-Rub, *High Performance Control of AC Drives with Matlab/Simulink Models*, 1st ed. United Kingdom: John Wiley & Sons, 2012.
- [11] Muhammad Mubeen, “Brushless DC Motor Primer,” Technical Report, Aspen Motion Technologies, USA, 2008.
- [12] P. Pillay and R. Krishnan, “Application Characteristics of Permanent Magnet Synchronous and Brushless dc Motors for Servo Drives,” *IEEE Trans. Ind. Appl.*, vol. 21, no. 5, pp. 986–996, 1991.
- [13] S. Derammelaere and et al., “A Quantitative Comparison between BLDC , PMSM , Brushed DC and Stepping Motor Technologies,” in *19th International Conference on Electrical Machines and Systems , Japan*, 2016, pp. 1–5.
- [14] M. S. F. Ludwig, “Integrated high-speed PMSM Drive with IMS PCB-Technology for Mobile Applications,” in *IEEE 11th International Conference on Power Electronics and Drive Systems , Australia*, 2015, pp. 1070–1073.
- [15] S. Chi, Z. Zhang, and L. Xu, “Sliding-Mode Sensorless Control of Direct-Drive PM Synchronous Motors for Washing Machine Applications,” *IEEE Trans. Ind. Appl.*, vol. 45, no. 2, pp. 582–590, 2009.
- [16] C. S. Soh and et al., “Contactless Measurement Method for Hard Disk Drive Spindle Motor Impedance,” *IEEE Trans. Magn.*, vol. 45, no. 11, pp. 5168–5171, 2009.
- [17] Y.-C. Chin, “A Permanent Magnet Synchronous Motor for an Electrical Vehicle-Design Analysis,” PhD thesis, Depatement of Electrical Engineering, Royal Institute of Technology, Sweden, 2004.

- [18] H. Jiang, “Audible Noise Reduction in the High Frequency Injection based Sensorless Torque Control for EPS Applications,” PhD thesis, Nottingham University, UK, 2012.
- [19] K. Matsuoka and S. Member, “Development Trend of the Permanent Magnet Synchronous Motor for Railway Traction,” *IEEJ Trans Electr. Electron. Eng.*, vol. 2, pp. 154–161, 2007.
- [20] K. T. Chau and et al., “Overview of Permanent-Magnet Brushless Drives for Electric and Hybrid Electric Vehicles,” *IEEE Trans. Ind. Electron.*, vol. 55, no. 6, pp. 2246–2257, 2008.
- [21] M. Liserre and et al., “Overview of Multi-MW Wind Turbines and Wind Parks,” *IEEE Trans. Ind. Electron.*, vol. 58, no. 4, pp. 1081–1095, 2011.
- [22] B. Z. Q. Zhu and D. Howe, “Electrical Machines and Drives for Electric , Hybrid , and Fuel Cell Vehicles,” *Proc. IEEE*, vol. 95, no. 4, pp. 746–765, 2007.
- [23] R. Mecke, “Permanent magnet synchronous motor for passenger ship propulsion,” in *European Conference on Power Electronics and Applications, Spain, 2009*, pp. 1–10.
- [24] C. S. Postiglione and et al., “Propulsion System for an All Electric Passenger Boat employing Permanent Magnet Synchronous Motors and Modern Power Electronics,” in *IEEE, Railway and Ship Propulsion Electrical Systems for Aircraft, Italy, 2012*, pp. 1–6.
- [25] A. Maria, R. Mar, and A. I. Nicu, “Permanent Magnet Synchronous Machines for Small Energy-Efficient Applications,” in *The 5th IEEE International Conference on E-Health and Bioengineering, Romania, 2015*, pp. 12–15.
- [26] H. Nak and A. F. Ergenç, “A PMSM Driven Rotationally Oscillating Micro Drill,” in *10th International Conference on Electrical and Electronics*

- Engineering, Turkey*, 2017, pp. 309–313.
- [27] P. Karimaghaee, “Adaptive Control Application on Syringe Pump Pressure Control Systems in Oil and Gas Industries,” in *15th International Conference on Control, Instrumentation, and Automation, Iran*, 2017, pp. 259–264.
- [28] R. Nukke, T. Lehtla, A. Kilk, and T. Kangru, “Design of the Exterior-Rotor PM Synchronous Motor for an Electrical Powered Paraglider,” in *56th International Scientific Conference on Power and Electrical Engineering of Riga Technical University, Latvia*, 2015, pp. 1–4.
- [29] “Magnetic Materials: History.” [Online]. Available: <https://www.birmingham.ac.uk/Documents/college-eps/metallurgy/research/Magnetic-Materials-Background/Magnetic-Materials-Background-1-History.pdf>. [Accessed: 15-Apr-2018].
- [30] Wikipedia, “Alnico.” [Online]. Available: <https://en.wikipedia.org/wiki/Alnico>. [Accessed: 16-Apr-2018].
- [31] Wikipedia, “Samarium cobalt_magnet.” [Online]. Available: https://en.wikipedia.org/wiki/Samarium-cobalt_magnet. [Accessed: 09-Jul-2017].
- [32] First4Magnets, “What Are Neodymium Magnets.” [Online]. Available: <https://www.first4magnets.com/tech-centre-i61/information-and-articles-i70/neodymium-magnet-information-i82/what-are-neodymium-magnets-i93>. [Accessed: 15-Apr-2018].
- [33] TEXAS INSTRUMENTS, “Motor Drive and Control.” [Online]. Available: <http://www.ti.com/lscds/ti/applications/industrial/motor-drives/overview.page>. [Accessed: 21-Jul-2017].
- [34] ThomasNet, “Types of Magnets.” [Online]. Available:

- <https://www.thomasnet.com/articles/electrical-power-generation/magnet-types>. [Accessed: 22-Jul-2017].
- [35] Supermagnete, “Demagnetisation through heat, temperature resistance magnet,,” 2017. [Online]. Available: <https://www.supermagnete.de/eng/faq/What-temperatures-can-magnets-sustain>. [Accessed: 22-Jul-2017].
- [36] ARNOLD MAGNETIC TECHNOLOGY, “Arnold Magnetic Technologies | Samarium Cobalt, Magnetic Assemblies.” [Online]. Available: <http://www.arnoldmagnetics.com/en-us>. [Accessed: 24-Jul-2017].
- [37] G. D. Andreescu, C. I. Pitic, F. Blaabjerg, and I. Boldea, “Combined flux observer with signal injection enhancement for wide speed range sensorless direct torque control of IPMSM drives,” *IEEE Trans. Energy Convers.*, vol. 23, no. 2, pp. 393–402, 2008.
- [38] S. Kim and P. Nae-Chun, “Simple Sensorless Algorithm for Interior Permanent Magnet Synchronous Motors Based on High-Frequency Voltage Injection Method,” *IET Electr. Power Appl.*, vol. 8, no. 2, pp. 68–75, 2014.
- [39] H. Rasmussen, P. Vadstrup, and H. Børsting, “Sensorless field oriented control of a PM motor including zero speed,” *IEMDC 2003 - IEEE Int. Electr. Mach. Drives Conf.*, vol. 2, pp. 1224–1228, 2003.
- [40] V. Zhao, Z. Zhang, and M. Cong, “Sensorless Control of Surface-Mounted Permanent-Magnet Synchronous Machines for Low-Speed Operation Based on High-Frequency Square-Wave Voltage Injection,” in *IEEE Industry Applications Society Annual Meeting, USA*, 2013, pp. 1–8.
- [41] C. Liu and et al., “A Novel Claw Pole Permanent Magnet Motor with SMC and Ferrite PM,” in *17th International Conference on Electrical Machines and Systems, China*, 2014, pp. 430–434.

- [42] S. Range, "Identification and Fuzzy-PI Controller Design for a Novel Claw Pole Eddy Current dynamometer in Wide," in *IEEE 24th Iranian Conference on Electrical Engineering, Iran, IEEE*, 2016, pp. 1038–1042.
- [43] S. Il Kim, J. Cho, S. Park, T. Park, and S. Lim, "Characteristics Comparison of a Conventional and Modified Spoke-type Ferrite Magnet Motor for Traction Drives of ILw-speed Electric Vehicles," *IEEE Trans. Ind. Appl.*, vol. 49, no. 6, pp. 2516–2523, 2013.
- [44] W. Kakihara, M. Takemoto, and S. Ogasawara, "Rotor Structure in 50 kW Spoke-type Interior Permanent Magnet Synchronous Motor with Ferrite Permanent Magnets for Automotive Applications," in *2013 IEEE Energy Conversion Congress and Exposition, USA*, 2013, vol. 2, pp. 606–613.
- [45] S. Murakami and et al., "Encoderless Servo Drive with Adequately Designed IPMSM for Pulse-Voltage-Injection-Based Position Detection," *IEEE Trans. Ind. Appl.*, vol. 48, no. 6, pp. 1922–1930, 2012.
- [46] P. Akiki and et al., "Performance Comparison of a Doubly-Salient Motor with Multi-V-shape Ferrite Magnets," in *International Symposium on Power Electronics, Electrical Drives, Italy*, 2016, pp. 205–212.
- [47] P. Crause, O. Wasynczuk, S. Sudhoff, and S. Pekarek, *Analysis of Electric Machinery and Drive Systems*, 3rd ed. New Jersey: John Wiley & Sons, 2013.
- [48] Power Electronics A to Z, "Comparison of Inverters: VSI vs CSI," 2018. [Online]. Available: <http://www.completepowerelectronics.com/vsi-vs-csi-comparison-inverters/>. [Accessed: 05-Apr-2018].
- [49] A. El Shahat and H. El Shewy, "Permanent Magnet Synchronous Motor Drive System for Mechatronics Applications," *Int. J. Res. Rev. Appl. Sci.*, pp. 323–338, 2010.

- [50] J. Zambada, "Sensorless Field Oriented Control of PMSM Motors," Application note AN1078, Microchip Technology Inc., 2007.
- [51] R. Balachandar, S. Vinoth, and C. Vignesh, "Sensorless Speed Control for PMSM Based On the DTC Method with Adaptive System," *Int. J. Innov. Res. Sci. Eng. Technol.*, vol. 3, no. 1, pp. 767–772, 2014.
- [52] M. A. Rahman, D. M. Vilathgamuwa, and M. N. Uddin, "Nonlinear Control of Interior Permanent-Magnet Synchronous Motor," *IEEE Trans. Ind. Appl.*, vol. 39, no. 2, pp. 408–416, 2003.
- [53] J. Bastos, A. Monti, and E. Santi, "Design and Implementation of Nonlinear Speed Control for a PM Synchronous motor Using the Synergetic Approach to Control Theory," *35th Annu. IEEE Power Electron. Spec. Conf.*, vol. 5, pp. 3397–3402, 2004.
- [54] M. Ouassaid, M. Cherkaoui, A. Nejmi, and M. Maaroufi, "Nonlinear Torque Control for PMSM : A Lyapunov Technique Approach," *Int. J. Electr. Comput. Eng.*, vol. 1, no. 6, pp. 918–921, 2007.
- [55] G. M. Schoonhoven, S. M. Ieee, M. N. Uddin, and S. M. Ieee, "Wide Speed Range Operation of PMSM Drives Using Nonlinear Flux Control Techniques," in *8th International Conference on Electrical and Computer Engineering*, 2014, pp. 603–606.
- [56] C. I. Xia, *Permanent Magnet Brushless DC Motor Drives and Controls*, 2nd ed. Singapore: John Wiley & Sons, 2012.
- [57] R. S. A and S. Wekhande, "Comparison of High Frequency Signal Injection Techniques for Rotor Position Estimation at Low Speed to Standstill of PMSM," *5th India Int. Conf. Power Electron.*, 2012.
- [58] E. E. Montalvo-Ortiz and et al., "Comparison between a Spoke-type PMSM and

- a PMASynRM using Ferrite Magnets,” *Proc. 2013 IEEE Int. Electr. Mach. Drives Conf. IEMDC 2013*, pp. 1080–1087, 2013.
- [59] R. Madhu and A. Mathew, “MATLAB / Simulink Model of Field Oriented Control of PMSM Drive Using Space Vectors,” *Int. J. Adv. Eng. Technol.*, vol. 6, no. 3, pp. 1355–1364, 2013.
- [60] W. Mieslinger, “Control circuit for a commutatorless D.C. motor,” Patent 3475668, United States Patent Office, US, 1969.
- [61] J. Davoine, R. Perret, and H. Le-Huy, “Operation of a Self-Controlled Synchronous Motor Without a Shaft Position Sensor,” *IEEE Trans. Ind. Appl.*, vol. IA-19, no. 2, pp. 217–222, 1983.
- [62] K. Iizuka, H. Uzuhashi, M. Kano, T. Endo, and K. Mohri, “Microcomputer Control for Sensorless Brushless Motor,” *IEEE Trans. Ind. Appl.*, vol. IA-21, no. 3, pp. 595–601, 1985.
- [63] B. Wu, *High-power Converters and ac Drives*. New Jersey, USA: IEEE press, John Wiley & Sons, 2006.
- [64] B. Liu, B. Zhou, J. Wei, H. Liu, J. Li, and L. Wang, “A Rotor Initial Position Estimation Method for Sensorless Control of SPMSM,” in *IECON Proceedings (Industrial Electronics Conference)*, 2014, pp. 354–359.
- [65] L. Shenzhen Gozuk Co., “Frequency inverter design.” [Online]. Available: <http://www.frequencyinverters.org/frequency-inverter-design-559198.html>. [Accessed: 26-Apr-2018].
- [66] O. Kechiche, H. Sethom, H. Sammoud, and I. Belkhodja, “Optimized High Frequency Signal Injection Based Permanent Magnet Synchronous Motor Rotor Position Estimation Applied to Washing Machines,” *Am. J. Eng. Appl. Sci.*, vol. 4, no. 3, pp. 390–399, 2011.

- [67] M. C. Huang, "Comparison of Shaft Position Estimation and Correction Techniques for Sensorless Control of Surface Mounted PM Synchronous Motors," *Cardiff, UK PhD thesis, Wolfson Cent. Magn. Sch. Eng. Cardiff Univ.*, 2009.
- [68] J. Holtz, "Initial Rotor Polarity Detection and Sensorless Control of PM Synchronous Machines," in *41st IAS Annual Meeting. Conference IEEE Industry Applicationsm USA*, 2006, vol. 4, pp. 2040–2047.
- [69] H. Takashima, M. Toita, Z. Chen, and M. Satoh, "Sensorless Position and Velocity Control of Cylindrical Brushless DC Motors at Low Speed Using Eddy Currents," *Proc. Power Convers. Conf.*, vol. 3, pp. 1300–1303, 2002.
- [70] J. Jang, K. Sul, I. Ha, Ide.K, and M. Sawamura, "Sensorless Drive of Surface-Mounted Permanent-Magnet Motor by High-Frequency Signal Injection Based on Magnetic Saliency," *IEEE Trans. Ind. Appl.*, vol. 39, no. 4, pp. 1031–1039, 2003.
- [71] S. Seman and J. Luomi, "Application of Carrier Frequency Signal Injection in Sensorless Control of a PMSM Drive with Forced Dynamics," *Fifth Int. Conf. Power Electron. Drive Syst.*, vol. 2, pp. 1663–1668, 2003.
- [72] A. Arias, G. Ashe, M. Sumne, P. Wheeler, L. Emprhgham, and C. Silva, "High Frequency Voltage Injection for the Sensorless Control of Permanent Magnet Synchronous Motors using Matrix Converters," *30th Annu. Conf. IEEE Ind. Electron. Soc.*, vol. 1, pp. 969–974, 2004.
- [73] J. Jang, J. Ha, M. Ohto, K. Ide, and S. Sul, "Analysis of Permanent-Magnet Machine for Sensorless Control Based on High-Frequency," *IEEE Trans. Ind. Appl.*, vol. 40, no. 6, pp. 1595–1604, 2004.
- [74] X. Yunxiang, Z. Ping, and N. Haiqing, "A Study on High Frequency Signal Injection Method of Aiming at Detecting the Rotor Position of the Salient - pole

- Brushless DC Motor,” *IEEE Int. Conf. Electr. Mach. Syst.*, vol. 3, pp. 2369–2373, 2005.
- [75] Y. Zhang, J. Gu, Z. Wu, and J. Ying, “Investigation of High Frequency Injection Method for Surface-mounted PMSM Sensor-less Drive,” *Int. Conf. Electr. Mach. Syst.*, vol. 1, pp. 306–309, 2005.
- [76] Z. Feng, W. Xuhui, X. Shan, and G. Jinwen, “Sensorless Control of Interior Permanent Magnet Machine at Standstill and Low Speed,” in *12th International Conference on Power Electronics and Motion Control, 2006. Slovenia, 2006*, pp. 1289–1294.
- [77] C. Ortega, A. Arias, C. Caruana, C. Staines, and J. Balcells, “Sensorless Direct Torque Control of a Surface Mounted PMSM using High Frequency Injection,” *IEEE Int. Symp. Ind. Electron.*, vol. 3, pp. 2332–2337, 2006.
- [78] N. Urasaki, T. Senjyu, T. Kinjo, T. Funabashi, and H. Sekine, “Dead-time Compensation Strategy for Permanent Magnet Synchronous Motor Drive Taking Zero-current Clamp and Parasitic Capacitance Effects into Account,” *IEE Proc. - Electr. Power Appl.*, vol. 152, no. 4, pp. 845–853, 2005.
- [79] C. Silva, G. Asher, and M. Sumner, “Influence of Dead-time Compensation on Rotor Position Estimation in Surface Mounted PM Machines Using HF Voltage Injection,” *Proc. Power Convers. Conf. 2002 (Cat. No.02TH8579)*, vol. 3, pp. 1279–1284, 2002.
- [80] N. Teske, G. Asher, M. Sumner, and K. Bradley, “Analysis and Suppression of High-Frequency Inverter Modulation in Sensorless Position-Controlled Induction Machine Drives,” *IEEE Trans. Ind. Appl.*, vol. 39, no. 1, pp. 10–18, 2003.
- [81] C. Choi and J. Seok, “Compensation of Zero-Current Clamping Effects in High Frequency-Signal-Injection-Based Sensorless PM Motor Drives,” *IEEE Trans. Ind. Appl.*, vol. 43, no. 5, pp. 1258–1265, 2007.

- [82] C. Ortega, A. Arias, J. Balcells, and C. Caruana, "High Frequency Injection in a Matrix Converter DTC Drive for Sensorless Operation of a PMSM," *12th Int. Power Electron. Motion Control Conf.*, pp. 2278–2283, 2007.
- [83] C. CHOI and J. SEOK, "Pulsating Signal Injection-Based Sensorless Control of PMSM Using Injection Axis Switching Scheme Without Wdditional off Line Commissioning Test," *42nd IAS Annu. Meet. Ind. Appl. Conf.*, pp. 2365–2370, 2007.
- [84] S. Wu, Y. Li, and X. Miao, "Two Signal Injection Methods for Sensorless Control of PMSM at Very Low Speeds," *IEEE Power Electron. Spec. Conf.*, pp. 568–573, 2007.
- [85] M. Nour, N. Ee, and E. Radwan, "Improvements on the High Frequency Signal Injection Method for Permanent Magnet Synchronous Motors and its Application in the Hybrid Drive Position Control," *IEEE 2nd Int. Power Energy Conf.*, pp. 295–300, 2008.
- [86] J. Salomäki, J. Luomi, and J. Luomi, "Signal Injection in Sensorless PMSM Drives Equipped With Inverter Output Filter," *IEEE Trans. Ind. Appl.*, vol. 44, no. 5, pp. 1614–1620, 2008.
- [87] A. Khan and O. Mohammed, "Neural Network based Modeling of Audible Noise for High Frequency Injection based Position Estimation for PM Synchronous Motors at Low and Zero speed," *IEEE 2nd Int. Power Energy Conf.*, pp. 119–122, 2009.
- [88] H. Jiang, "Audible Noise Reduction in the High Frequency Injection based Sensorless Control for EPS Application," Nottingham, UK: Thesis submitted to the University of Nottingham for the degree of Doctor of Philosophy, 2012.
- [89] Q. Xin, X. Zhou, C. Wang, X. Wang, and K. Zhou, "Rotor Position Estimation for a Sensorless PMSM Using High-Frwquency Signal Indiction Method," in

- IEEE Youth Conference on Information, Computing and Telecommunication*, 2009, pp. 54–57.
- [90] C. Nino, A. Tariq, C. Jurkovic, and E. Strangas, “High Performance Low Speed Sensorless Control of Interior Permanent Magnet Synchronous Motor,” in *IEEE International Symposium on Industrial Electronics*, 2010, pp. 1314–1320.
- [91] Y. Wang, J. Zhu, Y. Guo, Y. Li, and W. Xu, “Torque Ripples and Estimation Performance of High Frequency Signal Injection based Sensorless PMSM Drive Strategies,” in *IEEE Energy Conversion Congress and Exposition*, 2010, pp. 1699–1706.
- [92] Y. D. Yoon, S. K. Sul, S. Morimoto, and K. Ide, “High Bandwidth Sensorless Algorithm for AC Machines Based on Square-Wave Type Voltage Injection,” in *IEEE Energy Conversion Congress and Exposition*, 2009, pp. 2123–2130.
- [93] C. Yu, J. Tamura, D. Reigosa, and R. Lorenz, “Position Self-Sensing Evaluation of a FI-IPMSM based on High Frequency Signal Injection Methods,” *IEEE Trans. Ind. Appl.*, vol. 49, no. 2, pp. 880–888, 2013.
- [94] R. Leidhold, “Position Sensorless Control of PM Synchronous Motors Based on Zero-Sequence Carrier Injection,” *IEEE Trans. Ind. Electron.*, vol. 58, no. 12, pp. 5371–5379, 2011.
- [95] S. Bolognani, S. Calligaro, R. Petrella, and M. Sterpellone, “Sensorless Control for IPMSM using PWM Excitation: Analytical Developments and Implementation Issues,” in *Symposium on Sensorless Control for Electrical Drives*, 2011, pp. 64–73.
- [96] O. Mohammed, A. Khan, A. Mohamed, A. Nejadpack, and M. Roberts, “A Wavelet Filtering Scheme for Noise and Vibration Reduction in High-frequency Signal Injection-Based Sensorless Control of PMSM at Low Speed,” *IEEE Trans. Energy Convers.*, vol. 27, no. 2, pp. 250–260, 2012.

- [97] W. Jianmin and G. Jianwei, "Influence of Speed EMF on Position Estimation Error in Carrier Signal Injection Based Sensorless Control of PMSM," in *15th International Conference on Electrical Machines and Systems (ICEMS)*, 2012, pp. 1–6.
- [98] F. Cupertino, A. Guagnano, A. Altomare, and G. Pellegrino, "Position Estimation Delays in Signal Injection-Based Sensorless PMSM Drives," in *3rd IEEE International Symposium on Sensorless Control for Electrical Drives*, 2012, pp. 1–6.
- [99] Z. Ma and R. Kenel, "System-on-Chip Sensorless Control of PMSM Combining Signal Injection and Flux Observer," in *IEEE 7th International Power Electronics and Motion Control Conference - ECCE*, 2012, pp. 1201–1205.
- [100] A. Setty, S. Wekhande, and K. Chatterjee, "Adaptive Signal Amplitude for High Frequency Signal Injection Based Sensor less PMSM Drives," in *IEEE International Symposium on Sensorless Control for Electrical Drives and Predictive Control of Electrical Drives and Power Electronics (SLED/PRECEDE)*, 2013, pp. 1–5.
- [101] E. Sebastian, S. Markus, and P. Bernhard, "Flatness Based Sensorless Control of PMSM Using Test Current Signal Injection and Compensation for Differential Cross-Coupling Inductances at Standstill and Low Speed Range," in *IEEE International Symposium on Sensorless Control for Electrical Drives and Predictive Control of Electrical Drives and Power Electronics*, 2013, pp. 1–7.
- [102] M. Ali, G. Moghadam, and F. Tahami, "Sensorless Control of PMSMs with Tolerance for Delays and Stator Resistance Uncertainties," *IEEE Trans. POWER Electron.*, vol. 28, no. 3, pp. 1391–1399, 2013.
- [103] K. Landsmann, D. Paulus, and A. Dötlinger, "Silent Injection for Saliency based Sensorless Control by means of Current Oversampling," in *IEEE International Conference on Industrial Technology (ICIT)*, 2013, pp. 398–403.

- [104] J. Choi, I. Jeong, K. Nam, and S. Jung, "Sensorless Control for Electrically Energized Synchronous Motor Based on Signal Injection to Field Winding," in *39th Annual Conference of the IEEE Industrial Electronics Society*, 2013, pp. 3120–3129.
- [105] D. Reigosa, F. Briz, C. Charro, and A. Gioia, "Sensorless Control of Doubly Fed Induction Generators Based on Rotor High-Frequency Signal Injection," *IEEE Trans. Ind. Appl.*, vol. 49, no. 6, pp. 25-93–2601, 2013.
- [106] B. Yuanjun, G. Xinhua, S. Xiaofeng, W. Yanfeng, and C. Yin, "Initial Rotor Position Estimation of PMSM Based on High Frequency Signal Injection," in *IEEE Conference and Expo Transportation Electrification Asia-Pacific (ITEC Asia-Pacific)*, 2014, pp. 1–4.
- [107] Y. Li, A. Taylor, and K. Bai, "A Hybrid Observer for the Full-Speed-Range Sensorless Control of Interior Permanent Magnet Motor Drives," in *IEEE Transportation Electrification Conference and Expo (ITEC)*, 2014, pp. 1–5.
- [108] Y. Chen, T. Liu, S. Syu, and C. Nguyen-Manh, "A Sensorless Matrix-Converter IPMSM Drive Based on High Frequency Injection Method," in *40th Annual Conference of the IEEE Industrial Electronics*, 2014, pp. 360–366.
- [109] T. Yoon, H. Sim, J. Lee, and K. Lee, "A Simplified Method to Estimate the Rotor Position Using the High Frequency Voltage Signal Injection," in *IEEE Applied Power Electronics Conference and Exposition - APEC 2014*, 2014, pp. 2453–2458.
- [110] T. Tuovinen and M. Hinkkanen, "Adaptive Full-Order Observer with High-Frequency Signal Injection for Synchronous Reluctance Motor Drives," *IEEE J. Emerg. Sel. Top. Power Electron.*, vol. 2, no. 2, pp. 181–189, 2014.
- [111] Y. Tauchi and H. Kubota, "Audible Noise Reduction Method in IPMSM Position Sensorless Control based on High Frequency Current Injection," in *International*

- Power Electronics Conference (IPEC-Hiroshima 2014 - ECCE ASIA)*, 2014, pp. 3119–3123.
- [112] V. Repecho, D. Bie, and A. Arias, “Enhanced High Frequency Injection Algorithm For Sensorless Sliding Mode Control PMSM Drives,” in *11th International Multi-Conference on Systems, Signals & Devices*, 2014, pp. 1–6.
- [113] V. Repecho, D. Biel, and A. Arias, “Finite-Element Analysis of Electrical Machines for Sensorless Drives with High-Frequency Signal Injection,” *IEEE Trans. Ind. Appl.*, vol. 50, no. 3, pp. 1871–1879, 2014.
- [114] Y. Shih-Chin, “Initial Rotor Position Estimation of Permanent Magnet Synchronous Machines Using Square-Wave Voltage Injection with a Single Current Sensor,” in *IEEE Applied Power Electronics Conference and Exposition - APEC 2014*, 2014, pp. 2430–2437.
- [115] M. Seilmeier and B. Piepenbreier, “Initial Start-Up and Magnet Polarity Estimation Method for HF Test Current Injection Based Sensorless Control of PMSM,” in *16th International Power Electronics and Motion Control Conference and Exposition*, 2014, pp. 59–64.
- [116] A. Chibah, M. Mena, and K. Yazid, “Rotor Speed Estimation of Doubly Fed Induction Motor Using High Frequency Carrier Signal Injection,” in *16th International Power Electronics and Motion Control Conference and Exposition*, 2014, pp. 751–756.
- [117] Z. Chen, J. Gao, F. Wang, Z. Ma, Z. Zhang, and R. Kennel, “Sensorless Control for SPMSM With Concentrated Windings Using Multisignal Injection Method,” *IEEE Trans. Ind. Electron.*, vol. 61, no. 12, pp. 6624–6634, 2014.
- [118] R. Hu, Z. Deng, J. Cai, and C. Wang, “Sensorless Control of Switched Reluctance Motors Based on High Frequency Signal Injection,” in *17th International Conference on Electrical Machines and Systems*, 2014, pp. 3558–3563.

- [119] Y. Yoon and S. Sul, "Sensorless Control for Induction Machines Based on Square-Wave Voltage Injection," *IEEE Trans. Power Electron.*, vol. 29, no. 7, pp. 3637–3645, 2014.
- [120] J. Liu and Z. Zhu, "Sensorless Control Strategy by Square-Waveform Sensorless Control Strategy by Square-Waveform Stationary Reference Frame," *IEEE J. Emerg. Sel. Top. Power Electron.*, vol. 2, no. 2, pp. 171–180, 2014.
- [121] T. Glasberger, V. Muzikova, V. Smidl, and Z. Peroutka, "Sensorless Permanent Magnet Synchronous Drive with DTC Based on High Frequency Injections," in *40th Annual Conference of the IEEE Industrial Electronics*, 2014, pp. 850–856.
- [122] D. Kim, Y. Kwon, S. Sul, J. Kim, and R. Yu, "Suppression of Injection Voltage Disturbance for High Frequency Square-Wave Injection Sensorless Drive with Regulation of Induced High Frequency Current Ripple," in *International Power Electronics Conference (IPEC-Hiroshima 2014 - ECCE ASIA)*, 2014, pp. 925–932.
- [123] D. Wang, C. Zhou, M. Zou, J. Liao, and Y. Du, "Study on Inspection of the Initial Rotor Position of BLDC Based on High-frequency Signal Injection," in *IEEE Conference and Expo Transportation Electrification Asia-Pacific (ITEC Asia-Pacific)*, 2014, pp. 1–4.
- [124] N. S. Pillai and R. Radhakrishnan, "Analysis and Simulation Studies for Position Sensorless BLDC Motor Drive with Initial Rotor Position Estimation," in *International Conference on Nascent Technologies in the Engineering Field , India*, 2015, pp. 1–6.
- [125] S. Medjmadj, D. Diallo, M. Mostefai, and C. Delpha, "PMSM Drive Position Estimation: Contribution to the High-Frequency Injection Voltage Selection Issue," *IEEE Trans. Energy Convers.*, vol. 30, no. 1, pp. 349–358, 2015.
- [126] T. Wang and J. Xu, "Rapid Demodulation of Rotor Position for High Frequency

- Voltage Injection Based IPM Machine Sensorless Control,” in *IEEE 11th International Conference on Power Electronics and Drive Systems*, 2015, pp. 873–879.
- [127] P. Pan, T. Liu, and U. Madawala, “Adaptive Controller with an Improved High Frequency Injection Technique for Sensorless Synchronous Reluctance Drive Systems,” *IET Electr. Power Appl.*, vol. 10, no. 4, pp. 240–250, 2016.
- [128] M. Glasberger, M. TomášVendula and G. Tomáš, “Control Strategies Enabling High Frequency Injections for PMSM Position Estimation,” in *International Conference on Applied Electronics (AE)*, 2015, pp. 161–164.
- [129] J. Agrawal and S. Bodkhe, “Low Speed Sensorless Control of PMSM Drive Using High Frequency Signal Injection,” in *Annual IEEE India Conference (INDICON)*, 2015, pp. 1–6.
- [130] X. Qiu, J. Yang, J. Shi, J. Chen, and A. Guo, “The Influence of Phase Inductance Harmonics on PMSM Position Estimation Using High Frequency Signal Injection,” in *18th International Conference on Electrical Machines and Systems (ICEMS)*, 2015, pp. 1615–1618.
- [131] E. Song, J. Im, S. Kim, and R. Kim, “A Rotor Position Estimation Method in Stationary Reference Frame of High Frequency Rotating Voltage Signal Injection IPMSM Sensorless Control,” in *IEEE 2nd International Future Energy Electronics Conference (IFEEEC)*, 2015, pp. 1–6.
- [132] S. Kim and R. Kim, “Analysis and Compensation of Band-Pass-Filter Delay for a High Frequency Signal Injected Sensorless Control,” in *17th European Conference on Power Electronics and Applications (EPE'15 ECCE-Europe)*, 2015, pp. 1–8.
- [133] D. Wang, K. Lu, and P. Rasmussen, “A New High Frequency Injection Method Based on Duty Cycle Shifting without Maximum Voltage Magnitude Loss,” in

- IEEE International Electric Machines & Drives Conference (IEMDC)*, 2015, pp. 811–817.
- [134] T. Sun, J. Wang, and X. Chen, “Maximum Torque Per Ampere (MTPA) Control for Interior Permanent Magnet Synchronous Machine Drives Based on Virtual Signal Injection,” *IEEE Trans. Power Electron.*, vol. 30, no. 9, pp. 5036–5045, 2015.
- [135] D. Reigosa, D. Fernandez, H. Yoshida, T. Kato, and F. Briz, “Permanent-Magnet Temperature Estimation in PMSMs Using Pulsating High-Frequency Current Injection,” *IEEE Trans. Ind. Appl.*, vol. 51, no. 4, pp. 3159–3168, 2015.
- [136] S. C. Yang, “Online Turn Fault Detection of Interior Permanent-Magnet Machines Using the Pulsating-Type Voltage Injection,” *IEEE Trans. Ind. Appl.*, vol. 52, no. 3, pp. 2340–2349, 2016.
- [137] S. C. Yang, “Performance evaluation of stator winding fault detection in the inverter-fed permanent magnet machine using high frequency voltage injection,” in *IECON 2015 - 41st Annual Conference of the IEEE Industrial Electronics Society*, 2015, pp. 3810–3815.
- [138] D. Fernandez, D. Reigosa, J. M. Guerrero, Z. Zhu, and F. Briz, “Permanent Magnet Magnetization State Estimation Using High Frequency Signal Injection,” *Energy Convers. Congr. Expo. (ECCE), 2015 IEEE*, vol. 52, no. 4, pp. 3949–3956, 2016.
- [139] D. D. Reigosa, D. Fernandez, Z. Zhu, F. Briz, S. Member, and A. P. Pm, “PMSM Magnetization State Estimation Based on Stator-Reflected PM Resistance Using High-Frequency Signal Injection,” *IEEE Trans. Ind. Appl.*, vol. 51, no. 5, pp. 3800–3810, 2015.
- [140] O. Ojo, M. Ramezani, and A. Gautam, “Sensor-less Vector Control of the Nine-phase Concentrated Wound Interior Permanent Magnet Motor Drive Using a

- Unique Third Sequence High Frequency Injection into the Stator Windings,” in *2015 IEEE Energy Conversion Congress and Exposition, ECCE 2015*, 2015, pp. 853–859.
- [141] A. Srivorakul, S. Suwankawin, I. I. M. Odel, O. F. D. Oubly, and E. D. I. Nduon, “A Synchro-Perspective High-Frequency Signal Injection Method for Position-Sensorless Vector Control of Doubly-Fed Induction Machines,” no. 4, pp. 1–5, 2015.
- [142] J. Cai and Z. Deng, “Initial Rotor Position Estimation and Sensorless Control of SRM Based on Coordinate Transformation,” *IEEE Trans. Instrumentations Meas.*, vol. 64, no. 4, pp. 1004–1018, 2015.
- [143] X. Luo, Q. Tang, A. Shen, and Q. Zhang, “PMSM Sensorless Control by Injecting HF Pulsating Carrier Signal into Estimated Fixed-Frequency Rotating Reference Frame,” *IEEE Trans. Ind. Electron.*, vol. 63, no. 4, pp. 2294–2303, 2016.
- [144] P. Xu and Z. Zhu, “Novel Carrier Signal Injection Method Using Zero-Sequence Voltage for Sensorless Control of PMSM Drives,” *IEEE Trans. Ind. Electron.*, vol. 63, no. 4, pp. 2053–2061, 2016.
- [145] Y. Lai, S. Member, F. Shyu, and S. Tseng, “New Initial Position Detection Technique for Three-phase Brushless DC Motor without Position and Current Sensors,” *IEEE Trans. Ind. Appl.*, vol. 39, no. 2, pp. 485–491, 2003.
- [146] P. Somsiril, P. Champal, P. Wipasuramonton, K. Tungpimonrut, and P. Aree, “Voltage Injection Based Initial Rotor Position Estimation Method for Three-Phase Star-Connected Switched Reluctance Machines,” pp. 494–500, 2007.
- [147] P. B. Schmidt, M. L. Gasperi, and A. H. Wijenayake, “Initial Rotor Angle Detection of a Non-Salient Pole Permanent Magnet Synchronous Machine,” vol. 0, no. c, pp. 8–12, 1997.

- [148] G. Wang, "Rotor Position Estimation of PMSM in Low-Speed Region and Standstill Using Zero-Voltage Vector Injection," *IEEE Trans. Power Electron.*, vol. 33, no. 9, pp. 7948–7958, 2018.
- [149] X. Wu, S. Huang, X. Liu, K. Lu, J. Gao, and J. Zheng, "Design of Position Estimation Strategy of Sensorless Interior PMSM at Standstill Using Minimum Voltage Vector Injection Method," vol. 53, no. 11, 2017.
- [150] G. H. Jang, J. H. Park, and J. H. Chang, "Position Detection and Start-Up Algorithm of a Rotor in a Sensorless BLDC Motor Utilising Inductance Variation," *IEE Proc. - Electr. Power Appl.*, vol. 149, no. 2, p. 137, 2002.
- [151] H. L. D. Q. J. Kdqj, P. Zdqjzhl, V. H. X. Hgx, T. R. V. T. L. T, H. À H. Fdq, and E. H. Vlpsoilhg, "A Simple Initial Rotor Position Identification Method for PMSM," pp. 1–4, 2015.
- [152] G. Meng, H. Yu, M. Hu, and L. Huang, "Initial Position Estimation of Permanent Magnet Synchronous Motors Based on Variation Behavior of Winding Inductances," *9th Int. Conf. Power Electron. ECCE Asia (ICPE-ECCE Asia)*, pp. 1609–1616, 2015.
- [153] G. Wang, R. Yang, Y. Wang, Y. Yu, and D. Xu, "Initial Rotor Position Estimation for Sensorless Interior PMSM with Signal Injection," *Int. Power Electron. Conf. - ECCE ASIA*, pp. 2748–2752, 2010.
- [154] H. Zhaobin, Y. Linru, and W. Zhaodong, "Sensorless initial rotor position identification for non-salient permanent magnet synchronous motors based on dynamic reluctance difference," *IET Power Electron.*, vol. 7, no. January, pp. 2336–2346, 2014.
- [155] X. Wu *et al.*, "Initial Rotor Position Detection for Sensorless Interior PMSM With Square-Wave Voltage Injection," vol. 53, no. 11, 2017.

- [156] T. Meng, W. Liu, N. Jiao, J. Peng, and Y. Zhu, "Initial Rotor Position Estimation for Wound-Rotor Synchronous Starter / Generators Based on Multi-Stage-Structure Characteristics," pp. 540–545, 2018.
- [157] E. Suganya and S. Vijayashaarathi, "Smart Vehicle Monitoring System for Air Pollution Detection using Wsn," *2016 Int. Conf. Commun. Signal Process. (ICCSP)*, pp. 719–722, 2016.
- [158] A. Solum and M. Leijon, "Investigating the overload capacity of a direct-driven synchronous permanent magnet wind turbine generator designed using high-voltage cable technology," *Int. J. Energy Res.*, vol. 31, no. 1, pp. 1076–1086, 2007.
- [159] V. Krithika and C. Subramani, "A comprehensive review on choice of hybrid vehicles and power converters , control strategies for hybrid electric vehicles," *Int. J. Energy Res.*, vol. 42, no. 5, pp. 1789–1812, 2007.
- [160] P. Dost, "Mechanical and Electrical Behaviour of an Electric Vehicles Drive Train due to the Choice of the Control-System," in *37th Annual Conference of the IEEE Industrial Electronics , Australia*, 2011, pp. 1426–1431.
- [161] A. Assega, A. Purwadi, and Y. Haroen, "Dynamic response analysis of Permanent Magnet Brushless DC Motor drives for city electric car based on Matlab/Simulink," in *International Conference on Rural Information & Communication Technology and Electric-Vehicle Technology, Indonesia*, 2013, no. I, pp. 1–5.
- [162] S. Fang, B. Zhou, and Y. Liu, "Design and realization of dual redundancy PMSM electrical drive systems," in *4th IEEE Conference on Industrial Electronics and Applications, China*, 2009, pp. 1985–1989.
- [163] A. K. Jebai *et al.*, "Sensorless Position Estimation and Control of Permanent-Magnet Synchronous Motors Using a Saturation Model," *Int. J. Control*, vol.

- 7179, no. February, 2016.
- [164] K. Jash, P. Pradip, K. Saha, P. Goutam, and K. Panda, "Vector Control of Permanent Magnet Synchronous Motor Based On Sinusoidal Pulse Width Modulated Inverter with Proportional Integral Controller," *Int. J. Eng. Res. Appl.*, vol. 3, no. 5, pp. 913–917, 2013.
- [165] J. Hu, L. Xu, F. Ieee, and J. Liu, "Magnetic Pole Identification for PMSM at Zero Speed Based on Space Vector PWM," in *5th International Power Electronics and Motion Control , China*, 2006, pp. 1–5.
- [166] Z. Taylor and R. Subramanyam, "Modeling and Reliability Basics," in *Designing High Availability Systems:DFSS and Classical Reliability Techniques with Practical Real Life Examples, Chapter 7*, IEEE press, John Wiley & Sons, 2014, pp. 72–109.
- [167] M. J. Corley and R. D. Lorenz, "Rotor Position and Velocity Estimation for a Salient-Pole Permanent Magnet Synchronous Machine at Standstill and High Speeds," *IEEE Trans. Ind. Appl.*, vol. 34, no. 4, pp. 784–789, 1998.
- [168] G. Feng, C. Lai, and S. Member, "A Closed-Loop Fuzzy-Logic-Based Current Controller for PMSM Torque Ripple Minimization Using the Magnitude of Speed Harmonic as the Feedback Control Signal," *IEEE Trans. Ind. Electron.*, vol. 64, no. 4, pp. 2642–2653, 2017.
- [169] D. W. J. and P. SMITH, *Mathematical Techniques, an Introduction for the Engineering, Physical, and Mathematical Sciences*, 3rd ed. New York: Oxford University Press, 2002.
- [170] C. Xia, *Permanent magnet brushless dc motor drives and controls*, 1st ed. Singapore: John Wiley & Sons Singapore Pte. Ltd., 2012.
- [171] Atmel Corporation, "Atmel 8-bit microcontroller with 4/8/16/32Kbytes in-system

- programmable flash,” Datasheet, USA, 2015.
- [172] A. AL-Dhaher, “Integrating hardware and software for the development of microcontroller-based systems,” *ESEVIER, Micoprocessors and Microsystems*, vol. 25, pp. 317–328, 2001.
- [173] E. Monmasson, *Power Electronic Converters*, 1st ed. USA: John Wiley & Sons, Inc, 2011.
- [174] SSD Drives GmbH, “Parker SSD 3.2Nm x 4000RPM 230V AC Servo-Motor Resolver ACM2n 0320-4/2-3.” [Online]. Available: <https://inverterdrive.com/group/Servo-Motors-AC/ACM2n-0320-4-2-3-Servo-Motor-SSD-Drives-Eurotherm/>. [Accessed: 09-May-2018].
- [175] Applied Motion, “M, N and A Series Brushless Servo Motors.” [Online]. Available: <https://www.valinonline.com/Userfiles/Documents/AMP-Brushless-Servo-Motors.pdf>. [Accessed: 09-May-2018].
- [176] Atmel corporation, “Atmel AVR443 : Sensor-based Control of Three Phase Brushless DC Motor,” Application Note, USA, 2013.
- [177] V. Duka, “Importance of Mathematical Modelling Skills in Engineering Education for Master and Doctoral Students of Latvia University of Agriculture,” in *15th International Conference on Interactive Collaborative Learning, Austria*, 2012, pp. 1–6.
- [178] H. E. Gross, “The Importance of Mathematical Modelling for University Education in Mathematics,” *Int. J. Math. Educ. Sci. Technol.*, vol. 12, no. 5, pp. 549–555, 2006.
- [179] Difference Between.com, “Difference Between Modelling and Simulation.” [Online]. Available: <https://www.differencebetween.com/difference-between-modelling-and-vs-simulation/>. [Accessed: 16-Apr-2018].

- [180] MathWorks, “Physical Modelling,” 2018. [Online]. Available: <https://uk.mathworks.com/solutions/physical-modeling.html>. [Accessed: 12-Jan-2018].
- [181] S. Kim and E. Song, “A New Rotor Position Estimation Method of IPMSM Using All-Pass Filter on High-Frequency Rotating Voltage Signal Injection,” *IEEE Trans. Ind. Electron.*, vol. 63, no. 10, pp. 6499–6509, 2016.
- [182] H. Injections, M. Ramezani, and O. Ojo, “The Modeling and Position-Sensorless Estimation Technique for A Nine-Phase Interior Permanent-Magnet Machine Using High-Frequency Injections,” *IEEE Trans. Ind. Appl.*, vol. 52, no. 2, pp. 1555–1565, 2016.
- [183] J. Xu *et al.*, “A Modular Control Scheme for PMSM Speed Control With Pulsating Torque Minimization,” *IEEE Trans. Ind. Electron.*, vol. 51, no. 3, pp. 526–536, 2004.
- [184] Y. Zhang, B. Xia, and H. Yang, “Performance Evaluation of an Improved Model Predictive Control with Field Oriented Control as a Benchmark,” *IET Electr. Power Appl.*, vol. 11, no. 5, pp. 677–687, 2017.
- [185] P. Tran, “MATLAB/Simulink Implementation and Analysis of Three Pulse-Width-Modulation (PWM) Techniques,” Dissertation in Electrical Engineering, Boise State University, 2012.
- [186] C. Gerald and P. Wheatley, *Applied Numerical Analysis*, 7th ed. Greg Tobia, 2006.
- [187] L. Wang and et al., *PID and Predictive Control of Electrical Drives and Power Converters using Matlab®/Simulink®*. Singapore: John Wiley & Sons Singapore Pte. Ltd, 2015.
- [188] B. Bose, *Power Electronics and Variable Frequency Drives*. New York: IEEE

- press, John Wiley & Sons, 1998.
- [189] Y. Yan, J. G. Zhu, and Y. G. Guo, “Initial Rotor Position Estimation and Sensorless Direct Torque Control of Surface-Mounted Permanent Magnet Synchronous Motors Considering Saturation Saliency,” *IET Electr. Power Appl.*, vol. 2, no. 1, pp. 42–48, 2008.
- [190] Y. Li, H. Lu, W. Qu, S. Sheng, and Z. Wang, “Sensorless Control of PMSM Based on Low Frequency Voltage Injection at Low Speeds and Standstill,” *Energy Convers. Congr. Expo.*, no. 6, pp. 781–787, 2013.
- [191] J. Lara, J. Xu, and A. Chandra, “Effects of Rotor Position Error in the Performance of Field-Oriented-Controlled PMSM Drives for Electric Vehicle Traction Applications,” *IEEE Trans. Ind. Electron.*, vol. 63, no. 8, pp. 4738–4751, 2016.
- [192] J. Alacoque, *Direct Field Control for Induction Machines and Synchronous Motors*. United Kingdom: A John Wiley & Sons, Ltd., 2013.
- [193] N. P. Quang and J. A. Dittrich, “Inverter Control with Space Vector Modulation,” in *Vector Control of Three-Phase AC Machines*, Springer-Verlag Berlin Heidelberg, 2015, pp. 17–59.
- [194] Brett Beauregard, “PID Library.” [Online]. Available: <https://playground.arduino.cc/Code/PIDLibrary>. [Accessed: 25-Jan-2018].
- [195] BRAODCOM, “HCPL-2530 Dual Channel, High Speed Optocouplers.” [Online]. Available: <http://www.mouser.com/ds/2/149/HCPL2531-189259.pdf>. [Accessed: 02-Feb-2017].
- [196] RAIRCHILD on Semiconductors, “Design and Application Guide of Bootstrap Circuit for High-Voltage Gate-Drive IC,” Application Note AN6076, 2008.

- [197] ALLDATASHEET.COM, “L6388 Datasheet (PDF).” [Online]. Available: <https://www.alldatasheet.com/datasheet-pdf/pdf/170605/STMICROELECTRONICS/L6388.html>. [Accessed: 03-Feb-2017].
- [198] DIGITAL CONTROLS, “British Encoder 755HS Incremental Blind Hollow Shaft Encoder.” [Online]. Available: <http://digitalcontrols.biz/british-encoder-755hs-incremental-blind-hollow-shaft-encoder>. [Accessed: 30-May-2018].
- [199] US Digital, “US DIGITAL PRODUCTS.” [Online]. Available: <https://www.usdigital.com/products>. [Accessed: 29-Apr-2016].
- [200] IS LEROY SOMER, “300 W Rotating Machines Test Bed Manual,” France, 2002.
- [201] Infineon Technologies AG, “Start-up Control Algorithm for Sensorless and Variable Load BLDC Control Using Variable Inductance Sensing Method,” Application Note, V1.0, Oct 2006, Germany.
- [202] Oskar Liang, “Check RAM Memory Usage In Arduino and Optimization.” [Online]. Available: <https://oscarliang.com/check-ram-memory-usage-arduino-optimization/>. [Accessed: 12-Dec-2017].
- [203] J. Bayle, *C Programming for Arduino*, 1st ed. Birmingham, UK: Packt Publishing Ltd, 2013.
- [204] ST TECHNOLOGY, “Transducer Display Interface [E301/2].” [Online]. Available: <http://www.wentec.com/rotarytorque/products/pdf/e301datasheet.pdf>. [Accessed: 08-Mar-2018].

Appendices

Appendix A, C-language codes for μ Cs programming

A.1 Codes of zero speed position estimation

The ports PD3, PD4, and PD5 (pins 3, 4, 5) were chosen as output ports to output the three high frequency injection pulses.

1) Definitions to initialize the estimation program

```
#include <EEPROM.h>      //call the embedded EEPROM library
#include <LiquidCrystal.h> //call liquid crystal library to display rotor position
#include <math.h>        //call the mathematic library
LiquidCrystal lcd(12,11,6,7,8,10); // initializing the liquid crystal

// create six voltage variables to be employed in prediction the rotor position
int VNB1, VNA1, VNB2, VNC2, VNC3, VNA3, RP; // RP for rotor position
recording

// create the binary variables to be used in formatting the sector number
int A, B, C, D, E, F, G, H, I, K, L, M, N, P, R;

// create the subsectors variables
int BB, AA, CC, HH, EE, DD, FF, RR, GG, KK, LL, MM, NN, PP, II, BBB,
AAA, CCC, HHH, EEE, DDD, FFF, RRR, GGG, KKK, LLL, MMM, NNN,
PPP, III;

// create other useful variables .....
int d; // index of sector variable
```

```

int VNC22, avr; // to be used in creating the average analogue value
float addr; // addr is to form the final memory address
unsigned int address; // address is to form the y-address
int sector; // sector is to form the x-address

// Temporary utilized variables .....
int q; int V; int i; float floatt; int total; int indicator; int avrg; int minimum_error;
int e;

// specify a space for all rotor positions 0 through 360
int position_array[361];

```

2) Initializing the microcontroller, μC

```

// Programming the  $\mu\text{C}$  ports, let ports 2,3,4, and 9 output ports
pinMode(3, OUTPUT); // this port is wired to gates of IGBTs "AH" and "BL"
pinMode(3,OUTPUT); // this port is wired to gates of IGBTs "BH" and "CL"
pinMode(4,OUTPUT); // this port is wired to gates of IGBTs "CH" and "AL"
pinMode(9,OUTPUT);

*****

// Sselect baud rate
Serial.begin(9600);

*****

// Initialize the used registers
total=0; indicator=0; e = 1;

*****

// Initialize the liquid crystal display LCD
lcd.begin(16,2);

*****

```

```

// modify the ADC resolution .....
// defines for setting and clearing register bits
#ifndef cbi
#define cbi(sfr, bit) (_SFR_BYTE(sfr) &= ~_BV(bit))
#endif
#ifndef sbi
#define sbi(sfr, bit) (_SFR_BYTE(sfr) |= _BV(bit))
#endif
// set prescale to 16
sbi(ADCSRA,ADPS2) ;
cbi(ADCSRA,ADPS1) ;
cbi(ADCSRA,ADPS0) ;

// printing layout .....
//Serial.println(" Rotor Position    d    S    VNC22    addr    addr
V    i");
//Serial.print(" -----    ---    ---    ---    ---    -----    -----
-----");

```

3) Running

```
===== START EXECUTION =====
```

```
===== STEP1 =====
```

```
// DETERMINE THE Y-ADDRESS, find the average analogue value, avrg, for VC22
```

```
// Read the motor terminal voltage six times and find the average
```

```
for (q=6 ; q > 0 ; q--){
```

```
digitalWrite(3,HIGH); // set the injected pulse to high state, 5V
```

```
delayMicroseconds(85);
```

```

VNC22 = analogRead(A1); // Read the motor terminal voltage

delayMicroseconds(50);

digitalWrite(3,LOW); // set the injected pulse to low state, 0V

delayMicroseconds(150);

avr[q]=VNC22;

    total = total + VNC22; // stack the voltage readings

    delay(1000);

}

    avrg=(total-avr[6])/5; // remove the last voltage and find the average

    total = 0; // reset the stack to be ready for next proces

// remove the outlier values, any reading 1V greater than the average is outlier

for (i=1 ; i<6 ; i++){

if ( (abs(avr[i] - avrg)) > 1) { avr[i] = avrg ; }

    total = total + avr[i];

}

avrg = total/5;

VNC22=avr[q] ; // final value for the y-address

*****

===== STEP2 =====

// DTERMINE THE X-ADDRESS

```

// through injecting 3 pulses and finding the corresponding sector from the responses

STEP (2-1): pulse generations, pulse injections, and response readings

// generate the first pulse through output port3 and inject in windings A and B

```
digitalWrite(3,HIGH); // set the 1st injected pulse to high state, 5V
```

```
delayMicroseconds(85);
```

```
VNB1 = analogRead(A5); // Read the motor terminal voltage, VNB1
```

```
delayMicroseconds(50);
```

```
digitalWrite(3,LOW); // set the injected pulse to low state, 0V
```

```
delayMicroseconds(85);
```

```
VNA1 = analogRead(A5); // Read the motor terminal voltage, VNA1
```

```
delayMicroseconds(33);
```

// generate the second pulse through output port4 and inject in windings B and C

```
digitalWrite(4,HIGH); // set the 1st injected pulse to high state, 5V
```

```
delayMicroseconds(84);
```

```
VNC2 = analogRead(A4); // Read the motor terminal voltage, VNC2
```

```
delayMicroseconds(45);
```

```
digitalWrite(4,LOW); // set the injected pulse to low state, 0V
```

```
delayMicroseconds(85);
```

```
VNB2 = analogRead(A4); // Read the motor terminal voltage, VNB2
```

```
delayMicroseconds(35);
```

```

// generate the third pulse through output port5 and inject in windings C and A

digitalWrite(5,HIGH); // set the 1st injected pulse to high state, 5V

delayMicroseconds(85);

VNA3 = analogRead(A3); // Read the motor terminal voltage, VNA3

delayMicroseconds(45);

digitalWrite(5,LOW); // set the injected pulse to low state, 0V

delayMicroseconds(85);

VNC3 = analogRead(A3); // Read the motor terminal voltage, VNC3

delayMicroseconds(35);

```

STEP (2-2): reset all the variables

```

A=0,B=0,C=0,D=0,E=0,F=0,G=0,H=0,I=0,K=0,L=0,M=0,N=0,P=0,R=0;BB=0;AA=0
;CC=0;HH=0;EE=0;DD=0;FF=0;RR=0;GG=0;II=0;BB=0; AA=0; CC=0; HH=0;
EE=0; DD=0; FF=0; RR=0; GG=0; KK=0; LL=0; MM=0; NN=0; PP=0; II=0;BBB=0;
AAA=0; CCC=0; HHH=0; EEE=0; DDD=0; FFF=0; RRR=0; GGG=0; KKK=0;
LLL=0; MMM=0; NNN=0; PPP=0; III=0;

```

STEP (2-3): voltage comparisons and set the variable values accordingly

```

if (100<(VNB1-VNA1)&& (VNB1-VNA1)<300){A=1;}

    if ((VNB1-VNA1)<100) {AA=1;}

    if ((VNB1-VNA1)>300) {AAA=1;}

if (100<(VNB1-VNC2)&& (VNB1-VNC2)<300){B=1;}

```

```
if ((VNB1-VNC2)<100) {BB=1;}

if ((VNB1-VNC2)>300) {BBB=1;}

if (100<(VNB1-VNB2) && (VNB1-VNB2)<300){C=1;}

if ((VNB1-VNB2)<100) {CC=1;}

if ((VNB1-VNB2)>300) {CCC=1;}

if (100<(VNB1-VNA3)&& (VNB1-VNA3)<300){D=1;}

if ((VNB1-VNA3)<100) {DD=1;}

if ((VNB1-VNA3)>300) {DDD=1;}

if (100<(VNB1-VNC3)&& (VNB1-VNC3)<300){E=1;}

if ((VNB1-VNC3)<100) {EE=1;}

if ((VNB1-VNC3)>300) {EEE=1;}

if (100<(VNA1-VNC2)&& (VNA1-VNC2)<300){F=1;}

if ((VNA1-VNC2)<100) {FF=1;}

if ((VNA1-VNC2)>300) {FFF=1;}

if (100<(VNA1-VNB2)&& (VNA1-VNB2)<300){G=1;}

if ((VNA1-VNB2)<100) {GG=1;}

if ((VNA1-VNB2)>300) {GGG=1;}

if (100<(VNA1-VNA3)&& (VNA1-VNA3)<300){H=1;}

if ((VNA1-VNA3)<100) {HH=1;}

if ((VNA1-VNA3)>300) {HHH=1;}
```

```

if (100<(VNA1-VNC3)&& (VNA1-VNC3)<300){I=1;}

    if ((VNA1-VNC3)<100) {II=1;}

    if ((VNA1-VNC3)>300) {III=1;}

if (100<(VNC2-VNB2)&& (VNC2-VNB2)<300){K=1;}

    if ((VNC2-VNB2)<100) {KK=1;}

    if ((VNC2-VNB2)>300) {KKK=1;}

if (100<(VNC2-VNA3)&& (VNC2-VNA3)<300){L=1;}

    if ((VNC2-VNA3)<100) {LL=1;}

    if ((VNC2-VNA3)>300) {LLL=1;}

if (100<(VNC2-VNC3)&& (VNC2-VNC3)<300){M=1;}

    if ((VNC2-VNC3)<100) {MM=1;}

    if ((VNC2-VNC3)>300) {MMM=1;}

if (VNB2>=VNA3){N=1;}

    if ((VNB2-VNA3)<100) {NN=1;}

if (VNB2>=VNC3){P=1;}

    if ((VNB2-VNC2)<100) {PP=1;}

if (VNA3>=VNC3){R=1;}

    if ((VNA3-VNC3)<100) {RR=1;}

```

STEP (2-4): calculate sector number, x-address

```
d= (15*A + 14*B + 13*C + 12*D + 11*E + 10*F + 9*G + 8*H + 7*I + 6*K + 5*L +
4*M + 3*N +2*P + R); //dmin=0 and dmax=120
```

```
// reformatting sector number
```

```
int  coloums[100]  =  {0,0,1,1,2,3,4,4,5,6,7,      8,9,10,11,12,6,13,14,15,16,17,
18,18,18,1,2,3,19,6,5,6,5, 8,9,10,4,7,13,11,7,9,12,15, 16,17,18,21,21,21,1,4,4,1,2,
                20,12,22,22,15,15,15,13,20,4,14,                10,5,8,13,1,15,19,19,19,20,16,
17,18,19,18,21,15,22,15,15,19,2, 1,3,20,20,31,6,1,6,4,11,4,4}; //this is corresponding
to values of d with the adding resistors and replacing the highest sector numbers
(31,30,29 ...) by lower ones.
```

```
// final value of sector number
```

```
sector = coloums[d]; x-address
```

```
// reformatting x-address
```

```
if  (sector  ==  0){sector=sector+24*(AA+AAA);};  if  (sector  ==
1){sector=sector+24*(BB+BBB);};  if  (sector  ==  2){sector=sector+24*(CC+CCC);} ;
if  (sector  ==  3){sector=sector+24*(DD+DDD);};
```

```
if  (sector  ==  4){sector=sector+24*(EE+EEE);};  if  (sector  ==
5){sector=sector+24*(FF+FFF);} ;  if  (sector  ==  6){sector=sector+24*(GG+GGG);} ;  if
(sector  ==  7){sector=sector+24*(HH+HHH);};
```

```
if  (sector  ==  8){sector=sector+24*(II+III);};  if  (sector  ==
9){sector=sector+24*(KK+KKK);};  if  (sector  ==  10){sector=sector+24*(LL+LLL);} ;
if  (sector  ==  11){sector=sector+24*(MM+MMM);};
```

```

if (sector == 12){sector=sector+24*NN;}; if (sector == 13){sector=sector+24*PP;}; if
(sector == 14) {sector=sector+24*RR;}; if (sector == 15)
{sector=sector+24*max(AA,BB);};

```

```

if (sector == 16){sector=sector+24*max(AA,CC);}; if (sector ==
17){sector=sector+24*max(PP,DD);}; if (sector == 18)
{sector=sector+24*max(RR,EE);}; if (sector == 19){sector=sector+24*max(BB,CC);}

```

```

if (sector == 20){sector=sector+24*max(BB,DD);}; if (sector ==
21){sector=sector+24*max(FF,GG);}; if (sector ==
22){sector=sector+24*max(HH,II);}; if (sector ==
23){sector=sector+24*max(KK,LL);}

```

STEP (2-5): calculate final memory address

```
// combine both portions of memory address
```

```
floatt= VNC22;
```

```
addr = sector + floatt/1000;
```

```
address = 1000*addr; // final address value
```

```
*****
```

===== STEP3 =====

===== MEMORY, LOOK-UP TABLE, LOADING =====

// create address memory matrix

int position_array[360] = {

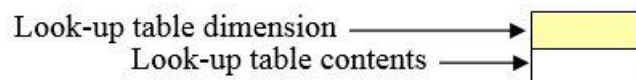
31366	31394	31427	31467	5502	5532	5555	5582	30606	30633
1	2	3	4	5	6	7	8	9	10
33655	33670	33672	42668	40673	40675	40671	40661	40640	12620
11	12	13	14	15	16	17	18	19	20
12598	12572	42548	42521	43492	30462	25429	25384	25340	25299
21	22	23	24	25	26	27	28	29	30
25260	32234	27223	27201	33175	33163	33171	33194	7210	7216
31	32	33	34	35	36	37	38	39	40
7225	7263	26306	14345	42377	42402	42420	31466	5524	5580
41	42	43	44	45	46	47	48	49	50
5622	5631	30632	40654	33689	42728	42746	42752	42756	40766
51	52	53	54	55	56	57	58	59	60
40790	40803	40798	40775	40760	45771	45770	45750	45707	43668
61	62	63	64	65	66	67	68	69	70
43615	43571	43524	30473	40431	40396	5368	5332	5303	27274
71	72	73	74	75	76	77	78	79	80

33246	33226	7218	7220	7227	7237	30253	42273	42296	42314
81	82	83	84	85	86	87	88	89	90
31344	31377	31415	5451	5495	5525	5556	5581	30612	30633
91	92	93	94	95	96	97	98	99	100
40655	33670	42680	42679	42687	40682	40672	40658	40644	30633
101	102	103	104	105	106	107	108	109	110
30615	12593	42562	42530	42512	42462	25414	25371	25323	10285
111	112	114	114	115	116	117	118	119	120
5236	32219	32204	27181	33152	33142	33151	33182	34203	7216
121	122	123	124	125	126	127	128	129	130
7245	30284	42336	42381	42316	31448	31467	31498	5538	5600
131	132	133	134	135	136	137	138	139	140
5648	5660	30652	30650	40667	42701	42720	42739	42740	42742
141	142	143	144	145	146	147	148	149	150
40763	40797	40813	40813	40785	40760	40763	45760	45740	39690
151	152	153	154	155	156	157	158	159	160
43635	43600	43547	7499	25461	25431	40395	5371	5343	27313
161	162	163	164	165	166	167	168	169	170
27290	33271	33254	33251	7254	7262	7279	30280	42294	42316
171	172	173	174	175	176	177	178	179	180

42339	31358	31384	31413	31444	5478	5512	5530	5563	5588
181	182	183	184	185	186	187	188	189	190
30607	30629	30648	33657	33662	42668	40669	40659	40647	30631
191	192	193	194	195	196	197	198	199	200
30618	12598	12574	42547	42517	43488	43448	25405	25361	25307
201	202	203	204	205	206	207	208	209	210
10260	10219	5185	27169	27154	33132	33109	33103	33126	33157
211	212	213	214	215	216	217	218	219	220
7176	7184	7206	30236	30280	42319	42358	42376	42392	31429
221	222	223	224	225	226	227	228	229	230
5485	5534	5571	5584	30583	30600	30639	42680	42710	42728
231	232	233	234	235	236	237	238	239	240
42741	40759	40778	40796	40791	40768	40755	45750	45744	45712
241	242	243	244	245	246	247	248	249	250
43667	43616	43574	43523	32477	40432	40394	5365	5331	27297
251	252	253	254	255	256	257	258	259	260
27270	33251	33234	34224	7223	7231	7236	30247	42259	42282
261	262	263	264	265	266	267	268	269	270
42303	42323	31354	31385	31321	5460	5496	5534	5560	5591

271	272	273	274	275	276	277	278	279	280
30621	40652	33674	33690	42696	42704	40703	40696	40678	40655
281	282	283	284	285	286	287	288	289	290
30630	12607	12579	42545	42511	42471	30438	25402	25360	25311
291	292	293	294	295	296	297	298	299	300
25263	9223	37201	32183	27165	33137	33117	33119	33139	33160
301	302	303	304	305	306	307	308	309	310
7168	7179	7207	30246	30287	42333	42365	42386	31418	5480
311	312	313	314	315	316	317	318	319	320
5535	5577	5597	30607	30630	33670	42706	42727	42732	42738
321	322	323	324	325	326	327	328	329	330
40750	40760	40764	40743	40720	40705	46700	39678	43651	43610
331	332	333	334	335	336	337	338	339	340
43566	43520	43380	25443	25414	25385	40359	5333	5311	5287
341	342	343	344	345	346	347	348	349	350
27257	33239	33229	7227	7234	7240	30253	42268	42286	42310
351	352	353	354	355	356	357	358	359	360

} ; // THE COLOURED MEMORY CELLS ARE THE ERRORS IN ESTIMATION PROCESS



===== STEP4 =====

===== DISPLAY ROTOR POSITION =====

```
// define permitted address deviation=0.4 otherwise display FAILURE
```

```
V= address;
```

```
for ( i = 0 ; i < 361 ; i++ ) {
```

```
  if ( (abs(V - position_array[i]))<4){RP = i ; i = 361 ;
```

```
    lcd.clear();
```

```
    lcd.setCursor(0,0);
```

```
    lcd.print("RP = ");
```

```
    lcd.setCursor(5,0);
```

```
    lcd.print(RP);
```

```
  }
```

```
else
```

```
if ( (abs(V - position_array[i]))>=4 && (abs(V - position_array[i])<=6)){RP = i ; i = 361 ;
```

```
  addr=address;
```

```
  lcd.clear();
```

```
  lcd.setCursor(0,0);
```

```
  lcd.print("RP= ");
```

```
  lcd.setCursor(3,1);
```

```
  lcd.print(RP+0.2);
```

```
    }  
  
    else  
  
if ( (abs(V - position_array[i]))>6 && (abs(V - position_array[i])<=8)){RP = i; i = 361  
;  
  
addr=address;  
  
lcd.clear();  
  
lcd.setCursor(0,0);  
  
lcd.print("RP= ");  
  
lcd.setCursor(3,1);  
  
lcd.print(RP+0.4);  
  
    }  
  
    else{  
  
    lcd.clear();  
  
    lcd.print("FAILURE");}  
  
}
```

===== **STEP5** =====

===== PRINT SUMMARY REPORT =====

```

Serial.print(" ");Serial.print(sector); Serial.print(" "); Serial.println(VNC22);

Serial.println(" "); Serial.print(" ");Serial.println(address); Serial.println(" ");
Serial.println(" ");Serial.print(" ");Serial.print(VNC22); Serial.print(" ");
Serial.print(VNB1); Serial.print(" ");Serial.print(VNA1); Serial.print(" ");
Serial.print(VNC2);Serial.print(" ");Serial.print(VNB2); Serial.print(" ");
Serial.print(VNA3);Serial.print(" ");Serial.print(VNC3); Serial.println(" ");
Serial.println(" "); Serial.println(" "); Serial.print(" "); Serial.print(d); Serial.print("
"); Serial.print(A); Serial.print(" ");Serial.print(B); Serial.print(" "); Serial.print(C);
Serial.print(" "); Serial.print(D); Serial.print(" "); Serial.print(E); Serial.print(" ");
Serial.print(F); Serial.print(" "); Serial.print(G); Serial.print("
");Serial.print(H);Serial.print(" ");Serial.print(I); Serial.print(" "); Serial.print(K);
Serial.print(" "); Serial.print(L); Serial.print(" "); Serial.print(M); Serial.print("
");Serial.print(N);Serial.print(" ");Serial.print(P);Serial.print(" "); Serial.println(R);
Serial.println(" "); Serial.println(" "); Serial.print(" "); Serial.println(address);
Serial.print(" d= ");Serial.println(d);

```

===== **END ZERO SPEED C-LANGUAGE PROGRAMMING** =====

A.2 Codes for low speed running and RPE

1 SV sequence generation, MEMORY WRITING CYCLE

// This software is built and executed by the master microcontroller. It implements the space vector pulse width modulation

===== STEP1 =====

===== INITIALIZATIONS =====

```
#include <math.h>          // call the mathematic library
```

```
#include <EEPROM.h>       // call the mathematic library
```

```
// define types the variables
```

```
float  m ,priormin priorVtri , Vqs , Vds , Vtri , Ts,T1 , T2 , T0,Vm, pi2fo,tss, Vdc , pi2
, pi , ts , tht , a , Tss ;
```

```
int  mS1 , mS2 , mS3 , mS4 , mS5 , mS6,T11,T22,T00,Thetta ,Ns , ns , fo, fs , c , i , b ,
j , SA , SB , SC;
```

```
byte  S ,Stg ;
```

```
// set look-up tables
```

```
byte  Sn[36]={1,1,1,1,1,1,  2,2,2,2,2,2,  3,3,3,3,3,3,  4,4,4,4,4,4,  5,5,5,5,5,5,
6,6,6,6,6,6};
```

```
float Scos[7] = { 1.0 , 0.5 , -0.5 , -1 , -0.5 , 0.5 , 1.0};
```

```
float Ssin[7] = { 0 , 0.866 , 0.866 , 0 , -0.866 , -0.866 , 0};
```

```

byte a1[6]={1,1,0,0,0,1}; byte a2[6]={0,1,1,1,0,0}; byte a3[6]={0,0,0,1,1,1};

byte b1[6]={1,0,0,0,1,1}; byte b2[6]={1,1,1,0,0,0}; byte b3[6]={0,0,1,1,1,0};

// define and initialize variable values

Vdc = 48; // Set the dc link voltage, 48V for M200 motor, 150V for Mac2n motor

Ns = 960, // number of samples

fo =25; // output frequency , speed=120*fo/p rpm

pi2=6.2832; c=0; pi2fo=pi2*fo;

fs = 3000; // Hz sampling frequency

Ts =1.0/fs; //sec samplin period

tss=1.0/(Ns-1); // sec tim sub-division

Vm=((1/sqrt(3))*Vdc); // max of output voltage and (sqrt(3))/2*(2/3)

m=0.9;      // define the modulation index

mS1=1;mS2=1;mS3=1;mS4=1;mS5=1;mS6=1;

// define baud rate

Serial.begin(115200);

// ensure to reset all EEPRM cells

for (i=0 ; i<Ns ; i=i+1){

EEPROM.write(i,0);

}

```

===== STEP2 =====

===== START SV SEQUENCE GENERATION =====

// step 2-1, start rotating in SV // % % % % % % % % % % % % % % % % % %

for (i=0 ; i<Ns ; i=i+1){

xxx:

a=1.0*i*pi2/(Ns-1); // rotate through the SV space

step 2-1-1, eliminate the SV counting near the boundaries *****

if ((360.0-(180.0*a/PI))<11.0 && i<Ns){i=i+1;goto xxx;}

if ((180.0*a/PI)<11.0){i=i+1;goto xxx;}

if ((180.0*a/PI)>50 && (180.0*a/PI)< 72){i=i+1;goto xxx;}

if ((180.0*a/PI)>108 && (180.0*a/PI)< 132){i=i+1;goto xxx;}

if ((180.0*a/PI)>170 && (180.0*a/PI)< 192){i=i+1;goto xxx;}

if ((180.0*a/PI)>227 && (180.0*a/PI)< 252){i=i+1;goto xxx;}

if ((180.0*a/PI)>288 && (180.0*a/PI)< 311){i=i+1;goto xxx;}

//*****

step 2-1-2, define $\alpha\beta$ -frame voltages

Vm=m*((1/sqrt(3))*Vdc); // define the peak of the motor terminal voltage

Valpha=Vm*cos(a); Vbeta=Vm*sin(a);

step 2-1-3, define sector number

```
b=(a*179.9999/pi)/10; S=Sn[b]; Stg=S-1;
```

step 2-1-4, use volt sec balance to calculate the active vectors timing *****

```
T1 = (Ts/(sin(pi/3)*Vdc))*( Valpha *Ssin[S] - Vbeta *Scos[S]);/(sin(pi/3)*Vdc)
```

```
T2 = (Ts/(sin(pi/3)*Vdc))*(- Valpha *Ssin[Stg] + Vbeta *Scos[Stg]);/(sin(pi/3)*Vdc)
```

```
T0 = (Ts-T1-T2);
```

```
T00 = (1000000*T0/2)/2;T11=(1000000*T1)/2;T22=(1000000*T2)/2;// microseconds
```

```
if(T11<=0.5){T11=T11+1;} // avoid small IGBT turning ON
```

```
if(T22<=0.5){T22=T22+1;} // avoid small IGBT turning ON
```

```
// *****
```

step 2-1-5, start defining SV sequences, SA, SB, and SC and store in EEPROM

```
// sector No.1, 0< angle <= 60 =====
```

```
if (S==1 | S==0){
```

```
switch(mS1){
```

```
case 1:
```

```
EEPROM.write(i+Ns,0);EEPROM.write(i+2*Ns,0);EEPROM.write(i+3*Ns,0);
```

```
;EEPROM.write(i,T00);
```

```
break;
```

```
case 2:
```

```
EEPROM.write(i+Ns,1);EEPROM.write(i+2*Ns,0);EEPROM.write(i+3*Ns,0);
```

```
EEPROM.write(i,T11);
```

```
break;
```

```
case 3:
```

```
EEPROM.write(i+Ns,1);EEPROM.write(i+2*Ns,1);EEPROM.write(i+3*Ns,0);
```

```
EEPROM.write(i,T22);
```

```
break;
```

```
case 4:
```

```
EEPROM.write(i+Ns,1);EEPROM.write(i+2*Ns,1);EEPROM.write(i+3*Ns,1);
```

```
EEPROM.write(i,T00);
```

```
break;
```

```
case 5:
```

```
EEPROM.write(i+Ns,1);EEPROM.write(i+2*Ns,1);EEPROM.write(i+3*Ns,1);
```

```
EEPROM.write(i,T00);
```

```
break;
```

```
case 6:
```

```
EEPROM.write(i+Ns,1);EEPROM.write(i+2*Ns,1);EEPROM.write(i+3*Ns,0);
```

```
EEPROM.write(i,T22);
```

```
break;
```

```
case 7:
```

```
EEPROM.write(i+Ns,1);EEPROM.write(i+2*Ns,0);EEPROM.write(i+3*Ns,0);
```

```

        EEPROM.write(i,T11);

    break;

case 8:

        EEPROM.write(i+Ns,0);EEPROM.write(i+2*Ns,0);EEPROM.write(i+3*Ns,0);

        EEPROM.write(i,T00);

    break;

}

mS1=mS1+1;

if (mS1==9){mS1=1;}

}

// =====

// sector No.2, 60< angle <= 120  =====

if (S==2){

    switch(mS2){

        case 1:

            EEPROM.write(i+Ns,0);EEPROM.write(i+2*Ns,0);EEPROM.write(i+3*Ns,0);

            EEPROM.write(i,T00);

            break;

        case 2:

```

```
EEPROM.write(i+Ns,0);EEPROM.write(i+2*Ns,1);EEPROM.write(i+3*Ns,0);
```

```
EEPROM.write(i,T22);
```

```
break;
```

```
case 3:
```

```
EEPROM.write(i+Ns,1);EEPROM.write(i+2*Ns,1);EEPROM.write(i+3*Ns,0);
```

```
EEPROM.write(i,T11);
```

```
break;
```

```
case 4:
```

```
EEPROM.write(i+Ns,1);EEPROM.write(i+2*Ns,1);EEPROM.write(i+3*Ns,1);
```

```
EEPROM.write(i,T00);
```

```
break;
```

```
case 5:
```

```
EEPROM.write(i+Ns,1);EEPROM.write(i+2*Ns,1);EEPROM.write(i+3*Ns,1);
```

```
EEPROM.write(i,T00);
```

```
break;
```

```
case 6:
```

```
EEPROM.write(i+Ns,1);EEPROM.write(i+2*Ns,1);EEPROM.write(i+3*Ns,0);
```

```
EEPROM.write(i,T11);
```

```
break;
```

```
case 7:
```

```
EEPROM.write(i+Ns,0);EEPROM.write(i+2*Ns,1);EEPROM.write(i+3*Ns,0);
```

```

        EEPROM.write(i,T22);

    break;

case 8:

        EEPROM.write(i+Ns,0);EEPROM.write(i+2*Ns,0);EEPROM.write(i+3*Ns,0);

        EEPROM.write(i,T00);

    break;

}

mS2=mS2+1;

if (mS2==9){mS2=1;}

}

// =====

// sector No.3, 120< angle <= 180  =====

if (S==3){

    switch(mS3){

        case 1:

            EEPROM.write(i+Ns,0);EEPROM.write(i+2*Ns,0);EEPROM.write(i+3*Ns,0);

            EEPROM.write(i,T00);

            break;

        case 2:

```

```
EEPROM.write(i+Ns,0);EEPROM.write(i+2*Ns,1);EEPROM.write(i+3*Ns,0);
```

```
EEPROM.write(i,T11);
```

```
break;
```

```
case 3:
```

```
EEPROM.write(i+Ns,0);EEPROM.write(i+2*Ns,1);EEPROM.write(i+3*Ns,1);
```

```
EEPROM.write(i,T22);
```

```
break;
```

```
case 4:
```

```
EEPROM.write(i+Ns,1);EEPROM.write(i+2*Ns,1);EEPROM.write(i+3*Ns,1);
```

```
EEPROM.write(i,T00);
```

```
break;
```

```
case 5:
```

```
EEPROM.write(i+Ns,1);EEPROM.write(i+2*Ns,1);EEPROM.write(i+3*Ns,1);
```

```
EEPROM.write(i,T00);
```

```
break;
```

```
case 6:
```

```
EEPROM.write(i+Ns,0);EEPROM.write(i+2*Ns,1);EEPROM.write(i+3*Ns,1);
```

```
EEPROM.write(i,T22);
```

```
break;
```

```
case 7:
```

```
EEPROM.write(i+Ns,0);EEPROM.write(i+2*Ns,1);EEPROM.write(i+3*Ns,0);
```

```

        EEPROM.write(i,T11);

    break;

case 8:

        EEPROM.write(i+Ns,0);EEPROM.write(i+2*Ns,0);EEPROM.write(i+3*Ns,0);

        EEPROM.write(i,T00);

    break;

}

mS3=mS3+1;

if (mS3==9){mS3=1;}

}

// =====

// sector No.4, 180< angle <= 240 =====

if (S==4){

    switch(mS4){

        case 1:

            EEPROM.write(i+Ns,0);EEPROM.write(i+2*Ns,0);EEPROM.write(i+3*Ns,0);

            EEPROM.write(i,T00);

            break;

        case 2:

            EEPROM.write(i+Ns,0);EEPROM.write(i+2*Ns,0);EEPROM.write(i+3*Ns,1);

            EEPROM.write(i,T22);

```

```
break;
```

```
case 3:
```

```
EEPROM.write(i+Ns,0);EEPROM.write(i+2*Ns,1);EEPROM.write(i+3*Ns,1);
```

```
EEPROM.write(i,T11);
```

```
break;
```

```
case 4:
```

```
EEPROM.write(i+Ns,1);EEPROM.write(i+2*Ns,1);EEPROM.write(i+3*Ns,1);
```

```
EEPROM.write(i,T00);
```

```
break;
```

```
case 5:
```

```
EEPROM.write(i+Ns,1);EEPROM.write(i+2*Ns,1);EEPROM.write(i+3*Ns,1);
```

```
EEPROM.write(i,T00);
```

```
break;
```

```
case 6:
```

```
EEPROM.write(i+Ns,0);EEPROM.write(i+2*Ns,1);EEPROM.write(i+3*Ns,1);
```

```
EEPROM.write(i,T11);
```

```
break;
```

```
case 7:
```

```
EEPROM.write(i+Ns,0);EEPROM.write(i+2*Ns,0);EEPROM.write(i+3*Ns,1);
```

```
EEPROM.write(i,T22);
```

```
break;
```

```

case 8:

    EEPROM.write(i+Ns,0);EEPROM.write(i+2*Ns,0);EEPROM.write(i+3*Ns,0);

    EEPROM.write(i,T00);

    break;

}

mS4=mS4+1;

if (mS4==9){mS4=1;}

}

// =====

// sector No.5, 240< angle <= 300  =====

if (S==5){

    switch(mS5){

        case 1:

            EEPROM.write(i+Ns,0);EEPROM.write(i+2*Ns,0);EEPROM.write(i+3*Ns,0);

            EEPROM.write(i,T00);

            break;

        case 2:

            EEPROM.write(i+Ns,0);EEPROM.write(i+2*Ns,0);EEPROM.write(i+3*Ns,1);

            EEPROM.write(i,T11);

            break;

```

case 3:

```
EEPROM.write(i+Ns,1);EEPROM.write(i+2*Ns,0);EEPROM.write(i+3*Ns,1);
```

```
EEPROM.write(i,T22);
```

```
break;
```

case 4:

```
EEPROM.write(i+Ns,1);EEPROM.write(i+2*Ns,1);EEPROM.write(i+3*Ns,1);
```

```
EEPROM.write(i,T00);
```

```
break;
```

case 5:

```
EEPROM.write(i+Ns,1);EEPROM.write(i+2*Ns,1);EEPROM.write(i+3*Ns,1);
```

```
EEPROM.write(i,T00);
```

```
break;
```

case 6:

```
EEPROM.write(i+Ns,1);EEPROM.write(i+2*Ns,0);EEPROM.write(i+3*Ns,1);
```

```
EEPROM.write(i,T22);
```

```
break;
```

case 7:

```
EEPROM.write(i+Ns,0);EEPROM.write(i+2*Ns,0);EEPROM.write(i+3*Ns,1);
```

```
EEPROM.write(i,T11);
```

```
break;
```

case 8:

```

EEPROM.write(i+Ns,0);EEPROM.write(i+2*Ns,0);EEPROM.write(i+3*Ns,0);

EEPROM.write(i,T00);

break;

}

mS5=mS5+1;

if (mS5==9){mS5=1;}

}

// =====

// sector No.6, 300< angle <= 360  =====

if (S==6){

switch(mS6){

case 1:

EEPROM.write(i+Ns,0);EEPROM.write(i+2*Ns,0);EEPROM.write(i+3*Ns,0);

EEPROM.write(i,T00);

break;

case 2:

EEPROM.write(i+Ns,1);EEPROM.write(i+2*Ns,0);EEPROM.write(i+3*Ns,0);

EEPROM.write(i,T22);

break;

case 3:

```

```
EEPROM.write(i+Ns,1);EEPROM.write(i+2*Ns,0);EEPROM.write(i+3*Ns,1);
```

```
EEPROM.write(i,T11);
```

```
break;
```

```
case 4:
```

```
EEPROM.write(i+Ns,1);EEPROM.write(i+2*Ns,1);EEPROM.write(i+3*Ns,1);
```

```
EEPROM.write(i,T00);
```

```
break;
```

```
case 5:
```

```
EEPROM.write(i+Ns,1);EEPROM.write(i+2*Ns,1);EEPROM.write(i+3*Ns,1);
```

```
EEPROM.write(i,T00);
```

```
break;
```

```
case 6:
```

```
EEPROM.write(i+Ns,1);EEPROM.write(i+2*Ns,0);EEPROM.write(i+3*Ns,1);
```

```
EEPROM.write(i,T11);
```

```
break;
```

```
case 7:
```

```
EEPROM.write(i+Ns,1);EEPROM.write(i+2*Ns,0);EEPROM.write(i+3*Ns,0);
```

```
EEPROM.write(i,T22);
```

```
break;
```

```
case 8:
```

```
EEPROM.write(i+Ns,0);EEPROM.write(i+2*Ns,0);EEPROM.write(i+3*Ns,0);
```

```

EEPROM.write(i,T00);

break;

}

mS6=mS6+1;

if (mS6==9){mS6=1;}

}

}

//

=====

// %%%%%%%%%%% END WRITING ROUTINE %%%%%%%%%%%

```

2 SV sequence executing and motor running, READING CYCLE

This software is built and executed by the master micro controller, ATmega2560 to control running of the under test motors.

```

===== STEP1 =====

===== INITIALIZATIONS =====

#include <EEPROM.h>      // call EEPROM library

Step1-1: define the variable types *****

int i , b,z,Ns,c,v;

byte j ,k, q , SA , SB , SC , start; // start determines the startup period

```

```
unsigned int cc, wait;
```

```
float m ,Ts;
```

```
// *****
```

Step 1-2: define the output ports through port manipulation

```
DDRA = B11111111; // pins 22 through 27, 1/output, 0/input
```

```
Serial.begin(115200); // define baud rate
```

Step 1-3: define variable values

```
Ns=960;
```

```
start=20; // start determines the startup period
```

```
b=0;
```

```
cc=500; // define startup period
```

```
*****
```

```
===== STEP2 =====
```

```
===== START PROGRAM RUNNING =====
```

```
v=analogRead(A2); // read the setting speed
```

```
yyy:
```

```
if (analogRead(A7)<20){goto yyy;} // check if Vdc is turned ON
```

```
delay(4000); // wait 4 seconds after Vdc turning ON
```

Step 2-1: start execution loop

```
for (i=35 ; i<930 ; i=i+1){ // start from counting state 35 to avoid boundaries
```

```
wait=EEPROM.read(i); // read T0, T1, or T2
```

```
// read status of firing commands of the upper IGBTs SA, SB, and SC from EEPROM
and transfer the statuses to the pins of the output port
```

```
//
```

PINS PORTA	X	27	26	25	24	23	22
	X	S _{CL}	S _{BL}	S _{AL}	S _{CH}	S _{BH}	S _{AH}

```
SA =EEPROM.read(i+Ns); SB =EEPROM.read(i+2*Ns); SC =EEPROM.read(i+3*Ns);
```

```
if (SA ==0 && SB ==0 && SC ==0){PORTA = B0111000;}
```

```
if (SA ==1 && SB ==0 && SC ==0){PORTA = B0110001;}
```

```
if (SA ==0 && SB ==1 && SC ==0){PORTA = B0101010;}
```

```
if (SA ==1 && SB ==1 && SC ==0){PORTA = B0100011;}
```

```
if (SA ==0 && SB ==0 && SC ==1){PORTA = B0011100;}
```

```
if (SA ==1 && SB ==0 && SC ==1){PORTA = B0010101;}
```

```
if (SA ==0 && SB ==1 && SC ==1){PORTA = B0001110;}
```

```
if (SA ==1 && SB ==1 && SC ==1){PORTA = B0000111;}
```

```
if (wait<20){wait=20;}, // 20 microsecond is the minimum timing T0, T1, or T2
```

```

delayMicroseconds(wait+cc-20+v); // cc startup timing, 20 to subtract execution time

if (i==133){i=191;}

if (i==287){i=351;}

if (i==452){i=511;}

if (i==604){i=671;}

if (i==767){i=828;}

}

v=analogRead(A2); // check the setting speed

cc=cc-10; // step down startuo period by 10

cc=min(cc,cc+10); // check if cc=0

if (analogRead(A7)<20){ setup(); } // if Vdc turned OFF go to waiting state

}

===== END ===== END =====

```

3 Rotor position estimation at low speed running

This software is built and executed by the slave microcontroller, ATmega328 to estimate the rotor position of the under test motors at low speed running. The final graph representation is observed at the output of DAC2 in the test bed.

===== **STEP1** =====

===== INITIALIZATIONS =====

```
#include <math.h> // call the mathematic library
```

```
#include <ResponsiveAnalogRead.h> // increase the sensitivity of analogue reading

ResponsiveAnalogRead analog(A3, true); // apply sensitivity increasing on input A3

// define the variables

float positionn,theta, prior_positionn,prior_theta;

int c , x;

byte y ,n;

// define variable values

Serial.begin(115200); // define baud rate

prior_theta=0;

prior_positionn=1000.0;

// define ports B and D as output ports

DDRD = B11111111; // sets Arduino pins 0 to 7 as outputs

DDRB = B11111111; // sets Arduino pins 8 to 13 as outputs

n=0;

}
```

```
*****
```

===== STEP2 =====

===== START PPSITION ESTIMATION =====

Step2-1; find the position estimation in digital form

xxx:

if (analogRead(A4)<10){goto xxx;}, check if Vdc is ON

delay(4000); // wait 4 seconds

positionn=(5.0*(analogRead(A3))/1023); // read value of sine waveform

positionn=constrain(positionn,0.0,1.66); // limit sine min=0V and sine max=1.66V

theta=(asin((positionn-0.83)/0.83))*180.0/PI; // normalize sine to -0.83V and +0.83V

//and find prior position estimation

if (prior_positionn >= positionn) // detect negative slope

{theta=180-theta;} // modify prior position estimation accordingly

if (positionn<0.83 && prior_positionn < positionn) // detect positive slope

{theta=theta+360.0;} // modify prior position estimation accordingly

// Step2-2, move the digital form of the position estimation to DAC2

if (theta>10.0 && theta < prior_theta){theta = prior_theta;}

prior_positionn=positionn;

if (prior_theta > 350 && theta < 10){n=n+1;} // detect transition from 360 to 0

```

prior_theta = theta;

theta=theta/4;

if (n==4){n=0;}

x=90*n+theta; // convert the estimation to straight forward

//Serial.println(x);// this command and the next three are only active in case of reading
the position data

//Serial.print("  ");

//Serial.println(millis()-c);

//goto yyy;

// move the estimation to DAC2

if (x>63 && x<128){x=x-64;y=1;}

if (x>127 && x<192){x=x-128;y=2;}

if (x>191 && x<256){x=x-192;y=3;}

if (x>255 && x<320){x=x-256;y=4;}

if (x>319){x=x-320;y=5;}

x=x<<2; // shift right twice

PORTD = x;

PORTB = y;

y=0;

```

```
}

```

```
***** END ***** END *****
```

4 Speed estimation

```
===== STEP1 =====
```

```
===== INITIALISATION =====
```

```
// preparing the PID statement
```

```
#include <PID_v1.h>           // call the PID library
```

```
double Setpoint, Input, Output; // determine type of PID variables
```

```
// define the PID statement with Kp=1 and Ki=2 primarily
```

```
PID (&Input, &Output, &Setpoint,1.2,0, DIRECT);
```

```
// define the program variable types
```

```
int setting_speed, Thetta, theta, x, y;
```

```
float k1; float k2, float initialSpeed, float Speed, pi, T;
```

```
// define the variables initial values
```

```
float voltage = 0;
```

```
float LastVoltage = 0;
```

```

float rate = 0;

unsigned long lastTime = 0;

unsigned long dt = 100; // dt in milliseconds

Serial.begin(2000000); // define baud rate

initialSpeed = 0;

*****

===== STEP2 =====

===== START SPEED ESTIMATION =====

myPID.SetMode(AUTOMATIC);

setting_speed= analogRead(A1); // read the value of desired speed

// range the speed from 0 to 255 instead of 0 to 1023

setting_speed= map (setting_speed, 0,1023,0,255);

Setpoint = setting_speed;

if (millis() - lastTime >= dt) // wait for dt milliseconds

{

    lastTime = millis();

    int sensorValue = analogRead(A2);

    voltage = sensorValue * (5.0 / 1023.0); // this line changed !!

rate = (voltage-LastVoltage);

```

```
Speed = ((1000*rate/dt)*(360/5)/(360/60)); // (360/5) is to change dV/dt from  
volt/Sec to degree/Sec and (360/60) is to change degree/Sec to rpm
```

```
if ( Speed <= 10 ){
```

```
    Speed = setting_speed; // initialSpeed; }
```

```
else{
```

```
    initialSpeed = Speed; }
```

```
LastVoltage = voltage;
```

```
delay= myPID.Compute(); // give output of PID varying numerically from 0 to 255
```

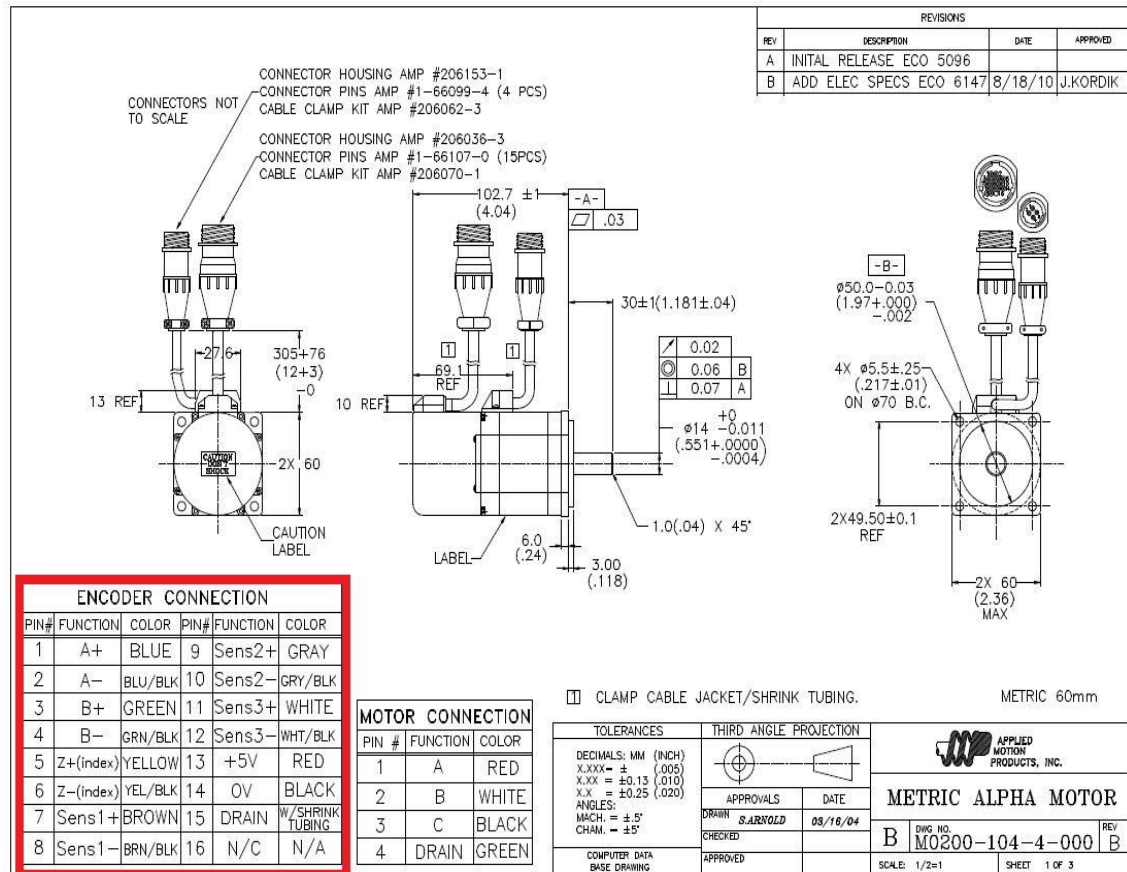
```
v= delay
```

```
}// back to monitoring and measuring speed
```

```
***** END *****
```

Appendix B, References for the main peripherals

B.1 Encoder inside the motor M0200



B.2 Incremental encoder 755HS

This peripheral is an incremental encoders which is separately supplied to be coupled with a motor shaft to provide square waveforms of frequencies directly proportional to rotor speed. Next the datasheets for this peripheral as it are published by the manufacturer.



Model 755HS 38mm High Precision Hollow Bore Encoder

Incremental Thru-Bore & Motor Mount Encoders



Features

- Miniature Size (38.1mm Diameter)
- Up to 30,000 Pulses per Revolution
- Hollow Bore sizes up to 14 mm
- Flex Mounting
- High Temperature Option

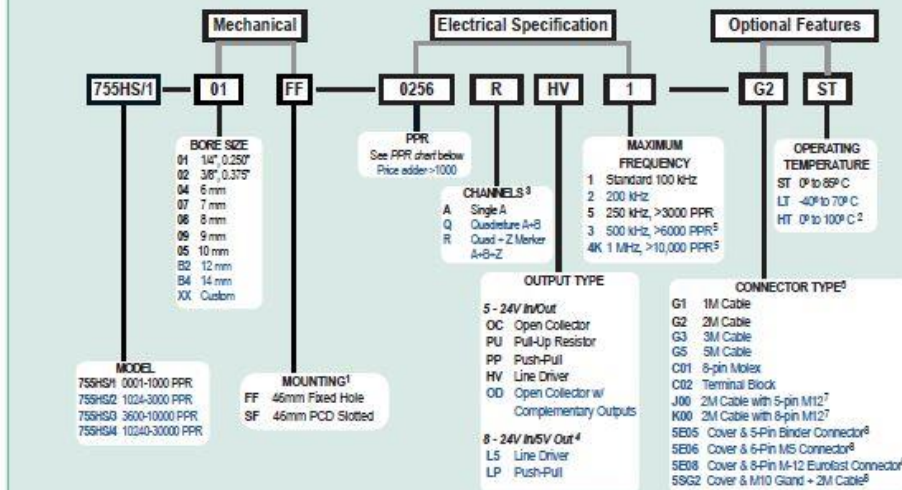
The Model 755HS is ideal for applications requiring a small, high precision, high performance encoder. Approximately 38.1mm in diameter and 38.1mm long, it will fit where many encoders cannot. All metal construction and shielded ball bearings provide years of trouble-free use. A variety of blind hollow bore sizes are available. Large bores allow for shafts up to 14 mm. Attaching directly to a motor is quick and simple with the innovative flex mount. This industry standard mount eliminates couplings and increases reliability, while reducing overall length and cost. Where critical alignment is required, a Slotted Flex Mount (SF) is available. A perfect replacement encoder where high reliability is required.

Common Applications

Robotics, Assembly Machines, Motor-Mounted Feedback, Phototypesetters, Printers & Digital Plotters, Elevator Controls, Medical Diagnostic Equipment

Model 755HS Ordering Guide

Blue type indicates price adder options. Not all configuration combinations may be available. Contact Customer Service for details.



Model 755HS PPR Options

0001*	0002*	0004*	0005*	0005*	0007*	0008*	0010*	0011*
0012*	0014*	0020	0021*	0024*	0025*	0028*	0030*	0032*
0033*	0034*	0035*	0038*	0040*	0042*	0045*	0050*	0060
0064*	0100	0120	0125	0128*	0144*	0150*	0160*	0192*
0200	0240*	0250	0254*	0256*	0300	0333*	0360	0400
0500	0512	0600	0625*	0635	0665*	0720	0768*	0800
0889	0900*	1000	1024	1200	1201*	1203*	1204*	1250*
1270*	1440	1500	1800	2000	2048	2400*	2500	2540*
2880*	3000*	3600*	4000*	4096*	5000*	6000*	7200*	7500*
9000*	10,000*	10,240*	12,000*	12,500*	14,400*	15,000*	18,000*	20,000*
20,480*	25,000*	30,000*						

* Contact Customer Service for High Temperature Option.
 † High Temperature Option (H) limited to 85° C maximum for these PPR options.
 Contact Customer Service to determine all currently available PPR values. Special disk resolutions are available upon request. A one-time NRE fee may apply.

For specification assistance call Customer Service at +44 (0)1978 262100

- NOTES:
- 1 See 755 Appendix sheet for flange options or Contact Customer Service for additional options.
 - 2 0° to 85° C for certain resolutions - Please see PPR options table.
 - 3 Contact Customer Service for marker galling options.
 - 4 Standard temperature, 60 to 3000 PPR only.
 - 5 Standard cable lengths only.
 - 6 For non-standard cable lengths, please call our sales office.
 - 7 5-pin not available with Line Driver (HV, LS) outputs. Additional cable lengths available. Please consult Customer Service.
 - 8 See 755 Special Covers page 41 for Cover Diagrams & options.

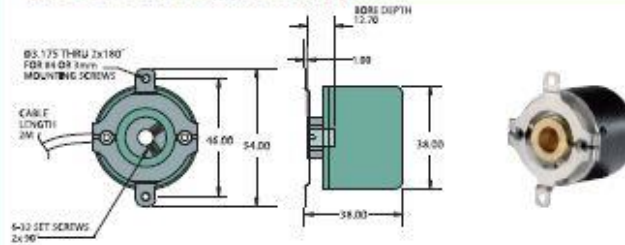


Model 755HS 38mm High Precision Hollow Bore Encoder

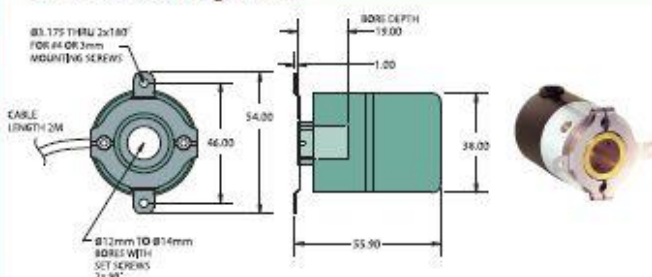
Model 755HS Specifications

- Electrical**
- Input Voltage.....4.75 to 28 Vcc max for temperatures up to 70° C
4.75 to 24 Vcc for temperatures between 70° C to 100° C
 - Input Current.....100 mA max with no output load
 - Input Ripple.....100 mV peak-to-peak at 0 to 100 kHz
 - Output Format.....Incremental- Two square waves in quadrature with channel A leading B for clockwise shaft rotation, as viewed from the encoder mounting face. See *Waveform Diagrams* below.
 - Output Types.....Open Collector- 100 mA max per channel
Pull-Up- 100 mA max per channel
Push-Pull- 20 mA max per channel
Line Driver- 20 mA max per channel (Meets RS 422 at 5 Vcc supply)
 - Index.....Occurs once per revolution. The index for units >3000 CPR is 90° gated to Outputs A and B. See *Waveform Diagrams* below.
 - Max Frequency.....Up to 1 MHz
 - Noise Immunity.....Tested to BS EN61000-4-2; IEC601-3; BS EN61000-4-4; DDENV 50141; DDENV 50204; BS EN55022 (with European compliance option); BS EN61000-6-2; BS EN50081-2
 - Symmetry.....1 to 6000 PPR: 180° (±18°) electrical at 100 kHz output
8001 to 20,480 PPR: 180° (±36°) electrical
 - Quad Phasing.....1 to 6000 CPR: 90° (±22.5°) electrical at 100 kHz output
8001 to 20,480 PPR: 90° (±36°)
 - Min Edge Sep.....1 to 6000 PPR: 67.5° electrical at 100 kHz output
8001 to 20,480 PPR: 54° electrical
 - Rise Time.....Less than 1 microsecond
 - Accuracy.....Instrument and Quadrature Error: For 200 to 1999 PPR, 0.017° mechanical (1.0 arc minutes) from one cycle to any other cycle. For 2000 to 3000 PPR, 0.01° mechanical (0.6 arc minutes) from one cycle to any other cycle. Interpolation error (units > 3000 PPR only) within 0.005° mechanical. (Total Optical Encoder Error = Instrument + Quadrature + Interpolation)
- Mechanical**
- Max Shaft Speed.....7500 RPM. Higher shaft speeds may be achievable, contact Customer Service.
 - Bore Size.....Up to 14 mm
 - Bore Tolerance.....H7, Sliding fit for g5
- User Shaft Tolerances**
- Radial Runout.....0.2mm max
 - Axial End Play.....±0.8mm max
 - Starting Torque.....2.985 x 10⁻⁴ typical
 - Max Acceleration.....1 x 10³ rad/sec²
 - Electrical Conn.....2M cable (foil and braid shield, 24 AWG conductors), 5- or 8-pin M12 (12 mm) in-line connector with 2M cable (braid shield), 8-pin Molex, Terminal Block, 5 Pin Cover, 8 Pin Cover, 8 Pin Cover, Gland Cover (See appendix sheet for cover options)
- Housing**.....Black non-corrosive finish
- Bearings**.....Precision ABEC ball bearings
- Mounting**.....Flex, and Slotted Flex Mounting
- Weight**.....100 grams typical
- Environmental**
- Operating Temp.....0° to 70° C for standard models
-40° to 70° C for low temperature option
0° to 100° C for high temperature option
(0° to 85° C for certain resolutions, see PPR Options.)
 - Storage Temp.....-25° to +85° C
 - Humidity.....98% RH non-condensing
 - Vibration.....10 g @ 58 to 500 Hz
 - Shock.....50 g @ 11 ms duration
 - Sealing.....IP50 Standard

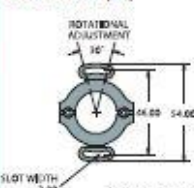
Model 755HS Flex Mount (FF)



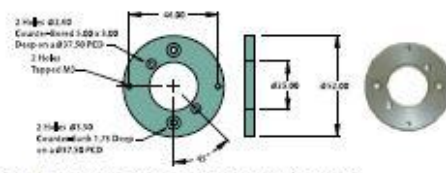
Model 755HS Large Bore



Optional Slotted Flex Mount (SF)



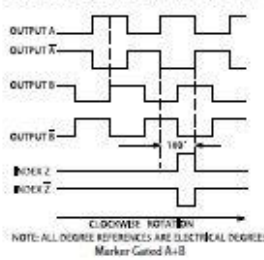
Also Available - PARVEX Flange Kit (M-9)



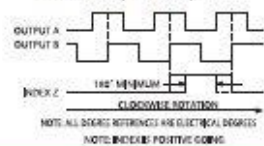
All dimensions are in mm with a tolerance of +0.127 or -0.254 unless otherwise specified

Waveform Diagrams

Line Driver (HV), Push-Pull (PP - No A, B & Z)



Open-Collector, Pull-Up (OC, PU)



Wiring Table

Function	Cable Wire Color	Terminal Block	8-pin Molex	5-pin M12	8-pin M12	8-pin MS1
0 Vcc	Black	7	2	3	7	A
+ Vcc	White	8	1	1	2	B
A	Brown	1	8	4	1	D
A'	Yellow	2	7	—	3	—
B	Red	3	4	2	4	E
B'	Green	4	3	—	5	—
Z	Orange	6	6	5	6	C
Z'	Blue	5	5	—	6	—
Shield	Bare	—	—	—	—	—

See Appendix Data Sheet for Connector Cover Options

Incremental Thru-Bore & Motor Mount Encoders

B.3 Binary converter

The function of this peripheral is to count the pulses coming from the encoder and convert the counting states into binary digital word. Following is the datasheet for this peripheral as it is given by the manufacturer.

ECOUNT Encoder to Binary Counter Converter

Description:

The ECOUNT converts the A/B quadrature output of an incremental encoder into a 24-bit parallel binary count value. A DIP switch provides a convenient way to configure various modes.

The ECOUNT draws its power from an external unregulated DC power supply (PS-12) included. The ECOUNT has an internal voltage regulator that provides +5V to the encoder connector.

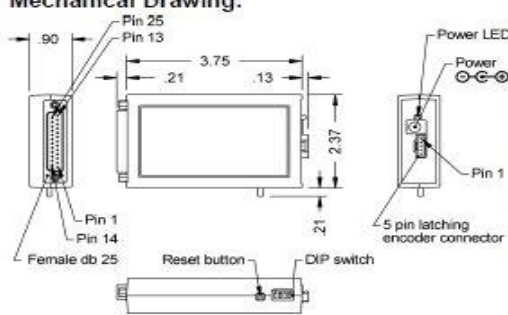
There are three ways that the 24-bit counter can be reset to zero. The user can cycle the unit power off and on, press the reset button, or select the reset on index mode with the DIP switch.

An encoder cable can be plugged into the 5-pin finger-latching connector. A DB25 female connector allows the user to connect to the 24-bit parallel output. The DV-option provides 23-bits of parallel output, and a low true data valid signal line on counter bit 24. DIN rail mounting is available. The ECOUNT only draws 5mA of current without an encoder connected.

US Digital warrants its products against defects in materials and workmanship for two years. See complete warranty for details.



Mechanical Drawing:



Absolute Maximum Ratings:

Parameter	Min.	Max.	Units
Storage Temperature	-40	100	°C
Operating Temperature	0	70	°C
Humidity (non-condensing)	0	95	%
Encoder Inputs (diode clamped)	-0.6	5.6	Volts

Electrical Specifications:

Parameter	Min.	Typ.	Max.	Units
Supply Voltage (into ECOUNT)	6	-	16	Volts
Supply Current (without encoders)	-	-	5.0	mA
Voltage Supply to Encoder	4.85	5.0	5.25	Volts
Quadrature Input Frequency	0	-	1.2	MHz
Quadrature Inputs from Encoder - Logic Low	-	-	0.8	Volts
Quadrature Inputs from Encoder - Logic High	3.1	-	-	Volts
Counter Outputs - Logic Low @ +0.5mA	-	0.4	-	Volts
Counter Outputs - Logic High @ -0.5mA	-	4.6	-	Volts
Quadrature Input Impedance	10K	-	-	Ohms

DIP Switches:

SW	Name	Up	Down	Notes
1	Count Mode	X4	X1	Once per cycle / once per edge
2	Up Count	B / A	A / B	Count direction
3	Index	Reset	No reset	
4	-	-	-	

Compatible Cables & Connectors:

Finger-latching:

5-pin	Description
CON-FC5-22*	Connector
CA-3133-1FT	Connector on one end with 4 12" wires
CA-3132-1FT	Connector on one end with 5 12" wires
CA-3131-8FT	Connector on one end of a 6' shielded round cable
CA-3620-8FT	Connectors on both ends of a 6' shielded round cable

* 22 AWG is standard. 24, 26 and 28 AWG are also available.

Attention:

- > Specify cable length when ordering.
- > Custom cable lengths are available.

Encoder Input Connector Pin-out:

Pin	Description
1	Ground
2	Index
3	A channel
4	+5VDC power
5	B channel

DB25 Output Connector Pin-out:

Pin	Description
1-23	Data bits 0-22
24	Data bit 23 or data valid for DV-option
25	Ground

Ordering Information:

Price:

- \$103.95 / 1
- \$95.55 / 10
- \$87.15 / 50
- \$79.80 / 100

Part #:

ECOUNT -

DV = Low true data valid signal.
 R = DIN rail (35mm wide) mounting.
 NP = No power supply.

Cost Modifiers:

- > Add \$10 for R-option.
- > Subtract \$5 for NP-option (no PS-12).

Includes:

- > PS-12 (power supply).

Technical Data, Rev. 06.28.06, June 2006
All information subject to change without notice.

US DIGITAL

info@usdigital.com • www.usdigital.com
 Local: 360.260.2468 • Sales: 800.736.0194
 Support: 360.397.9699 • Fax: 360.260.2469

page 1

B.4 Pins out description for the μ C ATmega328

Following is a brief scheduling for the function assigned for each pin in the body structure of the DIL integrated circuit ATmega328.

Functional pins configuration for ATmega328		
Pin Number	Description	Function
1	PC6	Reset
2	PD0	Digital Pin (RX)
3	PD1	Digital Pin (TX)
4	PD2	Digital Pin
5	PD3	Digital Pin (PWM)
6	PD4	Digital Pin
7	Vcc	Positive Voltage (Power)
8	GND	Ground
9	XTAL 1	Crystal Oscillator
10	XTAL 2	Crystal Oscillator
11	PD5	Digital Pin (PWM)
12	PD6	Digital Pin (PWM)
13	PD7	Digital Pin
14	PB0	Digital Pin
15	PB1	Digital Pin (PWM)
16	PB2	Digital Pin (PWM)
17	PB3	Digital Pin (PWM)
18	PB4	Digital Pin
19	PB5	Digital Pin
20	AVcc	Positive voltage for ADC (power)
21	AREF	Reference Voltage
22	GND	Ground
23	PC0	Analog Input
24	PC1	Analog Input
25	PC2	Analog Input
26	PC3	Analog Input
27	PC4	Analog Input
28	PC5	Analog Input

B.5 Pins out description for the μ C ATmega2560

Pin Number	Pin Name	Mapped Pin Name
1	PG5 (OC0B)	Digital pin 4 (PWM)
2	PE0 (RXD0/PCINT8)	Digital pin 0 (RX0)
3	PE1 (TXD0)	Digital pin 1 (TX0)
4	PE2 (XCK0/AIN0)	
5	PE3 (OC3A/AIN1)	Digital pin 5 (PWM)
6	PE4 (OC3B/INT4)	Digital pin 2 (PWM)
7	PE5 (OC3C/INT5)	Digital pin 3 (PWM)
8	PE6 (T3/INT6)	
9	PE7 (CLK0/ICP3/INT7)	
10	VCC	VCC
11	GND	GND
12	PH0 (RXD2)	Digital pin 17 (RX2)
13	PH1 (TXD2)	Digital pin 16 (TX2)
14	PH2 (XCK2)	
15	PH3 (OC4A)	Digital pin 6 (PWM)
16	PH4 (OC4B)	Digital pin 7 (PWM)
17	PH5 (OC4C)	Digital pin 8 (PWM)
18	PH6 (OC2B)	Digital pin 9 (PWM)
19	PB0 (SS/PCINT0)	Digital pin 53 (SS)
20	PB1 (SCK/PCINT1)	Digital pin 52 (SCK)
21	PB2 (MOSI/PCINT2)	Digital pin 51 (MOSI)
22	PB3 (MISO/PCINT3)	Digital pin 50 (MISO)
23	PB4 (OC2A/PCINT4)	Digital pin 10 (PWM)
24	PB5 (OC1A/PCINT5)	Digital pin 11 (PWM)
25	PB6 (OC1B/PCINT6)	Digital pin 12 (PWM)

26	PB7 (OC0A/OC1C/PCINT7)	Digital pin 13 (PWM)
27	PH7 (T4)	
28	PG3 (TOSC2)	
29	PG4 (TOSC1)	
30	RESET	RESET
31	VCC	VCC
32	GND	GND
33	XTAL2	XTAL2
34	XTAL1	XTAL1
35	PL0 (ICP4)	Digital pin 49
36	PL1 (ICP5)	Digital pin 48
37	PL2 (T5)	Digital pin 47
38	PL3 (OC5A)	Digital pin 46 (PWM)
39	PL4 (OC5B)	Digital pin 45 (PWM)
40	PL5 (OC5C)	Digital pin 44 (PWM)
41	PL6	Digital pin 43
42	PL7	Digital pin 42
43	PDO (SCL/INT0)	Digital pin 21 (SCL)
44	PD1 (SDA/INT1)	Digital pin 20 (SDA)
45	PD2 (RXD1/INT2)	Digital pin 19 (RX1)
46	PD3 (TXD1/INT3)	Digital pin 18 (TX1)
47	PD4 (ICPI)	
48	PD5 (XCK1)	
49	PD6 (T1)	
50	PD7 (T0)	Digital pin 38

51	PG0 (WR)	Digital pin 41
52	PG1 (RD)	Digital pin 40
53	PC0 (A8)	Digital pin 37
54	PC1 (A9)	Digital pin 36
55	PC2 (A10)	Digital pin 35
56	PC3 (A11)	Digital pin 34
57	PC4 (A12)	Digital pin 33
58	PC5 (A13)	Digital pin 32
59	PC6 (A14)	Digital pin 31
60	PC7 (A15)	Digital pin 30
61	VCC	VCC
62	GND	GND
63	PJ0 (RXD3/PCINT9)	Digital pin 15 (RX3)
64	PJ1 (TXD3/PCINT10)	Digital pin 14 (TX3)
65	PJ2 (XCK3/PCINT11)	
66	PJ3 (PCINT12)	
67	PJ4 (PCINT13)	
68	PJ5 (PCINT14)	
69	PJ6 (PCINT15)	
70	PG2 (ALE)	Digital pin 39
71	PA7 (AD7)	Digital pin 29
72	PA6 (AD6)	Digital pin 28
73	PA5 (AD5)	Digital pin 27
74	PA4 (AD4)	Digital pin 26
75	PA3 (AD3)	Digital pin 25

76	PA2 (AD2)	Digital pin 24
77	PA1 (AD1)	Digital pin 23
78	PA0 (AD0)	Digital pin 22
79	PJ7	
80	VCC	VCC
81	GND	GND
82	PK7 (ADC15/PCINT23)	Analog pin 15
83	PK6 (ADC14/PCINT22)	Analog pin 14
84	PK5 (ADC13/PCINT21)	Analog pin 13
85	PK4 (ADC12/PCINT20)	Analog pin 12
86	PK3 (ADC11/PCINT19)	Analog pin 11
87	PK2 (ADC10/PCINT18)	Analog pin 10
88	PK1 (ADC9/PCINT17)	Analog pin 9
89	PK0 (ADC8/PCINT16)	Analog pin 8
90	PF7 (ADC7)	Analog pin 7
91	PF6 (ADC6)	Analog pin 6
92	PF5 (ADC5/TMS)	Analog pin 5
93	PF4 (ADC4/TMK)	Analog pin 4
94	PF3 (ADC3)	Analog pin 3
95	PF2 (ADC2)	Analog pin 2
96	PF1 (ADC1)	Analog pin 1
97	PF0 (ADC0)	Analog pin 0
98	AREF	Analog Reference
99	GND	GND
100	AVCC	VCC

B.6 Transducer Display Interface [E301/2]

According to the manual of this instrument:

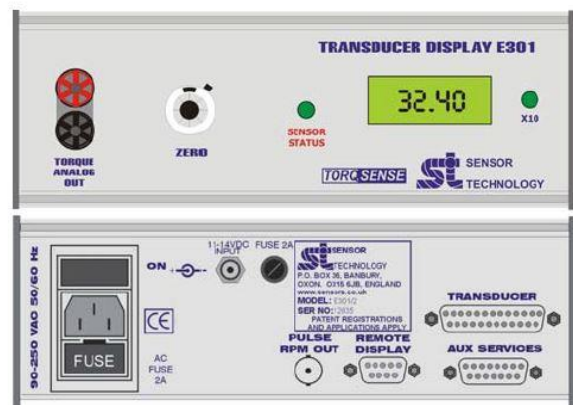
“The E302 interface is an advanced instrument, digitally displaying the output signals of the E300 RWT1 torque transducer. Torque and RPM are displayed together with the computed power. There also an option to display transducer temperature. The E302 can be powered either from 96-250V, 50/60 Hz A.C mains supply, or from an 11-14V D.C source. Power to the transducer is also supplied from the E302.” It works in conjunction with a torque sensor and a cable to connect them as shown below. More details are given in [204].



A typical E-302 Transducer Display unit. Front panel

Common Features

- Automatically detects the full-scale range of any E300 RWT1 transducer.
- The display is automatically programmed to read the full scale of the transducer.
- Continuous self-auditing (sensor status is indicated on a front panel LED or remotely available).
- $\pm 5\text{v}$ analog output for Torque FSD.
- 90-250V ac operation or 12v dc operation.





Torque sensor and connection cable

Appendix C, Miscellaneous

C.1 Datasheets for electronic components

C.1.1 Brief datasheet for IGBT FGH40N60SFD


March 2015

FGH40N60SFD

600 V, 40 A Field Stop IGBT

Features

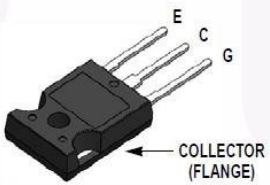
- High Current Capability
- Low Saturation Voltage: $V_{CE(sat)} = 2.3 \text{ V @ } I_C = 40 \text{ A}$
- High Input Impedance
- Fast Switching
- RoHS Compliant

Applications

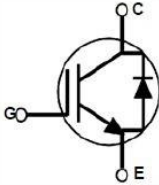
- Solar Inverter, UPS, Welder, PFC, Microwave Oven, Telecom, ESS

General Description

Using novel field stop IGBT technology, Fairchild's field stop IGBTs offer the optimum performance for solar inverter, UPS, welder, microwave oven, telecom, ESS and PFC applications where low conduction and switching losses are essential.



COLLECTOR (FLANGE)



IGBT used in implementation the platform of zero speed rotor position estimation

C.1.2 Brief datasheet for IGBT FGH40T100SMD



ON Semiconductor®

FGH40T100SMD

1000 V, 40 A Field Stop Trench IGBT

Features

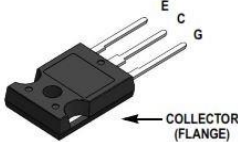
- High Current Capability
- Low Saturation Voltage: $V_{CE(sat)} = 1.9 \text{ V(Typ.) @ } I_C = 40 \text{ A}$
- High Input Impedance
- Fast Switching
- RoHS Compliant

General Description

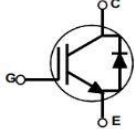
Using innovative field stop trench IGBT technology, ON Semiconductor new series of field stop trench IGBTs offer the optimum performance for hard switching application such as UPS, welder and PFC applications.

Applications

- UPS, welder, PFC



← COLLECTOR (FLANGE)



IGBT used in implementation the test bed of low speed rotor position estimation

C.1.3 Brief datasheet for digit to analogue converter AD767



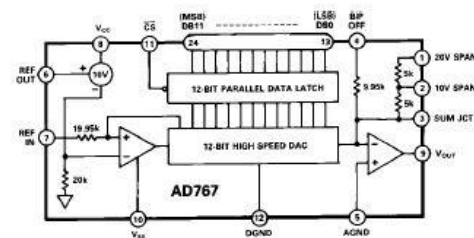
Microprocessor-Compatible 12-Bit D/A Converter

AD767

FEATURES

Complete 12-Bit D/A Function
On-Chip Output Amplifier
High Stability Buried Zener Reference
Fast 40 ns Write Pulse
0.3" Skinny DIP and PLCC Packages
Single Chip Construction
Monotonicity Guaranteed Over Temperature
Settling Time: 3 μ s max to 1/2 LSB
Guaranteed for Operation with ± 12 V or ± 15 V Supplies
TTL/5 V CMOS Compatible Logic Inputs
MIL-STD-883 Compliant Versions Available

FUNCTIONAL BLOCK DIAGRAM



PRODUCT DESCRIPTION

The AD767 is a complete voltage output 12-bit digital-to-analog converter including a high stability buried Zener reference and input latch on a single chip. The converter uses 12 precision high-speed bipolar current steering switches and a laser-trimmed thin-film resistor network to provide high accuracy.

Microprocessor compatibility is achieved by the on-chip latch. The design of the input latch allows direct interface to 12-bit buses. The latch responds to strobe pulses as short as 40 ns, allowing use with the fastest available microprocessors.

The functional completeness and high performance of the AD767 result from a combination of advanced switch design, high-speed bipolar manufacturing process, and the proven laser wafer-trimming (LWT) technology.

The subsurface (buried) Zener diode on the chip provides a low-noise voltage reference which has long-term stability and temperature drift characteristics comparable to the best discrete reference diodes. The laser trimming process which provides the excellent linearity is also used to trim the absolute value of the reference as well as its temperature coefficient. The AD767 is thus well suited for wide temperature range performance with $\pm 1/2$ LSB maximum linearity error and guaranteed monotonicity over the full temperature range. Typical full-scale gain T.C. is 5 ppm/ $^{\circ}$ C.

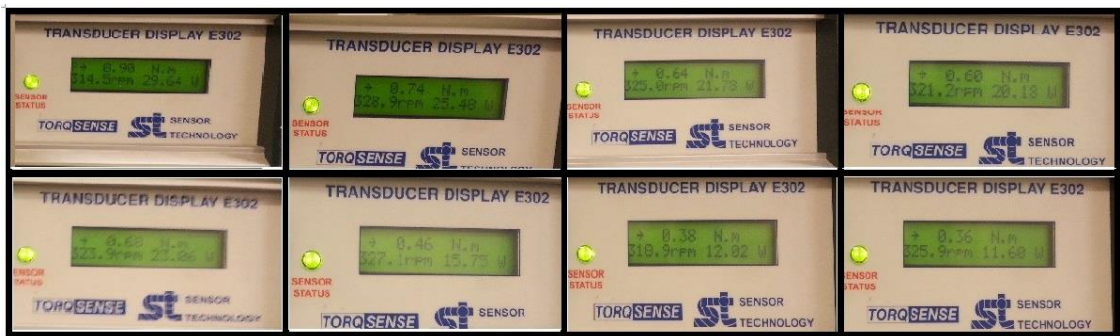
PRODUCT HIGHLIGHTS

1. The AD767 is a complete voltage output DAC with voltage reference and digital latches on a single IC chip.
2. The input latch responds to write pulse widths as short as 40 ns assuring direct interface with the industry's fastest microprocessors.
3. The internal buried Zener reference is laser-trimmed to 10.00 volts with a $\pm 1\%$ maximum error. The reference voltage is also available for external application.
4. The gain setting and bipolar offset resistors are matched to the internal ladder network to guarantee a low gain temperature coefficient and are laser trimmed for minimum full-scale and bipolar offset errors.
5. The precision high-speed current steering switches and on-board high-speed output amplifier settle within 1/2 LSB for a 10 V full-scale transition in 3.0 μ s when properly compensated.
6. The AD767 is available in versions compliant with MIL-STD-883. Refer to the Analog Devices Military Products Databook or current AD767/883B data sheet for detailed specifications.

C.2 Snaps for load test results



Load test reading MAc2n320-4/2-3



Load test reading for the motor M0200-104-4-000

C.3 Motor M0200 datasheet

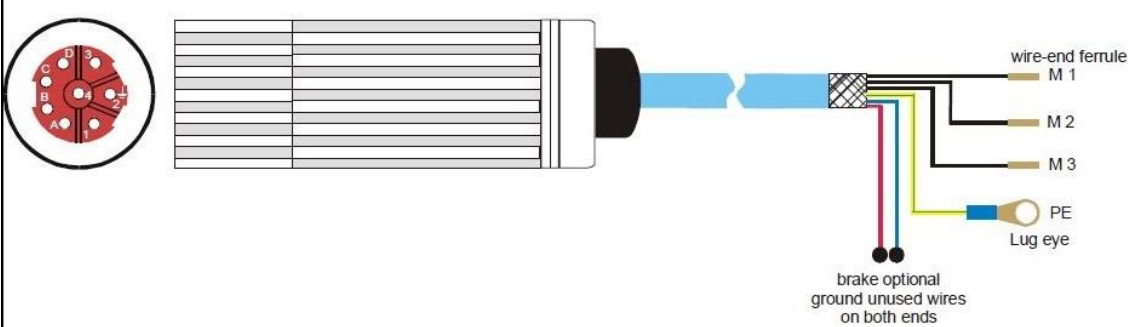
Applied Motion Products		Applied Motion Products, Inc. 404 Westridge Dr. Watsonville, CA 95076, USA		1-800-525-1609 Tel (831) 761-6555 Fax (831) 761-6544		Product Datasheet www.Applied-Motion.com	
M0200-104-4-000 60mm Servo Motor, 200W							
				<p>Product Features</p> <ul style="list-style-type: none"> • High torque density • Low rotor inertia • Compact size • High-resolution, incremental encoders (2000 lines, 8000 counts) <p>RoHS</p>			
Description							
Frame Size	60 mm	Armature Inductance	1.7 mH				
Continuous Torque	5.7 in-lb	Motor Length	4.04 inch				
Peak Torque	17 in-lb	Rotor Inertia	2.55E-03 oz-in-sec ²				
Rated Power	200 watts	Weight	1.9 lbs				
Rated Voltage	48 volts	Storage Temperature	-10 to 85 °C				
Rated Speed	3000 rpm	Operating Temperature	0 to 40 °C				
Peak Speed	5000 rpm	Insulation Class	Class B (130 °C)				
Rated Current	6.4 A rms	Maximum Radial Load	44 lbs				
Peak Current	18.0 A rms	Concentricity	0.002 inches				
Torque Constant	0.93 in-lb/A	Maximum Thrust Load	15.4 lbs				
Voltage Constant	11 V/krpm	Shaft Run Out	0.0008 inch T.I.R. max				
Armature Resistance	0.6 ohms	Perpendicularity	0.003 inches				

C.4 Motor AC M2n0320 datasheet

AC Servo - Motors



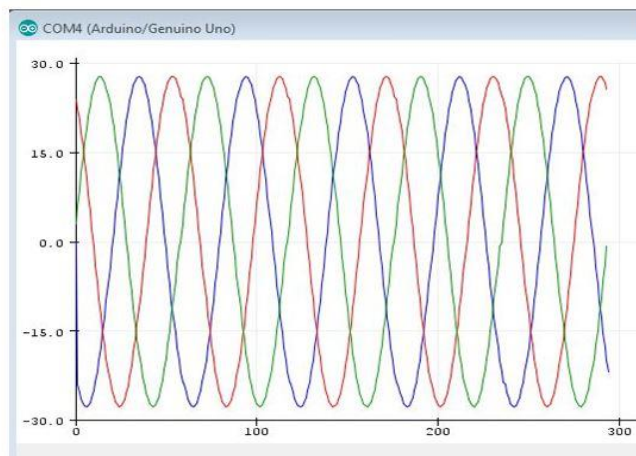
Rated Torque	3.2 Nm	Rotor Inertia	2.4 kg.cm ²
Rated Power	1300 watts	Weight	6 kg
Rated Voltage	325 volts	Armature Inductance	2.4 mH
Rated Speed	4000 rpm	Armature Resistance	1 ohms
Rated Current	6.4 A rms	Ingress protection	IP54
Torque Constant	0.49 Nm/A	Voltage Constant	30 V/krpm
Magnetic material	NdFeB	No. of pole pars	3



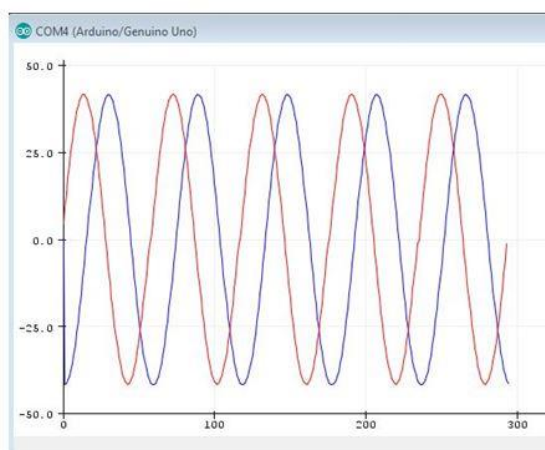
wire-end ferrule
 M 1
 M 2
 M 3
 PE
 Lug eye
 brake optional
 ground unused wires
 on both ends

C.5 Virtual voltages and sectors of the proposed SV sequence

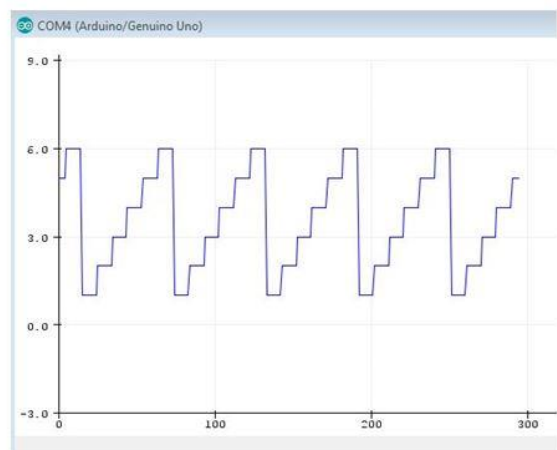
Following are snaps for the injected virtual voltages and the corresponding obtained sector divisions as they were plotted by the employed master microcontroller.



Virtual injected voltages

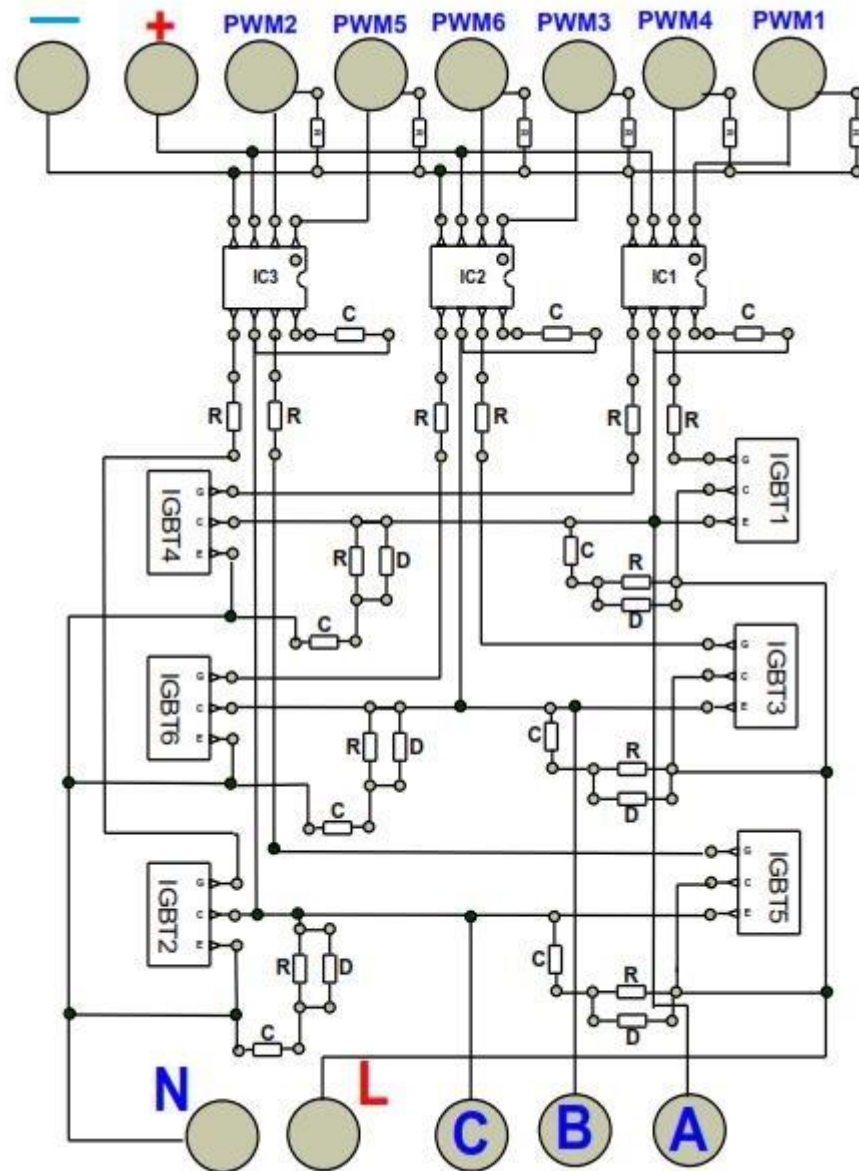


V_α and V_β

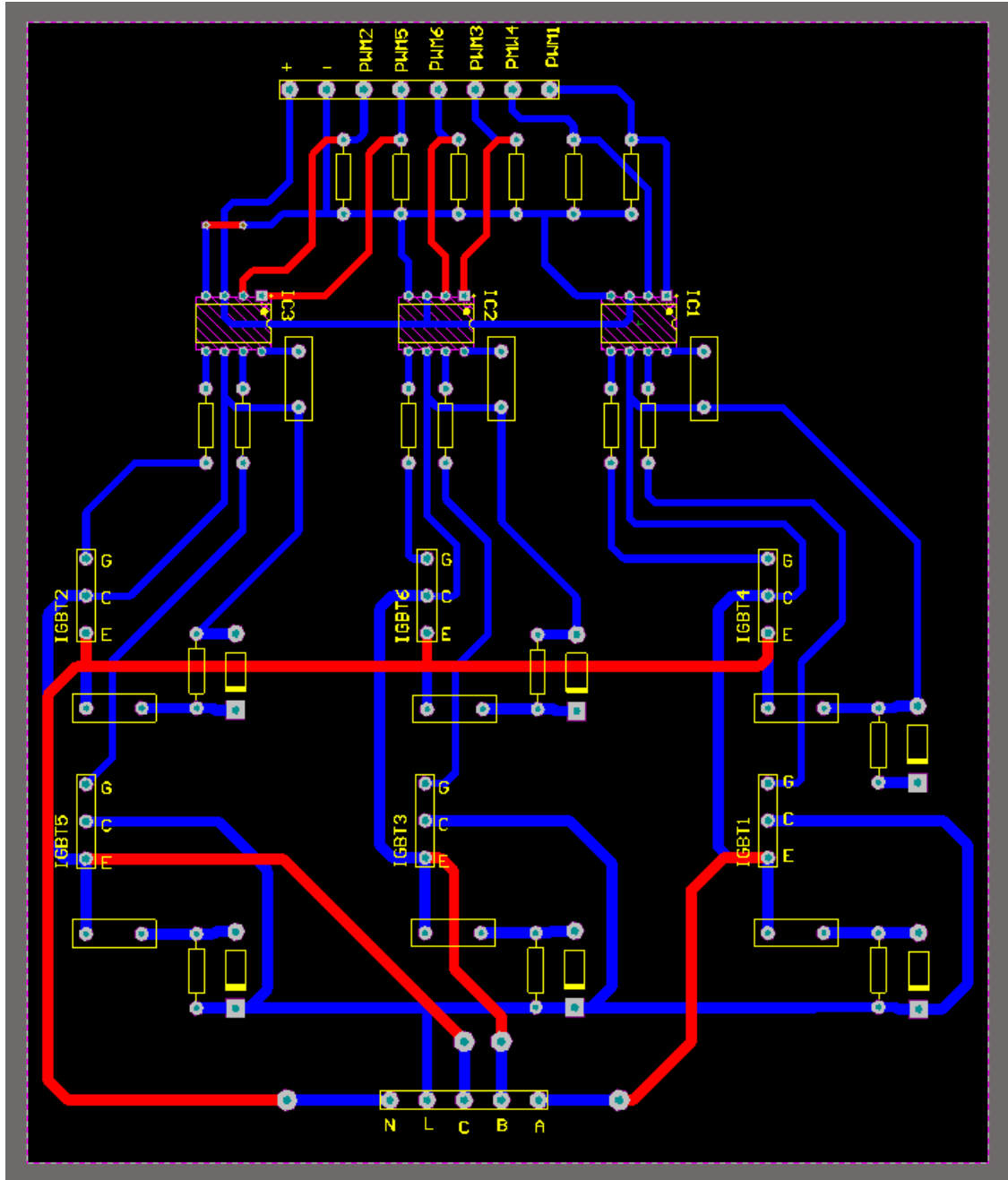


Sectors

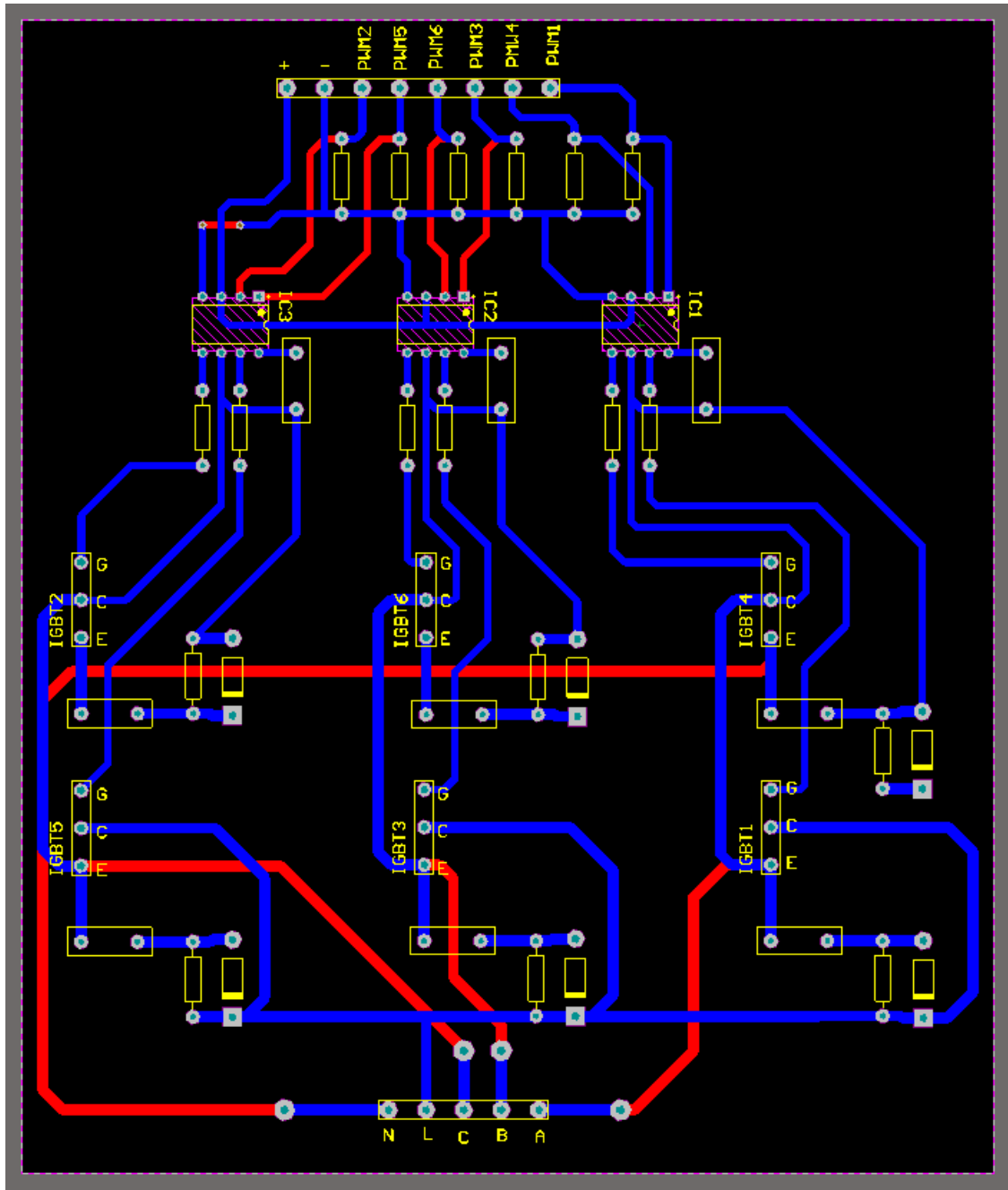
C.6 The inverter printed circuit board, PCB



Electronic drawing for the inverter circuit with the bootstrap ICs

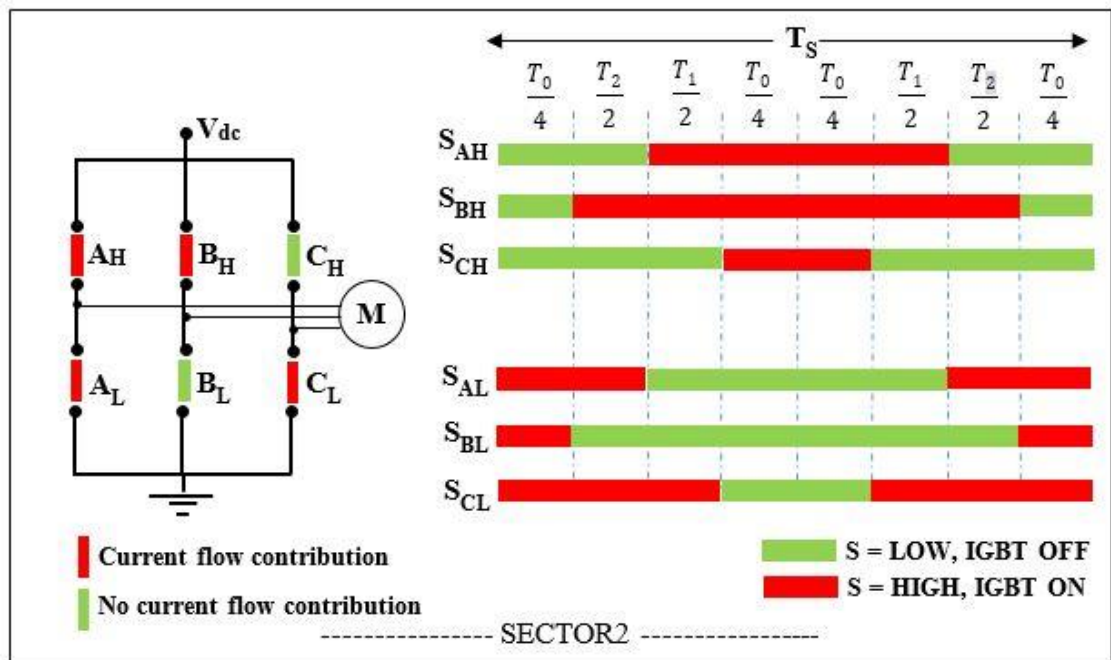
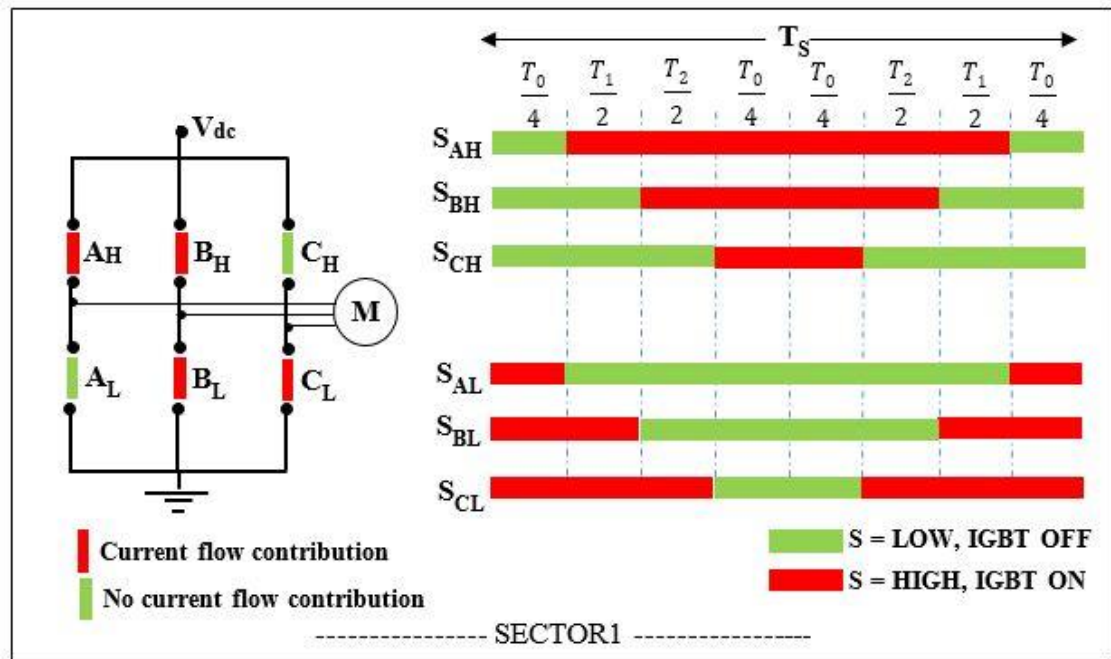


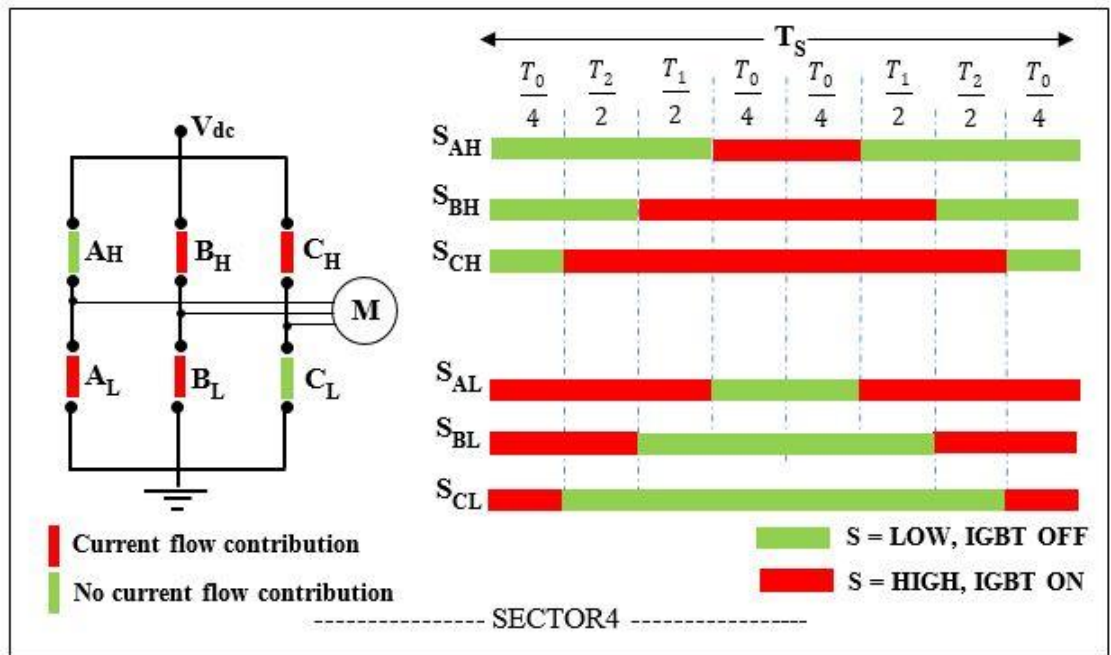
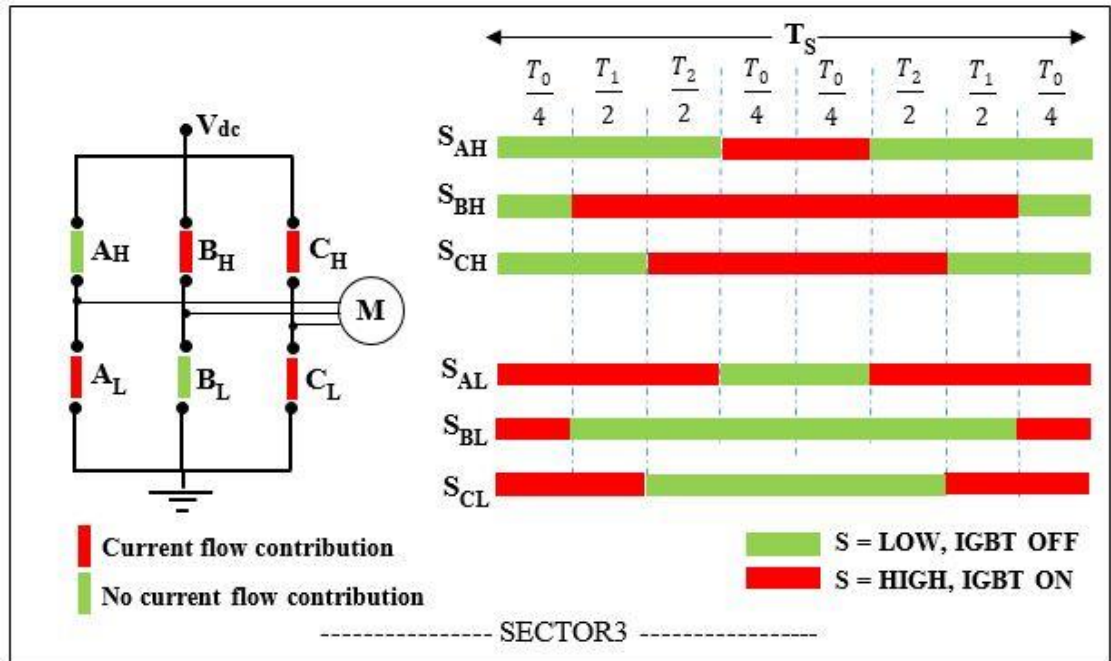
Top layer of the inverter printed circuit board

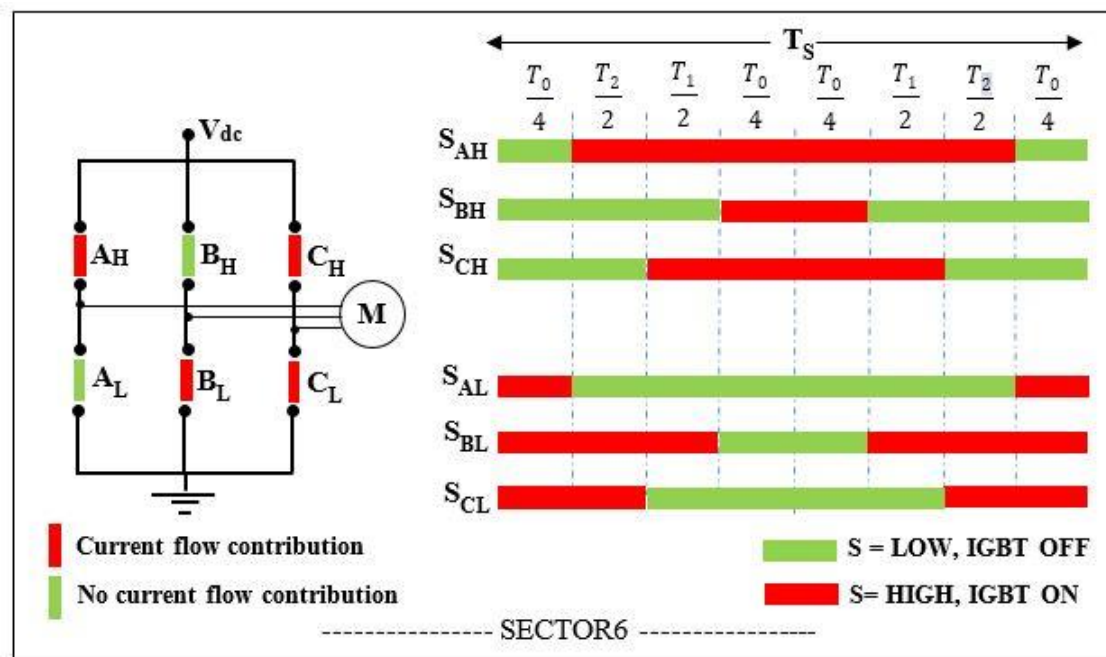
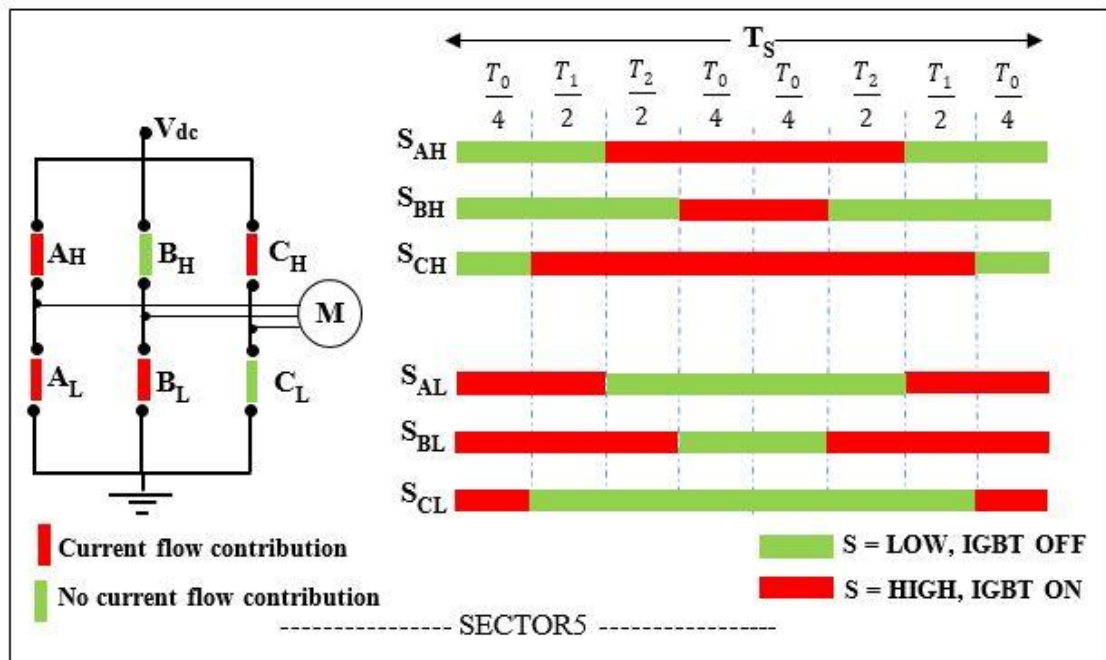


Bottom layer of the inverter printed circuit board

C.7 Standard patterns of space vector technique







C.8 Details of the block IGBT switching in figure 4.21

